Role of Caf proteins in outer membrane vesicle release from *Escherichia coli*

Mouna Jassim Al-Houli

Thesis submitted in partial fulfilment of
the requirements of the regulations for the degree of
Doctor of Philosophy

Biosciences Institute

Faculty of Medical Sciences

Newcastle University

February 2023

Abstract

Outer membrane vesicles (OMVs) are nanostructures that are spontaneously produced by Gram-negative bacteria during all phases of growth and often in response to stress. Gram-negative bacteria display a variety of surface proteinaceous appendages by which they attach to objects or move in their environments. These structures mainly involve repetitive assemblies organised into filamentous polymers; one example is the F1 antigen which uses the chaperone-usher pathway to assemble an amorphous capsule (Caf1) to help *Yersinia pestis* evade phagocytosis. In this study, flocculated materials, consisting of OMVs trapped in a polymeric network of Caf1, were observed in *Escherichia coli* cultures expressing Caf1 proteins. It was demonstrated that the flocculent layer is Caf1 polymer dependent and that expression of several *caf1* operon genes increases OMV formation. The deletion of the molecular usher Ca1fA was found to prevent Caf1 polymer formation at the cell surface and to cause hypervesiculation and an increase in liposaccharide (LPS) release. In addition to LPS, OMVs contain an abundance of outer membrane proteins (OMPs), such as OmpF and OmpA. To measure OMV production a range of fluorescent OmpA proteins were created. These included truncated and full-length forms of OmpA fused with GFP or mCherry or containing a tetra-cysteine motif which binds the FlAsH-EDT_2 fluorescent probe. This study showed that full length OmpA-mCherry fusions are highly expressed and insert into the OM making them the most suitable probes for measuring OMV levels. It was also shown that the level of Caf1A present in the OM may not be the limiting factor in polymer production and that only a very low level of Caf1A is needed to produce flocculent. Also, these findings demonstrated for the first time that the *caf1R* gene directly regulates the *caf1A* gene. Disappointingly, overexpression of *caf1A* did not elevate Caf1A levels, increase Caf1 polymer production or decrease OMV formation by reducing Caf1 aggregation in the periplasm. This may be due to a limit on the amount of Caf1A that can be inserted into the OM. These results will help maximise Caf1 production for biomaterials applications and may suggest the use of OMVs for vaccine applications containing Caf1 as a protein scaffold for antigen delivery.

Dedication

To My Children,

Shoug, Reem, Bader, Ali, Suliman and Hassan

Acknowledgement

The completion of this PhD thesis would not have been possible without the social and emotional support of many people.

First and foremost, I would like to express my sincere thanks and deepest appreciation to my great supervisor Professor Jeremy Lakey for his immense guidance, continual encouragement, endless support, and his unlimited patience throughout this PhD study. Without his support, I would not have seen the light at the end of the tunnel. I have been very fortunate to have a great supervisor like Jeremy. I have learned great deal from his expertise and professionalism, and for everything he has given, thanks see to me far less small a return, but I sincerely and humbly offer him.

I wish to express my sincere gratitude to my dearest friend Dr Helen Waller who has never failed to offer me her advice when things went out of track. Her wisdom and perception of things have given me the strength to overcome hurdles and to focus on my goal.

I am deeply grateful to Dr Daniel Peters for his friendship and assistance for the joyful time that we both spent in the lab. It has been a pleasure working with you.

Members of the Lakey research group, Dr Abdulmajeed Al-jawdah, Dr Nicolo Paracini are thanked for their friendship, good advice, and collaboration.

In addition, Many thanks to all the Thai students who made the lab more enjoyable place.

I am thankful for the members of my panel (Dr Anjam Khan and Dr Colin Harwood) who gladly gave their time to provide constructive advice an encouragement.

I would like to express my gratitude to Dr Henrik Strahl for his assistance and guidance in carrying out the Fluorescence microscopy experimental work, as well as for his stimulating discussions.

I would like to thank the Newcastle University Biosciences Institute (NUBI) for their continuous support throughout the PhD study. A special thanks to Dr Tim Cheek, Louise Campbell and Dr Simon Whitehall.

I would like to extend my sincere gratitude to Tracy Davey and the entire Newcastle University Electron Microscopy Research Services.

Many thanks to Marian Rixhan of the EndNote team at the Walton Library for assistance just two days before the submission deadline. Thank you Loads!

I would like also to extend to thanks to the IT department for their help during this journey .

Special thanks to Dr Azzeldin Madkour for his continuous support and encouragement.

Also, I warmly Thanks all my friends especially Maria Stringer and Abdulkarim Alessa for their continuous support and for always believe in me!

Last, but not the least, words fall far short from expressing my appreciation for everything that my mother has done to me throughout my life. Without her being there, I would not have reached this stage. I would like to deeply thank my aunt Lila, for being not just aunt but a caring and kind older sister. Many thanks extend to my brothers, Mohammad, Abdulrahman and Omar, and my sweet sister Nour, for being there whenever I needed them.

Table of contents

List of figures

List of Tables

List of Abbreviations

Abbreviation	Definition
ABC	ATP-binding cassette
ANOVA	Analysis of variance
BAM	β-barrel assembly machinery
Caf1	Capsular antigen F1
CDT	C-terminal domain
CUP	Chaperone-usher pathway
DegP	Periplasmic serine endoprotease
DSC	Donor strand complementation
DSE	Donor strand exchange
DsRed	*Discosoma* species red
EDTA	Ethylenediaminetetraacetic acid
EGFP	Enhanced fluorescent protein
FGL	F1-G1 loop long
FGS	F1-G1 loop short
FlAsH-EDT_2	4,5-bis (1,3,2-dithiarsolan-2-yl) fluorescein

Abbreviation	Definition
FP	Fluorescent protein
FUP	Fimbrial usher protein
GFP	Green fluorescent protein
GlcNAc	N-acetylglucosamine
GSP	General secretion-independent pathway
HD	High density
IFN	Interferon factor
Ig	Immunoglobulin
IL-lB	Interleukin-lB
IM	Inner membrane
IMP	Inner membrane protein
IPTG	Isopropyl β-D-1-thiogalactopyranoside
Kdo	3-deoxy-D-manno-octulosonic acid
KWC	Killed-whole cell vaccine
LamB	Lambda phage receptor protein or Maltoporin
LB	Luria-Bertani
Lpp	Braun's lipoprotein

Abbreviation	Definition
LPS	Lipopolysaccharide
Mdo	Membrane-derived oligosaccharides
Mla	Maintenance of lipid asymmetry
mRFP	Monomeric red fluorescent protein
MurNAc	N-acetylmuramic acid
NMR	Nuclear magnetic resonance
NTD	N-terminal domain
OD_{600}	Optical Density at a light wavelength of 600 nm
OM	Outer membrane
OMP	Outer membrane protein
OmpA	Outer membrane protein A
OmpF	Outer membrane protein F
OMV	Outer membrane vesicle
PAGE	Poly Acrylamide Gel Electrophoresis
Pap	Pyelonephritis associated pili
PBS	Phosphate Buffered Saline
PD	Plug domain

Abbreviation	Definition
PGN	Peptidoglycan
PhoE	Phosphoporin
PldA	Phospholipase A
PMF	Proton-motive force
pMT1	Murine toxin
POTRA	Polypeptide transport-associated domains
pPCP1	Pestis-specific pesticin, plasminogen and coagulase
PQS	Pseudomonas quinolone signal
rCaf1	Recombinant Caf1
R-Form	Rough LPS
RT-PCR	Real-Time Polymerase Chain Reaction
SDS	Sodium Dodecyl Sulphate
Sec	Secretion translocase
sfGFP	Superfolder green fluorescent protein
S-Form	Smooth LPS
SRP	Signal recognition particle
SurA	Survival protein

Abbreviation	Definition
TB	Terrific Broth medium
TCM	Tetra-cysteine motif
TD	Transmembrane β-barrel domain
TEM	Transmission electron microscopy
TLC	Thin layer chromatography
TLR-4	Toll-like receptor 4
TNF	Tumour necrosis factor
UPEC	Uropathogenic
UTI	Urinary tract infections
Yops	Yersinia outer membrane proteins

Chapter One

Introduction

"We are what we repeatedly do. Excellence then is a habit"

Aristotle

1 Introduction

1.1 Gram-negative bacteria

Prokaryotes comprise two groups: archaea (formerly archaebacteria) and bacteria (formerly eubacteria) which have some characteristics in common. Most importantly, they generally possess a single circular chromosome, have a protective layer (cell wall) outside their plasma membrane and reproduce asexually via the binary fission process, which involves the division of a cell in half to yield a pair of identical cells. Based on their characteristics, archaea are divided into different groups, such as methanogens, extreme halophiles, and thermoacidophiles. Contrastingly, bacteria are usually segregated based on their response to Gram staining, which is the most commonly applied detection tool, originally developed by Christian Gram in 1884 (Wu *et al.*, 2020). This divides bacteria into two main types: Gram-positive (monoderm prokaryotes) and Gram-negative (diderm prokaryotes). Gram-positive bacteria retain the crystal violet-iodine colour and stain violet or purple when they are stained using the eponymous Gram staining procedure. By contrast, Gram-negative bacteria completely lose their colour and stain pink or pale red instead (Wu *et al.*, 2020). These two bacterial types differ in terms of the morphology or composition of their cell walls, particularly the presence of an outer membrane in Gram-negative bacteria and the thick cell wall of peptidoglycan (PGN) layer in the periplasm of Gram-positive bacteria (Silhavy *et al.*, 2010).

Gram-negative bacteria have been successfully used for many decades as a valuable source of practical bio-products, such as proteins, food processing enzymes and biopharmaceuticals (Singh *et al.*, 2017). However, these bacteria are also pathogens that have been implicated with hospital-acquired infections including pneumonia, urinary tract, venereal and wound or surgical site infections (Miller, 2016; Kubas *et al.*, 2018). These pathogens spread rapidly and are responsible for significant mortality and morbidity (Furuyama *et al.*, 2021). Recently, Gram-negative pathogens have become more prevalent, mostly due to excessive dispensing and imprudent use of antibiotics and we have witnessed a steep decline in the efficacy of antibiotics against Gram-negative bacteria (Jan, 2017). In order to tackle this growing crisis of antibiotic resistance, a tremendous effort needs to be devoted to the study of Gram-

negative bacteria in terms of identifying which of their components should be targeted for the development of new, safe and efficient antibiotic drugs.

The cell envelope of Gram-negative bacteria is more elaborate than that of Gram-positive bacteria (Silhavy *et al.*, 2010; Pajerski *et al.*, 2019). This cellular architecture consists of an outer membrane (OM) and a cytoplasmic or inner membrane (IM) (**Figure 1.1**). These two structures are separated by an aqueous periplasm (also referred to as the periplasmic space) containing a thin peptidoglycan cell wall. The various proteins and soluble enzymes within these three compartments enable the transport of molecules and provide support for metabolic processes (Galdiero *et al.*, 2012). The biosynthesis of the Gram-negative cell envelope is a complex process in which the protein components of the cell envelope are initially synthesised either in the cytoplasm or at the inner surface of the IM as soluble precursors with signal sequences. These precursors are subsequently translocated across the IM and through the periplasmic space to the OM (Silhavy *et al.*, 2010).

The IM is a symmetric phospholipid-rich bilayer that encloses the cytoplasm and serves as an electrochemical barrier (Schwechheimer *et al.*, 2015). This cytoplasmic membrane is mostly composed of ~70% phosphatidylethanolamine, ~15% phosphatidylglycerol and ~15% cardiolipin (Ruiz *et al.*, 2006; Horne *et al.*, 2020). In addition to phospholipids, the IM contains lipoproteins and integral proteins. The IM lipoproteins are attached to the outer leaflet of the IM by lipid alterations of the N-terminal cysteine residue of their own mature form. The integral IM proteins (IMPs) traverse the IM with α-helical transmembrane domains and carry out various cellular activities, including structural maintenance, nutrient transport, lipid biosynthesis, protein secretion and chemotaxis (Ruiz *et al.*, 2006). IMPs are synthesised in a co-translational manner via the signal recognition particle (SRP) pathway and its FtsY receptor. The synthesised IMPs then are inserted into the IM via the general secretion pathway (GSP), which has one or two copies of the heterotrimeric SecYEG translocon with a cytoplasmic ATPase motor SecA (Luirink *et al.*, 2012).

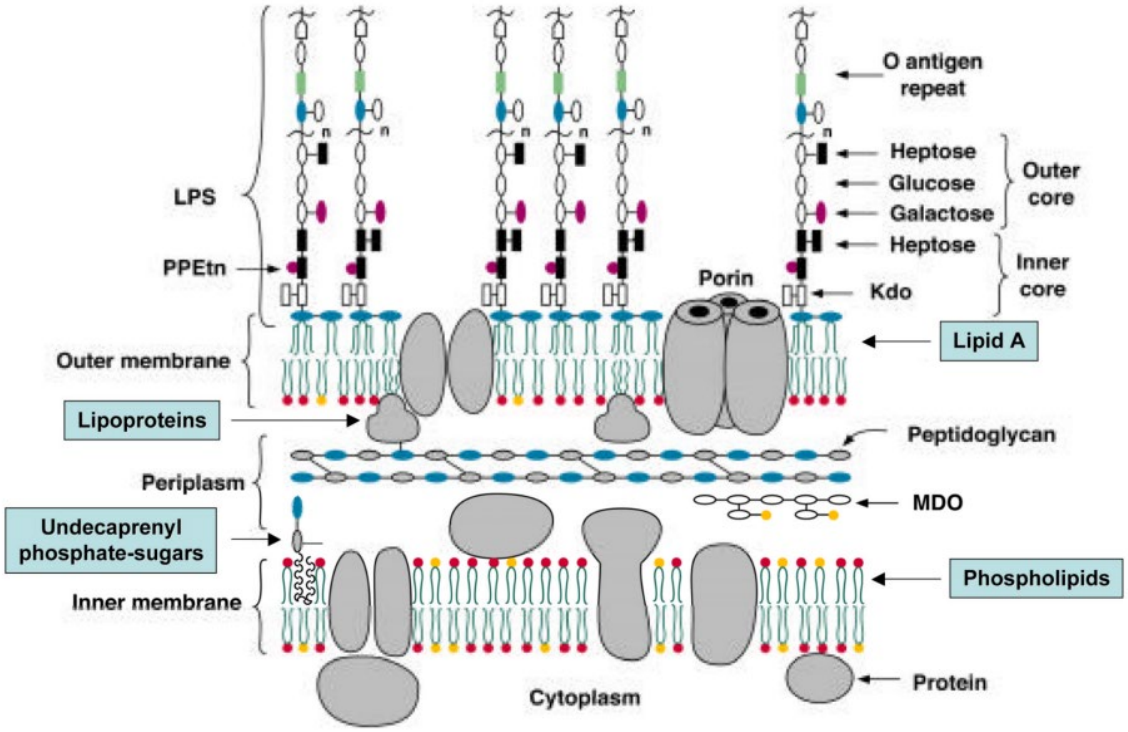

Figure 1.1: Structure of the Gram-negative bacterial cell envelope.

Gram-negative bacteria have a protein rich outer, asymmetric, bilayer membrane (OM) composed of an outer leaflet almost exclusively containing lipopolysaccharide (LPS) and inner leaflet mainly containing mainly phospholipids. LPS consists of a lipid A moiety, a core oligosaccharide with inner and outer cores and an outer O-specific chain. The periplasm contains many proteins, a thin peptidoglycan (PGN) layer and membrane-derived oligosaccharides (MDO). The inner membrane (IM) is symmetrical and composed of phospholipids and proteins. Image adapted from Raetz *et al.* (2002).

The periplasm of Gram-negative bacteria has a gel-like conformation that occupies approximately 10% of the total cell volume (Ruiz *et al.*, 2006). This viscous compartment is an oxidative environment for protein folding but lacks nucleotide energy sources, such as adenosine triphosphate (ATP). It contains a high concentration of soluble proteins and a thin peptidoglycan (PGN) layer. The periplasmic proteins are essential components of the cell envelope by virtue of their serving as substance transporters, protein folding chaperones, enzymes, and receptors of chemotaxis (Silhavy *et al.*, 2010; Schwechheimer *et al.*, 2015) . These vital functions thus make the periplasm the site for protein folding and trafficking the factors that build and maintain the cell envelope (Ruiz *et al.*, 2006).

The PGN (also called murein) sacculus is an extra-cytoplasmic cytoskeleton that offers shape and rigidity to the cell wall in Gram-negative bacteria (Silhavy *et al.*, 2010). It is a complex heteropolymer containing long glycan chains crosslinked by short peptides and is made up of alternating molecules of disaccharide N-acetylglucosamine (GlcNAc

or NAG) and N-acetylmuramic acid (MurNAc or NAM) with the peptide chains made up of amino acid residues: L-alanine (L-ala), D-glutamic acid (D-glu), meso-diaminopimelic acid (mDAP), and D-alanine (D-ala) (Vollmer *et al.*, 2008; Bouhss *et al.*, 2008; Garde *et al.*, 2021). The PGN is covalently crosslinked to the OM by Braun's lipoprotein (Lpp), which is a small α-helical lipoprotein that controls the width of the periplasmic space (Braun *et al.*, 1969). The length of Lpp and the OM-PGN covalent linkage are critical for the transmission of stress signals from the OM to the IM, and functional mutations of Lpp substantially contribute to increasing bacterial susceptibility to antibiotics (Mathelié-Guinlet *et al.*, 2020).

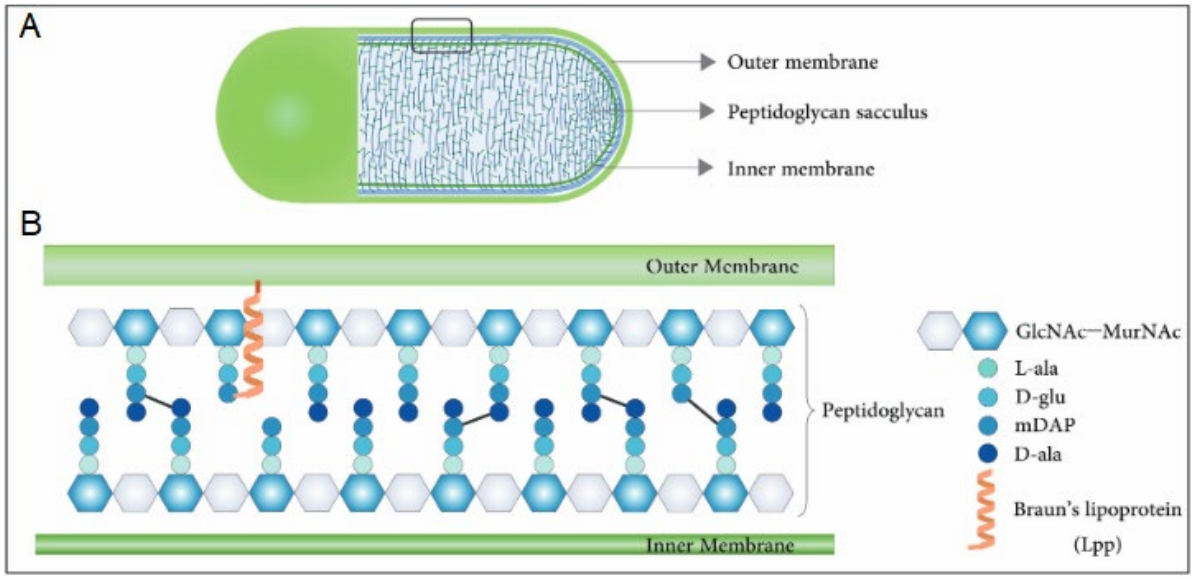

Figure 1.2: Structure of peptidoglycan.

(A) Schematic diagram of a rod-shaped *E. coli* cell with its peptidoglycan sacculus (blue mesh) located between the OM and IM. (B) Glycan chains are made up of repeating disaccharide units of GlcNAc (grey hexagons) and MurNAc (blue hexagons) with the peptide chains made up of amino acid residues: L-alanine (L-ala), D-glutamic acid (D-glu), meso-diaminopimelic acid (mDAP), and D-alanine (D-ala). The glycan chains are linked to each other through peptide cross-linking between either D-ala and mDAP residues to form a net-like sacculus. The Braun's lipoprotein (Lpp) (orange helix) covalently tethers PGN to the OM. Image adapted from Garde *et al.* (2021).

1.2 Outer membrane

The OM is the most distinctive feature that distinguishes between Gram-negative and Gram-positive bacteria since it is entirely lacking in Gram-positive bacteria. The OM of Gram-negative bacteria is a highly asymmetric bilayer with an exterior lipid leaflet containing almost entirely lipopolysaccharide (LPS) and an interior leaflet containing mainly phospholipids identical to those found in the IM. The OM serves as a selective permeation barrier that allows the passage of beneficial hydrophilic compounds such as nutrients from the external environment (Nikaido, 2003). In addition to LPS, the OM is composed of an intricate combination of phospholipids, lipoproteins, outer membrane proteins (OMPs) and a few enzymes confined to the outer leaflet of the OM, such as phospholipase PldA, protease OmpT and PagP (Sperandeo *et al.*, 2017). To fulfil its barrier function, the OM largely counts on its asymmetric lipid distribution, established by the LPS transport (Lpt) protein system and always maintained by the OM maintenance of lipid asymmetry (Mla) proteins.

1.2.1 Lipopolysaccharide

LPS is a complex glycolipid molecule that comprises up to 80% of the outer leaflet of *Escherichia coli* OM (Avila-Calderón *et al.*, 2021) and its interaction with OMPs is required for the OM to perform its primary function as a potent permeability barrier (Arunmanee *et al.*, 2016). LPS is a macrophage-activating, highly negatively charged agent (Rollauer *et al.*, 2015; Huszczynski *et al.*, 2020). The peculiar asymmetric and tightly packed layer of LPS plays an instrumental role in enhancing the protective property of the OM against both hydrophobic and hydrophilic molecules (Galdiero *et al.*, 2012; Sperandeo *et al.*, 2017). As shown in **Figure 1.3**, the structural composition of LPS includes the hydrophobic lipid A, a core oligosaccharide, and a distal O-antigen (also known as O-polysaccharide or O-chain) (Bruneteau *et al.*, 2003; Ruiz *et al.*, 2008). These molecules bind tightly to one another through the interaction of divalent cations, such as Mg^{2+} and Ca^{2+}, with the negative charges of lipid A and oligosaccharide inner core phosphates and carboxylates (Sperandeo *et al.*, 2017) ensuring mechanical stability of the OM by forming a physical barrier that permits selective diffusion and transport of both hydrophobic and hydrophilic materials. It has been demonstrated that the removal or displacement of the divalent citations by exposure to EDTA causes the release of large quantities of LPS and destabilisation of the Gram-negative OM (Clifton *et al.*, 2015).

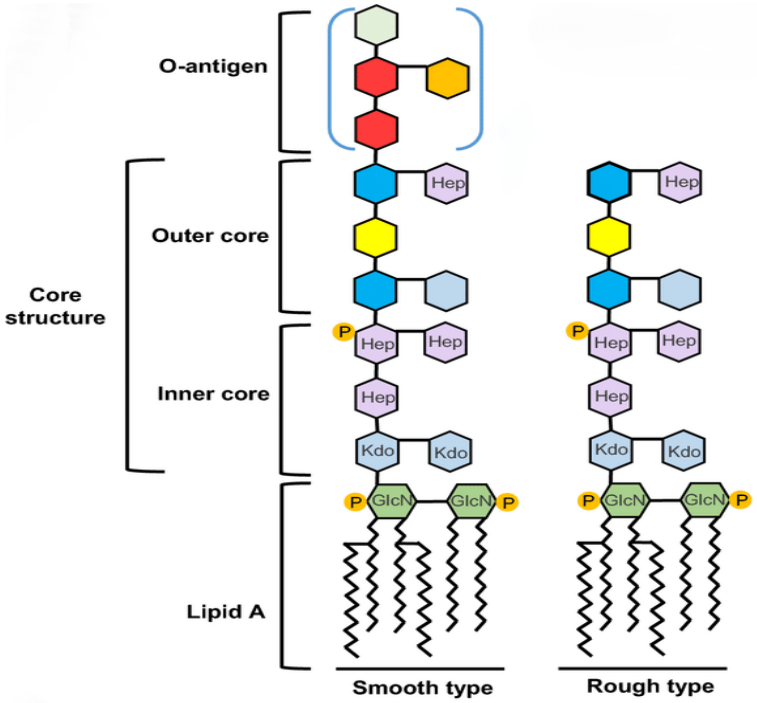

Figure 1.3: General structure of Lipopolysaccharides.

LPS consists of hydrophobic lipid A, core oligosaccharide with inner and outer regions covalently linked to an outer O-specific chain. Lipid A anchors LPS to the OM. The inner region is composed of Kdo (blue) and heptoses (purple) whilst the outer core is composed mostly of hexoses. The O-antigen repetitive unit is present in highly variable numbers in smooth LPS and is absent in rough LPS. P, phosphate groups; GlcN, glucosamine; Kdo, 3-deoxy-Dmanno-octulosonic acid; Hep, L-glycerol-Dmanno-heptose. Image adapted from García-Weber *et al.* (2021).

Lipid A is a glucosamine disaccharide with 6 or 7 largely saturated acyl chains and contains the OM-anchoring region of LPS (Maldonado *et al.*, 2016). Because of its hydrophobic nature, lipid A is regarded as the most toxic component of LPS. The toxicity of lipid A is caused by the specific interactions between the innate immunity of the host and LPS in the blood stream (Maldonado *et al.*, 2016). and emanates from the immense sensitivity of the immune system to LPS as a definite indicator of bacterial infection (Froning *et al.*, 2020) or pathogen associated molecular pattern (PAMP) (Ellis *et al.*, 2010). The negative effects of the endotoxin on humans range from fever, diarrhoea and weakness to toxic shock, sepsis and death. Lipid A binds to Toll-like receptor 4 (TLR-4), and thus it serves as an advanced warning of bacterial infection (Sperandeo *et al.*, 2017) . The activation of the innate immunity induces production of cytokines, such as interleukin-1β (IL-1β), IL-6, and tumour necrosis factor (TNF), which mediate the pathophysiological response to endotoxin (Li *et al.*, 2008).

The core oligosaccharide is composed of a branched oligosaccharide of 8 to 12 sugars extending from the external environment (Caroff *et al.*, 2003). It is divided into

an inner and outer core. Unlike the outer core which contains L-glycero-D-manno-heptose (heptose) residues, glucose and galactose, the inner core region mainly contains heptose and 3-deoxy-D-mannooctulosonic acid (KDO) which attaches it to lipid A. The O-antigen is the terminal part of LPS and contains more than 180 recognised forms in *E.coli* (Wang *et al.*, 2001). It is formed by repeating units of oligosaccharides which play a major role in shaping the serological and antigenic specificity of LPS. Therefore, the classification of LPS as rough (R-form) or smooth (S-form) is influenced by the absence, presence, and alteration in O-polysaccharides (Obeng *et al.*, 2017). Rough LPS comprises just the non-repeating core oligosaccharide whereas smooth LPS additionally contains the repeating O-polysaccharide (Galdiero *et al.*, 2012; Micciulla *et al.*, 2019). As opposed to smooth LPS, molecules lacking the O-antigen but having oligosaccharide structures up to 10 saccharide units are referred to as lipooligosaccharide (LOS) (Gorman *et al.*, 2022).

The LPS synthesis follows the 9-step enzymatic sequence known as the Raetz pathway which starts with soluble enzymes in the cytoplasm and ends on the cytoplasmic side of the IM with the synthesis of Kdo-lipid A (Raetz *et al.*, 2002). The core oligosaccharide is first synthesised at the cytoplasmic face of the IM inner leaflet and then flipped across the IM, catalysed by the essential ATP-binding cassette (ABC) MsbA transporter (Ruiz *et al.*, 2008). Afterwards, if the O-antigen is present, it attaches to the core and LPS is ultimately transported to the OM outer leaflet for assembly by the lipopolysaccharide transport (Lpt) machinery (Sperandeo *et al.*, 2008). The Lpt machinery consists of seven proteins (LptABCDEFG), and the assembly of LPS at the cell surface necessitates the involvement of LptA and LptB as well as the OM-mediated LptD/E (previously known as RlpB-IMP) complex (Ruiz *et al.*, 2006; Bos *et al.*, 2007; Tokuda, 2009). LPS is ultimately flipped to the cell surface across the OM, where individual LPS form ionic linkages between divalent cations and their phosphate and carboxylic acid moieties. It has been shown that LPS molecules are not shuttled to the OM but pushed through a physical bridge that connects the IM and the OM and is formed by the assembly of LptA proteins across the periplasm (Sherman *et al.*, 2018).

1.2.2 Outer membrane proteins

OMPs account for nearly 50% of the OM mass and mostly comprise lipoproteins and outer membrane porins (Galdiero *et al.*, 2012; Koebnik *et al.*, 2000; Sklar *et al.*, 2007) . It was estimated that approximately 2 to 3% of the genes of the Gram-negative

bacteria genome encode OMPs (Wimley, 2003). These proteins play a fundamental role in cellular pathogenicity and protection against external toxic agents owing to their extensive involvement in the interaction between pathogens and the host milieu. OMPs traverse the OM via a β-pleated sheet configuration that folds into β-barrels (Ruiz *et al.*, 2008; Paul *et al.*, 1985). Almost all β-barrel OMPs are arranged in an even number of β-strands ranging between 8-strands (e.g., OmpA) to 36-strands (e.g., T9SS protein SprA) and follow an antiparallel pattern (Khalid *et al.*, 2008; Rollauer *et al.*, 2015). The β-strands are connected to their neighbours by short turns ranging from 1 to 12 amino acids in length at the periplasmic surface and by extended hydrophilic loops ranging from 2 to 46 amino acids in length on the extracellular region of the OM (Tamber *et al.*, 2003; Galdiero *et al.*, 2012; Rollauer *et al.*, 2015). These strands form a cylindrical tube and contain polar (hydrophilic) residues that are inwardly directed towards the centre of the β-barrel to interact with internal folds of transporter protein, as well as non-polar residues that point outwards to interact with the hydrophobic membrane. Another class of proteins with large β-barrels has been identified. These large β-barrel (20-36 amphipathic β-strands) proteins, such as TonB-dependent receptors (e.g., FhuA and SusC), are energy-dependent transporters found in lower amounts in the OM and function as gated channels in the transport of large ligands, such as ferric chelates (siderophores), carbohydrates and vitamin B12 (Nikaido, 2003; Silhavy *et al.*, 2010). These high-molecular-weight OM proteins are involved in the uptake of large substrates that cannot pass through the diffusion channels and need to be pumped against a large concentration gradient (Koebnik *et al.*, 2000). The primary function of TonB is to connect the IM proton-motive force (PMF) to the receptor-mediated processes in the OM (Bos *et al.*, 2007). To perform this function, TonB links the large β-barrel proteins to the electrochemical potential of the cytoplasmic membrane via the TonB-ExbBD complex, which transduces the proton-motive force into conformational change (Koebnik *et al.*, 2000) .

1.2.3 Biogenesis of OMPs

The assembly of OMPs is defined as a secretion process which entails the export of native OMPs from a cytoplasmic location of synthesis to extra cytoplasmic sites (Tseng *et al.*, 2009) (**Figure 1.4)**. It initially starts with synthesising nascent OMPs as pre-proteins or precursors by ribosomes in the cytoplasm with an N-terminal signal sequence. The precursors bind to the chaperone SecB to prevent premature folding, and then the unfolded OMPs are delivered to SecA at the SecYEG translocon. The

translocation of the OMPs from the cytoplasm into the periplasm across the IM is mediated by the GSP. The secreted OMPs are subsequently exported across the periplasm to the OM where they are finally assembled in their mature conformations (Tsukazaki *et al.*, 2008; Du *et al.*, 2011; Park *et al.*, 2012; Rigel *et al.*, 2012). During the secretion process, a type I signal peptidase (Lep) is targeted to the IM by the signal recognition particle (SRP) pathway to cooperate with the GSP to accomplish co-translational translocation and to cleave the signal sequences of native OMPs at the periplasmic surface of the IM (Dalbey *et al.*, 2012; Auclair *et al.*, 2012).

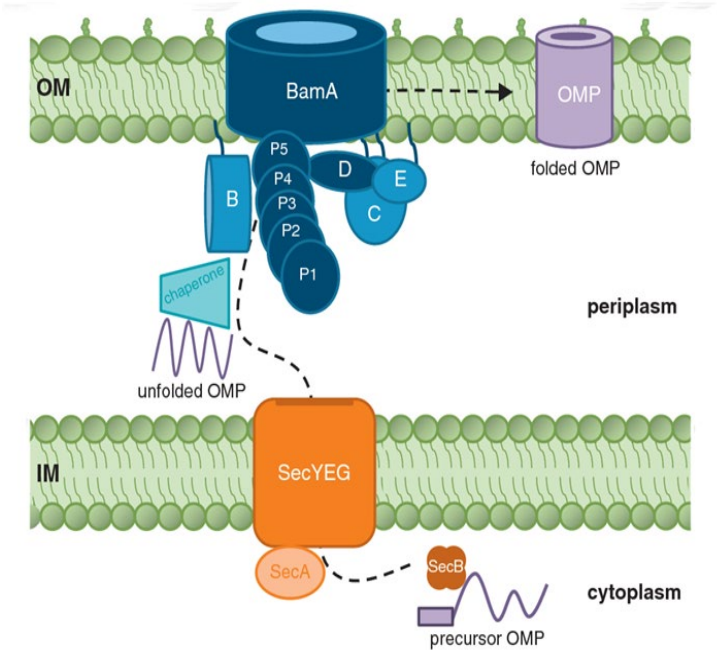

Figure 1.4: Biogenesis of Outer membrane proteins.

OMPs are synthesised as unfolded precursors in the cytoplasm and then translocated across the IM via the Sec translocase. Unfolded OMPs bind periplasmic chaperones, such as SurA and Skp, and are then transported across the periplasm to the BAM complex. The BAM complex proteins are labelled BamA-E, and the POTRA domains of BamA are labeled P1-5. Image adapted from Rigel *et al.* (2012).

The transport of OMPs across the periplasm is controlled by a network of periplasmic chaperones (folding factors), such as the Survival protein A (SurA), the Seventeen kilodalton protein (Skp) and periplasmic serine endoprotease (DegP). SurA is a periplasmic chaperone that functions as a peptidyl-prolyl isomerase and is critical for bacterial survival. Skp interacts with the OMPs once they leave the Sec-independent apparatus, assisting in their release from the IM and precluding their accumulation. Whereas Skp is a passive chaperone that firmly binds to unfolded OMPs to prevent them from misfolding in the periplasm (Tamm *et al.*, 2001), DegP is

indispensable for bacterial survival by acting as a protease to degrade misfolded and aggregated OMPs formed during heat shock conditions (Rollauer *et al.*, 2015). These chaperones provide a vital assistance in the transport of OMPs to the β-barrel assembly machinery (BAM) complex. Their essential role is to prevent secreted OMPs from misfolding or aggregating in the periplasm (Sklar *et al.*, 2007; Volokhina *et al.*, 2011; Rollauer *et al.*, 2015), ensuring proper insertion of synthesised OMPs into the OM. To direct the synthesised OMPs to the BAM complex, the three periplasmic chaperones are regulated by the σ^E envelope stress response and operate in two parallel pathways; SurA functions in one pathway whereas Skp and DegP follow another. However, Sklar and co-workers demonstrated that OMPs favoured SurA over Skp/DegP pathways since SurA depletion resulted in a significant drop in OM density as compared to the depletion of Skp and DegP (Sklar *et al.*, 2007).

The BAM complex of *E. coli* is a heterooligomer containing BamA (also known as YaeT) and its four lipoprotein partners (BamB, C, D and E). BamA is a 16-stranded β-barrel protein and is essential for cell viability, transport and assembly of other OMPs (Selkrig *et al.*, 2014). It belongs to the Omp85 family of proteins and is considered the core structural component of the BAM complex (Silhavy *et al.*, 2010; Bennion *et al.*, 2010; Galdiero *et al.*, 2012).The structure of BamA is composed of a large periplasmic amino-terminal (N-terminal) domain and a C-terminal β-barrel domain (Noinaj *et al.*, 2015). The N-terminal incorporates five globular polypeptides-transport-associated (POTRA) domains of which POTRA 5 is the most critical for OMP folding, localisation and bacterial survival (Silhavy *et al.*, 2010; Rollauer *et al.*, 2015; Mashburn-Warren *et al.*, 2006a). BamA and BamD are the essential components of the BAM complex in *E. coli* (Rollauer *et al.*, 2015; Rigel *et al.*, 2012). They operate independently but their interactions are stabilised by BamE, and their depletion results in rapid aggregation of OMPs in the periplasm (Galdiero *et al.*, 2012). The 26-stranded LptD depends on BamA for its assembly and forms a complex with LptE to insert LPS into the outer leaflet of the OM (Rollauer *et al.*, 2015; Storek *et al.*, 2019). Depletion of LptD can result in aggregation of intermediates and improper placement of LPS, leading to a breakdown in the integrity of the OM structure (Bojkovic *et al.*, 2015).

1.3 Bacterial porins

Amongst the most numerous OMPs are porin species (Khalid *et al.*, 2008; Rollauer *et al.*, 2015). The *E. coli* porin proteins were first isolated in 1974

(Rosenbusch, 1974), but the term “porin” was not coined to designate this class of OMPs until two years later (Nakae, 1976). The first porin structure, resolved by X-ray diffraction at 3 Å resolution in 1990, was from *Rhodobacter capsulatus* (Weiss *et al.*, 1990). Porins are trimeric transmembrane, β-barrel channel-forming proteins that are the most abundant pore forming proteins in the OM of Gram-negative bacteria but entirely absent in Gram-positive bacteria. These transmembrane proteins are present and make the OM more leaky than the IM as they allow the passive diffusion of water-soluble molecules with a size exclusion limit of less than 600 Da into cellular membranes (Koebnik *et al.*, 2000; Nikaido, 2003). This explains why these proteins are commonly referred to as diffusion channels. Porins also serve as receptor sites for phage and bacteriocin binding and their sequences include a high density of charged residues (Jeanteur *et al.*, 1991). Porins are classified as either general (non-specific) or substrate specific. Non-specific porins, such as the outer membrane C (OmpC or osmoporin) and the outer membrane F (OmpF or matrix porin), are the most abundant porins in the OM and are involved in managing the inflow and efflux of small solutes. Non-specific porin diffusion rises linearly with solute concentration, that is, these porins are more efficient at high solute concentrations. To perform their passive molecular sieving function, non-specific porins use charge, size and concentration gradient (Tamber *et al.*, 2003).

On the other hand, substrate-specific porins, such as LamB (maltoporin) and PhoE (phosphoporin), are trimers responsible for regulating the passage of specific substrates, such as maltose and anions, across the OM (Koebnik *et al.*, 2000) and appear to be part of an energy-driven uptake mechanism, such as the ABC system (Welte *et al.*, 1995). Whereas LamB (18 amphipathic β-strands) is specific for the uptake of maltooligosaccharide or maltodextrins, PhoE (16 amphipathic *β*-strands) is specific for the uptake of anions such as phosphate (Silhavy *et al.*, 2010). The expression of LamB is induced by low glucose conditions, whereas PhoE is expressed only under phosphate-starving conditions (Nikaido, 2003). PhoE shares a high degree of homology with OmpC and OmpF, but it has more preference for anions instead of cation-selective channels (Cowan *et al.*, 1995; Nikaido, 2003). PhoE, OmpC and OmpF are the best characterised porins in terms of structural and functional properties and thus commonly referred to as the classical porins (Nikaido, 2003). The genes of these proteins (*phoE*, *ompC* and *ompF*, respectively) encode the porins of *E. coli* with more than 50% of sequence identity (Jeanteur *et al.*, 1991).

1.3.1 Outer membrane proteins C and F

OmpC (or osmoporin) and OmpF (or matrix porin) account for 2% of the total cellular protein (Wang *et al.*, 2017) and inhibit the entry of hydrophilic solutes that surpass the threshold of 600 Da (Dutzler *et al.*, 1999). OmpC and OmpF form trimers and the inactivation of their genes in *E. coli* considerably hinders their adhesive, invasive and colonisation abilities (Hejair *et al.*, 2017). OmpC and OmpF play a crucial role in the adaptation of Gram-negative bacteria to the conditions of their external environment, such as temperature, osmotic pressure, and nutrient content of the medium (Guzev *et al.*, 2005). The expression of ompC and ompF genes are reciprocally regulated by osmolarity (Yoshida *et al.*, 2006; Hejair *et al.*, 2017; Cowan *et al.*, 1992). At low osmolarity, OmpF becomes more dominant porin than OmpC, and in the case of high osmolarity, OmpC predominates (Achouak *et al.*, 2001). Furthermore, OmpC and OmpF are tightly associated with LPS, and these interactions are critical for maintaining the selective OM permeability (Arunmanee *et al.*, 2016).

Although OmpC and OmpF are almost exactly similar in respect to the size of their constriction regions (the eyelets) and their charged residues, OmpF was found to have a higher uptake than OmpC (Nikaido *et al.*, 1983). OmpC and OmpF are most involved in antibiotic transport (Pagès *et al.*, 2008) and their loss is considered a contributing factor to antibiotic resistance as well as the suppression of antibody-dependent bacterial activity (Cepas *et al.*, 2020; Liu *et al.*, 2012). It was demonstrated that an OmpF-deficient mutant was resistant to a variety of antibiotics, including β-lactams, suggesting that OmpF serves as the primary pathway for many antibiotics to penetrate the OM (Choi *et al.*, 2019b).

The first structure of *E. coli* OmpF was elucidated in 1992 at 2.4 Å resolution (Cowan *et al.*, 1992) whereas the OmpC structure was determined to 2.0 Å resolution by X-ray crystallography in 2006 (Baslé *et al.*, 2006). In terms of structural and functional properties, OmpF is the porin protein that has been studied most extensively. The general OmpF structure consists of three identical copies of a 340-residue monomeric unit which is composed of a β-barrel of 16 transmembrane β-strands (**Figure 1.5**) These strands are connected by eight long extracellular loops and eight short periplasmic turns and are tilted to promote the stabilisation of the β-barrel water-filled pore. Loop 2, which connects strands 3 and 4, folds outwards to link with the adjacent monomer, that is, to establish monomer-monomer interactions,

whereas Loop 3, which is not exposed to the cell surface, joins strands 5 and 6 together and folds back into the lumen of the barrel to form the constriction zone at half the height of the channel (Koebnik *et al.*, 2000; Nikaido, 2003). This packed structure of OmpF allows it to be remarkably stable and highly resistant to adverse pH and temperature conditions. It was found in vitro that unless heated above 75°C, OmpF stayed intact and folded in detergents, and it endured pH levels between 1.6 and 12 without deterioration at room temperature (Schindler *et al.*, 1984).

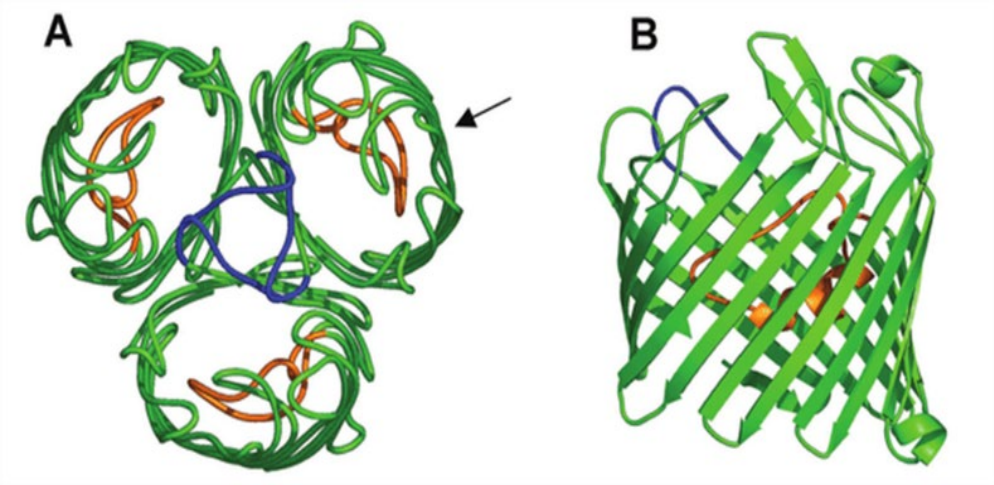

Figure 1.5: Structure of OmpF.

(A) Top view of the trimer, where Loop 2 (blue) links the monomers together and Loop 3 (orange) is exposed to the cell surface but folds back into the barrel to form the constriction zone (the eyelet), is in orange. (B) Side view of the OmpF monomer, in the direction of the arrow shown in (A). PDB code: 2OMF. Image adapted from (Nikaido, 2003).

1.3.2 Outer membrane protein A

The *ompA* gene was originally identified in *E. coli* in 1974 and purified in 1977 (Chai *et al.*, 1977). OmpA is a 35 kDa monomeric protein with typically more than 100,000 copies in *E. coli* and is classified as one of the major surface antigens of Gram-negative bacteria (Khalid *et al.*, 2008). The small size of OmpA and its monomeric nature have made it an ideal model for studying the insertion and folding of β-structured membrane proteins (Koebnik *et al.*, 2000; Kleinschmidt *et al.*, 1999). OmpA is highly regulated and is environmentally responsive (Smith *et al.*, 2007). It acts as a receptor for some phage and is regarded a key target in the immune defence against many Gram-negative bacterial pathogens(Arora *et al.*, 2001; Tamm *et al.*, 2001). In *E. coli*, OmpA is involved in multifaceted structural and physiological activities, including maintenance of structural integrity and stability, formation of biofilms, and hosting of

adhesin and invasion processes (Wang, 2002). OmpA is a structural protein classified as a PGN-associated protein since it interacts with PGN through its C terminal domain, and this interaction, supported by the Braun's lipoprotein (Lpp), has been found to be essential for preserving the OM integrity (Samsudin *et al.*, 2017). The OmpA association with the maintenance of membrane integrity results in increased susceptibility of OmpA mutants to many antibiotics (Choi *et al.*, 2019a).

The structure of OmpA has been solved by both X-ray crystallography (Pautsch *et al.*, 2000) and nuclear magnetic resonance (NMR)(Arora *et al.*, 2001) (**Figure 1.6**). These studies showed that OmpA is a distinct two-domain protein. Located in the OM, the N-terminal domain (19 kDa) is a transmembrane β-barrel with eight antiparallel, amphipathic transmembrane β-strands connected by four relatively long hydrophilic surface-exposed loops and three short turns on the periplasmic side. The C-terminal domain (16 kDa) resides in the periplasmic space interacting specifically with the PGN layer and containing a high proportion of α-helices(Koebnik, 1999; Power *et al.*, 2006). The N-terminal membrane-embedded domain is connected to the C-terminus by a proline-rich hinge region (Koebnik *et al.*, 2000). Evidence has been presented to show that the Skp binds the OmpA N-terminal domain in its cavity and maintains it in an unfolded state while simultaneously allowing folding of the C-terminal domain outside of the cavity (Walton *et al.*, 2009).

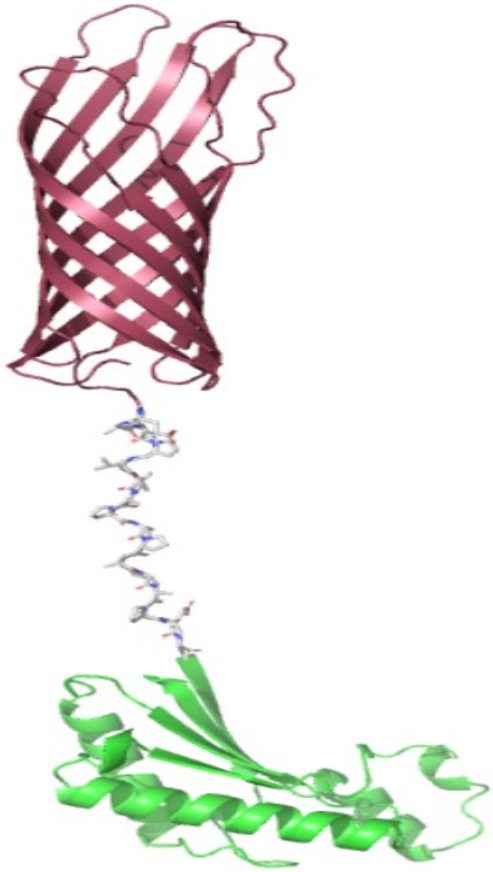

Figure 1.6: Structure of OmpA.

Full length OmpA protein model from the Alpha Fold Protein Structure Database. The structure of the N terminal domain was obtained from the 1BXW PDB file (Pautsch *et al.*, 1998). The structure of the C terminal domain was derived from the 2MQE PDB file (Ishida *et al.*, 2014). These structures were identified using X-ray crystallography and Nuclear Magnetic Resonance Spectroscopy, respectively.

1.4 Outer membrane vesicles

OMVs were initially observed in the 1960s by transmission-electron microscopy as controlled blebbing from the OM of the Gram-negative bacterium *Vibrio cholerae* (Chatterjee *et al.*, 2012). During the years following their discovery, OMVs were thought of as an alteration or instability of the OM, that is, as an artifact of bacterial growth instead of being a normal physiological phenomenon (Avila-Calderón *et al.*, 2021) (**Figure 1.7**). However, with the emergence of extensive OMV-focused research, the scientific community has come to understand that OMVs derived from the cell envelope of Gram-negative bacteria are heterogeneous in the sense that identical species can release different membrane vesicle types with different compositions (Nagakubo *et al.*, 2020). Although OMVs have been known for several decades, their prominence in academia has only lately risen. An array of Gram-negative bacterial species has been identified as producers of OMVs, including *E. coli, Neisseria meningitis, Pseudomonas aeruginosa, Salmonella typhi, Shigella dysenteriae, Vibrio cholerae, Porphyromonas gingivalis, Helicobacter pylori, Bacteroides fragilis and Borrelia burgdorferi*, to name some examples. Microvesicles, agrosomes, exosomes, and tolerasomes are other terms used interchangeably within the scientific community to refer to OMVs (Furuyama *et al.*, 2021). Due to their abundant presence in host tissues during infections, OMVs are believed to be utilised by pathogenic bacteria to regulate the activation or inhibition of the host immune system, suggesting that OMVs have a pathogenic function in a variety of infectious illnesses (Kaparakis-Liaskos *et al.*, 2015; Schwechheimer *et al.*, 2015).

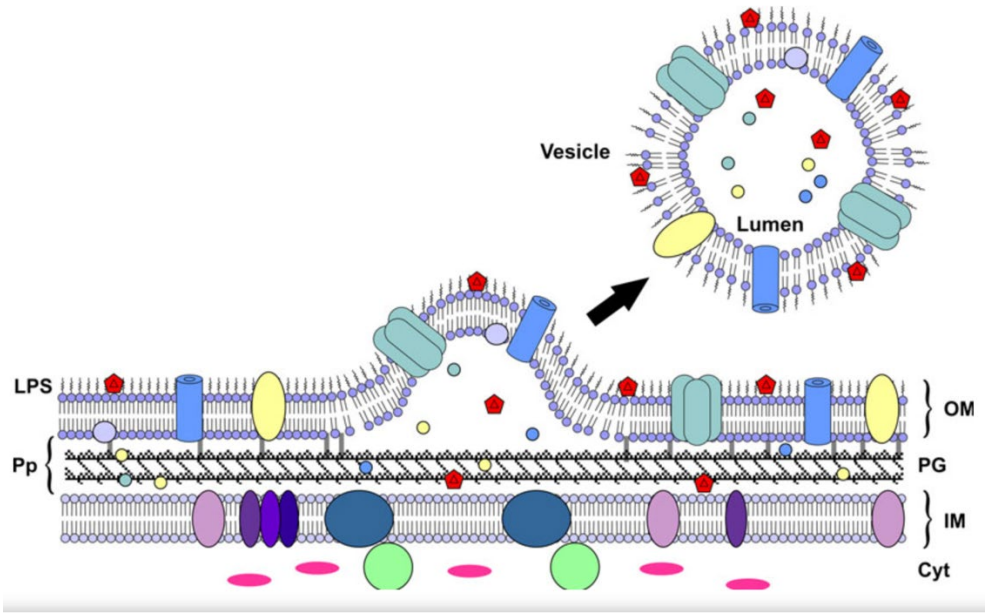

Figure 1.7: Biogenesis of outer membrane vesicles model.
A schematic diagram of outer membrane vesicles biogenesis. LPS, lipopolysaccharide; Pp, periplasm; OM, outer membrane; PG, peptidoglycan; IM, inner membrane; Cyt, cytosol. Image adapted from Kuehn *et al.* (2005).

1.4.1 OMV composition and functions

OMVs are small, lipid-encapsulated, spherical, bilayer membrane-enclosed entities, ranging between 10 to 300 nm in diameter, that are spontaneously produced by a range of pathogenic and non-pathogenic Gram-negative bacteria during all phases of growth (Lee *et al.*, 2011; Avila-Calderón *et al.*, 2014; Kulp *et al.*, 2015; Roier *et al.*, 2016; Jan, 2017). In Gram-negative bacteria, native OMVs contain an OM and periplasmic materials (McBroom *et al.*, 2007). The OMV cargo is typically composed of a variety of OMPs (including OmpC, OmpF and OmpA), LPS, phospholipids, nucleic acids (DNA and RNA), ionic metabolites, periplasmic and cytoplasmic proteins (including alkaline phosphatase and the AcrA-TolC transporter complex), and a series of virulence factors involved in the adhesion and evasion of host tissues (McMahon *et al.*, 2012; Kim *et al.*, 2013; Avila-Calderón *et al.*, 2014; Brown *et al.*, 2015) (**Figure 1.8**). It has been demonstrated that 0.2 to 0.5% of OM and periplasmic proteins are crowded with vesicles from *E. coli*, implying that OMV formation and release are an energy sink (Kuehn *et al.*, 2005).

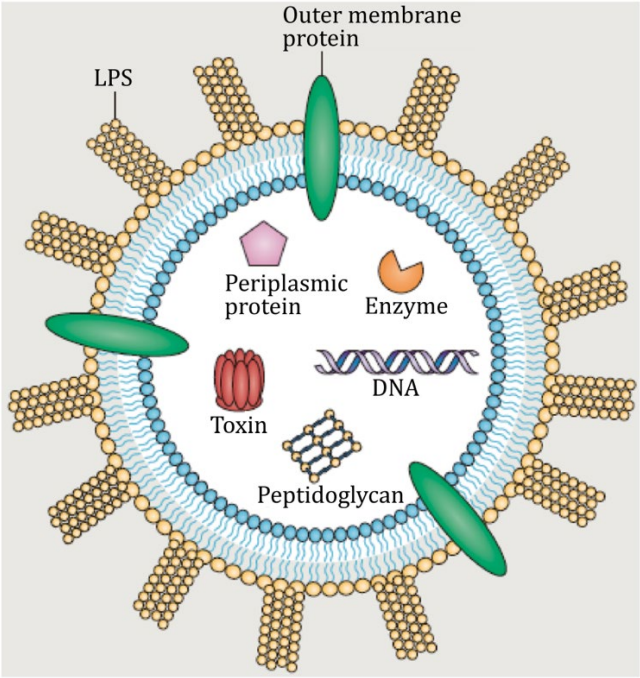

Figure 1.8: Gram-negative bacterial outer membrane vesicles contents.

Outer membrane vesicles contain lipopolysaccharide (LPS), peptidoglycan, outer membrane protein, periplasmic protein, DNA,RNA, enzymes, and toxins. Image adapted from Kaparakis-Liaskos *et al.* (2015).

The likelihood of inclusion of a protein in the OMV cargo is influenced by its cellular localisation. Periplasmic proteins associated with the IM, for example, exhibit decreased cellular localisation in OMVs as compared to proteins that are bound to the inner leaflet of the OM (Bonnington *et al.*, 2014). As a result of their complex and distinct composition, OMVs are engaged in a myriad of cellular, biological and pathophysiological functions, including envelope stress response, protein and horizontal gene transfer, cell-cell communication, biofilm nucleation, nutrient acquisition, host-immune response modulation, bacterial adherence and virulence factor transport (Deatherage *et al.*, 2009; Kulp *et al.*, 2010; Kunsmann *et al.*, 2015; Schwechheimer *et al.*, 2015). Virulence factors, such as toxins, adhesins, and immunomodulatory molecules, shield OMVs from degradation by the host tissue degradative enzymes and permit direct, simultaneous, and coordinated transport into host cells, thus boosting their pathogenic potential and survival scenarios (Huszczynski *et al.*, 2020). A consequence of this is that OMVs constitute a potent arsenal of bioweapons that can aid bacterial infections to establish colonisation niches, interfere with host cellular processes, induce inflammatory responses, and modify the immune system (Beveridge *et al.*, 1995). This also indicates that OMVs can serve as a

promising candidate for vaccine development and drug delivery (Kulp *et al.*, 2010; Furuyama *et al.*, 2021).

1.4.2 Biogenesis of outer membrane vesicles

OMV biogenesis can be described as a blebbing process forming vesicles with the outside of the OM at the surface of the OMV (van der Pol *et al.*, 2015). Despite the passing of six decades from the discovery of OMVs, the mechanism of vesiculation is still unclear (Kuehn *et al.*, 2005) and has been one of the most unsettled topics of OMV-related research (Kudryakova *et al.*, 2016). Although this process is still not fully understood, the existing knowledge derived from many biochemical and genetic studies most often has been grouped into four non-mutually exclusive blebbing models that are intended to explain the biogenesis of OMV (Qing *et al.*, 2019; Nagakubo *et al.*, 2020). The classification of these models is grounded on the significant involvement of stress-inducing conditions, PGN, LPS, and lipoproteins in OMV production.

The first model focuses on the breakdown in the covalent OM-PGN crosslink as a result of a loss or reduction in Lpp synthesis. According to this model, a modification of Lpp by exclusion, disruption or otherwise relocation causes the OM to bulge, resulting in OMV formation (McBroom *et al.*, 2006; Deatherage *et al.*, 2009; Elhenawy *et al.*, 2016). The modification of OmpA as a PGN-associated protein has also been shown to increase OMV formation (**Figure 1.9**) (Anand *et al.*, 2016; Volgers *et al.*, 2018).

The second model views OMVs as a primary vehicle that Gram-negative bacteria employ to thwart stress-inducing conditions from their own, host or external environments. According to this view, OMVs are produced during PGN turnover where OMV blebbing occurs as a consequence of increased turgor stress (Kulp *et al.*, 2015) induced by external osmolality or deficiency in PGN re-modelling (Kulkarni *et al.*, 2014; Roier *et al.*, 2016). The turgor pressure is imposed on the OM inner leaflet by misfolded proteins that aggregate in the periplasmic space, causing the OM to protrude and ultimately pinch off to release OMVs (Toyofuku *et al.*, 2018).

The third model suggests that OMV production increases when certain regions of the OM are enriched with lipid microdomains (lipid rafts) which contain certain protein components, LPS and phospholipids. This enrichment affects the asymmetric composition of the OM outer leaflet and curvature. Because of their charge, cargo, or

enhanced membrane fluidity, the lipid microdomains tend to pinch off outwards, causing the release of OMVs (Schwechheimer *et al.*, 2015).

The fourth model postulates that OMV formation in *Pseudomonas aeruginosa* is induced by direct interactions between the membrane curvature-inducing molecules LPS and *Pseudomonas* quinolone signal (PQS) (Roier *et al.*, 2016; Volgers *et al.*, 2018). According to this model, PQS employs a mechanism of expansion of the outer leaflet of the OM to induce OMV formation through localised membrane curvature (Schertzer *et al.*, 2012; Kulp *et al.*, 2015; Florez *et al.*, 2017). This expansion is characterised as asymmetric since the outer leaflet of the OM grows faster than the OM inner leaflet as a result of the enrichment of the OM with PQS.

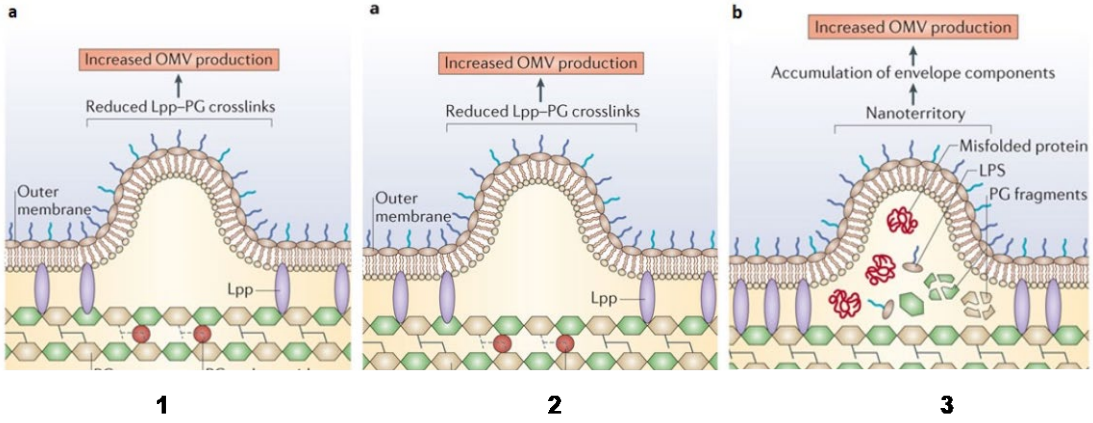

Figure 1.9: Biogenesis of outer membrane vesicles (OMV).
Three models of outer membrane vesicles biogenesis: 1) OMVs are produced in areas with reduced Lpp-PG crosslinks. 2) The outer membrane is enriched in lipid microdomains (LPS, phospholipids),This enrichment affects the asymmetric composition of the outer membrane leaflet and curvature. Due to their charge, cargo or increased membrane fluidity, lipid microdomains have a tendency to bulge, and results in OMV production. 3) OMV production can be increase by PQS insertion into the outer leaflet of the outer membrane. PQS, *Pseudomonas* quinolone signal; LPS, Lipopolysaccharide; Lpp, Lipoprotein; PG, Peptidoglycan ; FA, Fatty acid. Image adapted from Schwechheimer *et al.* (2015).

1.5 Bacterial surface structures

Gram-negative bacteria expose on their surface a variety of proteinaceous appendages by which they attach to or escape objects in their environments (Busch *et al.*, 2012). These bacterial surface structures mainly involve repetitive assemblies organised into filamentous polymers known as flagella and pili. Bacterial flagella are whip-like surface appendages that are distributed over the surface of Gram-negative bacterial cells as monotrichous (a single flagellum originate from one polar of the cell), lopotrichous (multiple flagella arise from both poles of the cell) or peritrichous (lateral

flagella are distributed over the entire cell). A bacterial flagellum is a helical filamentous organelle mostly composed of several thousand molecules of protein subunits called flagellins. The main function of flagellins is motility, that is, to provide motile bacteria with swimming movement (Nakamura *et al.*, 2019). Bacterial flagella are powered by the PMF established across the IM rather than ATP hydrolysis. The flagellar system includes a switch that creates either counter-clockwise or clockwise spin, allowing bacteria to alter direction to evade or connect to toxic compounds (Macnab, 2003).

Bacterial pili, on the other hand, are non-flagellar surface filaments that are attached to the OM of Gram-negative pathogens and are regarded as key virulence factors for various ailments, including infections of the urinary and gastrointestinal tracts. These filaments have hair-like extracellular structures that form a dense coating around the Gram-negative bacterium to allow it to bind to the cell structure (Proft *et al.*, 2009). They comprise several hundreds to thousands of pilus subunit proteins known as pilins (Waksman *et al.*, 2009) that polymerise via non-covalent interactions between repeated pilin subunits to create the mature pilus (Fronzes *et al.*, 2008; Salih *et al.*, 2008). The size of pilus subunits ranges between ~12 to ~20 kDa, and these subunits mediate various functions in Gram-negative bacteria, including receptor-mediated adhesion, evasion of immune surveillance, colonisation of surfaces, biofilm and microcolony formation, and protein and DNA transport (Salih *et al.*, 2008; Waksman *et al.*, 2009; Wurpel *et al.*, 2013; Werneburg *et al.*, 2017).

Based on their physical properties, antigenic determinants, adhesion characteristics in the primary amino acid sequence between their subunits, pili of Gram-negative bacteria are grouped into different classes, the best characterised of which are type I (or pyelonephritis-associated (Pap)) pili, curli pili and F1 antigen (Proft *et al.*, 2009; Dalbey *et al.*, 2012). Type 1 pili are filamentous protein complexes that are attached to the OM of uropathogenic (UPEC) *E. coli* and facilitate bacterial attachment to urinary epithelial cell surfaces.

Curli fimbriae are extensively studied in the context of pathogen-host interactions (Römling *et al.*, 1998). These fimbriae are unbranched, extracellular protein fibres that are highly flexible and stable filaments and are resistant to degradation by proteases and denaturation by detergents (Dalbey *et al.*, 2012; Evans *et al.*, 2014). They are functional amyloid fibres that constitute the major protein components of the *E. coli* extracellular matrix and are heavily involved in host cell adhesion and invasion, biofilm

formation and host colonisation (Proft *et al.*, 2009). Due to their wide range of interactions with many host proteins, curli pili serve as potent promoters of the proinflammatory response (Barnhart *et al.*, 2006; Fronzes *et al.*, 2008). Whilst curli subunits are assembled at the OM via the nucleation-precipitation pathway (Yan *et al.*, 2020), the secretion and assembly of type I pili or Pap and F1 antigen subunits occur via the chaperone-usher (CU) pathway (Dalbey *et al.*, 2012; Werneburg *et al.*, 2017). The following section will introduce CU mechanism in more details and is followed by another section to discuss *Yersinia pestis* F1 antigen with emphasis on its subunits and how the F1 capsule is assembled and secreted via CU pathway.

1.5.1 Chaperone-usher pathway

CU pathway is a secretion mechanism responsible for the assembly of virulence-associated pili cell surface structures in Gram-negative pathogenic bacteria (Psonis *et al.*, 2019; Wurpel *et al.*, 2013; Werneburg *et al.*, 2017). CU-assembled fimbriae are determinant factors of pathogenicity that promote host localisation and colonisation in Gram-negative bacterial species, such as UPEC, which is the major causative agent of urinary tract infections (UTI), and *Salmonella typhi,* which is a causative agent of typhoid fever (Waksman *et al.*, 2009). CU pathway assembles pilus subunits (pilins) in a highly regulated fashion and are normally encoded in single gene clusters each of which encodes one or more subunits. Each of these gene clusters encodes a structural subunit, a periplasmic chaperone and an OM pore-forming usher (Sauer *et al.*, 2004). The CU system is classified according to which of its constituent components is used as a base for the classification, the chaperone or the usher. The usher-based mode of CU classification uses the fimbrial usher proteins (FUP) whose sequences include six major phylogenetic clades: namely, σ-, β-, γ- (which comprises γ1, γ2, γ3, and γ4), κ-, π-, and σ-fimbriae (Nuccio *et al.*, 2007). These clades are divided into four clusters based on their gene organisation and relationship to the sequences of their pilus subunits. These clusters include α-, β-, and σ-clades as each one of them stands on its own as a separate cluster, and the fourth cluster contains γ-, κ- and π-clades (Psonis *et al.*, 2019).

The chaperone-based mode of CU classification, on the other hand, relates mainly to the chaperone structure, specifically the length of the loop that connects their F1 and G1 strands. Accordingly, CU pathways are divided into two: the short F1-G1 loop (FGS) and the long F1-G1 loop (FGL) subfamilies (Zavialov *et al.*, 2003). FGS is

associated with the assembly of fimbrial filaments and falls into most of the FUP clades: namely, β-, γ1, γ2, γ4, κ-, and π- clades. FGS-chaperone assembled pili are heteropolymeric and typified by the prototypical type I pili or Pap (Busch *et al.*, 2012). Conversely, FGL-chaperones are associated with the assembly of non-fimbrial (afimbrial or amorphous) surface structures and fall only into the γ3 phylogenetic clade of the FUP classification. This type of assembled pili (atypical pili) is homopolymeric and exemplified by *Yersinia pestis* F1 antigen, *Salmonella* Saf1 and *E. coli* afa/Dr adhesions (Salih *et al.*, 2008; Soliakov *et al.*, 2010). The heteropolymeric pili contain several subunits including an adhesion subunit with a single copy at the most distal site of the pit fibrillum whereas the homopolymeric pili include only one or two different subunits (Werneburg *et al.*, 2017).

The CU pathway involves the assembly of the FGS or FGL subunits in a process independent from an external source of energy, such as ATP or the PMF (Remaut *et al.*, 2008; Dalbey *et al.*, 2012). A schematic presentation of the CU composition and assembly of type I pili and Pap is shown in **Figure 1.10**. For the sake of clarity and simplicity, the focus here will be on Pap as a prototype of CU-assembled FGS subunits. Each Pap subunit is synthesised in a precursor form containing an N-terminal signal peptide and then transported from the cytoplasm across the IM to the periplasm using the GSP (Waksman, 2017). In the periplasm, the signal peptides of the translocated pilus subunits, are cleaved to allow their subsequent folding (Auclair *et al.*, 2012; Du *et al.*, 2011). The PapD chaperone next binds the nascent subunits as they enter the periplasm, assists in their folding and forms binary chaperone-subunit complexes (Dubnovitsky *et al.*, 2010; Mapingire *et al.*, 2009) via the donor strand complementation (DSC) mechanism.

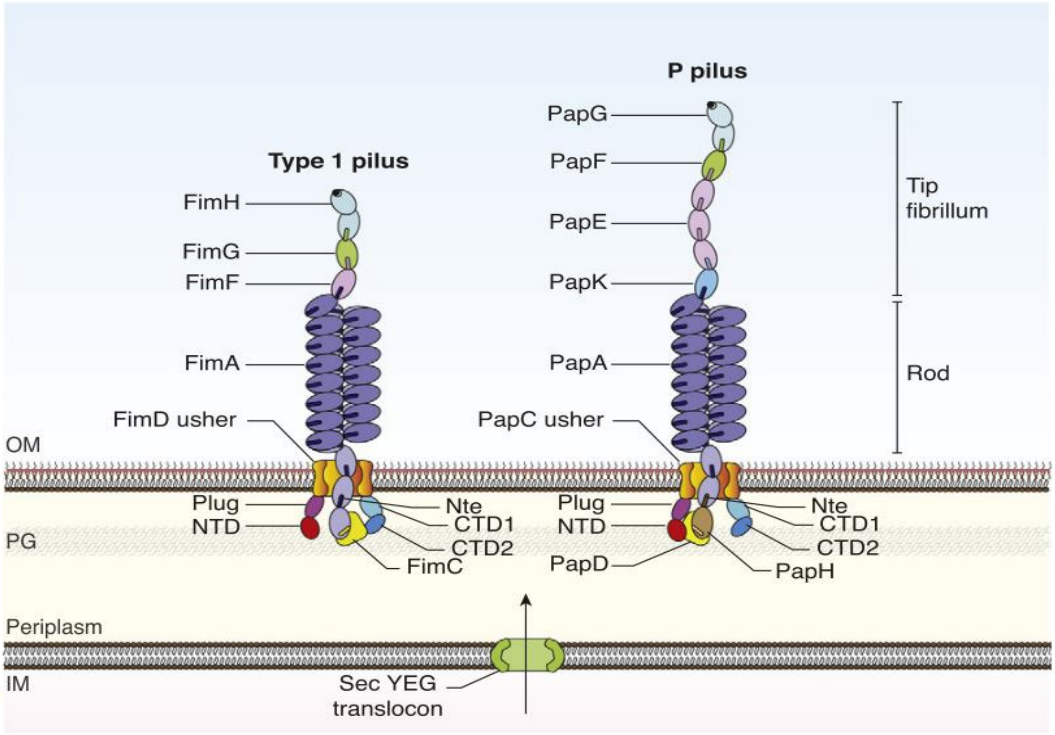

Figure 1.10: Schematic presentation of composition and assembly of type I pili and Pap.

Type I pili (Left) and Pap (Right) are composed of four (FimH, G, F and A) and six (PapG, F, E, K, A, and H) subunits, respectively, assembling in a defined order. Each subunit traverses the IM using the GSP, at the exit of which the subunit is received by the periplasmic chaperone FimC for type I pili or PapD for Pap. The chaperone assists in the subunit folding by donating one of its own strands to the Ig fold of the subunit to form a stable binary chaperone–subunit complex. The complexes are then transported for assembly to the usher (FimD for type I pili or PapC for Pap) which comprises the following domains: N-terminal (NTD), plug (PD) and C-terminal (CTD1 and CTD2). The usher orchestrates subunit polymerisation by catalysing the substitution of the chaperone-donated strand by the N-terminal extension (Nte) of the subunit next in assembly. For Pap, PapH is a terminator of subunit polymerisation. The black dots at the tip of FimH and PapG designate the receptor-binding site. Image adapted from Waksman (2017).

The DSC mechanism involves the donation by PapD of one of its own β-strands to the hydrophobic subunit groove (acceptor subunit) to complete the incomplete Ig-like fold of the pilus subunit. The donated β-strand inserts between the A and F strands of the pilus subunit to form a continuous β-sheet (Werneburg *et al.*, 2017; Fronzes *et al.*, 2008; Waksman, 2017). The chaperone-subunit complexes must then interact with the OM usher (PapC) in order to have the subunit assembled into a pilus fibre and to have the assembled fibres secreted to the cell surface. The recognition of PapC by the periplasmic chaperone-subunit complex at the periplasmic side of the OM is the most critical step in pili assembly. Without such a recognition, these complexes would accumulate in the periplasm, exposing them as targets for premature polymerisation and degradation (Fernández *et al.*, 2000). The activation of PapC requires binding of chaperone-subunit complex to the N-terminal domain (NTD) of PapC. This interaction

results in discharging the plug domain (PD) from the usher pore to house the polymer subunit and transferring the PapD-subunit complex from the NTD to the C-terminal domains (CDT1 and CDT2), freeing the NTD to recruit additional chaperone-subunit complexes. As a gated channel, PapC catalyses the exchange of chaperone-subunit to subunit-subunit interactions via a donor strand exchange (DSE) mechanism.

In DSE, the N-terminal extension (Nte) of an incoming subunit displaces the donated chaperone ß-strand from the preceding subunit, completing the Ig fold of the previous subunit. That is, every pilus subunit complements the Ig fold of its neighbour (Remaut *et al.*, 2008; Werneburg *et al.*, 2017; Fronzes *et al.*, 2008; Sauer *et al.*, 2000; Sauer *et al.*, 1999; Yu *et al.*, 2009; Zavialov *et al.*, 2003). The exchange reaction between the Nte and the chaperone-donated β-strand in the incoming subunit occurs via a zip-in-zip-out mechanism. This mechanism is instigated by the insertion of the Nte P5 residue into the P5 pocket of the groove in the preceding subunit. Polymerisation of the Pap pilus subunits by DSE in PapC is terminated by PapH which does not have a binding groove for Nte, rendering it unable to bind another pilus subunit (Dalbey *et al.*, 2012).

1.6 F1 antigen

1.6.1 Yersinia pestis F1 antigen

Yersinia pestis was recognised as the etiologic agent of pneumonic, primary septicaemic and bubonic plagues by the Swiss French physician Alexander Yersin in Hong Kong in 1894 (Butler, 2014). It has been implicated in the deaths of several hundred million people throughout the recorded history of mankind. The plague pathogen *Yersinia pestis* is a non-motile, rod-shaped, slow-growing organism that infects rodents and is transmitted to humans primarily by the bite of infected arthropods, mostly rat fleas (bubonic and septicaemic plagues) or aerosol (pneumonic plague) (MacIntyre *et al.*, 2001; Hatkoff *et al.*, 2012). *Yersinia pestis* can exist as a single organism, in pairs or in short chains. Moreover, colonies of *Yersinia pestis* are characterised by being small, translucent, and non-haemolytic.

Yersinia pestis is a species of the *Yersinia* genus which is a member of the *Enteropathogenic bacteria*. Out of eleven members of the *Yersinia* genus, only three are classified as Gram-negative human-pathogenic species: namely, *Yersinia pestis, Yersinia entercolitica* and *Yersinia pseudotuberculosis* (Perry *et al.*, 1997; Zhou *et al.*,

2006). These three pathogens share a 70-75 kb plasmid termed “calcium dependence” (pCD1, 100 – 110 kb) (Perry *et al.*, 1997; Du *et al.*, 2002) which encodes a virulence factor called low-calcium response virulence (LcrV or V antigen). LcrV is a major immunogen that upregulates interleukin-10 (IL-10) and simultaneously downregulates tumour necrosis factor-alpha (TNFα) and interferon-gamma (IFNγ) (Brubaker, 2003). Furthermore, pCD1 encodes a type III secretion system which exports *Yersinia* outer membrane virulence effector proteins (Yops) to the cytoplasm of target host cells, eventually causing inhibition of both phagocytosis and host cell demise (Hu *et al.*, 1998; Hatkoff *et al.*, 2012). A couple of hours following its penetration into the host, *Yersinia pestis* begins to rapidly express virulence determinants such as F1 antigens, LcrVs and Yops. A couple of days following infection, these virulence markers instigate disturbances in the host immune system, such as preventing cytokine production, inhibiting neutrophil chemotaxis, and inducing apoptosis (Li *et al.*, 2008).

The first complete genome of virulent *Yersinia pestis* was sequenced in 2001 from *Yersinia pestis* CO92 strain (Parkhill *et al.*, 2001). It contains a 4.65 Mb chromosome and harbours another two key plasmids: murine toxin (pMT1) and pesticin, coagulase, plasminogen activator (pPCP1). The pMT1 *pestis*-specific plasmid (also known as pFra plasmid, 96 kb) encodes a number of critical virulence markers, including the FGL non-pilus F1 antigen and phospholipase D (Du *et al.*, 2002). The F1 antigen accumulates on the surface of *Yersinia pestis* to form an amorphous capsule whereas phospholipase D is essential for *Yersinia pestis* proliferation and survival within the flea midgut (Hinnebusch *et al.*, 2002). The pPCP1 (9.5 kb) plasmid encodes a potent plasminogen activator (Pla). This plasmid is essential for enhancing *Yersinia pestis* capacity to activate host plasminogen into plasmin and to disseminate from the site of infection, consequently bestowing on the bacterium the capability to adhere to and invade into host cells (Hu *et al.*, 1998; Hatkoff *et al.*, 2012; Du *et al.*, 2002).

The F1 antigen helps *Yersinia pestis* evade phagocytosis through the formation of a proteinaceous capsule which is highly immunoprotective (Psonis *et al.*, 2019; Du *et al.*, 2002) but is also considered an important immunogenic protein that has been used in anti-plague vaccines and in plague detection tools (MacIntyre *et al.*, 2001). The F1 antigen is the primary component of killed-whole-cell (KWC) vaccines. Evidence from epidemiological and experimental studies however has shown that existing vaccine formulations, mostly KWC and live attenuated vaccines, provide poor protection against *Yersinia pestis* pneumonic plague (Williamson *et al.*, 2011). In

recent years, research has focused on the development of safe and highly effective vaccines against all forms of *Yersinia pestis* based on virulence determinants located on the bacterial surface (Titball *et al.*, 2001). Much work has been devoted to developing a vaccine that comprises both the F1 and V surface antigens. Williamson and colleagues found that F1 and V antigens have a high potential to induce a protective immune response in non-human primates (cynomolgus macaques) against pneumonic plague. Their experimental evidence showed that co-immunisation with the F1 and V antigens produced elevated protection against bubonic and pneumonic plague in the mouse model compared to the individual antigens. Therefore, they concluded that a vaccine based on combining F1 and V antigens offers more protection than either individual antigen, or the attenuated and KWC vaccines (Diane Williamson *et al.*, 1995; Williamson *et al.*, 2011).

1.6.2 Subunits of F1 antigen

The F1 antigen is a polymer that serves as a prototype for non-pilus aggregative subunits assembled via the FGL periplasmic CU mechanism (Chapman *et al.*, 1999). The F1 polymer is remarkably stable and disassociates into separate oligomers and monomers at a melting temperature above 87.5°C (Zavialov, 2005). The F1 operon consists of four gene products: *caf1, caf1M*, *caf1A* and *caf1R (Galyovl et al., 1991; Karlyshev et al., 1992b; Titball et al., 1997; Miller et al., 1998)* (**Figure 1.8)**. These gene products code a structural subunit (Caf1), a periplasmic chaperone (Caf1M), an OM-localised usher (Caf1A) and a DNA-binding transcriptional regulator (Caf1R), respectively. All of these gene products are in the *caf* operon which resides in the pMT1 plasmid (pFra) (Zhou *et al.*, 2006; Zavialov *et al.*, 2007b) and has more than 60% of homology with the proteins of the *pap* operon in uropathogenic *E. coli* (Abramov *et al.*, 2001). The F1 antigen is considered a vital immunogenic protein, previous studies have demonstrated that oral immunisation with bacteria expressing the *caf* operon conferred greater protection against plague than that with bacteria expressing solely the *caf1* gene which does not produce extracellular Caf1 protein (Titball *et al.*, 1997; Holtzman *et al.*, 2006).

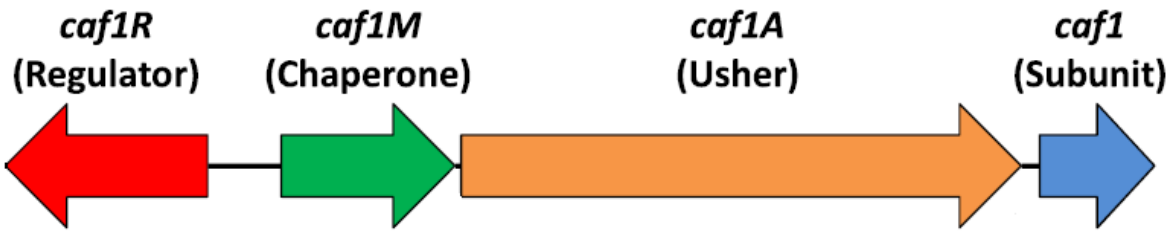

Figure 1.11: caf operon.

The *caf1* operon comprises four genes. Image adapted from Al-Jawdah *et al.* (2019).

1.6.2.1 Capsular antigen F1

The F1 antigen is classified as an FGL atypical pilus polymer, the assembly of which via the CU pathway produces an amorphously anti-phagocytic capsule which comprises linear fibres of a single gelatinous capsular antigen fraction 1 (Caf1) polypeptide subunit (Zavialov *et al.*, 2003) that is exported to the surface of the bacteria. Electron microscopic images of Caf1 have shown flexible polymers up to 1.5 µm long that resemble beads on a string (Soliakov *et al.*, 2010). Caf1 polymers are made of 15.6 kDa monomers and are extremely stable and soluble in aqueous solution(Galyov *et al.*, 1990; Ulusu *et al.*, 2017). Like the CU proteins described above, the Caf1 subunit comprises an immunoglobulin (Ig)-like domain of seven β-strands arranged in a β-sandwich and an N-terminal extension (Nte) that is naturally incomplete due to the absence of the C-terminal seventh strand (G). The absence of the G strand forms a long and profound hydrophobic groove (acceptor cleft) on the surface of the Caf1 subunit (Zavialov *et al.*, 2003).The chaperones attach Caf1 subunits though a process known donor strand complementation by inserting their G strand into the acceptor cleft (Zavialov *et al.*, 2003). It is necessary for Caf1 fibre assembly to proceed, the G1 donor strand of the chaperone must leave the acceptor cleft of the Caf1 subunit in order for the cleft to receive the N-terminal donor- strand extension of an incoming Caf1 subunit in complementary with the incomplete Ig fold of the previously assembled Caf1 subunit in the growing Caf1 fibre (Zavialov *et al.*, 2001; Zavialov *et al.*, 2002; Knight *et al.*, 2000)

The expression of the Caf1 subunit is temperature regulated by the product of the *caf1R* gene and its maximal expression on the surface of *Yersinia pestis* occurs at 37°C, with none at 22°C or below (Chen *et al.*, 1977; Miller *et al.*, 1998). Previous work has shown that the deletion of the Caf1 subunit gene causes an upsurge in the uptake of *Yersinia pestis bacilli* by macrophages, demonstrating that Caf1 plays a key protective function against host immune systems (Al-Jawdah *et al.*, 2019; Du *et al.*, 2002).

Caf1 was used in the early 1950s as a subunit protective antigen in animal models of plague (Baker *et al.*, 1952). Caf1 is normally shed into the culture medium in polymeric form by *Yersinia pestis* (Abramov *et al.*, 2002). However, its purification from *Yersinia pestis* was described as labour-intensive and time-consuming (Holtzman *et al.*, 2006). To overcome such challenges for the purpose of scaling up production,

Caf1 was purified from *E. coli* liquid cultures expressing the *caf* operon (Andrews *et al.*, 1996; Miller *et al.*, 1998) and hence large quantities of the purified recombinant Caf1 (rCaf1) have become readily available (Roque *et al.*, 2014; Dura *et al.*, 2018). rCaf1 has been shown to form an immuno-protective polymer around *E. coli* with identical behaviour to *Yersinia pestis* protein (Soliakov *et al.*, 2010; Dura *et al.*, 2020). Cultures of these *E. coli* present an unusual appearance when centrifuged in that the cell pellet is separated from the supernatant by a more diffuse “flocculent layer” (Miller *et al.*, 1998; Roque *et al.*, 2014). Other unique features of Caf1 are that it vigorously resists thermal and proteolytic degradation, it can easily be purified and its biological ability to thwart mammalian cell attachment is sustained when purified (Roque *et al.*, 2014; Levy *et al.*, 2018).

1.6.2.2 Caf1M and Caf1A

Caf1M and Caf1A are the prototype FGL-class (γ3-fimbrial clade) chaperone and usher, respectively. The *caf* operon encodes Caf1M as a 25.6 kDa periplasmic chaperone and Caf1A as a 90.4 kDa porin-like usher (Chapman *et al.*, 1999). Caf1M is an ATP-independent periplasmic chaperone that in collaboration with Caf1A assembles and secretes Caf1 subunits in Gram-negative pathogens (Zavialov *et al.*, 2007a). The structure of Caf1M has a boomerang-like shape composed of an N-terminal and C-terminal domains each of which is formed by an Ig-like fold (Sauer *et al.*, 1999; Geibel *et al.*, 2014). Caf1M possesses an accessory N-terminal sequence between its long F-G β-strands and a disulphide bond (bridge) that connects these strands (Chapman *et al.*, 1999; Zavialov *et al.*, 2001). The sequence of Caf1M is thus 18 residues longer than that of its FGS homolog, PapD (MacIntyre *et al.*, 2001). The primary functions of Caf1M involve precluding detrimental aggregation of the unfolded Caf1 subunit in the periplasmic space by forming a Caf1M:Caf1 complex and ensuring correct transport of this binary complex to Caf1A for surface localisation and assembly (Galyovl *et al.*, 1991; Zavialov *et al.*, 2001). Failure of Caf1M to fulfil these critical functions causes Caf1 subunits to be prematurely polymerised, unproductively accumulated in the periplasm, and proteolytically degraded (Sauer *et al.*, 2000; Salih *et al.*, 2008; Busch *et al.*, 2012).

Caf1A usher acts as a binding scaffold for coordinating the polymerisation of Caf1 into a linear fibre and promoting its anchorage into the OM (Dubnovitsky *et al.*, 2010; Yu *et al.*, 2009; Du *et al.*, 2002). Thus, unlike Karlyshev *et al.* (1992b) who found

Caf1A to be unessential for Caf1 secretion in their study of recombinant *E. coli* strains, Runco and team workers reported that Caf1A was required for both the secretion and assembly of the F1 capsule in *Yersinia pestis* (Runco *et al.*, 2008). It has been demonstrated that no binding between the usher and free chaperone has ever been detected; the usher only binds with chaperone-subunit complexes (Yu *et al.*, 2012). Therefore, Caf1A differentiates between free Caf1M and Caf1M:Caf1 intermediates. Caf1A was the first identified bacterial cytokine receptor, and the reported structural similarities between Caf1 and human IL-1β. Abramov *et al.* (2001) suggests potential interactions between IL-1β and Caf1A. Both Caf1 and IL-1β have been found to have a common binding site which overlaps on Caf1A (Högbom *et al.*, 2017).

1.6.2.3 Caf1R

Caf1R is a protein of 301 amino acid residues and 36.8 kDa (Karlyshev *et al.*, 1992a). Caf1R is encoded on the opposite DNA strand to the other *caf* operon genes by the associated *caf1R* gene product in the *caf* operon. The *caf1R* gene product assumes the role of a temperature regulator of Caf1 production to ensure the induction of the maximal expression of 37°C (Miller *et al.*, 1998). Caf1R is a positive regulator of DNA-binding transcription and is homologous to the widely distributed AraC family of bacterial transcriptional activators. The isoelectric point of Caf1R is computed to be 9.5, showing that it is a highly basic protein (Karlyshev *et al.*, 1992a). Caf1R has been found to orchestrate the thermal control of Caf1 in a transcriptional fashion, signifying that it is an essential virulence factor of *Yersinia pestis* (Karlyshev *et al.*, 1992a; Al-Jawdah *et al.*, 2019). Caf1R is a relatively unstable protein, and its structure is composed of two domains: DNA-binding domain of ~ 100 amino acids at the N-terminus and a sensing or oligomerisation binding domain of ~ 100 - 200 amino acids at the C-terminus. The N-terminus has been found to have a high structural homology with MarA (90%) and Rob (94%) from the AraC family (Gahlot *et al.*, 2021).

1.6.3 Assembly of the F1 antigen

Structural and functional studies revealed that the assembly of F1 antigen occurs by a mechanism similar to the one found in the CU apparatus involved in the assembly of type I pili and Pap (Runco *et al.*, 2008). The CUP-based assembly of F1 antigen is depicted in (**Figure 1.12**). The unfolded subunit is unstable, has a high tendency to aggregate and is vulnerable for degradation. In the periplasm, Caf1 binds

to Caf1M and the binding of Caf1 and Caf1M forms a soluble and stable Caf1M-Caf1 complex (Sauer *et al.*, 2004).

Caf1A provides a docking platform for the assembly of the F1 capsule and secretes Caf1 through its channel pore to form the gelatinous capsule on the cell surface. Both NTD and CTDs of Caf1A serve as Caf1M-Caf1 binding sites during assembly of the F1 capsule (Werneburg *et al.*, 2017).

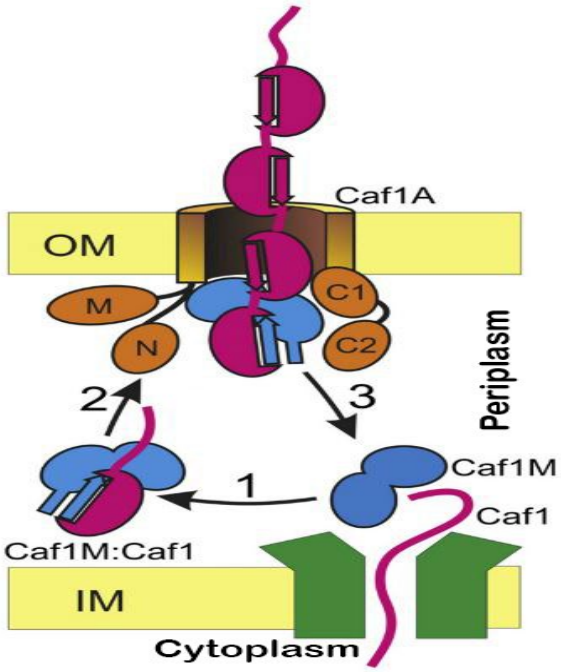

Figure 1.12: Schematic presentation of Caf1 Assembly.

Caf1 subunit is synthesised in the cytoplasm and then translocated across the IM into the periplasm. Step 1: Caf1M binds to Caf1 subunit by DSC to form a binary Caf1M:Caf1 complex. Step 2: The Caf1M:Caf1 complex is targeted to the OM-localised usher where it interacts with the N-terminal of Caf1A. Step 3: Caf1M disassociates from Caf1, and fibre is polymerised via DSE. The growing fibre is secreted to the surface. Arrows denote steps of assembly. IM, Inner membrane; OM, outer membrane; N, usher N-terminal domain; M, usher plug domain; C1 and C2, usher C-terminal domains. Image adapted from Yu *et al.* (2012).

At the usher, Caf1M disengages from Caf1 and allows for Caf1-Caf1 interaction to occur (Zavialov *et al.*, 2002). Caf1A catalyses the replacement of the Caf1M-Caf1 complex with the Caf1-Caf1 interaction (Werneburg *et al.*, 2017), and at this juncture, the Caf1 subunit is incorporated into the growing fibre. Multiple rounds of Caf1M-Caf1 binding and DSE reactions lead to the final formation of the capsule on the cell surface (Werneburg *et al.*, 2017).

1.7 Fluorescent proteins

Fluorescent proteins (FPs) are advantageous tools commonly used as biochemical markers for studying cellular processes. Although interests in FP research had a scientific history predating the 1960s, Osamu Shimomura is considered the first to purify and characterise GFP in the jellyfish *Aequorea Victoria*, which shows bright green fluorescence when exposed to UV light (Remington, 2011). GFPs have gained wide popularity in the cell, molecular and developmental biology since the 1990s thanks to the pioneering efforts of Prasher (who cloned and engineered the GFP gene), Tsuji (who made colour mutants of the GFP gene), Chalfie (who reported the functional expression of GFP in heterogenous tissues), and Tsien (who modified and developed GFP) (Prasher *et al.*, 1992; Chalfie *et al.*, 1994; Chalfie *et al.*, 1995; Inouye *et al.*, 1994). GFPs are thermally stable (up to 100°C) and extremely resistant to proteolysis due to their β-barrel architecture which forms a cylinder 40 Å in height and 25 Å in diameter (Remington, 2011). This β-barrel structure is composed of an internal oxygen-dependent fluorophore located near the centre of the barrel (Ormo *et al.*, 1996; Dammeyer *et al.*, 2012). To date, GFPs have been widely applied in a variety of species, including bacteria, fungi and human cells (Bogdanov *et al.*, 2010). These proteins have been used as genetically encoded fluorescent markers and unique reporters in living systems for monitoring gene expression, protein localisation and trafficking and structural relationships among viral and cellular proteins (Parthasarathy *et al.*, 2018; Cinelli *et al.*, 2000).

GFPs are considered an accessary emitter protein of the *Cnidarian* luminescent system and are formed as a result of a self-catalysed chromophore maturation mechanism. The initial step in this process is that the adjacent serine (Ser65), tyrosine (Tyr66) and glycine (Gly67) residues of the GFP chromophore react with each other and with oxygen for dehydration reactions to generate a fluorophore. The produced fluorophore then is excited by the absorption of blue light of 470 nm wavelength, and eventually vanishes with the emission of 505 nm green fluorescence (Drummen, 2012). One of the most distinctive properties of GFP is that it can be fused with special linkers to other proteins, effectively making them fluorescent, enabling any protein to be localised and tracked using standard fluorescent microscopy. However, it was shown that the formation of the GFP chromophore depends on the correct folding of the protein since the fused proteins can reduce the folding yield and fluorescence of GFPs (Waldo *et al.*, 1999). To circumvent this issue, multiple rounds of protein engineering led to the

development of the enhanced strain of GFP (EGFP). However, EGFP was found ineffective because its tag failed to be fluorescent when fused to bacterial proteins that form inclusion bodies (Valbuena *et al.*, 2020). As a result of such a drawback, a superfolder strain of GFP (sfGFP) was advanced (Pédelacq *et al.*, 2006). Previous research has revealed that sfGFP surpassed other common GFP variants with respect to protein localisation in the periplasm of Gram-negative bacteria (Dinh *et al.*, 2011). Another appealing characteristic of GFP is that under certain conditions modifications of its chromophore result in new fluorescent probes with various colours, such as blue, yellow, cyan and red (Bogdanov *et al.*, 2010).

Most red fluorescent proteins are derived from DsRed which is tetrameric protein isolated from *Discosoma species*. DsRed and its variants such as mFruits of the second-generation monomeric red fluorescent protein family (mRFP) were shown to have slow maturation rate and low photostability (Miyawaki *et al.*, 2012). To overcome these defects, Campbell *et al.* (2002) developed the monomeric mCherry fusion protein through directed evolution. mCherry is a very rapidly-maturing monomer with low acid sensitivity and is over tenfold more photostable than mRFP (Shaner *et al.*, 2004). As a result, it is regarded as the preferred choice of the red monomers as it combines red-shifted emission (610 nm wavelength), with reasonable photostability, brightness and performance in fusions (Davidson *et al.*, 2009; Ransom *et al.*, 2015). The structure of mCherry is similar to that of GFP. mCherry is commonly used in combination with sfGFP to fuse fluorescence protein tags to detect and quantify protein expression (Meyers *et al.*, 2019)**.** mCherry and sfGFP have distinctive maturation kinetics. The fluorophore of mCherry matures more slowly than that of sfGFP. Furthermore, the fluorophore of mCherry requires longer time than that of sfGFP to become fluorescent. The fluorescence intensities of mCherry and sfGFP can be monitored and quantified independently of each other.

1.8 Evidence for a role for Caf1 in OMV production

Previous research conducted in the Lakey group by Dr Helen Waller and two project students Isaac Goh and Rebecca McCamley showed the presence of OMVs and Caf1 in the flocculent layer of Caf1 expressing *E. coli* suggesting that OMV production is a stress response resulting from the production of Caf1.

The main findings of their work is presented in this section. They proposed the hypotheses that were used as the basis for the present study.

E. coli BL21(DE3) transformed with the pCaf1 plasmids(pCaf1, pΔCaf1A, pΔCaf1R, pCaf1, pΔT7) were used to produce the flocculent and supernatant samples which were analysed using sodium dodecyl sulphate-polyacrylamide gel electrophoresis (SDS-PAGE) and western dot blot techniques. Mass spectrometry, transmission electron microscopy (TEM) and thin layer chromatography (TLC) were also employed. The flocculent layer was shown by western blot and peptide mass fingerprinting to contain the proteins Caf1, OmpF, Caf1M and β-lactamase **(Figure1.10A**). Furthermore, the flocculent could be dissolved by SDS /EDTA solutions, suggesting that lipids are also a major constituent of the flocculent layer **(Figure 1.10B)**. The presence of LPS and phospholipids in the flocculent layer was then confirmed by TLC (**Figure 1.10C)**.

TEM images (not reported here) showed that OMVs were present in both the flocculent and supernatant of pCaf1 plasmid cultures, though these OMVs are more abundant in the flocculent sample. This finding indicates that Caf1 increases OMV production. Furthermore, a TEM image of the pCafΔ*caf1A* supernatant showed an abundance of OMVs **(Figure 1.11A)** and SDS PAGE revealed the presence of shorter Caf1 “oligomers” rather than polymers (**Figure 1.11B**). The pΔCaf1A supernatant also was found to have the highest LPS levels as compared to the supernatant samples from the other studied plasmids (all differences were statistically significant where *p* ranges between 0.01 and 0.5) (**Figure 1.11C**). Based on these results, the research team concluded that OMV production is a response to Caf1 production and that the flocculent layer is composed of OMV trapped within a Caf1 polymer network.

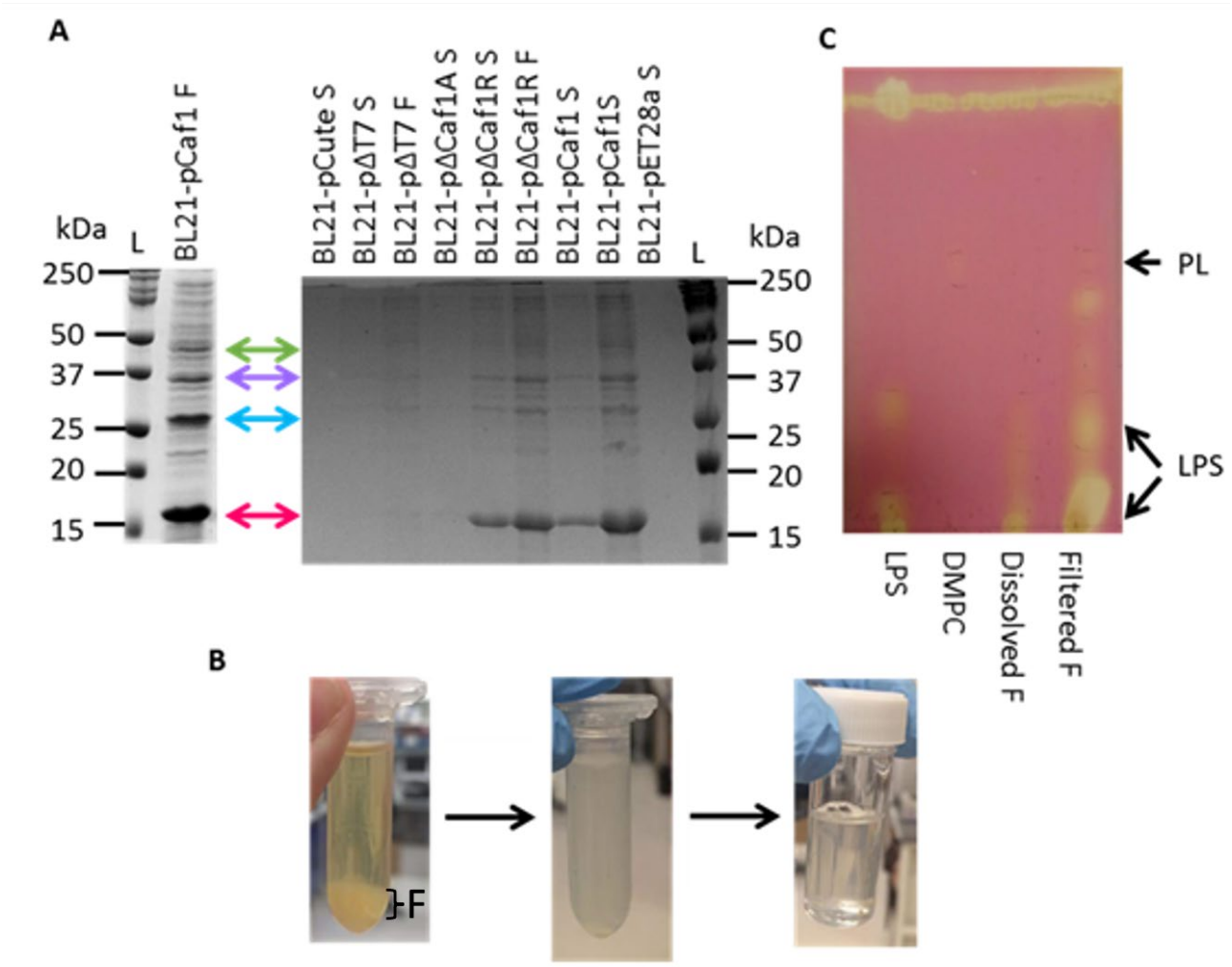

Figure 1.13: Components of the flocculent layer.

(A) Definition of proteins present in flocculents and supernatants. SDS PAGE Gel – 15% (left) prepared by Dr Helen Waller. Flocculent sample boiled with 2 x SDS Loading Dye. Stain – Coomassie Blue. Protein bands excised and analysed by the Pinnacle Mass spectrometry facility, Newcastle University. Green arrow – EF Tu1 (43.26 kDa); Purple arrow – OmpF (37 kDa); Blue arrow – Mixture: Caf1M (28.73 kDa) and β-lactamase (31.5 kDa); Pink arrow – Caf1 (15.56 kDa). SDS PAGE – 15% (right). Supernatant and flocculent sample drawn from *E. coli* transformant cultures boiled with SDS Loading Dye. BL21 has been transformed with five different plasmids :1. pCute, *caf1* gene has been knocked out; 2. pΔT7, the T7 promotor has been deleted; 3. pΔCaf1A; 4. pΔCaf1R,; 5. pET28a,a control plasmid. Stain – Coomassie Blue. L = Protein Ladder; F = Flocculent; S = Supernatant. (B) Photographs of Flocculent Dissolution Process. *E. coli* pCaf1 flocculent centrifuged (left). Supernatant discarded, suspended in Phosphate Buffer Saline by vortex (middle). Buffer added to a final concentration of 1% SDS 25 mM Tris 0.5 mM EDTA pH 8. Solution stirred until fully dissolved (right). (C) Thin Layer Chromatography of Lipids. Mobile phase – Chloroform, Methanol and Water (65:25:4 ml). Stain – Potassium Permanganate. LPS = Lipopolysaccharide; PL = Phospholipid; DMPC = 1,2-Dimyristoyl-sn-glycero-3-phosphorylcholine; F = Flocculent layer; S = Supernatant.

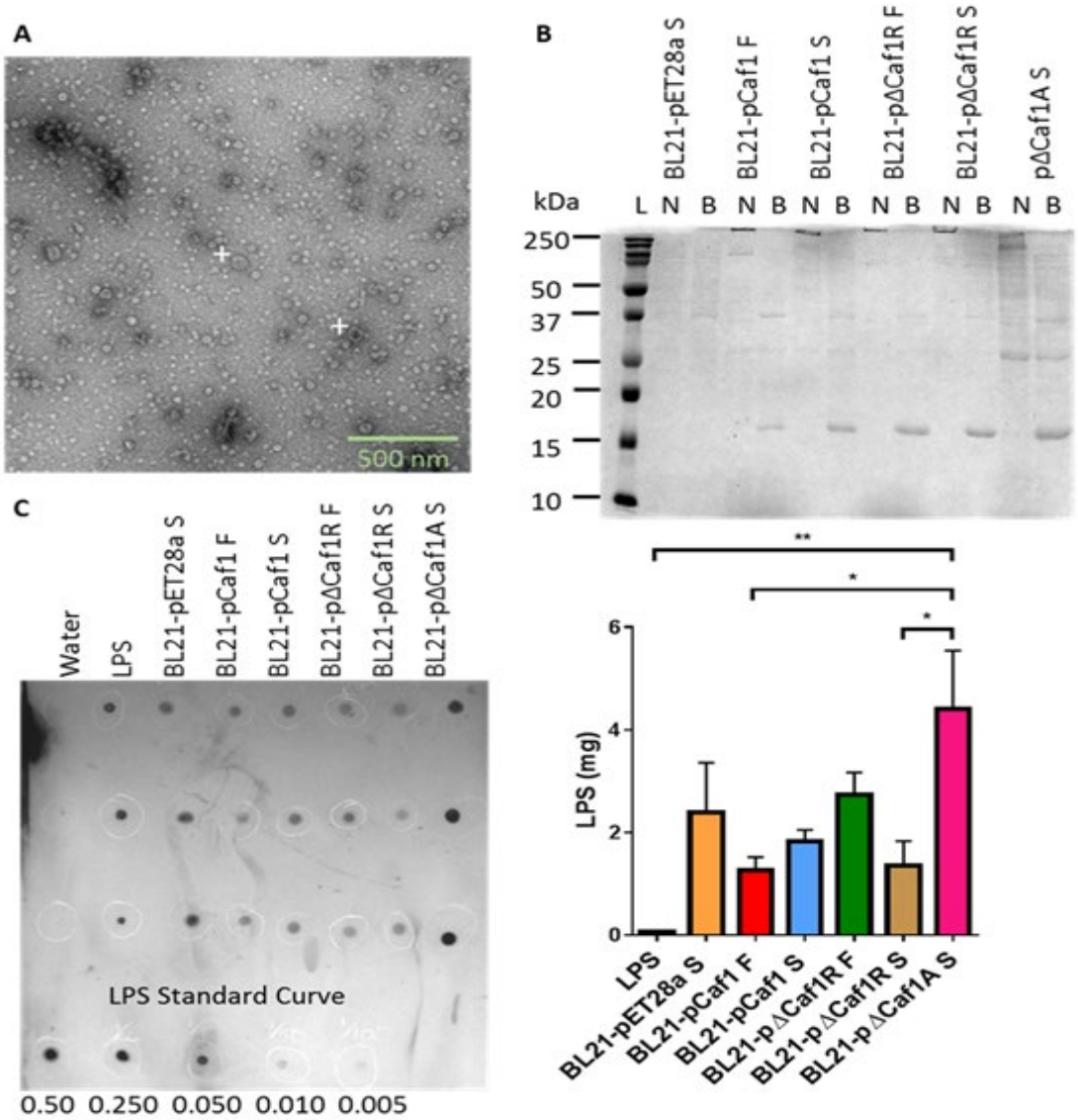

Figure 1.14: Effect of caf1A deletion.

(A) *E. coli* pΔCaf1A culture supernatant 0.2 µm filtered and concentrated (10,000 MW cut off). A 10 µL aliquot loaded on a copper grid. Stain – 2% Uranyl Acetate. Imaged using Transmission Electron Microscopy. + = Deflated OMV. (B) SDS PAGE gel of flocculent and supernatant samples used for TEM. The plasmid description is same as in Figure 1.10. L = Protein Ladder; F = Flocculent; S = Supernatant; N = Non-boiled; B = Boiled. (C) Western Dot Blot of Filtered Flocculents and Supernatants. *E. coli* transformants cultured in triplicate same as figure 1.10, flocculents and supernatants separated, filtered and diluted 1 in 10. LPS Standard Curve in mg. Primary Antibody – Sheep Anti-LPS IgG Monoclonal Antibody; Secondary Antibody – Donkey Anti-Sheep IgG conjugated to Alkaline Phosphatase; Visualisation - SIGMA*FAST*™ BCIP© /NBT. Bar chart shows pΔCaf1A contains most LPS. Western Dot Blot samples compared to LPS Standard Curve. F = Flocculent; S = Supernatant; ** p <0.01 * p<0.05.

1.9 Aims of study

The unpublished results of our research group presented above suggested a link between Caf1 and OMV production. These results are important if we wish to maximise the production of Caf1 polymers for biomaterials applications. Since OMV production is likely to be a burden on Caf1 producing cells, it could be hypothesised that if OMV formation can be reduced, it may increase yields of Caf1 polymer. On the other hand, Caf1 could be a means to produce OMVs for vaccine applications with Caf1 as a protein scaffold for antigen delivery. Thus, the present study seeks to answer the following research questions:

- How does Caf1 production cause vesiculation?
- What are the properties of the Caf1 induced OMVs?
- How does the knockout of Caf1A cause hypervesiculation?
- Can Caf1 production be altered to reduce vesiculation and the stress on the producer cells.

Chapter II

Materials and Methods

"I have learned more from my mistakes than from my successes."

Sir Humphry Davy

2 Materials and Methods

2.1 Materials

2.1.1 Buffers and Reagents

All buffers and reagents used in this thesis were sourced from Sigma-Aldrich Company Ltd. The kits of Phusion DNA polymerase, Monarch plasmid miniprep and Monarch DNA gel extraction were obtained from New England Biolabs® Inc. The In-Fusion HD cloning kit was obtained from Clontech, and the antibodies were sourced from Proteintech, GeneTex, Lifespan Biosciences, Stratech. A complete list of all the buffers and reagents used throughout this thesis are presented in **Table 2.1**.

Table 2.1: Lists of buffers and reagents

Buffer	Reagent
SDS loading buffer	2% (w/v) SDS, 0.1% (w/v) Bromophenol blue, 125 mM Tris-HCl pH 6.8, 15% glycerol, 1% (v/v) β-mercapto-ethanol
Running buffer (1X) SDS	1% (w/v) SDS, 14.4 g/l, 25 mM Tris-HCl pH 8.0, 192 mM glycine
Coomassie stain	10% (v/v) glacial acetic acid, 10% (v/v) propanol-2-ol, and 0.5% (w/v) Coomassie- Brilliant Blue G
Destain solution	10% (v/v) glacial acetic acid and 10% (v/v) propanol-2-ol
Transfer buffer	10 mM CAPS buffer, pH 11, 20 % (v/v) MeOH
TBST	2.7 mM KCl, 38 mM Tris-HCl, 140 mM NaCl, 0.05% Tween20 (v/v)
Primer mix	1μl 100 μM forward primer + 1μl 100 μM reverse primer + 8 μl Nuclease free water
TBE	90 mM Tris, 90 mM Boric Acid, and 500 mM EDTA

SDS, Sodium Dodecyl Sulfate; w, weight; v, volume; %, percentage; mM, millimolar; Tris, trisaminomethane; HCl, hydrochloric acid; CAPS, N-cyclohexyl-3-aminopropanesulfonic acid; MeOH,, methanol; KCl, potassium chloride; NaCl, sodium chloride; μl, microliter; μM, micromolar; EDTA, Ethylenediaminetetraacetic acid.

2.2 Microbiology

2.2.1 Bacterial strains

Three bacterial strains of *Escherichia coli* (*E. coli*) were used in this thesis: 1) *E. coli* BL21 (DE3); 2) *E*. BL21 AI*,* and 3) *E. coli* MachI, with the genotype and application of each of these strains are shown in **Table 2.2**. *E. coli* BL21 (DE3) and *E*. BL21 AI were sourced from New England Biolabs® Inc and *E. coli* MachI was obtained from Invitrogen (Life Technologies).

Table 2.2: Bacterial strains

***E.coli* Strains**	**Genotype**	**Supplier**	**Application**
BL21 (DE3)	*FhuA2 [lon] ompT gal (λ DE3) [dcm]deltahsdS λ DE3 = λ sBamHIodeltaEcoRI-B int::(lacI::PlacUV5::T7 gene1) i21deltanin5*	New England Biolabs® Inc	Protein expression
BL21 AI™	*F⁻ompT hsdS$_B$ (r_B^- m_B^-) gal dcm araB::T7RNAP-tetA*	Life Technologies	Protein Expression
Mach1™	*F⁻ φ80lacZΔM15 ΔlacX74 hsdR(r_K^-, m_K^+) ΔrecA1398 endA1 tonA*	Life Technologies	Cloning

2.2.2 Plasmid construction

Plasmids used here were constructed using an In-Fusion high definition (HD) cloning kit obtained from Clontech, described in more detail in **2.3.2** or from pCaf1 or pBad33SDCaf1, both of which were as previously described (Al-jawdah, 2019; Roque, 2012). Full details of the plasmid constructs are presented in **Table 2.3**.

Table 2.3: List of plasmid constructs

Plasmid Names	Description	Abbreviation
pCaf1	A pGEM-T plasmid with T7 promoter upstream of a wild type *caf* operon containing *caf1R, caf1M, caf1A* and *caf1* genes derived from pAHL34 (Miller *et al* 1998)	pCaf1
pCaf1ΔR	pCaf1 plasmid with *caf1R* gene deleted (this increases Caf1 polymer yield in T7 background (Al-Jawdah et al., 2019b). This plasmid was the basis for most Caf1 plasmids used in this study and so ΔR is omitted from their abbreviated names for simplicity	pCaf1ΔR
pCaf1Δ*R*Δ*A*	pCaf1 plasmid with *caf1R* and *caf1A* genes deleted (ΔA prevents polymer export)	pCaf1ΔA
pCaf1ΔRΔf1	pCaf1 plasmid with *caf1R* and *caf1* genes deleted	pCaf1Δf1
pGEM-T-Empty	Original pGEM-T (Promega)	pGEMT
pCaf1ΔRΔAM^{FLAG}	pCaf1 plasmid with *caf1R* and *caf1A* genes deleted. Addition of C-terminal FLAG tag to *caf1M*	pCaf1ΔAM^{FLAG}
pCaf1ΔRΔA**Caf*1M^{FLAG}	pCaf1 plasmid with *caf1R* and *caf1A* genes deleted. Addition of a stop codon at the start of *caf1M*^{FLAG}	pCaf1ΔA*M^{FLAG}
pCaf1ΔRΔACaf1M^{FLAG}ΔCaf1	pCaf1 plasmid with *caf1R, caf1A* and *caf1* genes deleted with addition of C-terminal FLAG tag to *caf1M*	pCaf1ΔAM^{FLAG}Δf1
pBad Caf1*A*	*caf1A* gene inserted in pBad33 (Al-Jawdah et al., 2019b)	pB*A*
pBad Caf1*A*^{FLAG}	FLAG-tag sequence inserted between proline and asparagine (467-468) of *caf1A* gene	pBA^{FLAG}
pCaf1ΔT7	The T7 promotor has been deleted of the pGEMT plasmid	pΔT7

Plasmid Names	Description	Abbreviation
pBad Empty	pBad33 plasmid created by adding Shine Dalgarno sequence to pBad33 (Roque et al., 2014b)	pBAD
pBad OmpA-NTD-mCherry	pBad vector with N-terminus end of OmpA with OmpA linker and mCherry insertion	pNAM
pBad Full OmpA-mCherry	pBad vector with OmpA NTD and OmpA CTD and mCherry inserted at the end of the CTD	pAM
pBad OmpA-NTD TCM-Linker-OmpA-CTD-mCherry	pBad vector with Tetra-Cysteine Motif inserted at the end of the OmpA NTD and mCherry at the end of CTD	pSAM
pBad OmpA-NTD-TCM-Linker OmpA-CTD	Same as the above except of the deletion of mCherry	pSA
pBad OmpA-NTD-Linker-TCM-OmpA-CTD-mCherry	pBad vector with OmpA NTD and Tetra-Cysteine Motif is inserted after the linker. mCherry is inserted at the end of the CTD	pASM
pBad-OmpA-NTD-Linker-TCM-OmpA-CTD-mCherry	Same as the above except of the deletion of mCherry	pAS
pGI10	Full length OmpA-mCherry pTHV037 OmpA-LEDPPAEF-mCherry (Verhoeven *et al.*, 2013)	pGI10
pBH501	*ori*-ColE1 *bla spc* (Ap^R $Spec^R$) *amyE*::P_{xyl}-*WALP23-mScarlet-I* (Gohrbandt *et al.*, 2019; Gohrbandt *et al.*, 2022)	

NTD, N-terminal domain; CTD, C-terminal domain; TCM, tetra-cysteine motif (Cys-Cys-Pro-Gly-Cys-Cys)

2.2.3 Preparation of Terrific Broth (TB) media

The TB medium was prepared by mixing 12 g/l of tryptone, 24 g/l of yeast extract, 0.05 M of NaCl and 0.4% v/v glycerol. The mixture was dissolved in 900 ml of deionised water and then autoclaved. Following autoclaving, 100 ml of potassium phosphate buffer (0.17 M K_2HPO_4 and 0.72 M K_2HPO_4) was added and mixed thoroughly.

2.2.4 Preparation of Lauria-Bertani (LB) media

The LB medium was prepared by mixing 10 g/l tryptone, 5 g/l yeast extract, and 5 g/l NaCl. The mixture was dissolved in 1 litre of deionised water and then autoclaved.

2.2.5 Preparation of LB agar for Petri dishes

A solid LB-agar media was used in Petri dishes. To make up LB-agar media 10 g/l tryptone, 5 g/l yeast extract, and 5 g/l NaCl, and agar (2% w/v) were dissolved in 1 litre of deionised water and then autoclaved. Prior to adding the molten LB agar media to plates, the appropriate antibiotics were added. The final concentrations of the added antibiotics were 100 and 20 µg/ml for ampicillin and chloramphenicol, respectively.

2.2.6 Bacterial cell transformation

E. coli BL21 (DE3) cells (New England Biolabs® Inc) were thawed on ice for 10 min and then were transformed with plasmid DNA, with full plasmids details presented in **Table 2.3.** Under sterile conditions, 25 µl of thawed competent *E. coli* BL21 (DE3) cells were added to 2 µl of each DNA plasmid 200 ng/µl solution and then incubated on ice for 30 min. The cells were heat shocked at 42°C for 30 seconds and were then immediately placed back on ice for 5 min. 150 µl of SOC (Outgrowth Medium - New England Biolabs ® Inc) was added to the mixture and incubated for 1 h at 37°C whilst continually shaking at 180 rpm. The required antibiotics (ampicillin and chloramphenicol at 100 and 20 µg/ml, respectively) were added to the LB media before pouring into the Petri dishes. 100 µl of the transformed cells were spread onto LB-agar plates and incubated overnight at 37°C.

2.2.7 Culture growth

Bacterial cultures were grown in 50 ml Falcon tubes. A single colony from the transformation plate was added to 45 ml TB medium with 5 ml phosphate buffer under sterile conditions. Antibiotics (ampicillin and chloramphenicol at 100 and 20 µg/ml,

respectively) were added to the medium. Bacterial cultures were then grown at 35°C for 7 and 22 h with continuous shaking at 180 rpm.

2.2.8 Measurement of flocculent layer height

Following flocculent layer generation, the height of the flocculent layer was measured using a ruler following centrifugation in glass capillary tubes containing 50 µl of Caf1 cultures. The bottoms of the glass capillary tubes were sealed with plasticine. The centrifugation was carried out at 2367 x g at 22 °C for 20 min as previously described (Al-jawdah, 2019).

2.3 Molecular biology

2.3.1 Polymerase chain reaction

Polymerase chain reaction (PCR) was used to mutate genes in the *caf* operon. The PCR was performed using the T100^{TM} Thermal cycler (BIO-RAD). The reaction mixture was prepared by mixing all of the components presented in **Table 2.4**. The PCR cycling conditions are presented in **Table 2.5** and a summary of the mutagenic oligonucleotide primers synthesised by Eurofins Genomics are present in **Table 2.6**.

Table 2.4: Polymerase chain reaction mixtures

Component	50 μl Reaction
Nanopure H_2O	27.5
5X Phusion GC Buffer	10
2mM dNTPs	5
10 mM primer mix *	5
100% DMSO	1.5
10 ng/mL Template	0.5
Phusion DNA Polymerase	0.5
Total Volume	50

*μl, microliters; dNTPs, deoxyribonucleotide triphosphate; DMSO, Dimethyl sulfoxide ng, nanogram, mL, millilitres; DNA, Deoxyribonucleic Acid. * denotes Primer mix (1ml of 100 mM forward primer + 1ml of 100 mM reverse primer + 8 ml nuclease free water.*

Table 2.5: Polymerase chain reaction cycling conditions

Step	Time	Temperature	Cycle
Initial Denaturation	3 min	98°C	1 cycle
Denaturation	10 s	98°C	35 cycles
Annealing	30 s	50-72°C	
Extension	25 s/kb	72°C	
Final Extension	10 min	72°C	1 cycle
Hold	-	4°C	Hold

Table 2.6: Mutagenic oligonucleotide primers for PCR

Name	Sequence (5'-3')	Function
Forward *Caf1M^{FLAG}*	AAA GAT GAT GAT GAT AAA TAA TGA TGA TTA AAG GGG ACG GG	Addition of C-terminal FLAG-tag to *caf1M*
Reverse *Caf1M^{FLAG}*	ATC ATC ATC ATC TTT ATA ATC TAA AGT CAC ATT TTT GGA ATA CAA	Addition of C-terminal FLAG-tag to *caf1M*
Forward stop *Caf1M^{FLAG}*	TTA AGT ACG TAA TAA TTA GGA ATT ATT ACT TTC GG CAT GC	Addition of two stop codons to *caf1M*
Reverse stop *Caf1M^{FLAG}*	TTA TTA CGT ACT TAA TCT ATT TAA AAT CAT GAG	Addition of two stop codons to *caf1M*
Forward Δ*caf1*	CGA TAG AGG TAA TAT GAA TTC CCC AAT CAC TAG TGA ATT CGC	Deletion of *caf1*
Reverse Δ*caf1*	ATA TTA CCT CTA TCG AAT AAT CCA ATC	Deletion of *caf1*
Forward *pBADCaf1AFLAG*	GAT TAT AAA GAT GAT GAT GAT AAA AAT ACC CGT AAT GAT TGC CGC	Addition of middle loop FLAG-tag to Caf1A
Reverse pBadCaf1AFLAG	ATC ATC TTT ATA ATC CGG TTT ACA ATA GGT ATT CAG GG	Addition of middle loop FLAG-tag to Caf1A
Forward-pBAD33	TGATAATCTAGAGTCGACCTGCAGGCA	Deletion of *GFP*
Reverse-pBAD33	GCTTTTGGTATCTGCACGCCAAACCATACC	Deletion of *GFP*
Forward ∆mCherry	ACTCAGCCGCAGGCTTGATAATCTAGAGTCGACCTGCAG GCATGCAAG	Deletion of *mCherry*
Reverse ∆mCherry	AGCCTGCGGCTGAGTTACAACGTCTTTGATACCTTTAACT TCGAT	Deletion of *mCherry*
Forward *Δcaf1A*	AGGGGACGGGAATAAACGGATGTTTATTTCAAACAGGAC	Deletion of *caf1A*
Reverse *Δcaf1A*	TATTCCCGTCCCCTTTAAACATC	Deletion of *caf1A*

2.3.2 In-Fusion HD cloning

To clone the Caf1 gene without the need for additional treatment of PCR products, e.g., restriction digestion, phosphorylation, or ligation, we used the In-fusion HD cloning protocol (Takara Biotech), depicted in **Figure 2.1.** This technique is based on 15 bp of homology between inserts and linearised vector backbones using the In-fusion polymerase enzyme. This approach provides the full range of mutagenesis of DNA including insertion, deletion, and substitution.

The target gene was amplified using PCR before being purified from agarose gel extraction using the Monarch Kit (New England Biolabs). To delete specific DNA segments, the relevant regions (genes) of the plasmid were generated by leaving out the relevant portion of the plasmid from the amplified region using two primers that surrounded the desired region with a 15-bp primer that was complementary to the opposite end of the linearised vector. PCR primers for the target gene were created with a 15-bp (5') tail complementary to the ends of the linearized vector for insertion cloning. This provided us with a linear amplified gene which was then ligated back to its circular form. Similar to deletion, a substitution reaction was carried out but in this case one of the two primers had the sequence inserted and the other contained a 15-bp that was complementary to the opposite end of the linearized vector. The PCR used here is described in detail in section **2.3.1** of this chapter. Agarose gel electrophoresis was used in each instance to analyse the PCR products. Using the Monarch Kit from New England Biolabs, the target DNA band was extracted from the gel as described in section **2.3.4** of this chapter. The In-Fusion HD cloning mix was prepared by mixing the following components: 2 µl of In-Fusion HD Enzyme Premix (Takara Biotech), and X µl of the insert, X µl of the linearised vector (using the In-Fusion HD cloning calculator, the volume and concentration of both linearized vector and insert are calculated), and finally adding nuclease-free water up to 10 µl as the final reaction volume.

The reaction mixture was incubated at 50˚C for 15 min, before being diluted 5-fold prior to its use in the transformation of competent cells as in section **2.2.6** of this chapter.

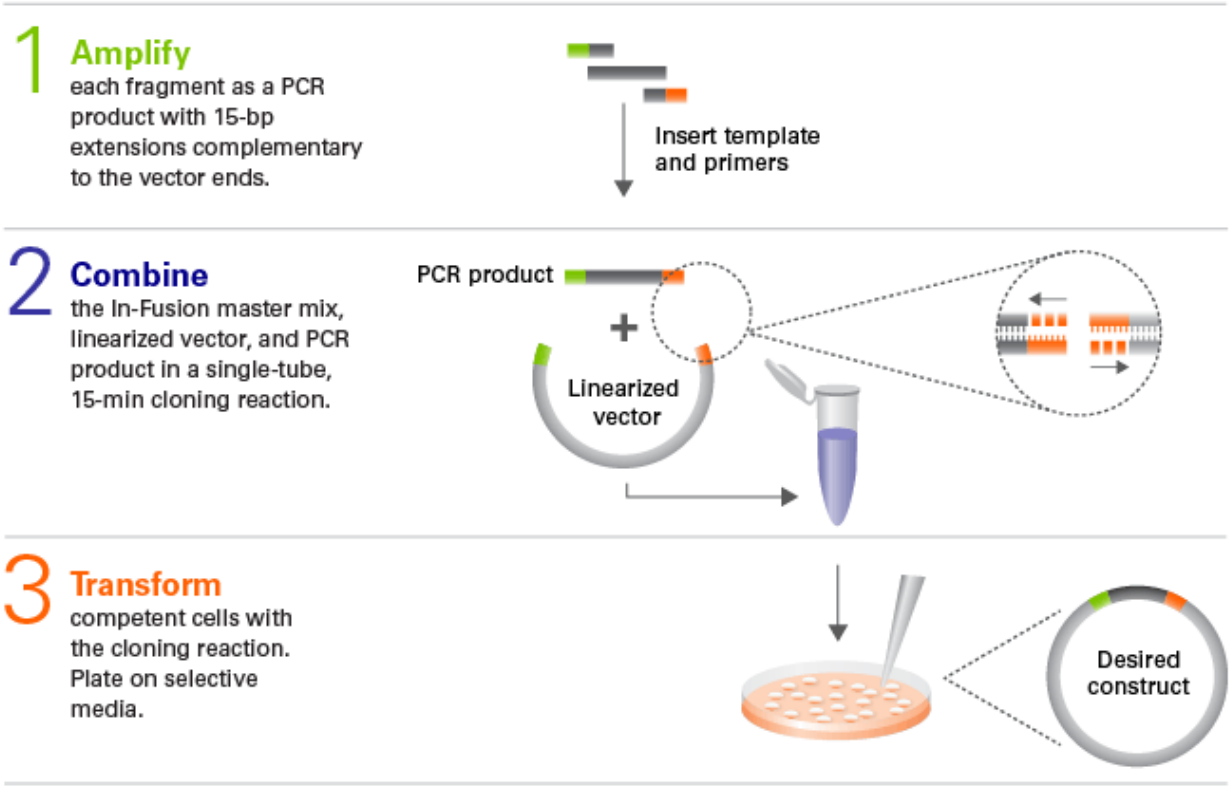

Figure 2.1: The In-Fusion HD cloning technique.

(Adapted from In-Fusion HD cloning guide (TaKaRa Bio Inc).

2.3.3 Agarose gel electrophoresis

DNA fragments were examined by agarose gel electrophoresis according to their molecular size. Therefore, 0.8% agarose stained with Midori Green Advance DNA stain was dissolved in 1 x Tris Borate EDTA (TBE) buffer and heated in a microwave for 30 seconds at medium power (800 watt). The mixture was then transferred into a sealed gel casting tray. The TBE buffer contains 90 mM Tris, 90 mM Boric Acid, and 500 mM EDTA. Next, 6 X loading dye were mixed with DNA samples and then loaded onto the gel. Gel electrophoresis was performed at 100 V for 30-50 min in a TBE buffer. DNA samples were visualised using UV light.

2.3.4 DNA gel extraction

The gel sections containing DNA fragments were cut out and added to 4 volumes of dissolving buffer, before being incubated at 50°C for 10 min while being vortexed periodically to fully dissolve the gel. The solution was placed in a spin column and centrifuged at 16000 x g for one minute, with the flow-through being discarded. The DNA was washed by adding 200 µl of DNA Wash Buffer and centrifuging for one minute at 16000 x g and was repeated twice. To elute the plasmid DNA, the column was shifted to a clean 1.5 ml tube and 12 µl of DNA Elution Buffer was added to the column, before being centrifuged for one minute at 16000 x g. The complete protocol described here is in accordance with the Monarch kit protocol (New England Biolabs).

2.3.5 Plasmid DNA preparation

We used the Monarch kit following the protocol described there in (New England Biolabs). Briefly, the transformed *E. coli* cells were pelleted in a 5 ml Eppendorf tube by centrifugation at 16000 x g for 30 seconds, and the supernatant was discarded. The pellet was resuspended in 200 µl of Resuspension Buffer (B1), and vortexed to ensure cell resuspension. The cells were then lysed by adding 200 µl of the Lysis Buffer (B2), before being inverted 5-6 times until a dark pink color appeared. The solution was incubated at room temperature for one minute. Neutralisation of the lysate was achieved by adding 400 µl of the plasmid neutralization Buffer (B3). The tube was then inverted until the precipitate formed and solution changed to a yellow color. The solution was incubated at room temperature for 2 min before being centrifuged at 16000 x g for 5 min. The supernatant was transferred to the supplied spin column, centrifuged for one minute at 16000 x g, and the flow-through was discarded. 200 µl of Plasmid Wash Buffer 1 was then added to the spin column and centrifuged again at

16000 x g for one minute to remove RNA, protein, and endotoxins. 400 µl of Plasmid Wash Buffer 2 was then added to the spin column and centrifuged for a further minute at 16000 x g. To elute the plasmid DNA, the column was transferred to a clean 1.5 ml tube and 30 µl of DNA Elution Buffer was added before centrifugation for one minute at 16000 x g.

2.3.6 DNA Sequencing analysis

Plasmids were sent for Sanger sequencing at GATC Biotech. All sequencing results and alignments were confirmed using Serial Cloner software Version 2.6.

2.4 Biochemical and General protocols

2.4.1 Isolation of outer membrane vesicles (OMVs)

A schematic diagram illustrating the process of isolating OMVs is depicted in **Figure 2.2.** The expression cultures were centrifuged in 50 ml Falcon tubes at 4200 rpm (2367 x g) for 20 min at 4ºC to remove bacterial cells and debris. The pellet was then discarded, and the supernatant then was centrifuged at 10000 rpm (Beckman, JA10 rotor) for 45 min. The supernatant was then transferred to an ultracentrifuge tube and centrifuged at 100,000 x g for 90 min at 4ºC (Beckman,70Ti rotor). The supernatant was discarded. To enhance the purity of OMVs, the collected pellet containing the OMV fraction was resuspended in PBS at pH 7.4 and then ultracentrifuged at 100,000 x g for 90 min at 4ºC. The pellet was resuspended in 5 ml PBS and then stored at -20ºC until further analysis.

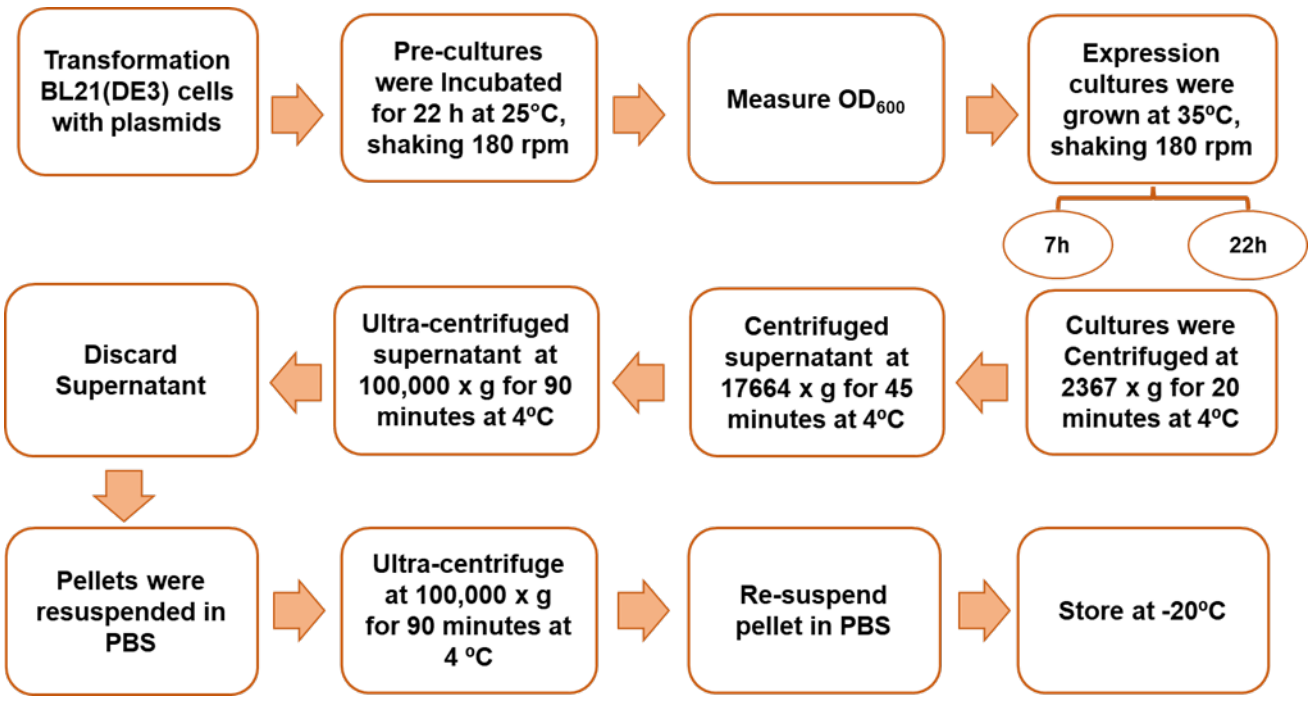

Figure 2.2: Schematic diagram of improved method for outer membrane vesicle (OMV) preparation.

2.4.2 Preparation of outer membrane fraction

To test the insertion of fluorescent OmpA derivatives into the OM, the Wolf-Watz method was employed (Wolf-Watz *et al.*, 1973) with some modification (**Figure 2.3**). Following this method, an overnight culture of BL21 (DE3) was grown in 1l LB medium at 37°C, with continuous shaking at 180 rpm. Cells were harvested by centrifugation at 10,000 rpm (17664 x g) (Beckman, JA10 rotor). Cell pellets were resuspended in 200 ml 0.05 M Tris buffer (pH 7.8) and 1 mM EDTA in a homogeniser for 1 minute. The cell pellet was collected by centrifugation at 10,000 rpm (17664 x g) (Beckman, JA10 rotor). The pellet was resuspended in 20 ml of 30% w/v sucrose in 0.05 M Tris buffer (pH 7.8), 1 ml of 0.1M EDTA, and lysozyme 20 mg, and incubated at RT for 20 min. Then, 1 ml of 0.2 M MgCl2, 5 mg RNase and 5 mg DNase were added, then centrifuged at 30,000 rpm (100,000 x g) (Beckman, 70Ti rotor) 4˚C for one hour. The pH of the supernatant was adjusted to 5.0 using 1 M HCl to precipitate the outer membrane fraction which was collected as the pellet of 20 min spin at 30,000 rpm (100,000 x g) (Beckman, 70Ti rotor), and washed twice in ice cold water.

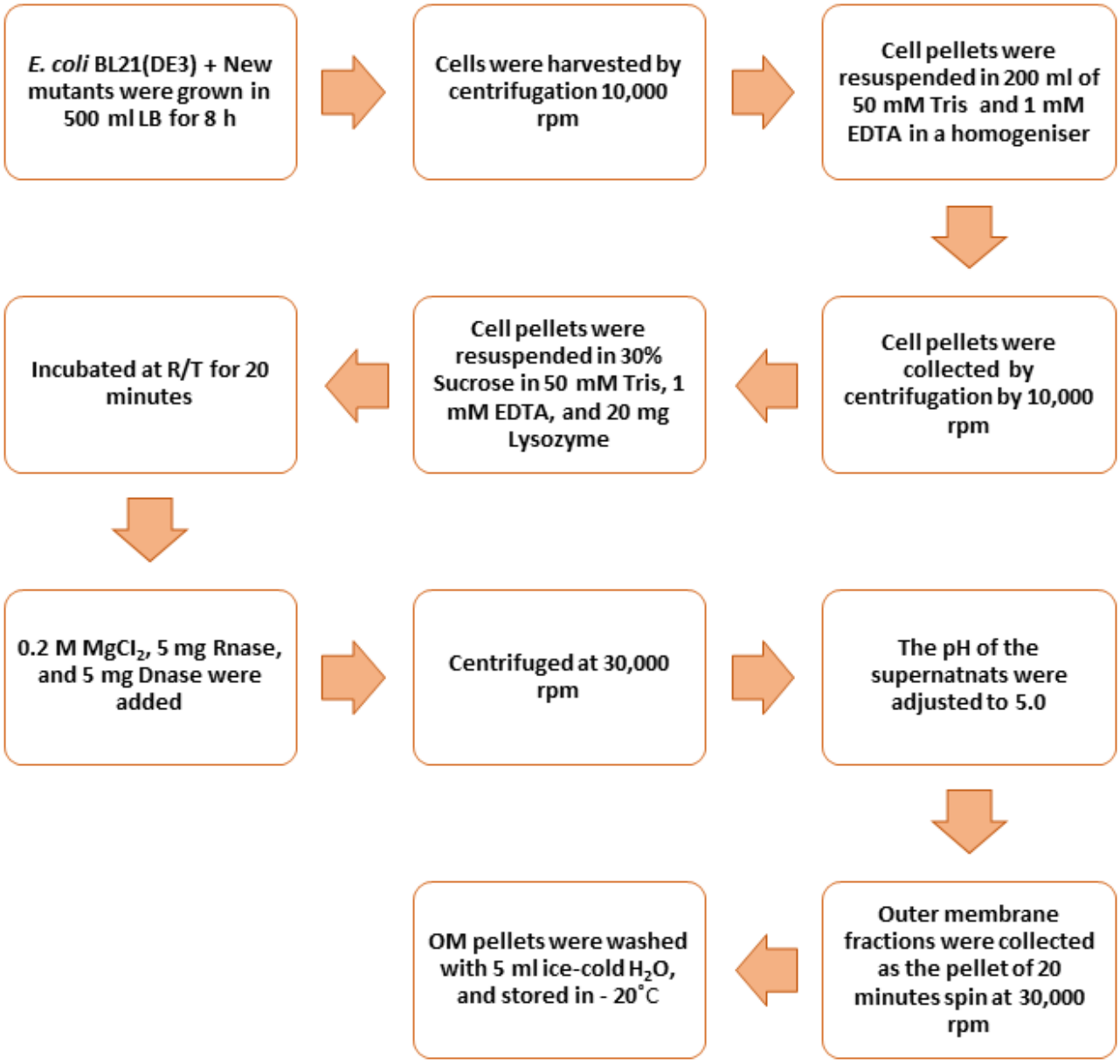

Figure 2.3: Schematic diagram of the modified method of outer membrane fraction purification.

2.4.3 Sodium Dodecyl sulfate Polyacrylamide Gel Electrophoresis (SDS-PAGE)

In all the SDS-PAGE experiments we used the standard methodology described by Laemmli (1970), based on a discontinuous acrylamide gel. The buffer for the resolving gel comprised of 375 mM Tris -HCl pH 8.8, 0.1% (w/v) SDS, and 12% (v/v) acrylamide. To catalyse the polymerisation reaction, 10% ammonium persulphate tetramethylethylenediamine (TEMED) was added. After the resolving gel had set. the stacking gel was applied. The stacking gel buffer contained 125 mM Tris-HCl,0.1% SDS, and 4% (v/v) acrylamide. The gel was polymerised in the same manner as the resolving gel, and then a gel well comb was securely placed into the top of the stacking gel. To prepare the protein samples, 20-30 µl of protein samples were mixed with sample loading buffer 2% SDS (w/v), 15% (v/v) glycerol ,0.1 (w/v) % Bromophenol blue, 125 mM Tris-HCl, 1% (v/v) β-mercapto-ethanol, at pH 6.8 at 1:1 ratio. 20 µl of the protein-dye mixture was then loaded into the wells of the stacking gel. The SDS-PAGE was carried out at 200 V in a running buffer containing 0.1% (w/v) SDS, 25 mM Tris-HCl (pH 8.0) and 192 mM glycine in a Mini PROTEAN tetra cell (BioRad).

2.4.4 Coomassie staining

Coomassie staining was used to stain the protein gels. The gel was stained with staining solution containing 0.05% (w/v) Coomassie Brilliant Blue (Sigma), 10% (v/v) glacial acetic acid and 10% (v/v) propan-2-ol. The samples were then microwaved at medium power (800 watt) for 30 seconds followed by 15 min of incubation at R/T. The gel was destained in destaining solution containing 10% (v/v) glacial acetic acid and 10 % (v/v) propan-2-ol until the bands developed. Using standard protein markers, protein bands are depicted in **Figure 2.4** (Precision plus protein dual colour standards from Bio-Rad) and the protein molecular weights were determined. The gels were imaged using Gel Doc XR+ (Bio-Rad).

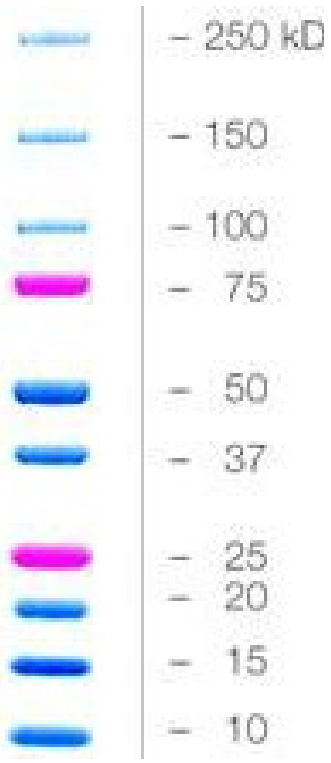

Figure 2.4: Bio-Rad Precision Plus Protein™ Standard

The molecular weight of the protein in (kDa) was determined using a standard protein ladder in Sodium Dodecylsulphate Polyacrylamide Gel Electrophoresis (SDS-PAGE) and western blot (Adapted from Bio-Rad instruction manual).

2.4.5 Western blot

Protein samples were first separated by SDS-PAGE before the transfer of proteins to nitrocellulose membranes. Nitrocellulose membranes (0.22 µm pore size) and blotting papers were cut to gel size and soaked with a blotting buffer. The blotting buffer contained 10 mM cyclohexyl-3-aminopropanesulfonic acid (CAPS) at pH 11, containing 20% (v/v) methanol for 20 min to prepare a gel sandwich. The protein bands were transferred onto the nitrocellulose membrane using the Trans-Blot Semi-Dry cell (Bio-Rad), at 10 V for 45-90 min. The nitrocellulose membrane was blocked with 5 ml of blocking buffer for two hours at room temperature. This approach blocks all areas of the nitrocellulose membrane that do not have any proteins attached to them. The blocking buffer contained TBST + 5% (w/v) milk powder. The TBST buffer contained Tris Buffered Saline (TBS) + 0.05% (v/v) Tween20. The TBS buffer comprised 2.7 mM KCl, 38 mM Tris-HCl and 140 mM NaCl. Throughout each step, the membrane was incubated with gentle agitation. The membrane was rinsed three times with the TBS buffer, and then incubated overnight at 4ºC with fresh TBST buffer containing 5% milk. Included in the incubation overnight, we added specific primary antibodies for each subject protein of interest, which had previously been diluted 1/500. We then washed

the membrane three times with TBS buffer for 5 min at room temperature in order to remove any excess antibodies and were then subsequently incubated for two hours with fresh TBST containing the appropriate secondary antibodies that had been diluted at 1/1000. The protein bands were detected by incubating the membrane with SIGMAFASTTM BCIP®/NBT (SLBT5588) Alkaline Phosphatase Substrate (one tablet dissolved in 10 ml Nanopure water) for 10 min. Once the bands had developed, the reaction was stopped by washing the membrane with Nanopure water. To visualise the protein bands, the membrane was imaged using Gel Doc XR+ (Bio-Rad).

2.4.6 Dot blot

In accordance with the method of Kulp *et al.* (2010), we extracted 0.5 µl of the diluted supernatant (1/100) and then added this to a nitrocellulose membrane (0.45 µm) and air dried for 2 min. The membrane was incubated with blocking buffer TBST + 5% (w/v) milk powder for one hour at room temperature on a 3D rocking platform. Each membrane was then washed three times with TBS buffer. Following this we incubated the membranes with TBST+ 5% milk powder and the LPS antibody diluted at 1:5000 with the sheep anti-LPS antibody (BIO-RAD) for two hours on a 3D rocking platform. We then washed the membrane three times in TBS for 5 min. Each membrane was then incubated in TBST for one hour on a 3D rocking platform with the secondary antibody, anti-sheep IgG alkaline phosphatase conjugate diluted at 1:5000 (Sigma). The membrane was then washed three times in TBS for 5 min each (SIGMAFASTTM BCIP®/NBT SLBT5588). One tablet of alkaline phosphatase substrate was then dissolved in 10 ml of Nanopure water for 15 min to visualize the dots. Once the dots had developed, the reaction was stopped by washing the membrane with Nanopure water. The dots were then imaged using Gel Doc XR+ (Bio-Rad).

2.4.7 Measurement of absorbance at OD_{600}

The cultures were diluted 1:10 and absorbance was measured at OD_{600} nm in a 1 cm path length cuvette using a UV-1800 Spectrophotometer (Shimadzu).

2.4.8 UV Spectrophotometry of proteins and DNA

Using a Nanodrop ND-1000 DNA concentrations were measured at 260 nm and protein concentrations at 280 nm.

2.4.9 Transmission electron microscopy (TEM)

A 20 µl of each OMV sample was added to a carbon coated glow discharged grid, which had been discharged of its glow prior to use. This preparation was adapted from the single droplet method (Harris, 2007; Harris *et al.*, 2014). The grid was incubated at room temperature for one minute and then washed three separate times, each with 20 µl of water. Excess liquid was removed from the grid using Whatman filter paper, before being dried under a heat lamp prior to use. Finally, 2% uranyl acetate was added to stain the sample. Excess liquid was removed using filter paper and grids air dried at room temperature prior to visualising the samples using the TEM. Micrographs were recorded at 100 kV on a HITACHT7800 EM (EM Research Services, Newcastle University). Digital images were recorded using a EMSIS XAROSA CMOS camera with RADIUS software.

2.4.10 Fluorescence microscopy and measurement

The slide preparation was carried out as described (te Winkel *et al.*, 2016). In brief, cell cultures were immobilised on Teflon-coated multi-spot microscope slides (Hendley-Essex) coated with a fine layer of agarose. Fluorescence microscopy was performed on 0.5 µl of cell culture, which was placed onto the exposed agarose surface, and allowed to air dry and covered with a microscopy coverslip.

Fluorescence microscopy images shown in Figure 4.2 were taken using the Nikon Eclipse Ti equipped with a Cool LED pE-4000 light source, a Photometrics BSI Camera (Nikon Plan Apo 100x/1.40 NA Oil Ph3). Two filter sets were used, the first was for GFP (Chroma 49002, EX470/40 DM495lpxr, EM525/50), and the second was for mCherry (Chroma 49008, EX560/40, DM585lpxr, EM630/75). The images were acquired with Metamorph 7.7 (Molecular Devices). All images were analysed using ImageJ 1.53t (National Institutes of Health).

Fluorescence microscopy images shown in Figure 4.17- 4.19 were carried out using a Total Internal Reflection Fluorescence (TIRF) microscopy. The microscope was Nikon Eclipse Ti2 equipped with a Photometric Kinetix sCMOS camera Nikon CFI SR HP Apo TIRF 100XAC Oil objective. Nikon NIS Elements AR v 5.30 imaging software. All images were analysed using ImageJ 1.53t (National Institutes of Health).

This work was carried out with collaboration with Dr Henrik Strahl (Centre for Bacterial Cell Biology- Newcastle University).

2.4.11 Plate reader assay

Cultures of growing bacteria expressing fluorescent proteins were analysed using a microplate reader. The OD_{600} and fluorescence was recorded using emission wavelengths 485 and 587nm for GFP and mCherry, respectively. Cultures were diluted to OD_{600nm} of 0.01 in a warm LB medium with appropriate antibiotics (100 and 20 µg/ml for ampicillin and chloramphenicol, respectively). Two hundred µl of the diluted cultures were immediately transferred to a 96-well plate (ThermoFisher- CoStar) and incubated at 37°C in a FLUOstar Omega plate reader. Absorbance and fluorescence were recorded every 10 min until the OD_{600} reached ~0.6, at which point the plate reader was paused, an inducer was added as appropriate (20% (w/v) arabinose, 1 mM IPTG) to each of the wells in the 96 well plate and then returned immediately to the plate reader. OD_{600nm} and fluorescence were then recorded every 10 min.

2.5 Statistics

In all experiments, three biological replicates were performed, except where explicitly stated. Statistical analysis was performed using GraphPad Prism software version 9.3.1. One way analysis of variance (ANOVA) was performed to compare data sets of two variables; in the case of comparisons of three variables or more a two-way ANOVA was employed. Three or more variables, and where repeated measures were present, respectively. The post-hoc Bonferroni corrections were used to identify significant interactions among variables. ****, *** and ** denote p values of < 0.0001, < 0.001 and < 0.01, respectively.

Chapter Three

Effect of Caf1 protein production on OMV formation

"Learn as if you will live forever, live like you will die tomorrow"

Mahatma Gandhi

3 Effect of Caf1 protein production on OMV formation

3.1 Introduction

The Gram-negative *Yersinia pestis* has been identified as a causative agent of the bubonic, pneumonic, and septicaemic plagues (Schubert *et al.*, 2004; Levy *et al.*, 2018). The *Y. pestis* pathogen produces large amounts of capsular antigen fraction 1 (F1 antigen) to protect itself from phagocytosis within the host environment (Du *et al.*, 2002; Peters *et al.*, 2022). The F1 antigen is a non-flagellar, protective, non-stick surface polymer, the assembly of which via the bacterial chaperone-usher machinery forms an amorphous anti-phagocytic capsule containing thousands of copies of a 15.5 kDa capsular antigen fraction 1 (Caf1) polypeptide subunit (Soliakov *et al.*, 2010; Dura *et al.*, 2018). The genome sequencing of Caf1 has four structural gene products: caf1 (Galyov *et al.*, 1990), caf1M (Galyovl *et al.*, 1991), caf1A and Caf1R (Karlyshev *et al.*, 1992a). These genes represent the components of the caf operon which codes for a structural subunit (Caf1), a periplasmic chaperone (Caf1M), an outer membrane localised usher (Caf1A), and a putative transcription regulator (Caf1R), respectively (Miller *et al.*, 1998; Abramov *et al.*, 2002). It has been reported that Caf1 deletion causes an upsurge in the uptake of *Y. pestis* bacilli by macrophage, demonstrating that Caf1 has a protective function against host immune systems (Du *et al.*, 2002).

Caf1 is a major constituent of *Y. pestis* outer membrane vesicles (OMVs) (Eddy *et al.*, 2014). One of the major models of OMV biogenesis views OMV production as a primary means that Gram-negative bacteria employ to cope with stress-inducing conditions from their own, host or external environments (Qing *et al.*, 2019; Nagakubo *et al.*, 2020; Avila-Calderón *et al.*, 2021). The OMV cargo is typically composed of a variety of OMPs (including OmpC, OmpF and OmpA), lipopolysaccharide (LPS), phospholipids, and nucleic acids (DNA and RNA) (Kim *et al.*, 2013; McMahon *et al.*, 2012; Avila-Calderón *et al.*, 2014). Previous studies have reported on the involvement of OMVs in *Escherichia coli* (*E. coli*) flocculation (Ojima *et al.*, 2015). However, the correlation between enhanced OMV production and flocculation remains unclear.

In unpublished work presented in detail in Chapter **1** Section **1.8**, our research group has previously demonstrated the presence of an outer membrane (OM)

component in the flocculent layer along with Caf1. The results of this experimental work also showed that the deletion of the *caf1A* gene causes large numbers of OMVs being observed by EM in the supernatant with a subsequent increase in the levels of LPS detected. Deletion of Caf1A stops formation of the Caf1 polymer at the surface and may therefore increase the concentration of Caf1 subunits in the periplasm (**Figure 3.1**). Therefore, it was suggested that the flocculent layer is composed of OMVs that are confined to the Caf1 polymer network. Furthermore, the envelope stress caused by periplasmic Caf1 and production of the Caf1 polymer could cause hypervesiculation.

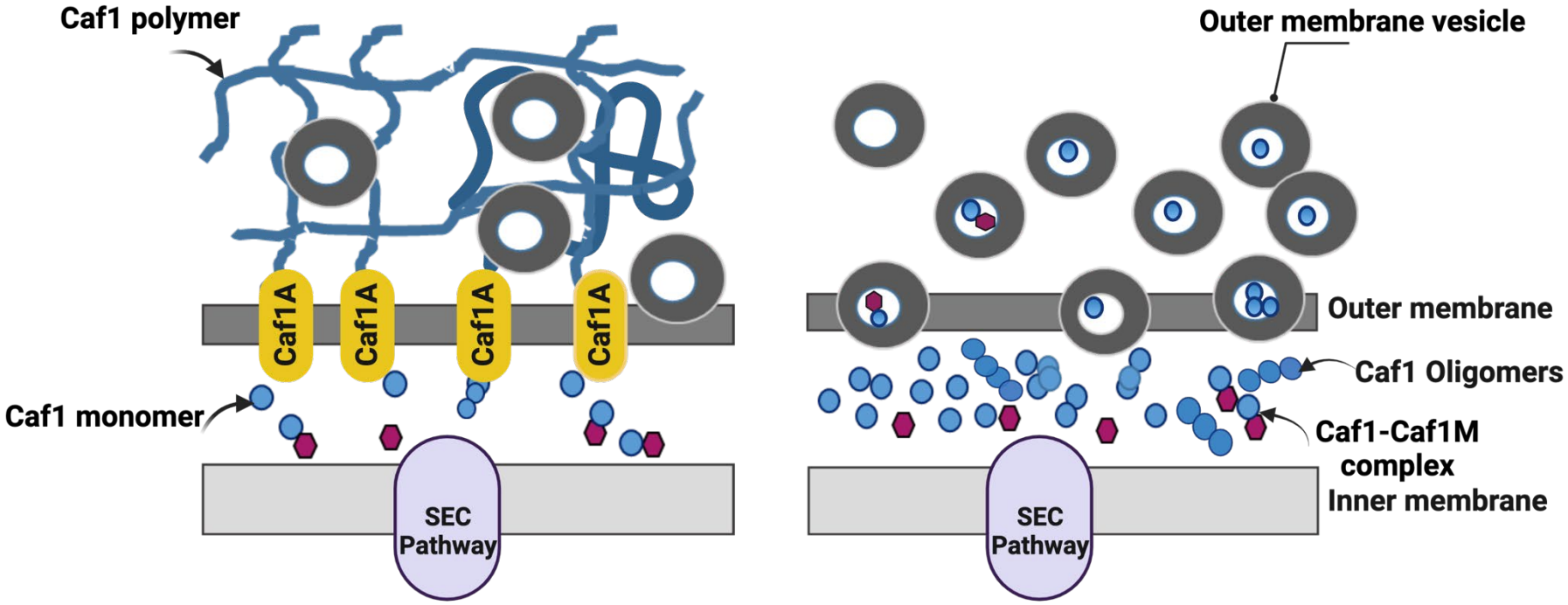

Figure 3.1: Effect of caf1A deletion.

A Schematic diagram showing that *caf1A* deletion prevents formation of Caf1 polymer, which may lead to an increase in the periplasmic concentration of Caf1 subunit. Moreover, it also leads to an increase in the release of outer membrane vesicles (OMVs). The outer membrane vesicles trap components of the periplasm such as the Caf1 monomer, Ca1-Ca1M complex, and Caf1 oligomers.

The main purpose of this chapter is to further develop the previous work from this laboratory, investigating the presence of an OM component in the flocculent layer along with Caf1. To do this, in this thesis, the effects of deleting different Caf1 genes on the flocculent and OMVs production will be measured. The aim is to test the hypothesis that Caf1 production stresses the OM, causing it to form OMVs which are then caught by Caf1 polymers to form the flocculent. More widely this work is anticipated to contribute to the emerging efforts and existing body of scientific knowledge regarding the development of safe and effective vaccines in response to the recent prevalence of antibiotic resistance to bacteria, particularly *Y. pestis*. Vaccines formed from OMVs have already shown promise for the prevention of meningitis and a Caf1-linked OMV vaccine could be useful as a plague vaccine, especially as Caf1 is already a component of existing vaccines, and that the V antigen (LcrV) is also an OMP. Finally, Caf1 is also being exploited as a biomaterial and the findings here may provide a unique insight into the development of novel biomaterials (Roque *et al.*, 2014; Soliakov *et al.*, 2010). Our laboratory is developing methods to increase the yield of Caf1 from bacterial fermentation and the metabolic cost of OMV formation may be limiting the efficiency of these methods. Therefore, we will aim to see if OMV formation can be reduced whilst maintaining high levels of Caf1 polymer production.

3.2 Results

3.2.1 Measuring Caf1 production

To quantify Caf1 production, *E. coli* BL21 (DE3) cells were transformed with the plasmid pCaf1 which contains the whole *caf* operon derived from the *Y. pestis* pMT plasmid (**Figure 3.2 A**). Cultures were grown at 35°C to induce Caf1 expression and incubated for 3, 7 and 22 h at 35ºC. Five ml samples were transferred into 5 ml Eppendorf sample tubes and centrifuged at 4200 rpm (2367 x g) for 15 minutes at 22ºC. Following centrifugation, a flocculent layer formed above the pellet and beneath the supernatant. Samples were taken at 3, 7 and 22 h and subjected to SDS-PAGE. The results showed that in the heated (H) samples, a clear band at 15.5 kDa was observed which corresponds to the Caf1 monomer (**Figure 3.3A**) and that the native, non-heated (N) samples did not show such a band. The absence of this band is due to Caf1 being in the form of large polymers, either preventing it from entering the gel or running near the top. Furthermore, the analysis also revealed that the H lanes also have a 37 kDa protein band compatible with the outer membrane protein F (OmpF) monomer size. This band was found to be weaker in the N samples where OmpF will migrate at its folded trimer mass. Although it is 111 kDa (3 x 37), the OmpF's folded conformation causes it to appear lower (75-85 kDa) as previously reported (Visudtiphole et al., 2005).

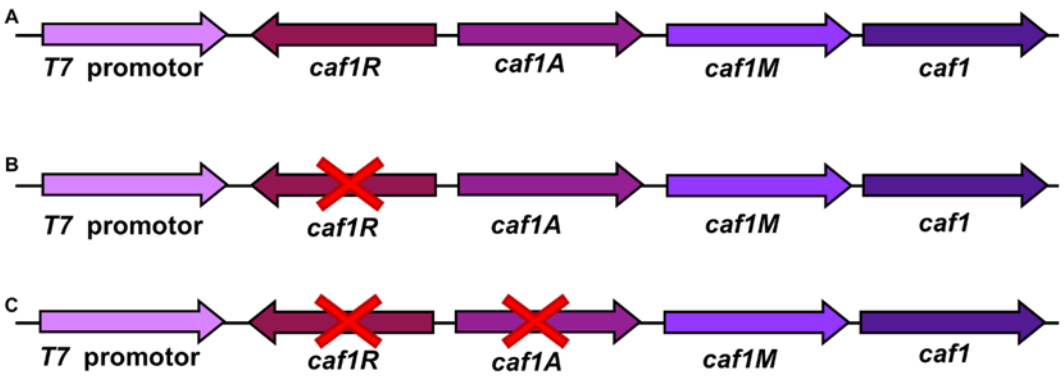

Figure 3.2: Schematic diagram of the Caf1 operon.

(A) The gene transcription of the caf operon is composed of four different genes: caf1 (encoding the subunit), caf1M (encoding the chaperone), caf1A (encoding the user) and caf1R (encoding the regulator). (B) The deletion of the regulator caf1R gene; the relevant plasmid is named here pCaf1ΔR, however, since it is the basis of all other plasmids created in this study the ΔR is omitted in their short names for simplicity. *caf1R gene* deletion was used as the background of all other plasmids to ensure that Caf1 production is driven by the leaky expression of the T7 polymerase. (C) Both caf1A and caf1R are deleted, thus in this study the relevant plasmid is named pCaf1ΔA rather than pCaf1ΔRΔA.

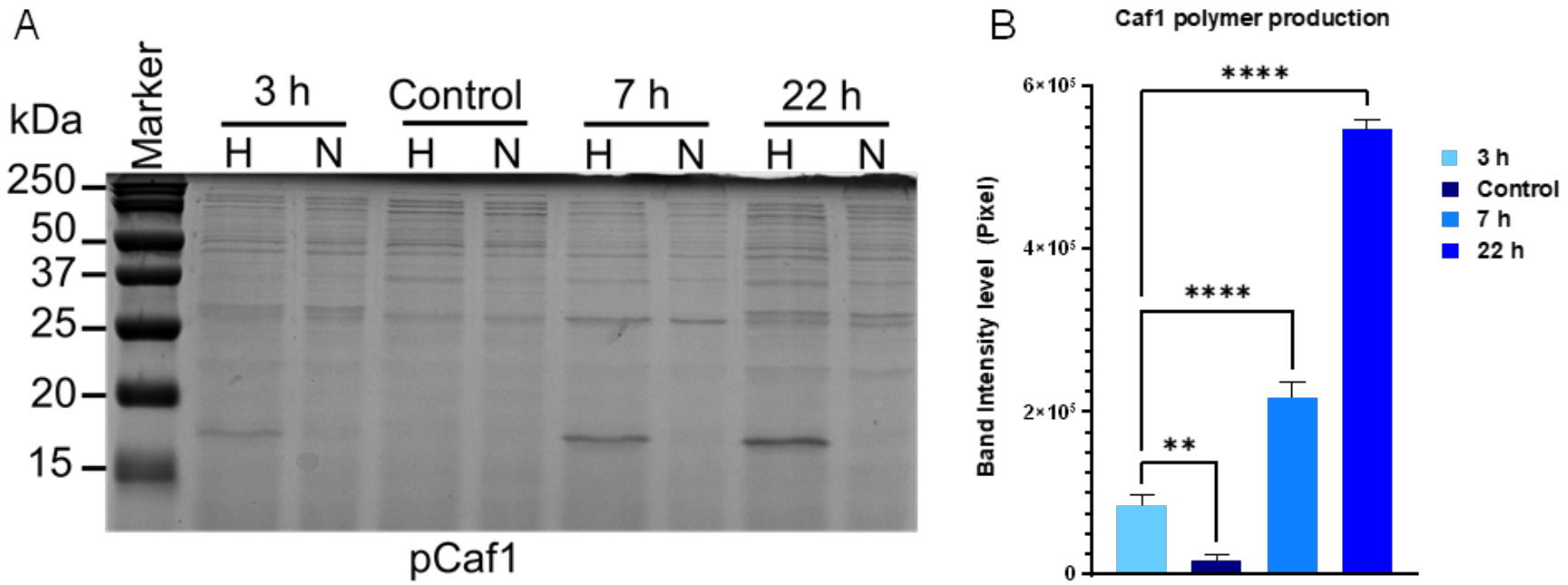

Figure 3.3: Caf1 production.

(A) Sodium dodecyl sulfate polyacrylamide gel electrophoresis (SDS-PAGE) for Caf1 production. *E. coli* BL21 (DE3) was transformed with the plasmid pCaf1. Cultures were grown at 35ºC for 3, 7 and 22 h, and centrifuged at 4200 rpm (2367 x g) for 15 minutes at 22ºC. Samples of flocculent and supernatant mixture were heated at 100ºC for 10 minutes and non-heated (N) samples were analysed by 12% SDS-PAGE and stained with Coomassie Blue. Caf1 is seen at 15.5 kDa in the heated lanes. Cells containing the plasmid pGEMT (empty vector) were used as the control. (B) Bar graph showing the results of densitometry measurements of the Coomassie Blue stained 15.5 kDa band as a measure of Caf1 polymer production at the three time points. Error bars represent standard error of the mean. Asterisks represent significant differences between groups (****, P< 0.0001, ** P< 0.001) determined by one way ANOVA. Biological replicates =3

3.2.2 Analysis of the flocculent layer following centrifugation

Centrifugation of Caf1 producing bacterial cultures has previously been shown to result in the appearance of a flocculent layer (Miller *et al*., 1998; Roque *et al*., 2014). To better define the components of the Caf1-producing bacterial cultures following centrifugation from *E. coli* BL21 (DE3) cells were transformed separately with four plasmids: pCaf1, pGEMT, pCaf1ΔA, and pCaf1ΔR (Table **2.3** of Chapter **II**). All samples were grown as described above in section 3.2.1 at 35ºC for 3, 7 and 22 h. Five ml samples were then isolated and centrifuged at 4200 rpm (2367 x g) at 22ºC for 15 minutes in 5 ml Eppendorf tubes. Cells containing plasmids pCaf1 or pCaf1ΔR produced a pellet, flocculent and supernatant. Cells transformed with pGEMT or pCaf1ΔA produced only a pellet and supernatant. **Figure 3.4** confirms a lack of a flocculent layer in pCaf1ΔA and the empty plasmid pGEMT, but a flocculent layer was present in the pCaf1 and pCaf1ΔR samples.

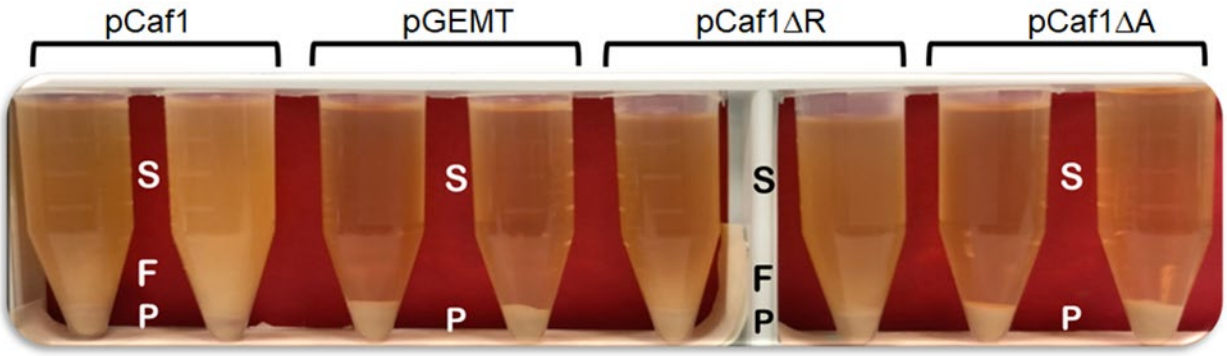

Figure 3.4: Centrifuged Caf1 expressing *E.coli* cultures.

Supernatant (S), flocculent layer (F), and the pellet (P). *E. coli* BL21 (DE3) was separately transformed with four plasmids. Cultures were grown at 35ºC for 7 h, and then 5 ml of samples were centrifuged in Eppendorf tubes at 4200 rpm (2367 x g) for 15 minutes at 22ºC.

The presence of a flocculent layer is considered as an indication of Caf1 polymer expression. To measure the height of the flocculent layer, we relied on using a glass capillary tubes instead of the Eppendorf tubes method, which tends to taper the diameter of the conical tube, affecting the precision of the measurement. The flocculent layer measurement was improved by using 50 µl glass capillary tube as previously described by (Al-jawdah, 2019). These tubes were filled with expression cultures, and the bottom end of the capillary tubes was then blocked with plasticine. The tubes were centrifuged at 2367 x g for 15 minutes supported in a Falcon tube (**Figure 3.5**). Using a ruler, the height of the flocculent layer was measured in mm above the pellet (**Figure 3.6**) and the level of the flocculent layer was found to be proportional with time and Caf1 protein expression level.

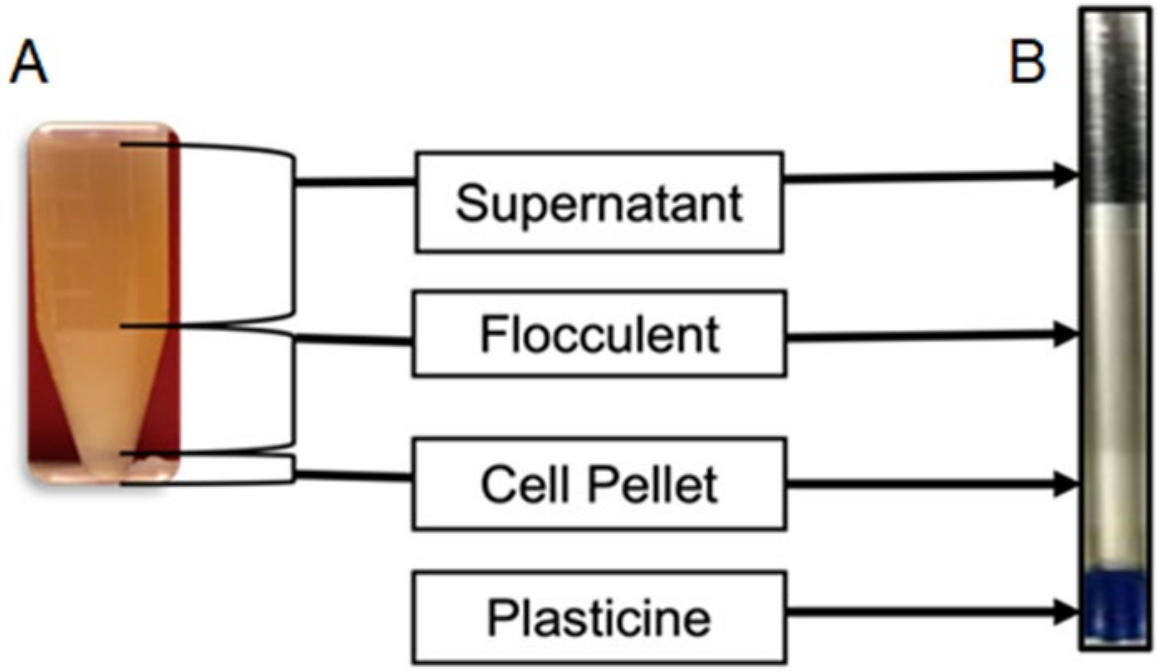

Figure 3.5: Two different methods of Flocculent layer measurement.

(A) Flocculent layer measurement using 5 ml Eppendorf tubes. (B) Flocculent layer measurement using 50 µl glass capillary tubes. Cultures of *E. coli* BL21 (DE3) transformed with pCaf1 and centrifuged at 2367 x g, 22 ºC for 15 minutes. The separation of the layers in the glass capillary tube shows the cell pellet to be above the blue plasticine at the bottom of the capillary tubes. The flocculent layer is in the middle and the supernatant at the top of the glass capillary tubes.

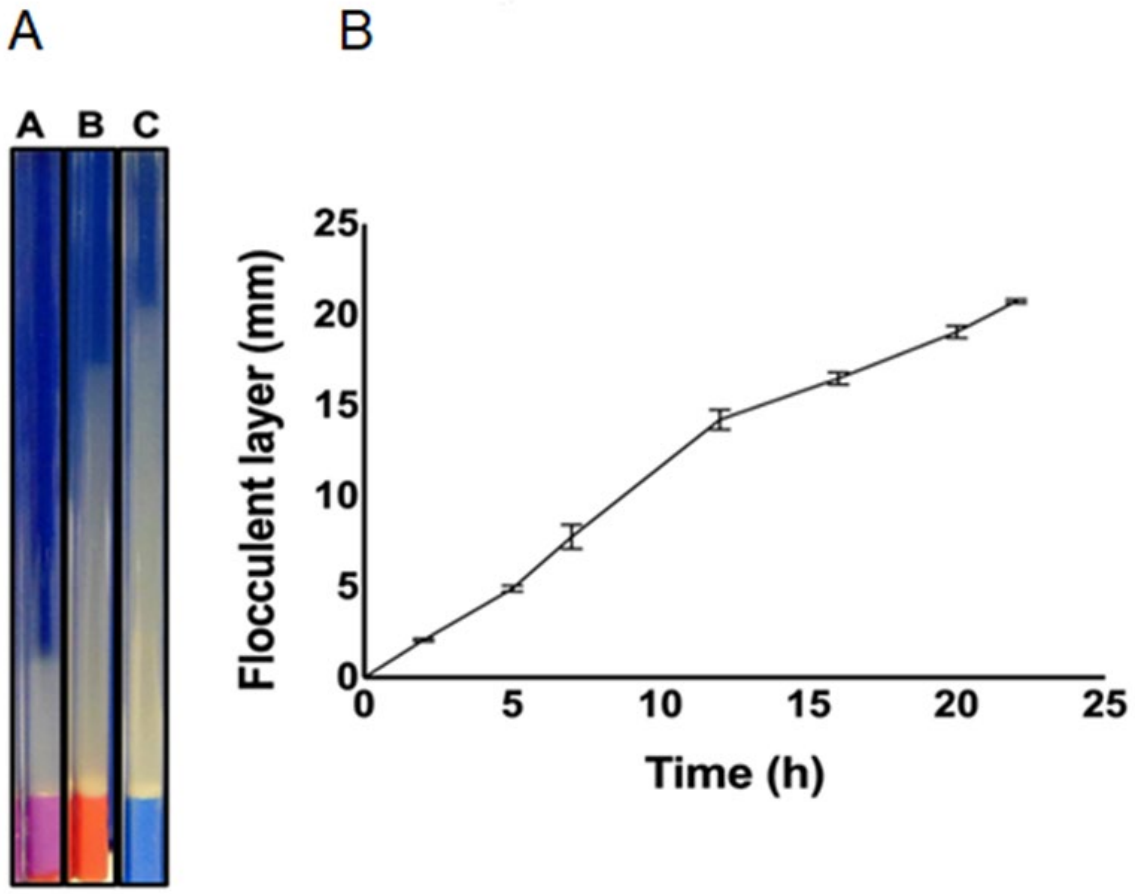

Figure 3.6: Measurement of the flocculent layer height.

(A) Cultures of pCaf1 were grown at 35ºC. (A) Three 50 μl glass capillaries tubes labelled A, B, and C (The remain glass capillaries tubes were not shown). Samples in tubes were taken after 2 (A), 7 (B) and 12 h (C). (B) The curve shows the production of flocculent layer. The height of the flocculent layer was measured using a ruler after the Caf1 expression cultures were centrifuged at 2367 x g in 50 μl glass capillaries tubes supported in a Falcon tube. Error bars represent standard error of the mean. Biological replicate = 3.

A 12% SDS-PAGE was used to analyse all samples (**Figure 3.7**). In the heated (H) flocculent and supernatant samples, a clear band at 15.5 kDa was observed corresponding to Caf1. In the non-heated (N) samples, the flocculent and supernatant samples containing large polymers of undenatured Caf1 did not present with this band. In **Figure 3.3**, Caf1 was produced at 3, 7 and 22 h using the original pCaf1 plasmid. In **Figure 3.7**, four plasmids pCaf1, pGEMT, pCaf1∆A, and pCaf1∆R were examined (**Figure 3.7B&C**). Aside from the control (pGEMT), all the plasmids expressed the *caf1* gene and the Caf1 protein band intensity increased over time from 3, to 7, and to 22 h. As shown in **Figure 3.5,** the flocculent layer was observed in pCaf1 and pCaf1∆R, confirming that the flocculent layer is dependent on the formation of Caf1 surface polymers, which do not form in the absence of the usher Caf1A. Nevertheless, Caf1 does form heat modifiable polymers in the absence of Caf1A as shown by the lack of a monomer band and a high molecular weight band shown clearly in lanes 5 and 6 (**Figure 3.7C)**. This suggests that at least oligomers of 10-20 subunits are forming in the periplasm and that this may be a significant factor in OMV production.

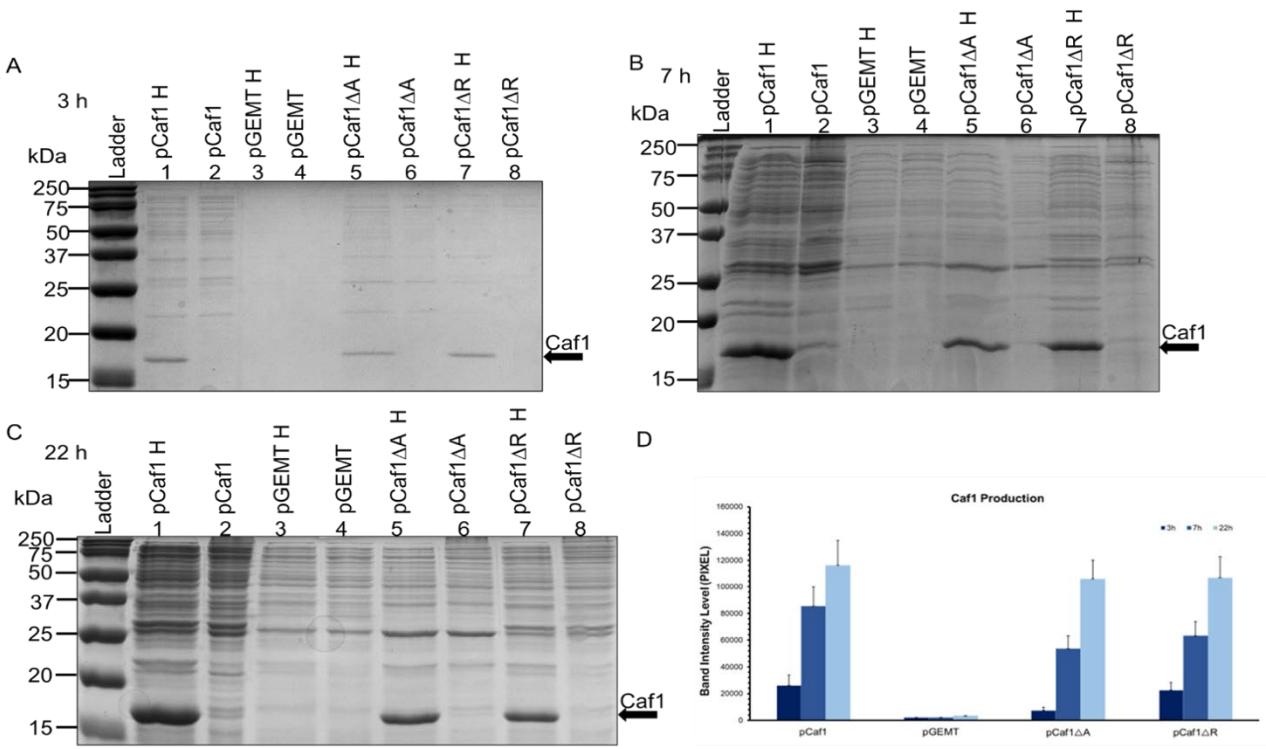

Figure 3.7: Caf1 production from cells containing different plasmids.

E. coli BL21 (DE3) was separately transformed with four plasmids: pCaf1, pGEMT, pCaf1ΔA, and pCaf1ΔR. Pre-cultures were grown at 25ºC for 22 h. The cultures were grown at 35ºC for 3 (A), 7 (B), and 22 h (C) and then centrifuged at 4200 rpm (2367 x g). A 20 μl sample of flocculent and supernatant, and a 20 μl sample of only supernatant in the cultures which produced no flocculent (pGEMT and pCaf1ΔA) were analysed on a 12% Sodium dodecyl sulfate polyacrylamide gel electrophoresis (SDS-PAGE). Samples in lanes 2, 4, 6 and 8 were non-heated (N) and showed no Caf1 bands since large polymers of undenatured Caf1 cannot enter the gel. Samples in lanes 1, 5, and 7, which were heated (H) at 100 ºC for 10 minutes presented a band at 15.5 kDa which is the Caf1 monomer. (D) The graph shows Caf1 band intensity level in pixels as measured by densitometry of the gels shown above (A, B, and C). Error bars represent standard error of the mean. Biological replicates =3.

3.2.3 Analysis of outer membrane content of Caf1 fractions

OMVs are comprised of a bilayer of lipopolysaccharide (LPS) in the outer leaflet and phospholipid in the inner leaflet, both originating from the Gram-negative OM. OMVs are derived by blebbing from the bacterial OM and will therefore contain OMPs and lipids. Furthermore, previous studies have shown that bacterial OMVs can also contain RNA, DNA, cytosolic and periplasmic proteins to aid in virulence factor transport (Beveridge & Kadurugamuwa, 1995). The OMVs originate from the surface of bacteria by poorly defined processes, and several studies have been performed to study the biogenesis of OMVs from the bacterial surface (Deatherage et al., 2009).

To test the hypothesis that Caf1 production increases the amount of OMVs, we measured the presence of OM markers in the supernatant. Firstly, we examined the OMP levels, specifically the abundant porin outer membrane protein F (OmpF). *E. coli* BL21 (DE3) cells were separately transformed using the four plasmids mentioned above (pCaf1, pGEMT, pCaf1ΔA, and pCaf1ΔR). Caf1 was then expressed by growing the cultures for 7 and 22 h at 35°C. Five ml samples were taken and then centrifuged at 4200 rpm (2367 x g). A 20 μl sample of both the flocculent and supernatant from pCaf1 and pCaf1ΔR, and another 20 μl sample of the supernatant from pGEMT and pCaf1ΔA were analysed on a 12% SDS-PAGE. Prior to the analysis, these samples were divided, and one was heated at 100°C for 10 minutes to see whether it produces monomeric OmpF or not (**Figure 3.8**). The lanes corresponding to the heated samples show a protein band at about 37 kDa compatible with OmpF monomer size. The same heated samples were applied to a nitrocellulose membrane to perform a western blot using a rabbit-OmpF antibody and (Goat anti-rabbit alkaline phosphatase as a secondary antibody, the results of which confirmed the appearance of monomeric OmpF (**Figure 3.9**), supporting the results obtained from the SDS-PAGE.

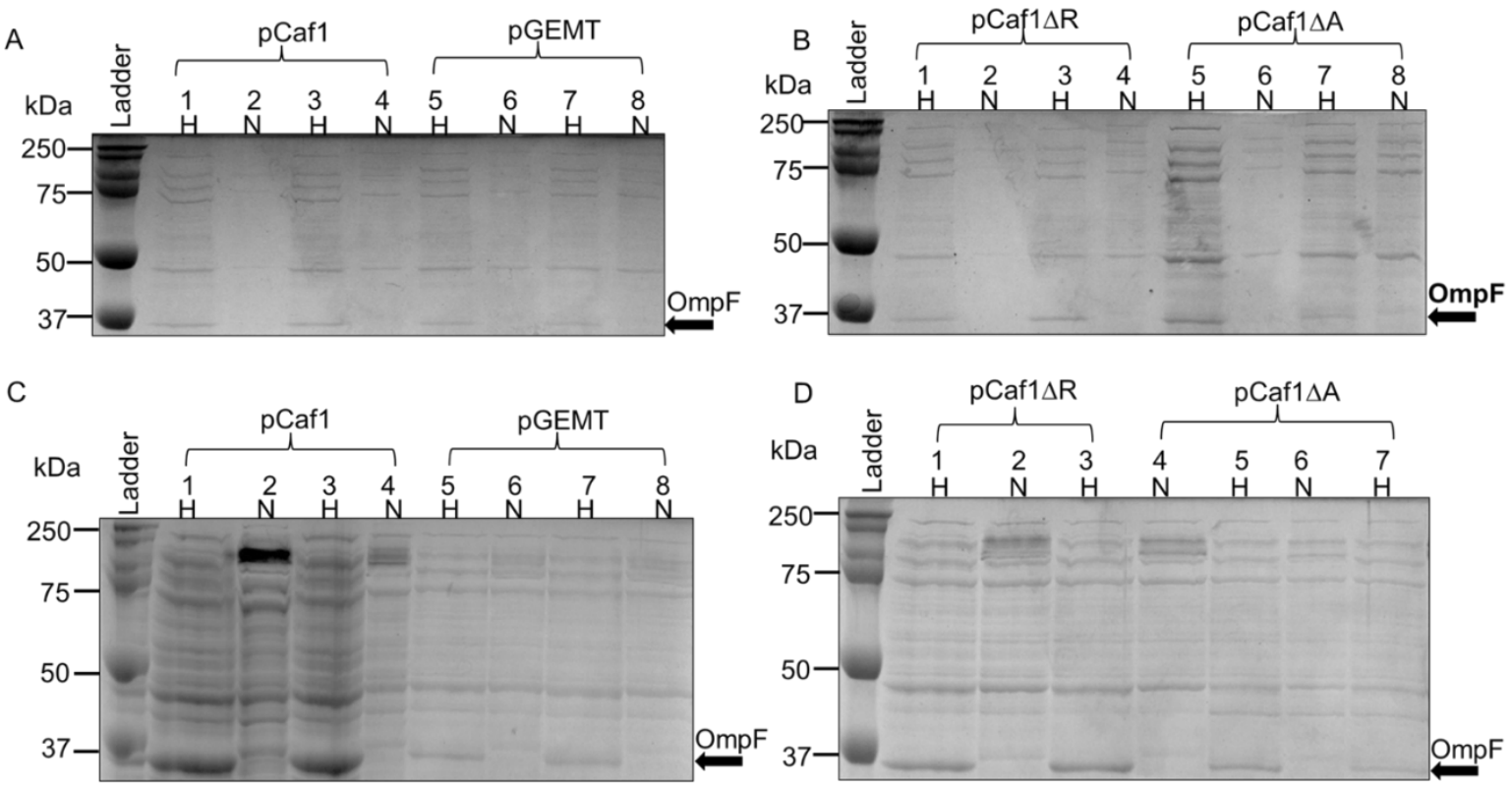

Figure 3.8: Outer membrane protein F (OmpF) in flocculents and supernatants.

A and B) 12% Sodium dodecyl sulfate polyacrylamide gel electrophoresis (SDS-PAGE). *E.coli* BL21(DE3) cells were separately transformed using four plasmids: pGEMT, pCaf1, pCaf1ΔA and pCaf1ΔR. Pre-cultures were grown at 25°C for 22 h. Following incubation for 7 h at 35 ºC, cultures were centrifuged at 4200 rpm (2367 x g) and a 20 μl sample of mixed flocculent and supernatant from pCaf1 and pCaf1ΔR, and then a 20 μl sample of supernatant from pGEMT and pCaf1ΔA were analysed. Heated and non-heated duplicate samples were analysed on the 12% SDS-PAGE and stained with Coomassie Blue. A band at 37 kDa was present in the heated (100 °C for 10 minutes) sample lanes 1, 3, 5, and 7 but not in the unheated samples corresponding to OmpF. C and D) Repeat of the description for images A and B but following incubation for 22 at 35 ºC.

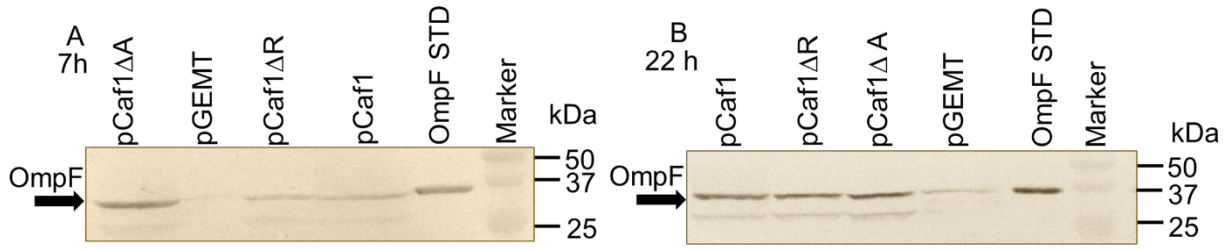

Figure 3.9: Western blot analyses of OmpF levels in supernatant and flocculent samples.

Samples of the same cultures mentioned in Figure 3.7 and the positive control (OmpF STD) were all heated, loaded and then separated on SDS-PAGE. After blotting OmpF was detected using a rabbit anti- OmpF antibody and secondary antibody (Goat anti-rabbit alkaline phosphatase conjugate). OmpF STD = Outer membrane protein F standard.

3.2.4 Dot blot analysis for Lipopolysaccharides (LPS)

The second OM marker we used to detect the presence of OMVs was LPS. The levels of LPS in cell culture supernatants and flocculants were measured after 7 and 22 h of cell culture using a sheep anti-LPS (*E. coli J5*) antibody in a dot blot as previously described in Section 2.6 of Chapter II. **Figure 3.10** demonstrates that LPS production was highest in pCaf1ΔA following 7 h of cell culture (**Figure 3.10A**) and had the highest density of LPS based on the pixel number at 7 and 22 h of cell culture (**Figure 3.10B**), which was significantly higher than pGEMT at both time points (p< 0.05). This most likely indicates an increase of OMVs in the supernatant when there is no flocculent layer to trap the OMVs. Also, a higher density of LPS based on pixel number was observed in pCaf1ΔR when compared to pCaf1 (**Figure 3.10B**), which is associated with Caf1 production, however, there was a lower LPS level than pCaf1ΔA, which may have been due to the OMV being trapped in the flocculent layer. Furthermore, pGEMT (control) does not carry the *caf1* operon and had the least LPS in the supernatant (**Figure 3.10**). The one-way ANOVA statistics revealed that there was a significant difference between pCaf1ΔR and pCaf1ΔA in both of the supernatant cell cultures at 7 and 22 h (p<0.0001). These findings are consistent with the data presented in **Figure 3.7**.

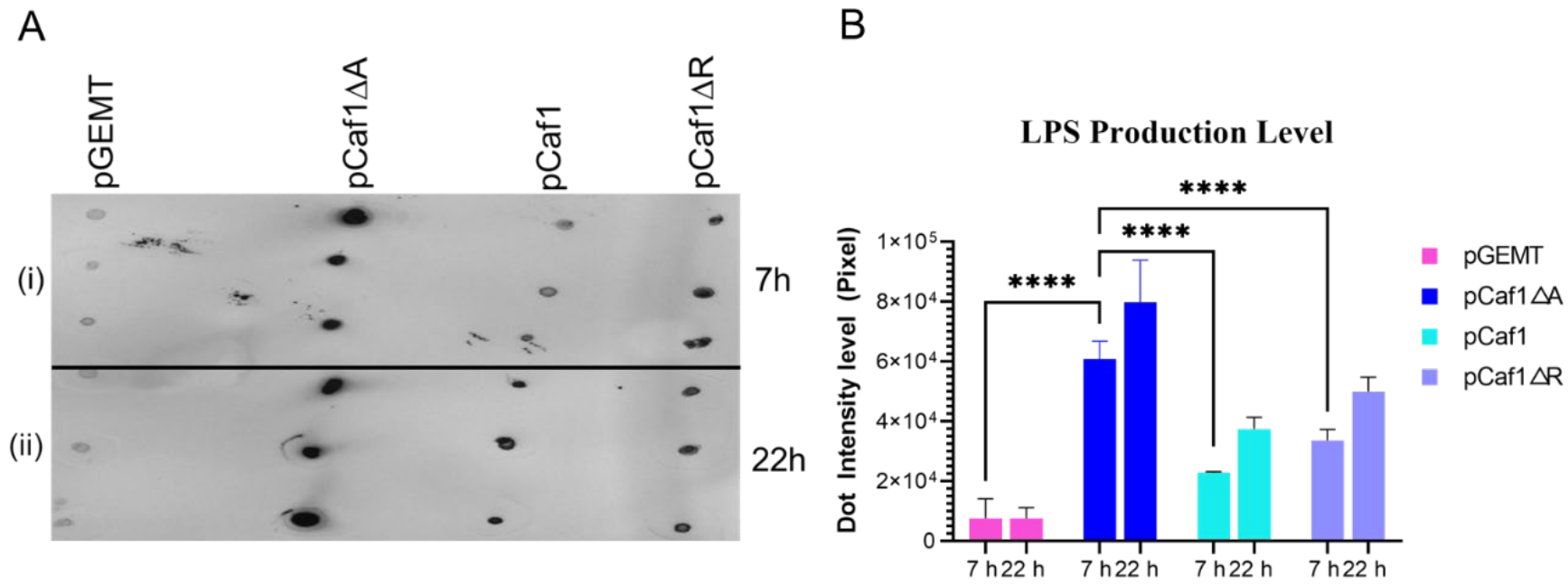

Figure 3.10: Analysis of lipopolysaccharide (LPS) amounts in the supernatants and flocculents

(A) Dot blot analyses of LPS release after culture for 7 and 22 h. Samples of the same cultures are analysed as those in Figure 3.7. A volume of 0.5 µl of mixed flocculent and supernatant from pCaf1 and pCaf1ΔR, and then a 0.5 µl samples of supernatant from pGEMT and pCaf1ΔA were added to a nitrocellulose membrane (0.45 µm) before being air dried for 2 minutes. A sheep anti-LPS and anti-sheep alkaline phosphatase antibody were used as the primary secondary antibody, respectively. (B) Bar graph of LPS quantification based on pixel number of band intensity level. Image J software was used for the dot blot analysis. The background density was subtracted. Error bars represent standard error of the mean. Asterisks represent significant differences between groups (**** denotes statistically significant $p<0.0001$) as determined by one way ANOVA. Biological replicates = 2.

3.2.5 Transmission Electron Microscopy (TEM)

E.coli BL21(DE3) were separately transformed with four plasmids (pGEMT, pCaf1ΔA, pCaf1ΔR, or pCaf1) previously described were used to produce samples for the TEM for imaging of OMVs. A 10 µl of each OMV sample was added to a carbon. Then negatively stained with 2% uranyl acetate. The method was adapted from the single droplet method (Harris, 2007; Harris *et al.*, 2014). **Figure 3.11** depicts OMVs in supernatant samples. Artefacts from sample preparation were visible, especially in pCaf1 samples that had a very dark stain, making it difficult to observe OMVs and construct comparisons among the samples. In the pCaf1ΔA plasmid, vesicles can be seen in abundance due to the absence of the flocculent layer, indicating that OMVs cannot be trapped and can be easily released in the supernatant as shown in **Figure 3.11B.**

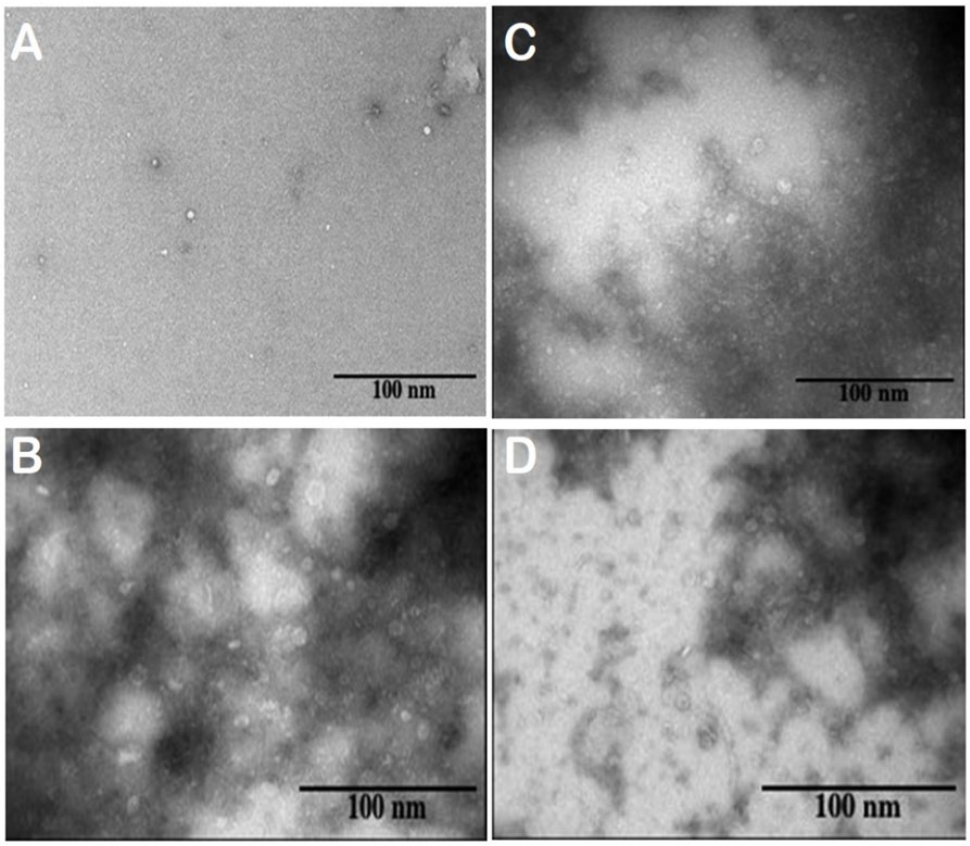

Figure 3.11: Transmission electron microscopy (TEM) of Outer Membrane Vesicles (OMV).

Initial examination of OMVs from supernatant samples. OMVs from *E. coli BL21* cultures transformed with A) pGEMT, B) pCaf1ΔA, C) pCaf1ΔR and D) pCaf1 were negatively stained with 2% (w/v) uranyl acetate. Initial examination of OMVs depicts artifacts from sample preparation. Images B, C, and D present with dark staining, making it difficult to observe OMVs. Vesicles in the pGEMT are small and scattered, whereas in the pCaf1ΔA sample the vesicles are visible. Images were captured using a HITACHI 7800 electron microscope at 100 kV in the EM Research Service at Newcastle University. Digital images were taken using the EMSIS XAROSA CMOS camera with RADIUS software (EMSIS GmbH). Image size 5120x3180 pixels.

3.2.6 Isolation of OMVs using ultracentrifugation

Ultracentrifugation is the most commonly utilised method for isolating vesicles as it outperforms other methods, including size-exclusion chromatography, with regards to sample preparation (An *et al*., 2018). The steps of a proposed modified ultracentrifugation approach used here to isolate OMVs is depicted in **Figure 2.2** of Chapter **II** section **2.4.1**. Briefly, the expression cultures of the plasmids were centrifuged at 2367 x g for 20 minutes at 4ºC to remove bacterial cells and debris. The collected supernatant containing the OMVs was then centrifuged at 10000 x g for 45 minutes and the pellet was discarded. Then the supernatant was ultracentrifuged at 100,000 x g for 90 minutes at 4ºC. To enhance OMV purity, the resulting pellets were resuspended in phosphate buffer saline (PBS) at pH 7.4, and then ultracentrifuged further at 100,000 x g for 90 minutes at 4ºC. The pellets were then resuspended in 5 ml PBS and stored at -20ºC for further analysis. This method was applied to cells transformed with plasmids pCaf1∆A and pCaf1∆R to test its efficacy. The results of OMVs examination from these samples using TEM are presented in **Figure 3.12**. We also used the modified ultracentrifugation approach to test the effects of different Caf1 mutants on OMV production as will be shown in the next section

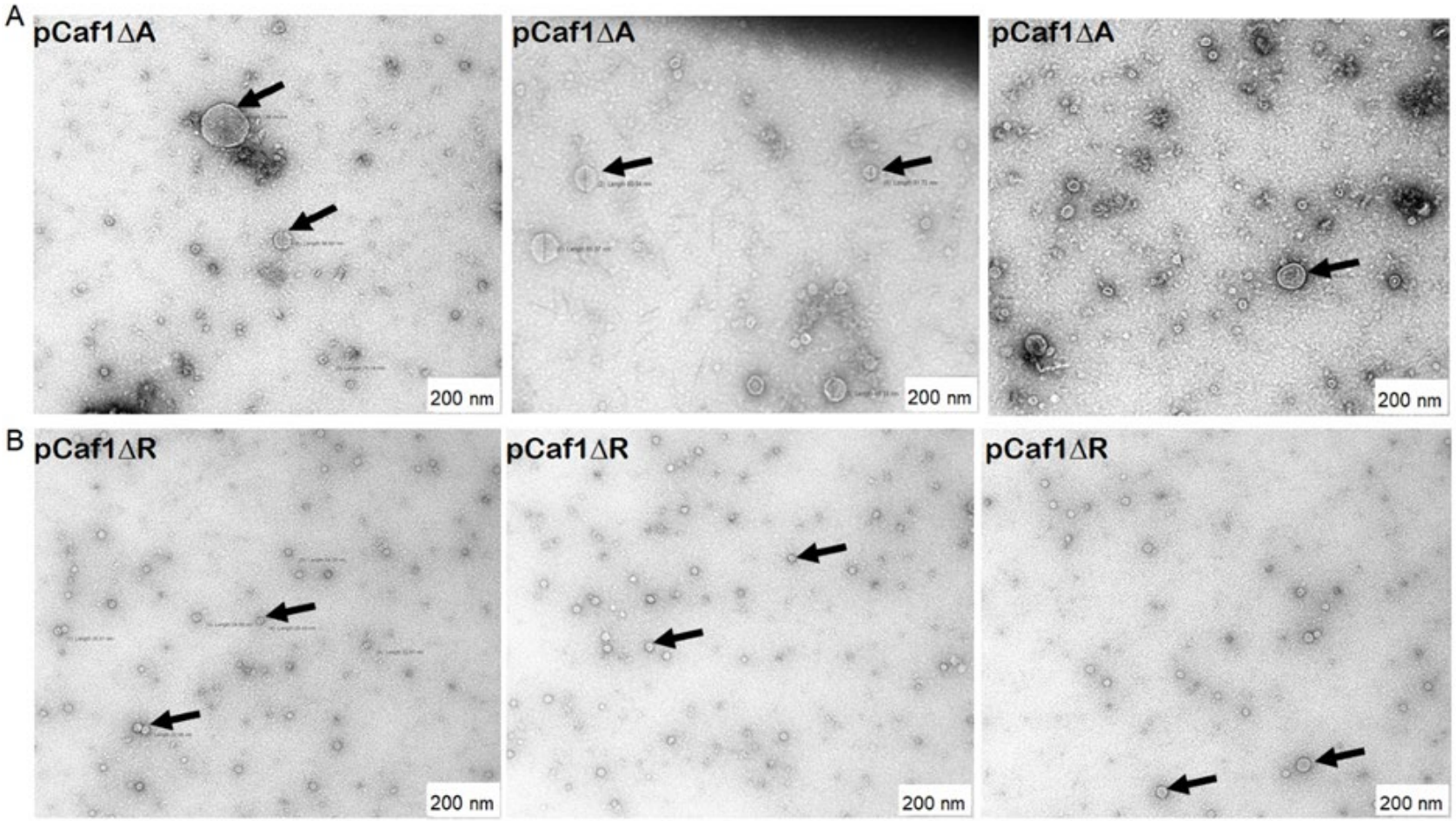

Figure 3.12: Transmission Electron Microscopy (TEM) of Outer Membrane Vesicles (OMVs).

OMVs were prepared using the modified ultracentrifugation approach. (A) The OMV from pCaf1ΔA cultures have a well-defined membrane. The OMV sizes range from 30 nm to 135 nm. (B) In the pCaf1ΔR sample, the OMVs are smaller than those present in pCaf1ΔA and their diameter sizes range between 22 nm to 67 nm

3.2.7 Effect on OMV production of adding a Flag tag to caf1M

3.2.7.1 The Chaperone protein Caf1M

It has been well established that the chaperone Caf1M is essential for preventing Caf1 subunit aggregation and for the formation of Caf1 subunits into thick gel-like structures in *Y. pestis* (Galyovl et al., 1991; Zavialov et al., 2001). However, it remains unclear if Caf1 will be degraded quickly or simply aggregate in the absence of caf1M. With no specific antibody for Caf1M, we added a FLAG tag to Caf1M in the pCaf1ΔA. As described in Section **3.2.3**, the production of OMVs is increased in the *caf1A* gene deletion background. The in-fusion technique described in Section **2.7** of Chapter **II** was used to carry out the addition of the FLAG tag sequence to the *caf1M* gene. Polymerase chain reaction (PCR) primers for *caf1M* were designed using a 15-bp (5') tail that was complementary to the linearised vector end of the *caf1M* gene (**Table 3.1**). The results of the addition of the Flag tag to the C-terminus of Caf1M are shown in **Figure 3.13**. In order to ascertain if the Caf1M FLAG was functional, we investigated whether adding a FLAG tag to the *caf1M* gene had any influence on OMV production. Using western blot and dot blot analyses, we observed that the FLAG tag added onto Caf1M did not have any effect on OMV production and we found no significant difference in the levels of either OmpF or LPS in the OMV samples of pCaf1ΔA and pCaf1ΔAM^{Flag} (**Figure 3.14A and B**).

Table 3.1: Oligonucleotide primers for the Flag tag insertion into caf1M gene

Primer	Nucleotide sequence (5' to 3')
Forward *Caf1M*^{FLAG}	AAA GAT GAT GAT GAT AAA TAA TGA TGA TTA AAG GGG ACG GG
Reverse *Caf1M*^{FLAG}	ATC ATC ATC ATC TTT ATA ATC TAA AGT CAC ATT TTT GGA ATA CAA

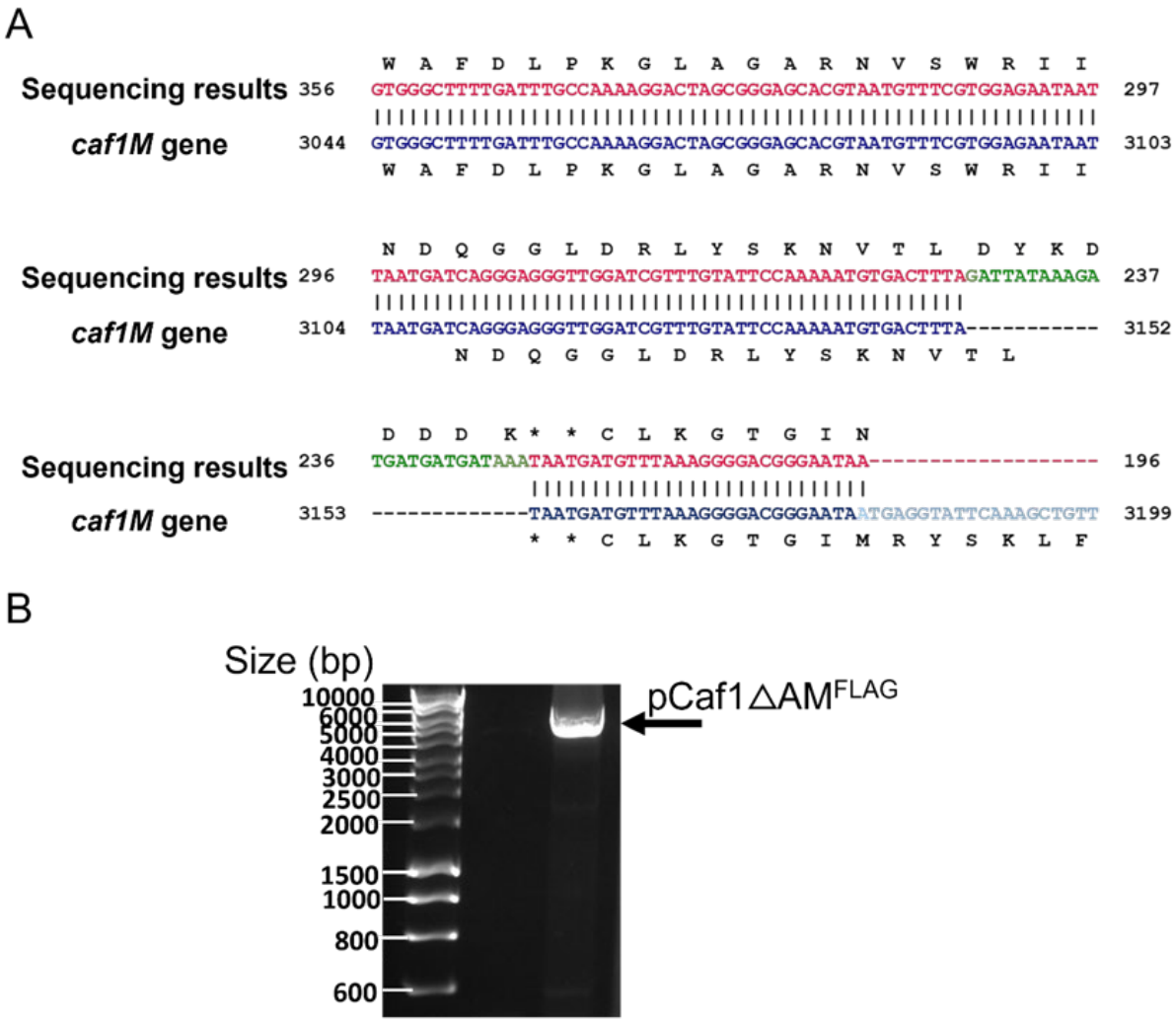

Figure 3.13: Addition of a FLAG tag to the 3' end of the *caf1M* gene.

(A) Eurofins Genomics sequencing results of the polymerase chain reaction product shown in red colour. The sequencing results show the insertion of a FLAG tag sequence at the C-terminus of the *caf1M* gene (green colour). Sequence 2 shown in blue colour is c*af1M* gene (GenBank accession number P26926) from the *caf* operon. (B) A 0.8 % agarose gel of the Caf1M FLAG plasmid preparation stained with Midori Green Advance DNA stain showing a band at approx. 5kbp which is size of the linearised pCaf1ΔAM^{FLAG} (5049 bp) Obtained from PCR reaction as described in Section **2.3.1** of Chapter **II**.

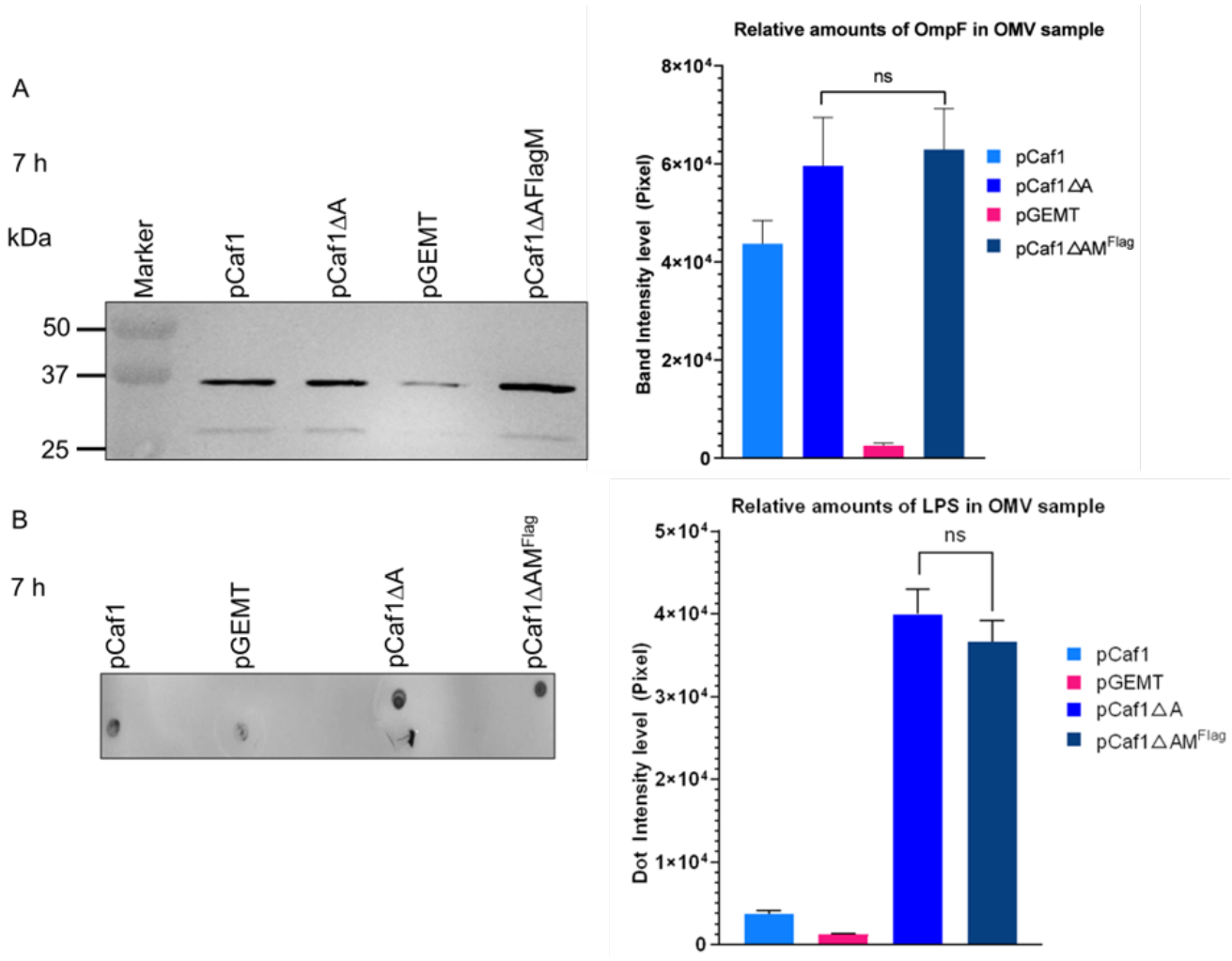

Figure 3.14: Effect of adding a FLAG tag to Caf1M on outer membrane vesicles (OMVs) production.

A) western blot to detect OmpF level was prepared by transferring OMV samples prepared by the modified ultracentrifugation method from SDS-PAGE onto a nitrocellulose membrane. Samples were analysed using a rabbit anti-OmpF and goat anti-rabbit alkaline phosphatase conjugate as the primary and secondary antibodies, respectively. The bar graph depicts densitometric quantification of OmpF bands using Image J. Biological replicates = 2. (B) A demonstration of a dot blot to detect LPS. OMVs samples were diluted 1 in 10. The dot blot was prepared by taking a 0.5 μl from the diluted OMVs and was added to a nitrocellulose membrane. A sheep anti-LPS polyclonal and anti-sheep alkaline phosphatase conjugated were used as the primary and secondary antibodies, respectively. Densitometric quantification of the LPS dots was performed using image J. Error bars represent standard error of the mean. For A and B, one way ANOVA was used to test for statistical significance of the differences among the samples. (ns denotes not significant).

3.2.8 Effect of caf1M or caf1 deletions on OMV production

We employed the in-fusion cloning technique described in Section **2.3.2** of Chapter **II** to examine the effect of deleting *caf1* on OMV production. To delete the *caf1* gene, the plasmid pCaf1ΔAM^{FLAG}Δcaf1 was constructed by deleting *caf1* gene from the pCaf1ΔAM^{FLAG} using in-Fusion high definition (HD) (**Figure 3.15**). PCR primers for the *caf1* gene were designed, and they included 15-bp overlaps with each other at their 5' ends and the bases to be deleted were omitted (**Table 3.2)**. For the insertion of a stop codon to pCaf1ΔAM^{FLAG}, PCR primers were designed with 15-bp (5') tail complementary to the linearised vector end (**Table 3.3**).

Table 3.2: Oligonucleotide primers for the deletion of caf1 gene.

Primer	Nucleotide sequence (5' to 3')
Forward *Δcaf1*	CGA TAG AGG TAA TAT GAA TTC CCC AAT CAC TAG TGA ATT CGC
Reverse *Δcaf1*	ATA TTA CCT CTA TCG AAT AAT CCA ATC

Table 3.3: Oligonucleotide primers for *caf1M* stop codon.

Primer	Nucleotide sequence (5' to 3')
Forward caf1*M^{FLAG}	TTAAGTACGTAATAATTAGGAATTATTACTTTCGGCATGC
Reverse caf1*M^{FLAG}	TTATTACGTACTTAATCTATTTAAAATCATGAG

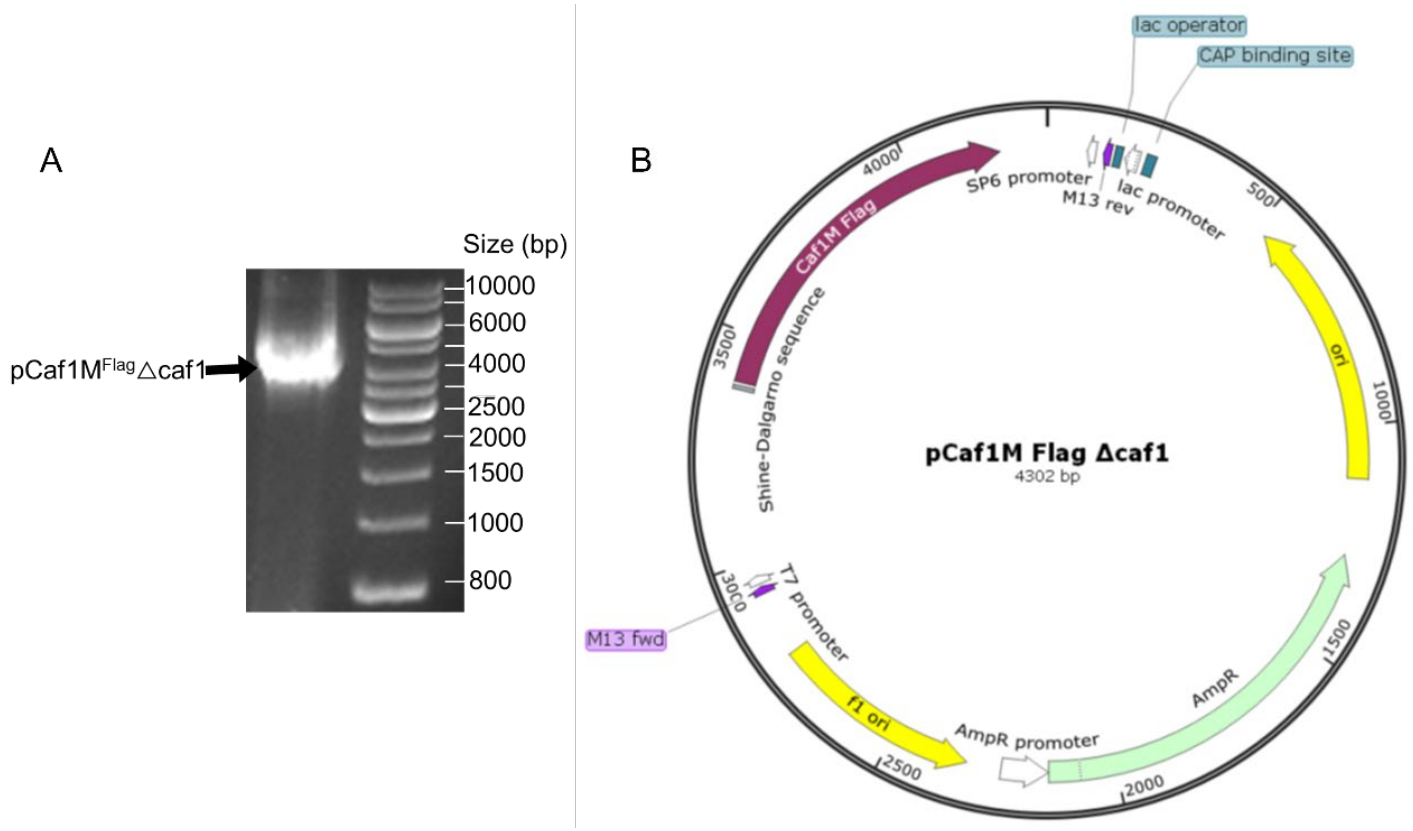

Figure 3.15: Deletion of *Caf1* gene.

(A) 0.8 % agarose gel of the deleted *caf1* plasmid preparation stained with Midori Green Advance DNA stain. A band is presented at approximately 4 kbp which is the size of the linearised pCaf1ΔAM^{FLAG}Δcaf1 (4302 bp).(B) Plasmid map of the new plasmid p Caf1ΔAM^{FLAG}Δcaf1. The new plasmid contains only the *caf1M* gene flagged .

We inserted a stop codon at the start of the *caf1M* gene to terminate *caf1M,* the new plasmid is called pCaf1ΔA*M^{FLAG}. *E.coli* BL21(DE3) cells were separately transformed with six plasmids:pCaf1,pGEMT,pCaf1ΔAM^{FLAG},pCaf1ΔAM^{FLAG}Δcaf1, pCaf1ΔA and pCaf1ΔA*M^{FLAG}. To induce Caf1 expression, the cells were cultured for 7 h at 35°C. OMV samples from each culture were prepared as described previously in this chapter (**Section 3.2.6**). *Y. pestis* F1 antigen antibody was used to confirm the presence of the Caf1 band. A western blot was used to confirm the Caf1 band using the monoclonal anti-Caf1 antibody. The results of this analysis are shown in **Figure 3.16**.

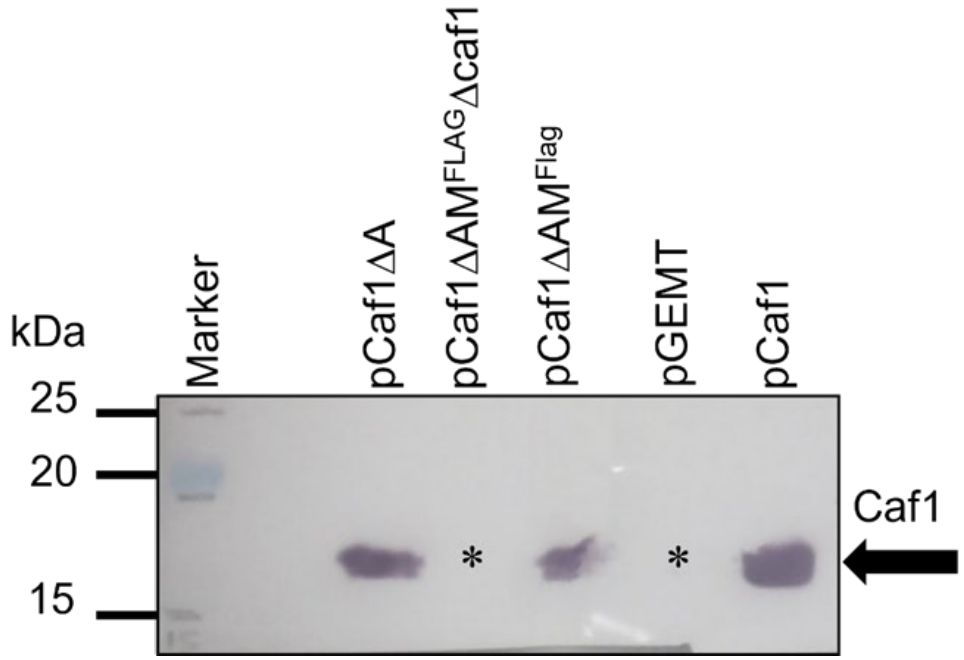

Figure 3.16: Western Blot Analysis to determine the level of Caf1 in the different OMV samples.

The *caf1* gene was detected using the mouse monoclonal anti-Caf1 antibody. OMV pellet samples were prepared as mentioned previously in section **3.2.6** of this chapter. A clear band at 15.5 kDa is depicted in the pCaf1ΔA, pCaf1M^{FLAG}, and pCaf1 samples. The pCaf1M^{FLAG}Δcaf1 has no band confirming the deletion of the caf1 gene. (∗) = Absence of Caf1. pCaf1 is a loading control.

To confirm the deletion of the *caf1M* gene, *E. coli* BL21 (DE3) cells were separately transformed with pCaf1M^{FLAG} a standard from (Al-jawdah, 2019), pCaf1ΔA*M^{FLAG}, pCaf1ΔAM^{FLAG}, and PGEMT. To induce Caf1 expression, cells were incubated for 7 h at 35°C, and then OMV samples from each culture were prepared as described above. Western blotting was utilised to confirm a Caf1M band by using the monoclonal anti-flag (**Figure 3.17)**.

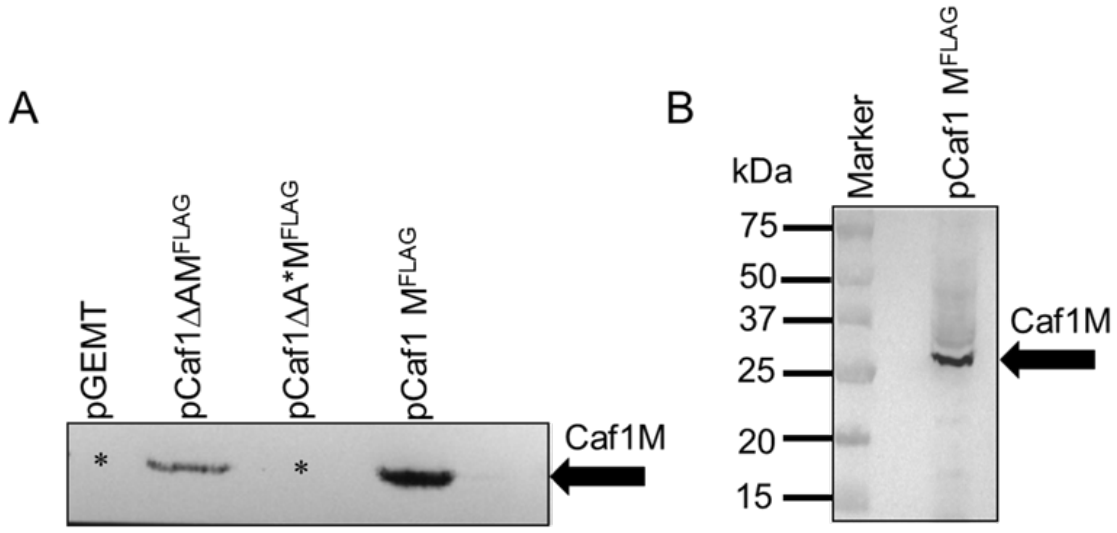

Figure 3.17: Western blot analysis to detect Caf1M in different OMV samples.

(A) Western blot of Caf1M protein from OMV samples, detected using anti-FLAG antibody. No band is evident in the pCaf1ΔA*M^{FLAG} confirming the effective insertion of the stop codon at the *caf1M* gene. (∗) denotes the absence of Ca1M. (B) Western blot of pCaf1M^{FLAG}. showing Caf1MFlag at 26.5 kDa.

Both, the knockout of *caf1* or the insertion of a stop codon at the beginning of *caf1M* resulted in a large decrease in Caf1 expression (**Figure 3.18**). However, for each knockout OMV production is much higher than pGEMT showing that OMV production can be induced by either Caf1M or Caf1 production and that both together produce the most OMV. (**Figure 3.19**). However, the high levels of oligomeric Caf1 in pCaf1ΔA derived OMVs indicates that they contain large amounts of Caf1 derived from the periplasm. The ANOVA statistical test revealed no significant differences in OMV Caf1 levels between

pCaf1ΔA and pCaf1ΔAM^{FLAG} (p> 0.05) (**Figure 3.19A**). Moreover, we found no statistically significant difference in LPS levels between pCaf1ΔAM^{Flag}Δcaf1 and pCaf1ΔA*M^{FLAG}. However, there was a significant difference between pCaf1ΔA and both pCaf1ΔAM^{FLAG}Δcaf1 and pCaf1ΔA*M^{FLAG} (p< 0.0001).

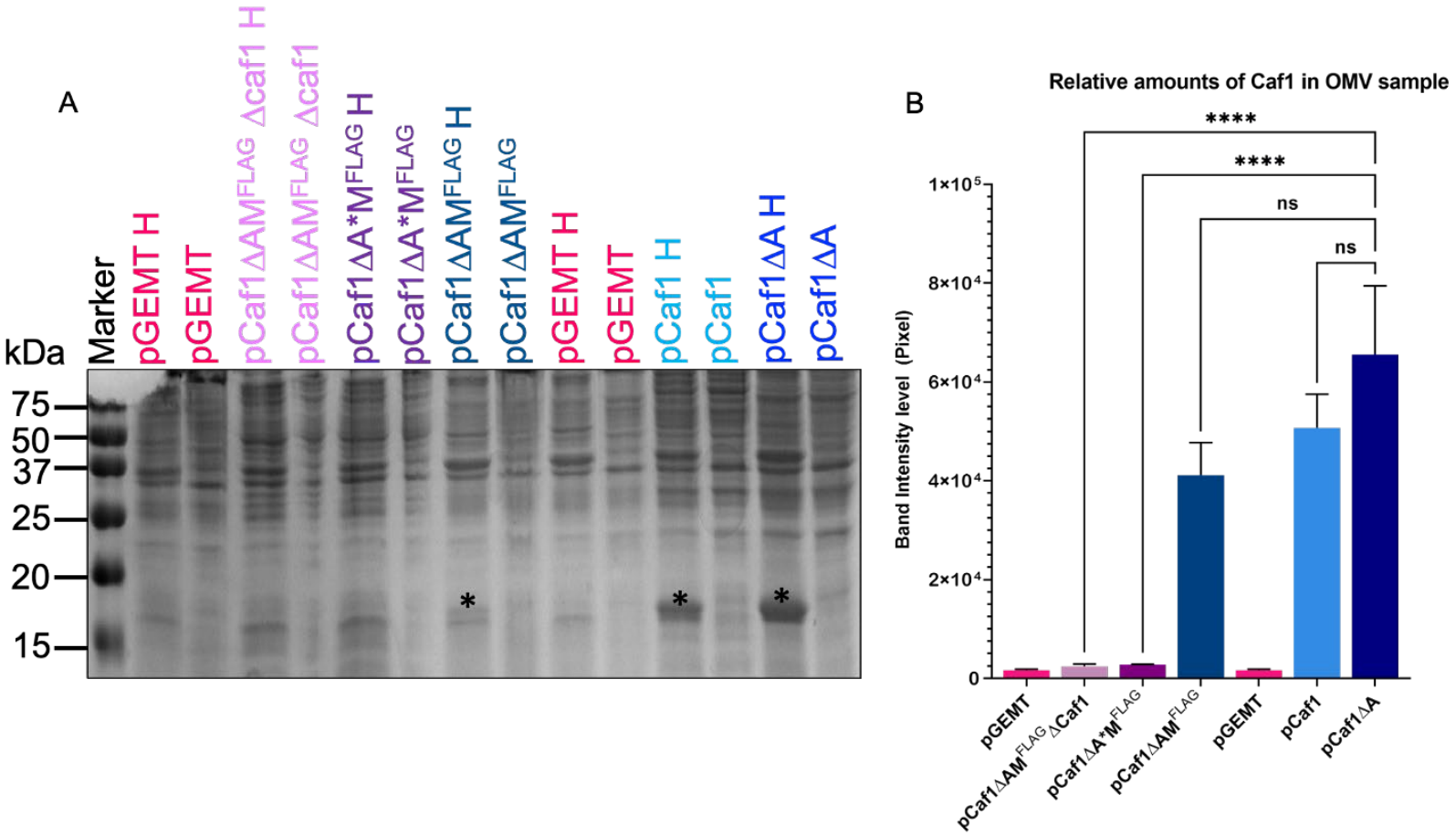

Figure 3.18: Effect of deletion of caf1M gene and caf1 gene on Caf1 levels in Outer Membrane Vesicles (OMV).

(A) Sodium dodecyl sulfate polyacrylamide gel electrophoresis (SDS-PAGE) analysis for Caf1 production. *E. coli* BL21 (DE3) cells were separately transformed with the 6 plasmids listed in Table 2.4 (pGEMT, pCaf1ΔAM^{FLAG}Δcaf1 and pCaf1ΔA*M^{FLAG} ,pCaf1ΔAM^{FLAG}pCaf1 and pCaf1ΔA). Cultures were expressed at 35°C for 7 h, and OMVs were prepared by the modified ultracentrifugation technique at 2367 x g, 10,000 x g, and 100,000 x g, respectively, as described in section 3.2.6. (B) Bar graph depicting densitometric quantification of Caf1 bands using Image J. All samples were heated at 100 ˚C. Asterisks denote significant differences between groups (****, p<0.0001) determined by one way ANOVA test. Biological replicates = 3

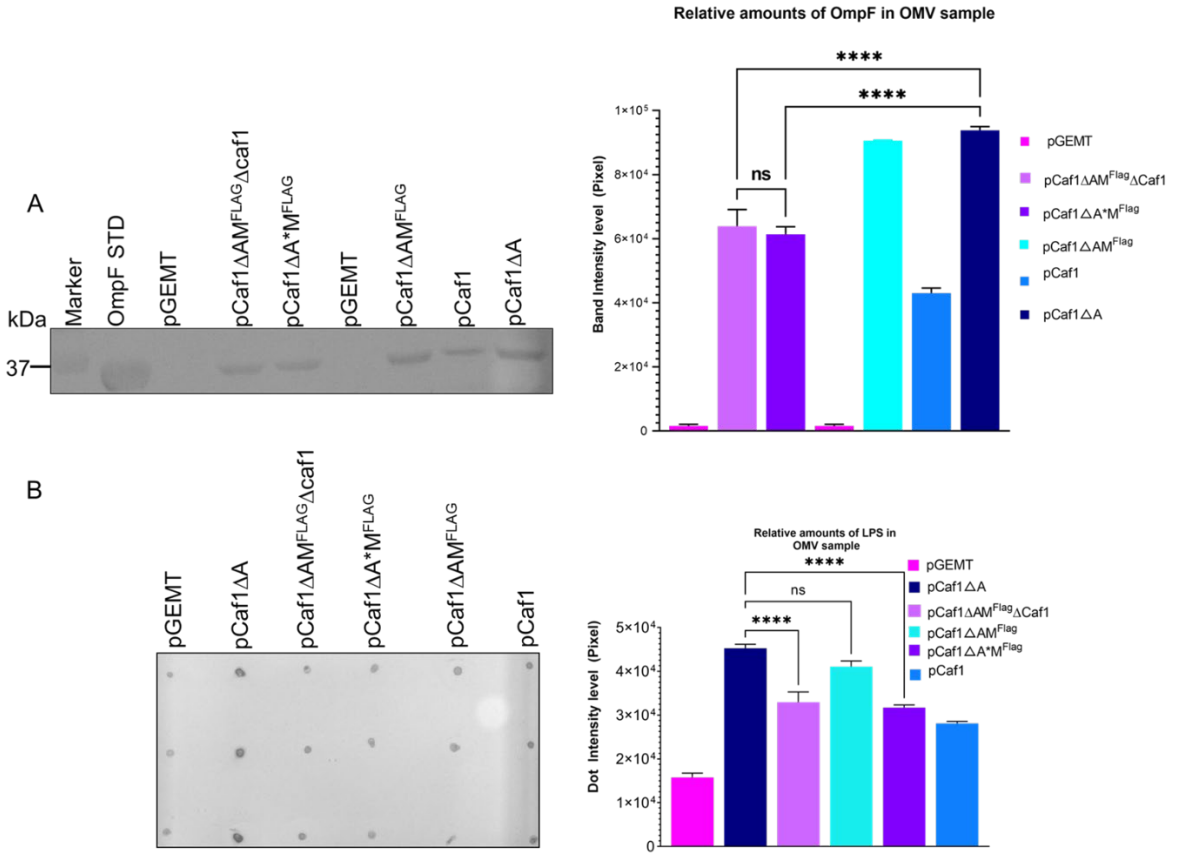

Figure 3.19: Effect of *caf1M* and *caf1* gene deletions on Outer Membrane Vesicles (OMV).

(A) Western blot analysis of OmpF levels in the same OMV preparation as in Figure 3.18. All Caf1 plasmids promote OMV production. Deletion of Caf1A caused a significant increase in OMV production. In contrast, OMV production decreases when this deletion is accompanied by deletions of either *caf1* or *caf1M* in comparison with *caf1A* gene deletion . Furthermore, both the knockout of *caf1* gene or the insertion of a stop codon at the start of *caf1M* gene resulting in an increase of OMV production in comparison with pGEMT, due to either an increase in the accumulation of Caf1 oligomers or accumulation of Caf1M in the periplasm. This increase will create a stress on the cell and enhance the production of OMV. Therefore, OMV production is increased when any protein is overexpressed in the periplasm. (B) Dot blot analysis of LPS levels shows a significant increase in OMV production due to the deletion of the *caf1A* gene. There was a statistically significant difference between pCaf1ΔA and pCaf1ΔAM^{FLAG}Δcaf1 or pCaf1ΔA*MFlag. There were no significant differences between pCaf1ΔA and pCaf1ΔAMFlag. Error bars represent standard error of the mean. Asterisks represent significant differences between groups (**** denotes statistically significant p<0.0001, and ns represents not significantly as determined by one way ANOVA test. Biological replicates = 3

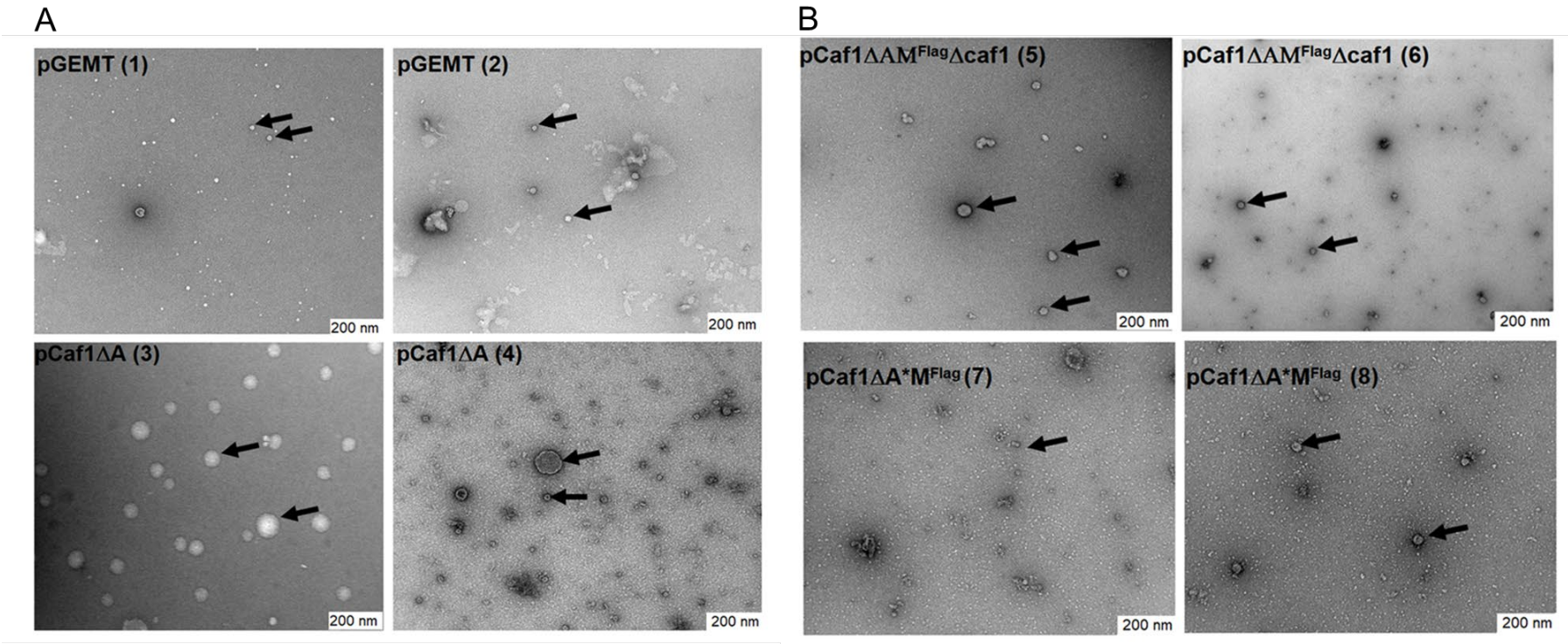

Figure 3.20: Electron microscopy of outer membrane vesicles (OMVs).

The images depict OMV samples from cells transformed with their respected plasmids. The differences in contrast between the image result from the grid preparation resulting in a variation in the depth of the uranyl acetate. Areas of positive stains are evident when the uranyl acetate stains the particle instead of sitting around it. The arrows show the vesicles with negative stain (darker edges). In images 5 through 8, vesicles are small, deteriorated and not well roundly shape.

3.3 Discussion

Since the 1960s, different models have been proposed to describe the formation of OMVs (Mashburn-Warren *et al.*, 2006b). All accumulated knowledge about OMV biogenesis agree that OMV production results from bulging or pinching off of the OM (Kudryakova *et al.*, 2016). However, how OMVs are produced and are able to perform their functions and what factors are involved in their formation are questions that have remained without definite answers. In this study, we focused on the actions of Caf1 to form OMVs from the bacterial OM. Based on previous unpublished data from our laboratory research group, we formulated the hypothesis that the flocculent layer is composed of OMVs trapped in the polymeric network of Caf1, and that Caf1 production is able to provoke the formation of OMVs. The experimental work presented in this chapter seeks to test this hypothesis. Furthermore, this study aims to examine whether the deletion of the *caf1A* gene has any impact on hypervesiculation and LPS levels.

Here we presented evidence for the presence of a flocculent layer as an indicator of Caf1 polymer production in bacterial cells following the separation of the cell pellet and supernatant by centrifugation of Caf1 producing cultures. Caf1 polymers are formed by the chaperone-usher pathway, which is the most common assembly mechanism of pili in bacteria belonging to the *Enterobacteriaceae* family and therefore deletion of either the chaperone or usher are likely to have significant effects on Caf1 polymer levels (Choudhury *et al.*, 1999). Miller *et al.* (1998) demonstrated that recombinant Caf1 polymer is the most dominant protein component of the flocculent layer and that the centrifugation of Caf1 producing cultures resulted in the separation of the capsule material, which subsequently formed the flocculent layer above the layer of sedimented bacterial cells. Using Coomassie-stained SDS-PAGE and western blot analyses, we confirmed that the flocculated material present in the studied bacterial cultures predominantly contained Caf1 polymers and OMVs. We found that OMVs produced by pCaf1 are retained by a network of polymeric Caf1 to produce the flocculent layer. We used a glass capillary tube method to measure the height of the flocculent layer present in each of the Caf1 producing cultures, primarily for the purposes of ensuring measurement, separation accuracy and efficiency in the use of bacterial culture volume. This method has been proven to be useful in serving these aims (Al-jawdah, 2019). The results presented here indicate that the level of the

flocculent layer was proportional to time (**Figure 3.6**) and the expression of Caf1 (**Figure 3.7**).

We used the finding that Caf1 and OMVs are major constituents of the flocculent layer to examine whether Caf1 production increases the amount of OMVs. For this we analysed the concentrations of OmpF and LPS to serve as markers of OMVs. It has been shown that OMVs contain an abundance of OMPs, such as OmpF (Rao *et al.*, 2020), and LPS (Vanaja *et al.*, 2016). An SDS-PAGE analysis of Caf1 producing cultures performed here also showed a protein band that is similar in size to OmpF. The presence of monomeric OmpF in the heated samples was further confirmed by a western blot. Our results based on a dot blot analysis showed high levels of LPS in the supernatant of cultures where the Caf1A usher has been deleted (pCaf1∆A), implying that the absence of the flocculent layer to trap the OMVs could be accountable for increases in the OMV levels in the supernatant.

In our examination of the effects of the deletions of *caf1*, *caf1A* and *caf1R* genes on flocculent and OMVs production, we found that a flocculent layer was present only in pCaf1 and pCaf1∆R, indicating that the flocculent is Caf1 and Caf1A dependent. We also observed that the pCaf1 flocculent had lower density of LPS , and therefore OMVs, than that of pCaf1ΔR. This result is consistent with previous findings that Caf1 expression increases when Caf1R is deleted (Karlyshev *et al.*, 1992a; Al-Jawdah *et al.*, 2019). However, the lower LPS levels of pCaf1 and pCaf1∆R in supernatant samples as compared to that of pCaf1ΔA may be attributed to OMVs being trapped in the flocculent layer (**Figure 3.19B**). As a result of their analysis of a *Y. pestis* ∆*caf1A* mutant, the work of Runco *et al.* (2008) demonstrated that the Caf1A is required for Caf1 assembly and secretion, and therefore, the increase in OMV production we observed using TEM in the supernatant of pCaf1∆A cultures confirms that OMVs are not trapped in the Caf1 polymer network leading to the absence of the flocculant layer. A western blot study of OmpF and LPS levels revealed that Caf1A deletion resulted in a considerable rise in OMV production, which diminished if the Caf1A deletion was coupled with knockouts of Caf1 or Caf1M. However, both deletions are sufficient to produce a lot of OMVs, much more than pGEMT. Our results thus demonstrated that OMV production is not only dependent on significant levels of Caf1 in the periplasm as expression of either Caf1 or Caf1M appears to be sufficient in pCaf1∆A background to result in increased OMV production (**Figure 3.18**).

Our findings demonstrate that pCaf1ΔA is the most prolific producer of OMVs, which have been characterised as OM spherical buds entrapping periplasmic content in the lumen (Kulp *et al.*, 2010). OMVs can serve as a response to toxic endogenous periplasmic protein accumulation under stress (Schwechheimer et al., 2015). In this chapter, there is evidence that Caf1 produce, heat labile, oligomers in the absence of Caf1A (**Figure 3.7**); and since they cannot be exported, these oligomers probably form in the periplasm. Furthermore, cells with Caf1A or M deletions show the highest levels of Caf1 in their OMVs (**Figure 3.18**). Thus, it seems likely that these OMVs are packaging Caf1 within their lumens which arises from the periplasm. The aggregation of Caf1 or the binary Caf1-Caf1M complexes in the periplasm owing to the lack of the usher may provoke the hypervesiculation observed in this study, demonstrating that OMV formation is a stress response to the packed periplasm (Klimentová *et al.*, 2015). Caf1 can also be misfolded when it does not bind with the chaperone Caf1M or the usher Caf1A proteins, triggering the periplasmic folding factors, such as DegP, SurA and Skp, to become active (Sklar *et al.*, 2007). These periplasmic folding factors operate in a parallel manner and are regulated by the σ^E stress response, whose primary function is to initiate damage-repair pathways (Lima *et al.*, 2013). McBroom *et al.* (2006) reported that alterations of the σ^E heat shock response was associated with increased OMV production in *E. coli*, and thus they postulated that misfolded toxic products or highly accumulated proteins in the periplasm prompt an increase in OMV production, supporting the results presented here.

As shown here, the level of Caf1 in the periplasm is a major determinant of vesiculation, and it has been indicated that vesiculation levels can be altered by an assortment of factors, such as temperature, antibiotics, oxidation and nutrient availability (Klimentová *et al.*, 2015; Schwechheimer *et al.*, 2014). It has been observed that temperature and vesiculation in *E. coli* are positively correlated (McBroom *et al.*, 2006; Mozaheb *et al.*, 2020), and that optimum Caf1 production occurs in temperature between 26-35◦C (Al-Jawdah *et al.*, 2019; Knight *et al.*, 2007). Thus, using a low temperature could reduce Caf1 production to a reasonable level in *Y. pestis* that prevents OMV production and flocculent formation. Therefore, this proposal could serve as a hypothesis to be tested in a future replication of this stud

Chapter Four

Development of fluorescent outer membrane proteins to measure OMV production

"Success is not final; failure is not fatal: It is the courage to continue that counts"

Winston S. Churchill

4 Development of fluorescent outer membrane proteins to measure OMV production

4.1 Introduction

Study of the OM and its components supports the development of new effective vaccinations, using OM and periplasmic components which are vitally important to manage the escalating worldwide crisis of antibiotic resistance (Ventola, 2015). In recent years there has been an increased interest in surface carbohydrates, predominantly LPS-based glycoconjugates (Zhu *et al.*, 2021), due to the potential of outer membrane vesicles (OMVs) to serve as novel platforms for the advancement of adjuvant-based vaccines against Gram-negative bacterial pathogens (Kashyap *et al.*, 2022). The main biotechnological advantage of this approach is that it combines the O-antigen polysaccharide biosynthesis with OMVs in *Escherichia Coli* (*E. coli*), which has been shown to initiate a strong T cell-independent responses (Hsia *et al.*, 2016).

The most abundant of these proteins is the integral OMPs is the outer membrane protein A (OmpA), which has been reported to play an essential role in mediating adhesion, biofilm formation, and antimicrobial resistance (Smith *et al.*, 2007; Maiti *et al.*, 2011; Nie *et al.*, 2020). OmpA is a 325-residue monomeric PGN-associated protein and is plentiful with more than 100,000 copies in each *E. coli* cell (Khalid *et al.*, 2008). It has previously been suggested that the formation of OMVs is dependent on the presence of OmpA as a monomer or homodimer, and its distribution on the OM (Avila-Calderón *et al.*, 2021). OmpA regulation has been shown to impact OMV production, and its deletion has been found to produce hypervesiculation in several bacterial species, including *Salmonella typhimurium* (Nevermann et al., 2019) and *Vibrio cholera* (Valeru et al., 2014). As described in chapter I section 1.3.2 the OmpA structure contains a pair of distinct domains. The N-terminal transmembrane (TM) domain (171 residues) is a transmembrane β-barrel with eight antiparallel, amphipathic β-strands connected by four relatively long hydrophilic surface-exposed loops and three short turns on the periplasmic side. The globular C-terminal periplasmic domain (135 residues) resides in the periplasm, interacting specifically with the PGN layer (Ishida *et al.*, 2014; Smith *et al.*, 2007), and contains a large fraction of α-helical structure (Sugawara *et al.*, 1996). These two domains are connected by an 18-residue Ala-Pro rich hinge-region, depicted in **Figure 1.6** (Koebnik *et al.*, 2000; Wang, 2002; Verhoeven *et al.*, 2013).

Among its vital multifaceted functions, OmpA acts as a receptor for some bacteriophages (K3,M1,and Ox2) and is considered a virulence factor that is crucial for bacterial survival (Liu *et al.*, 2012; Sun *et al.*, 2019; Smith *et al.*, 2007). OmpA has also been identified as a key surface antigen of many Gram-negative bacterial pathogens that the host immune system is able to recognise and initiate an immune response (Kleinschmidt *et al.*, 1999; Arora *et al.*, 2001). OmpA is synthesised in the cytoplasm and then transported across the IM and periplasm before being inserted into the OM for assembly (Kleinschmidt, 2003; Bulieris *et al.*, 2003).

The purpose of the present study is to investigate if a fluorescently tagged OmpA can be used as a probe to detect, measure and quantify OMV production. Fluorescent tagging or labelling is considered a powerful technique due to its simplicity, non-destructive nature, high selectivity, and applicability to various site-specific labelling strategies (*i.e.*, N-termini and C-termini) (Sahoo, 2012). This may provide a simpler and more quantitative approach compared with OMP/LPS western blots. In this study, superfolder green fluorescent protein (sfGFP) was initially used as a fusion platform as it has been shown to allow for real-time monitoring, quantification and fast analysis of protein integrity and membrane association (Wendel *et al.*, 2016). Moreover, sfGFP has been shown to have an enhanced tolerance for circular permutation, resistance to denaturants, and folding kinetics (Stepanenko *et al.*, 2013). Despite the potential strengths of sfGFP, its use in this study was not satisfactory to serve our primary purpose, and therefore, we adopted a full length OmpA linked to mCherry as an alternative. We utilised different variants of fluorescent OmpA in *E. coli* transformed with pCaf1∆A. Our choice of pCaf1∆A was guided by the data presented in Chapter III where we demonstrated that deletion of the *caf1A* gene from the *caf* operon produced a significant increase in OMV production and prevented Caf1 polymer formation.

4.2 Results

4.2.1 Subcloning OmpA-sfGFP into pBAD vector

Previous data has demonstrated that GFP-fusions can be utilised as tools to measure functional expression (Drew *et al.*, 2009). The fusion of the C-terminal GFP into a desired OMP enables GFP (25 kDa protein of 238 amino acids) to fold properly in the periplasm and become fluorescent. Providing that the desired protein integrates with the OM, the ensuing fluorescence may well be utilised as an appropriate measure of OM-integrated expression (Drew *et al.*, 2001; Stepanenko *et al.*, 2013). We therefore designed an OmpA-sfGFP fusion protein to serve as a fluorescent marker to quantify OMV production. The OmpA-sfGFP plasmid construct consisted of the N-terminal transmembrane domain of OmpA linked to a C-terminal sfGFP domain. The adoption of a superfolding version of GFP overcomes the deficiency of wild type GFP caused by its inadequate folding following export by the Sec pathway into the periplasm (Dinh *et al.*, 2011). Following the design of the OmpA-sfGFP we sent the sequence for synthesis by GeneArt-Fisher Scientific accompanied by the pBAD33 vector, which contained arabinose promoter and the chloramphenicol resistance gene (Roque, 2012). pBAD can be regulated over a different range of L-arabinose concentrations. OmpA-sfGFP was cloned into the pBAD33 vector between the *Kpn*I and X*ba*I restriction sites. The amino acid sequence of the OmpA-sfGFP plasmid is presented in **Table 4.1**.

Table 4.1: Amino acid sequence of OmpA-sfGFP protein.

Name	Amino acid sequence
OmpA-sfGFP	MKKTAIAIAVALAGFATVAQAAPKDNTWYTGAKLGWSQY HDTGFINNNGPTHENQLGAGAFGGYQVNPYGFEMGYDWL GRMPYKSVENGAYKAQGVQLTAKLGYPITDDLDIYTRLGG MVWRADTKSNVYGKNHDTGVSPVFAGGVEYAITPEIATRL EYQWTNNIGDAHTIGTRPDNGMLSLGVSYRFGQGEAAPVV APAPAPAPEVGSSKGEELFTG VVPILVELDG DVNGHKFSV R GEGEGDATNG KLTLKFICTT GKLPVPWPTL VTTLTYGV QC FSRYPDHMKR HDFFKSAMPE GYVQERTISF KDDGTY KTRA EVKFEGDTLV NRIELKGIDF KEDGNILGHK LEYNFN SHNV YITADKQKNG IKANFKIRHN VEDGSVQLAD HYQQN TPIGD GPVLLPDNHY LSTQSVLSKD PNEKRDHMVL LEFV TAAGIT HGMDELYK

Key: Orange; signal sequence peptide; Blue; OmpA N-terminus; Black; original 18-residue linker between N and C terminal domains of OmpA; Red; additional artificial 2-residue linker and Green; sfGFP.

To examine the expression of the OmpA-sfGFP fusion protein, we incubated the new pBAD-OmpA-sfGFP (pBAG) plasmid on a plate reader. The *E. coli* BL21 (DE3) plasmid was transformed with pBAG using chloramphenicol selection at a concentration of 20 µg/ml. Ten ml cultures were grown at 37°C until OD_{600} reached ~ 0.6. Each culture was then induced with 20% (w/v) arabinose at concentrations (0, 0.05, 0.1, 0.2, and 0.4% w/v) The induced cultures were then grown for 3 and 7 hours with constant shaking at 180 rpm. To quantify the level of sfGFP fluorescence, we transferred 200 µl of the cultures into a 96-well plate, which was subsequently read on an incubating plate reader at 485 nm. We observed a pattern of a varying sfGFP expression in pBAG and dependence of fluorescence intensity on both the incubation time and arabinose concentrations (**Figure 4.1**). The fluorescence intensity appeared significantly higher in all concentrations of arabinose when compared directly with the fluorescence intensity of the uninduced cells (all $p<0.01$). The highest level of fluorescence intensity associated with the 0.05% w/v arabinose (**Figure 4.1**.

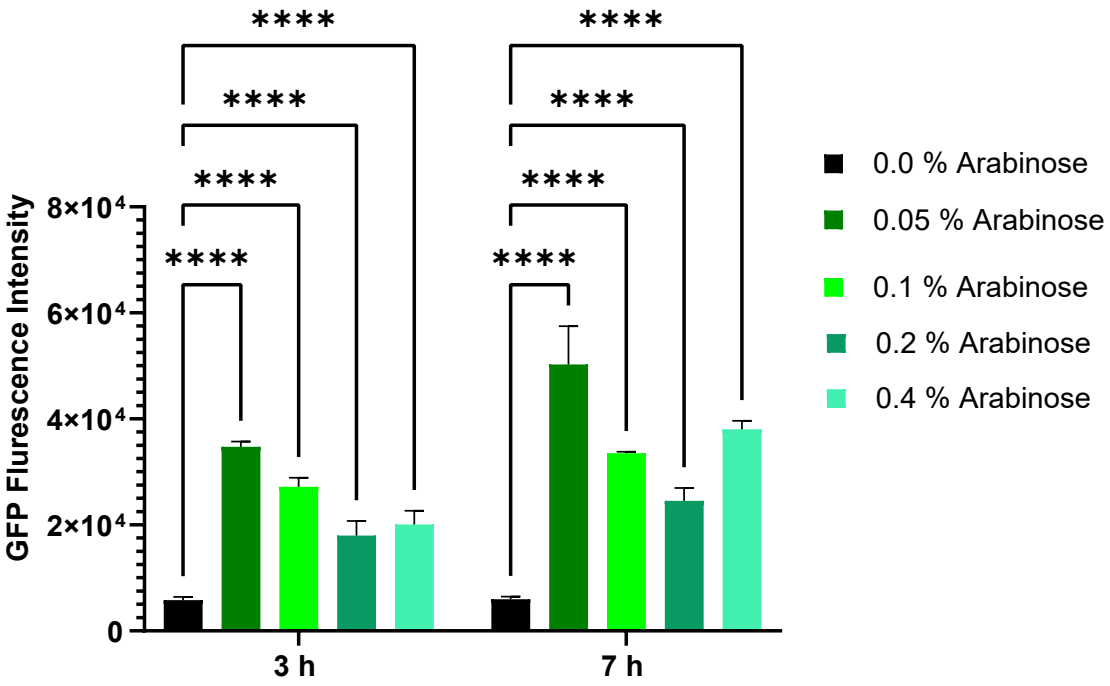

Figure 4.1: Green fluorescent protein (GFP) fluorescence in whole cells.

Escherichia coli BL21(DE3) cells were transformed with pBAG plasmid. Cultures were induced using different concentrations of 20% (w/v) arabinose (0, 0.05, 0.1, 0.2 and 0.4% (w/v)) until they reached approximately 0.6 OD_{600} nm. 200 µl of each culture at each incubation time point and arabinose concentration was transferred to a 96-well plate and subsequently excited at 485 nm and read at 510 nm on an incubating plate reader. Data presented as mean (standard error of the mean (S.E.M (±). Biological replicates = 2, n= 6. Statistical analysis was performed using a one-way ANOVA. All differences in the fluorescence intensities of the 3 and 7h corresponding to the different arabinose concentrations used and were highly significant (****p< 0.01).

4.2.2 Localisation of OmpA-sfGFP

Many localisation studies have shown that GFP can be fused with other proteins, effectively making the fusion partners fluorescent without interfering with their functions (Huang *et al.*, 2016). This form of fusion with any protein therefore indicates that they can be localised and tracked using standard fluorescent microscopy (Stepanenko *et al.*, 2013; Gunasinghe *et al.*, 2017). To confirm the presence of efficient insertion of the OmpA-sfGFP plasmid through the IM and across the periplasm into the OM, we osmotically shocked the IM cells, as it has been shown that the IM, which has a low permeability (Strahl *et al.*, 2010), shrinks and withdraws from the OM in reaction to osmotic stress (Oparka, 1994). The osmotic shock method is also commonly used for evaluating the release of periplasmic and cytoplasmic proteins associated with the inner leaflet of the IM (Kumamoto *et al.*, 1994; Gohrbandt *et al.*, 2019). Analysis of the images generated here for the GFP signal was performed using Total Internal Reflection Fluorescence (TIRF) microscopy. The pBH501 plasmid was co-expressed was co-expressed with pBAG in *E.coli* BL21 (DE3) cells with the appropriate antibiotics (ampicillin and chloramphenicol at a concentration of 100 and 20 µg/ml, respectively). All cell cultures were continuously shaken at 180 rpm for 10 hours at 37 °C prior to being placed onto microscope slides.

To inflict osmotic shock on the IM and provoke the retraction of the IM from the cell wall and OM (plasmolysis), 1M NaCl was added to the cell cultures, before adding 2 µg/ml of FM 5-95, a hydrophobic fluorescent dye specifically used for localising the OM, to the cell cultures for 5 minutes (te Winkel *et al.*, 2016). By examining the images presented in **Figure 4.2**, we were able to observe that OmpA-sfGFP was in the IM, which is likely to be due to a dysfunctional OmpA-sfGFP secretion process, implying that the fluorescent signal observed in the plate reader emanated from the IM. It has been shown that when cells were plasmolysed with 0.5 M NaCl, the IM detached from the OM, forming plasmolysis bays (Lewenza *et al.*, 2008). Pilizota *et al.* (2013) also demonstrated that up-shocking caused by an OM impermeable solute, such as sucrose, produces noticeable plasmolysis on a slow timescale, whereas up-shocking using OM permeable ions such as the ones used here results in plasmolysis immediately upon shock (Pilizota *et al.*, 2013).

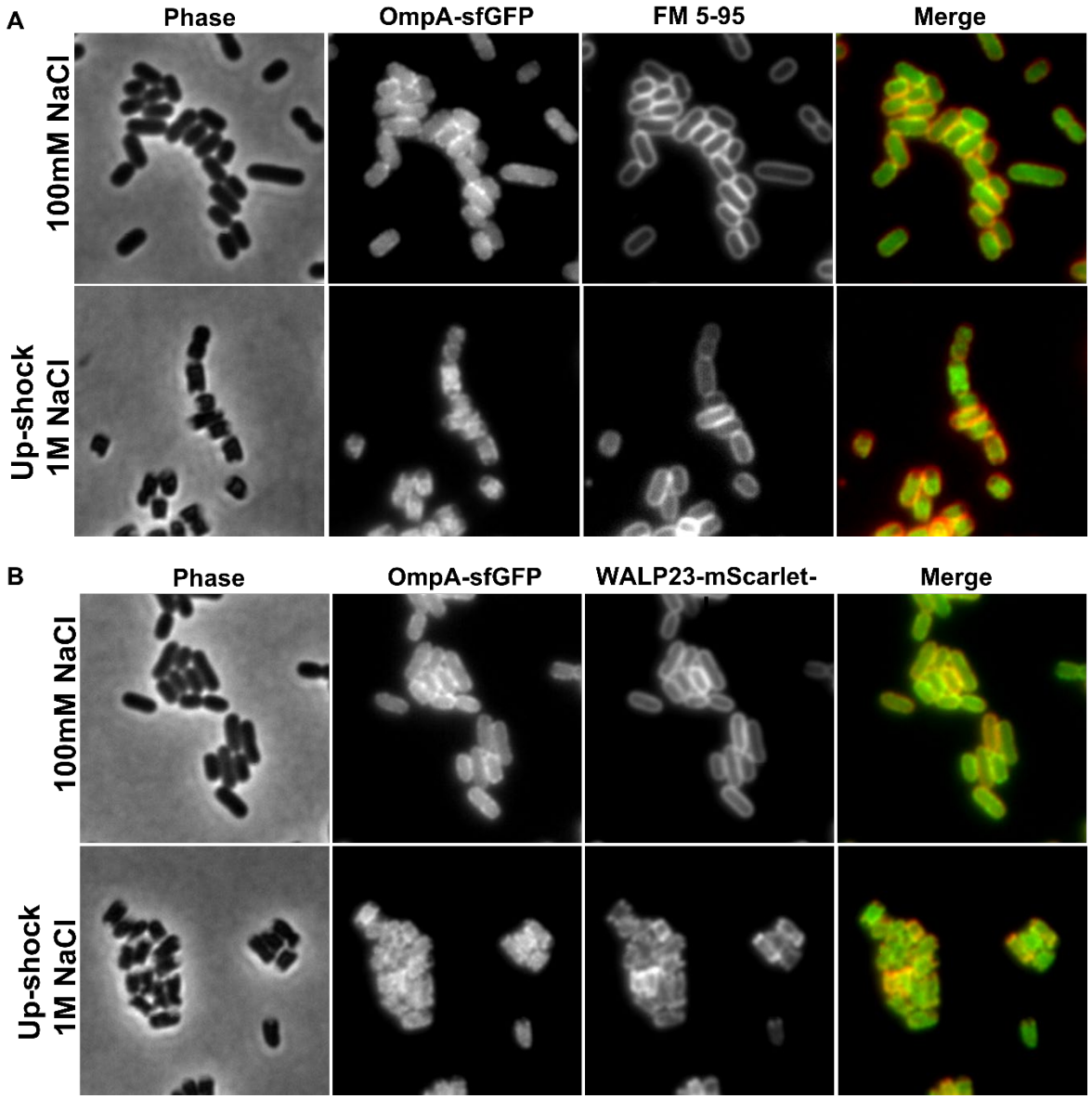

Figure 4.2: Fluorescence images of different localisation pattern of OmpA-sfGFP.

(A) OmpA-sfGFP fusion stained with FM 5-95 dye for the outer membrane (OM). (B) OmpA-sfGFP fusion co-transformed with WALP23-mScarlet-I, the latter is specifically for localising the inner membrane (IM). For (A) and (B), cell cultures were grown for 10 hours with shaking at 180 rpm. These cell cultures were washed and for (A) then incubated in the membrane dye (FM 5-95) for five minutes, and then applied to the slides and used immediately. The fusion protein OmpA-sfGFP doesn't follow the localisation of the OM upon up-shock and does follow the localisation of the IM upon up-shock. Differences between the localisation patterns of the OM (A) and IM (B) upon up-shock reflect that the membrane potential can be clearly identified. The localisation patterns of the IM appear similar; however, the OM localisation patterns are quite dissimilar. All microscopy analyses were performed using Nikon Eclipse Ti equipped with Cool LED pE-4000 light source Photometrics BSI Camera. Nikon Plan Apo 100x/1.40 NA Oil Ph3.

4.2.3 Design and production of OmpA-mCherry chimeras

Following the failure of the OmpA-sfGFP fusion protein to insert into the OM, we embarked upon using full length OmpA linked to C-terminal mCherry (Hsiao *et al.*, 1996; Shaner *et al.*, 2004) (**Figure 4.3**), which has been documented to fold efficiently into the periplasm (Verhoeven *et al.*, 2013). This approach was utilised following the successful use of the full length OmpA-mCherry fusion protein (pGI10) by the den Blaauwen group who kindly made their plasmid available (Verhoeven *et al.*, 2013). Moreover, a fluorescently labelled OmpA-mCherry fusion protein was found in the OMV fraction after co-expression as an OM marker (Stephan *et al.*, 2020). We thus pursued second-generation designs which we compared with pGI10. The DNA sequences for the new OmpA-mCherry chimeras listed in **Table 4.2** were designed and synthesised using Gene Art Strings by GeneArt-Fisher Science**.** The two primers depicted in **Table 4.3** were designed to delete the *sfGFP* gene from the pBAD vectors (**Figure 4.4**) prior to insertion of the four new genes (*NAM*, *AM*, *SAM,* and *ASM*) using In-Fusion HD as described in Section **2.3.2** of Chapter **II** . With exception of pNAM, which lacks the OmpA C-terminus, all designs of the new OmpA-mCherry chimeras were constructed using the pBAD vector as the backbone with the OmpA N-terminus followed by the various constructs and including the OmpA C-terminus (**Figure 4.5**).

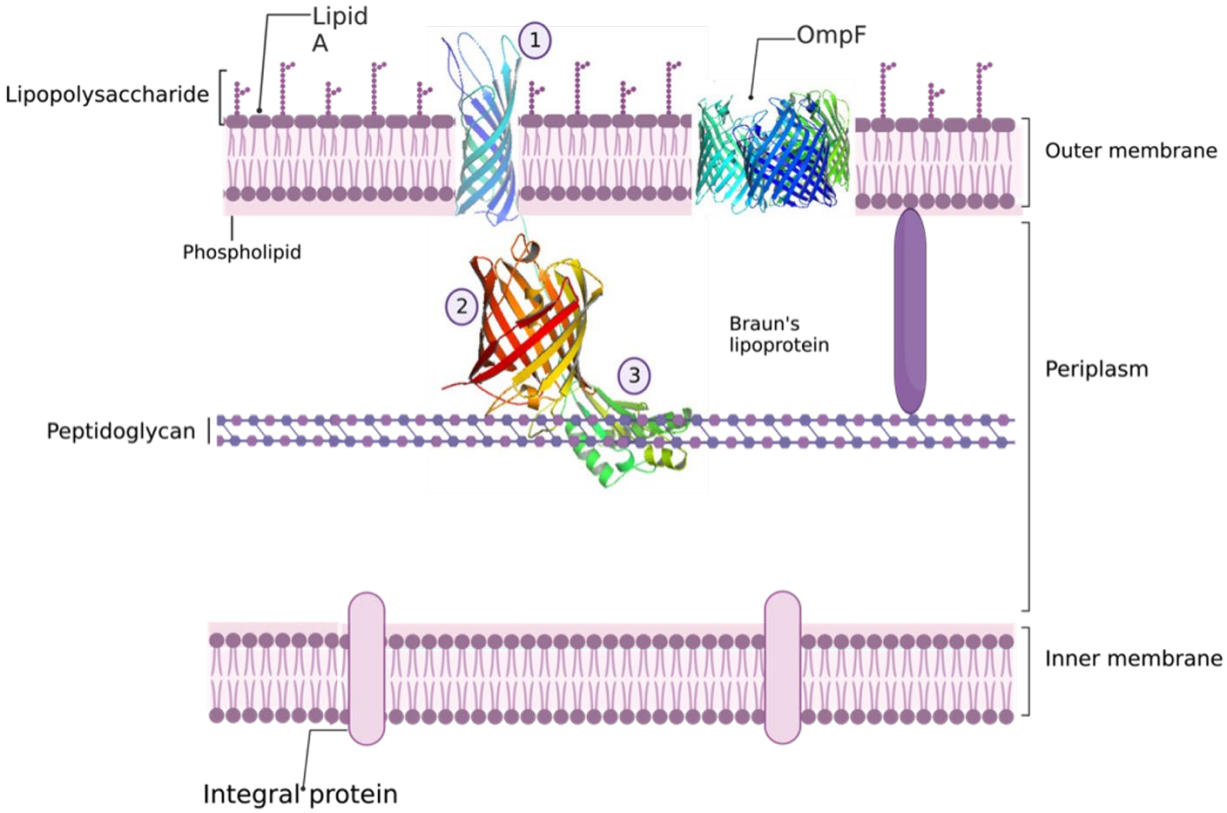

Figure 4.3: Model of OmpA-mCherry fusion in the envelope of Gram-negative bacteria.

The N-terminal domain of OmpA proteins is comprised of an eight-stranded, anti-parallel barrel that is embedded in the OM. The C-terminal domain of OmpA is positioned in the periplasmic space and interacts with the peptidoglycan layer. The mCherry is at the C terminus of OmpA, folded in the periplasm, and is shown here to sit between the peptidoglycan and OM. OM protein F Image created using BioRender.Com.
1 = Outer membrane protein A (OmpA) transmembrane domain, PDB file:1BXW; 2 = mCherry, PDB file: 2H5Q; 3 = Outer membrane protein A (OmpA) C-terminal domain, PDB file: 2MQE.

Table 4.2: OmpA-mCherry chimera design.

Full Name	Abbreviation	Construction	Number of amino acids	Molecular weight (kDa)
(1) Full OmpA_mCherry	pAM	OmpA (1-346) xx mCherry (349-582)	582	63.8
(2) OmpA-NTD_mCherry	pNAM	OmpA (1-210) xx mCherry (213-446)	446	49
(3) OmpA-NTD_TCM Linker_OmpA-CTD_mCherry	pSAM	OmpA (1-131) TCM (132-137) OmpA (138-198) Linker (199-216) OmpA (217-352) xx mCherry (355-588)	588	64.3
(4) OmpA-NTD-Linker_TCM_ OmpA-CTD_mCherry	pASM	OmpA (1-192) Linker (193-210) TCM (211-216) OmpA (217-352) xx mCherry (355-588)	588	64.3
(5) OmpA-NTD-Linker_TCM_ OmpA-CTD	pAS	OmpA (1-192) Linker (193-210) TCM (211-216) OmpA (217-352) xx	354	37.9
(6) OmpA-NTD_TCM_ Linker_OmpA-CTD	pSA	OmpA (1-131) TCM (132-137) OmpA (138-198) Linker (199-216) OmpA (217-352) xx	354	37.9

TCM refers to tetra-cysteine motif (Cys-Cys-Pro-Gly-Cys-Cys) and xx denotes an extra artificial linker.

The construction of the inserts described in Table 4.2 is as follows:

(1): OmpA N-terminal domain (NTD) – natural OmpA linker – OmpA C-terminal domain (CTD) – artificial additional linker – mCherry gene

(2): OmpA N-terminal domain (NTD) – natural OmpA linker – artificial additional linker – mCherry gene

(3): OmpA N-terminal domain (NTD) – tetra-Cysteine Motifs (TCM) – natural OmpA linker – OmpA C-terminal domain (CTD) – artificial additional linker – mCherry gene

(4): OmpA N-terminal domain (NTD) – natural OmpA linker – tetra-Cysteine Motifs (TCM) – OmpA C-terminal domain (CTD) – artificial additional linker – mCherry gene

(5): OmpA N-terminal domain (NTD) – natural OmpA linker – tetra-Cysteine Motifs (TCM)– OmpA C-terminal domain (NTD) – artificial additional linker

(6): OmpA N-terminal domain (NTD) – tetra-Cysteine Motifs (TCM) – natural OmpA linker – OmpA C-terminal domain (CTD) – artificial additional linker

For construct 3, the TCM was placed at amino acid numbers V-131 and Y-138 within the OmpA N-terminal. For construct 4, the TCM were placed at amino acid numbers V-210 and Q-217.

Table 4.3: Oligonucleotide primers for the deletion of superfolder green fluorescent protein.

Primer name	Nucleotide sequence (5’ to 3’)
pBAD33-Forward	TGATAATCTAGAGTCGACCTGCAGGCA
pBAD33-Reverse	GCTTTTGGTATCTGCACGCCAAACCATACC

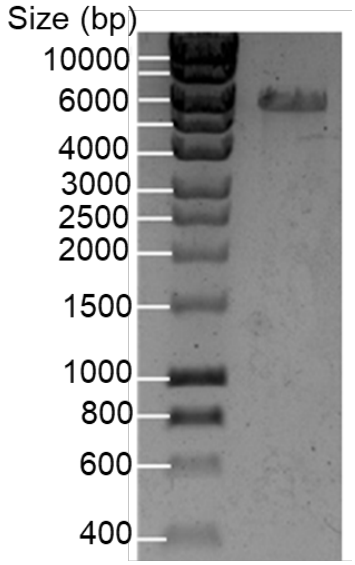

Figure 4.4: Agarose gel demonstrating the linearised vector.
0.8%(w/v) agarose gel demonstrating the linearised vector of pBAG. Midori Green Advance DNA was used for staining. Band depicted at approximately 6 kilobase pairs, which is the linearised vector (5925 bp).

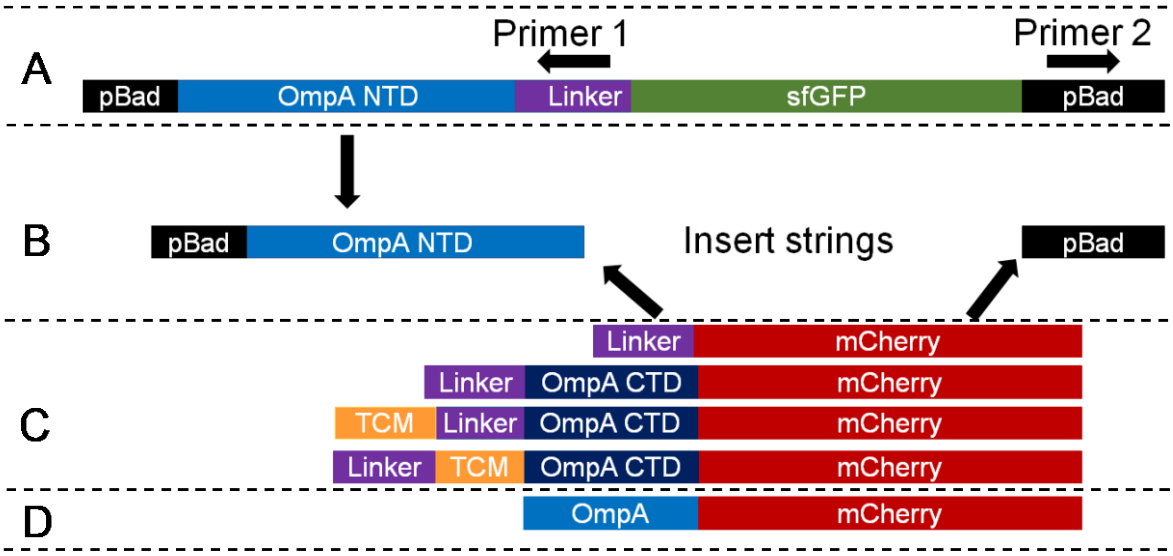

Figure 4.5: Schematic illustration of the OmpA-mCherry designs.

(A) denotes the original OmpA-sfGFP construct, (B) denotes the linear vector including the sfGFP deletion, (C) denotes strings obtained using GeneArt (1−4) and (D) denotes pGI10, a plasmid acting as a positive control obtained from Verhoeven et al. (2013). pBad vector; Protein expression vector, OmpA NTD; OmpA N-terminal domain, OmpA CTD; OmpA C-terminal domain, Linker; Natural OmpA linker, mCherry; mCherry protein, TCM; Tetra-Cysteine Motifs.

4.2.4 Analysis of outer membrane fractions

In order to assess if the new OmpA-mCherry chimeras were located in the OM, we conducted two experiments. The first experiment involved analysis of the OmpA-mCherry chimeras by harvesting the cells following 8 h of growth. The second experiment employed the OM fractionation method described by Wolf-Watz and colleagues (Wolf-Watz *et al.*, 1973) with some modifications, described in detail in the Materials and Methods (Section **2.4.2,** Chapter **II**)**.** *E. coli* BL21 (DE3) cells were transformed separately with the four new OmpA-mCherry chimeras (pNAM, pAM, pSAM, pASM), pGI10 (a positive control), and a pBAD empty vector (pBE) as a negative control.

Cell cultures were grown for 8 hours in 600 ml Luria-Bertani (LB) medium containing the appropriate antibiotics (100 µg/ml ampicillin for the pGI10 and 20 µg/ml chloramphenicol for the remaining pBAD plasmids) at 37°C whilst continually shaking at 180 rpm. When the OD_{600} reached approximately 0.6, these cultures were induced with L-arabinose at a concentration of 0.05% w/v. In contrast, the cell cultures of the pGI10 plasmid were induced with 1 mM Isopropyl β-d-1-thiogalactopyranoside (IPTG). Next, cell cultures were divided into 100 and 500-ml fractions. A 30 µl sample of the whole cell culture from the 100 ml aliquot was then incubated in an SDS-PAGE loading buffer at 95 ºC for 5 minutes. An additional 30 µl sample from the 100 ml aliquot was also mixed with an SDS-PAGE loading buffer and was not heated. All samples were then analysed using SDS-PAGE. The SDS-PAGE analysis highlighted the presence of an unexpected band at approximately 14 kDa (**Figure 4.6**). Using mass spectrometry, we identified this band as a periplasmic glutamine-binding protein (glnH), a two-domain protein with a 27 kDa molecular mass that appears to co-purify with OM fragments (Hsiao *et al.*, 1996). It is possible that the hinge region is liable to proteolysis leaving two equal sized products. Therefore, the lower band is likely to be the breakdown product of the 27 kDa band.

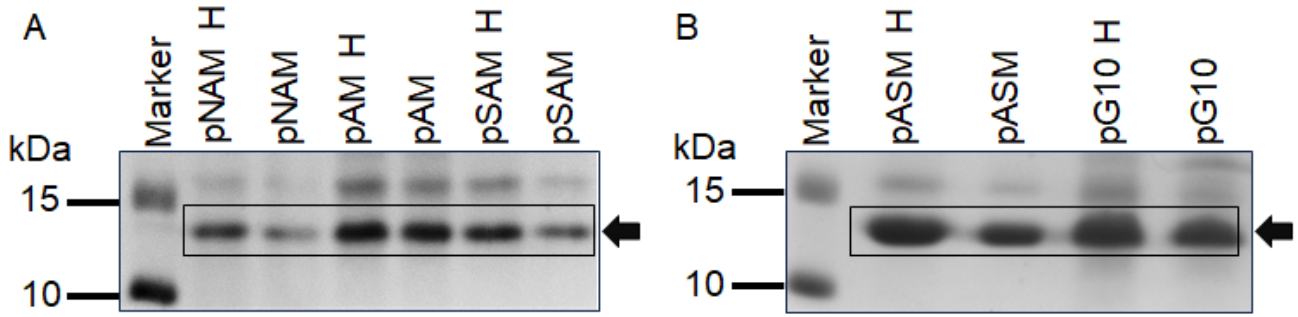

Figure 4.6: Coomassie blue stained Sodium dodecyl sulfate polyacrylamide gel electrophoresis (SDS-PAGE) of whole cell pellet samples.

A: 12% SDS-PAGE analysis of the whole cell cultures for OmpA-mCherry chimeras (pNAM, pAM, pSAM). (B) 12% SDS-PAGE analysis of the whole cells cultures for OmpA-mCherry chimera pASM and pGI10.The four new OmpA-mCherry chimeras (pNAM, pAM, pSAM, and pASM), and pGI10 (a positive control) were transformed separately into *Escherichia coli* BL21 (DE3) cells. Cell cultures were grown at 37°C for 8 h in Luria-Bertani (LB) media. Induction was performed after OD_{600} reached approximately 0.6. A 0.05% arabinose was added for the OmpA-mCherry chimaeras and 1 mM IPTG for the pGI10. 30 µl of heated and unheated samples of the whole cell culture were mixed with the SDS-PAGE sample buffer. The results show the presence of an unexpected band at approximately 14 kDa, which is the breakdown product of periplasmic glutamine-binding protein (glnH) identified by mass spectrometry.

The second experiment was conducted following the growth and culture of cells from the 500 ml fraction for 8 hours. The OM fractionation method described in section 2.4.1 in Chapter II was applied to all cultures (Wolf-Watz *et al.*, 1973) (**Figure 4.7**). The OM fractions were centrifuged at 30,000 rpm for 20 minutes and pellets collected. A western blot analysis was conducted using an anti-OmpA antibody, which confirmed the presence of OmpA with an intense band at 35 kDa in the whole cell pellets and numerous breakdown products presumably from proteolytic digestion at MW less than native OmpA (**Figure 4.8A**). A subsequent western blot analysis using the purified OM pellets revealed that the molecular weight of the OmpA-mCherry chimeras corresponded to the highest bands present in the western blot with breakdown products lower down the gel only as far as native OmpA (**Figure 4.8B**). These findings, resulting from the OM fraction, demonstrate that the OmpA-mCherry chimeras used here are expressed and inserted within the OM.

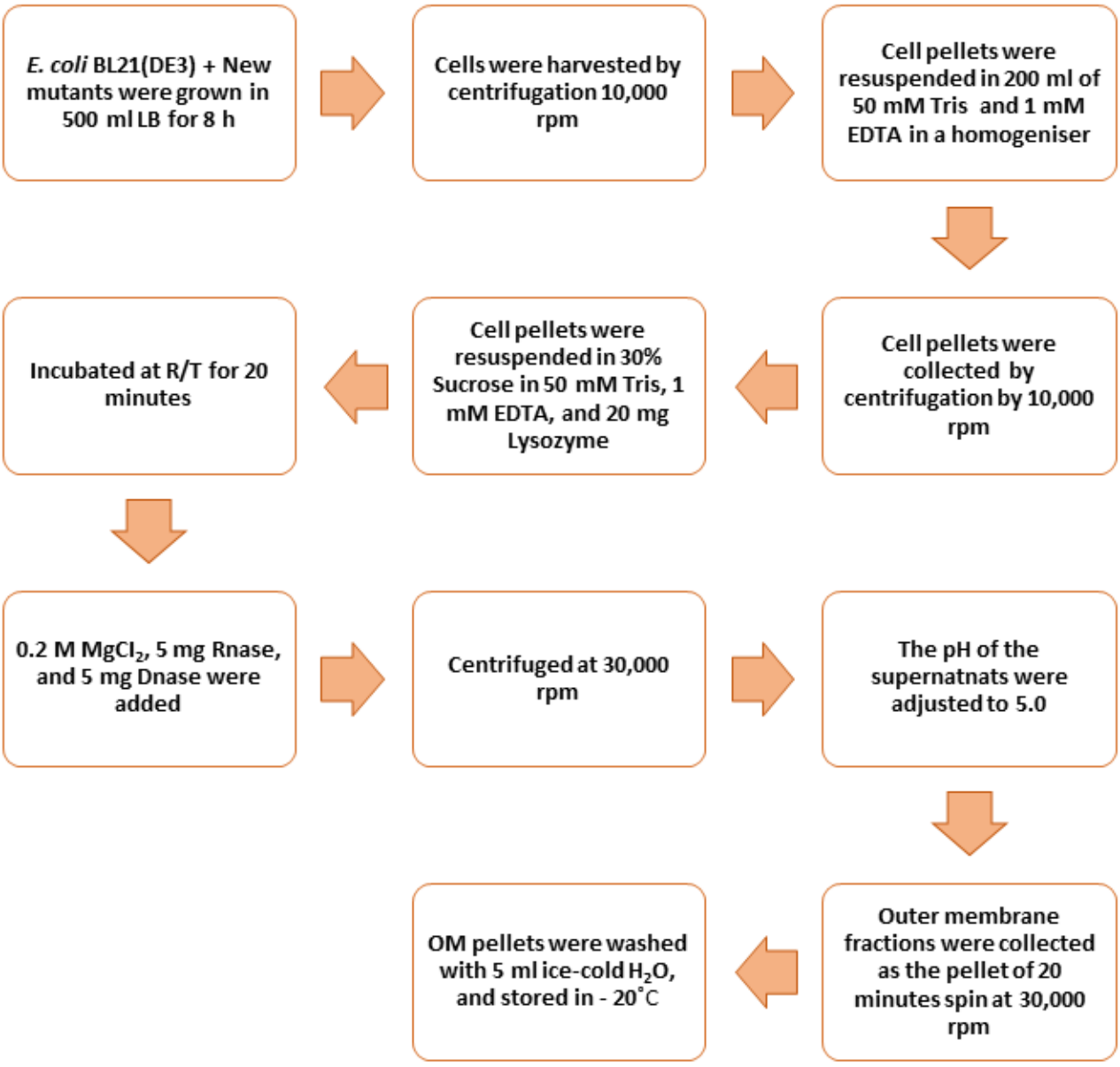

Figure 4.7: Schematic diagram of the modified method of outer membrane fraction purification

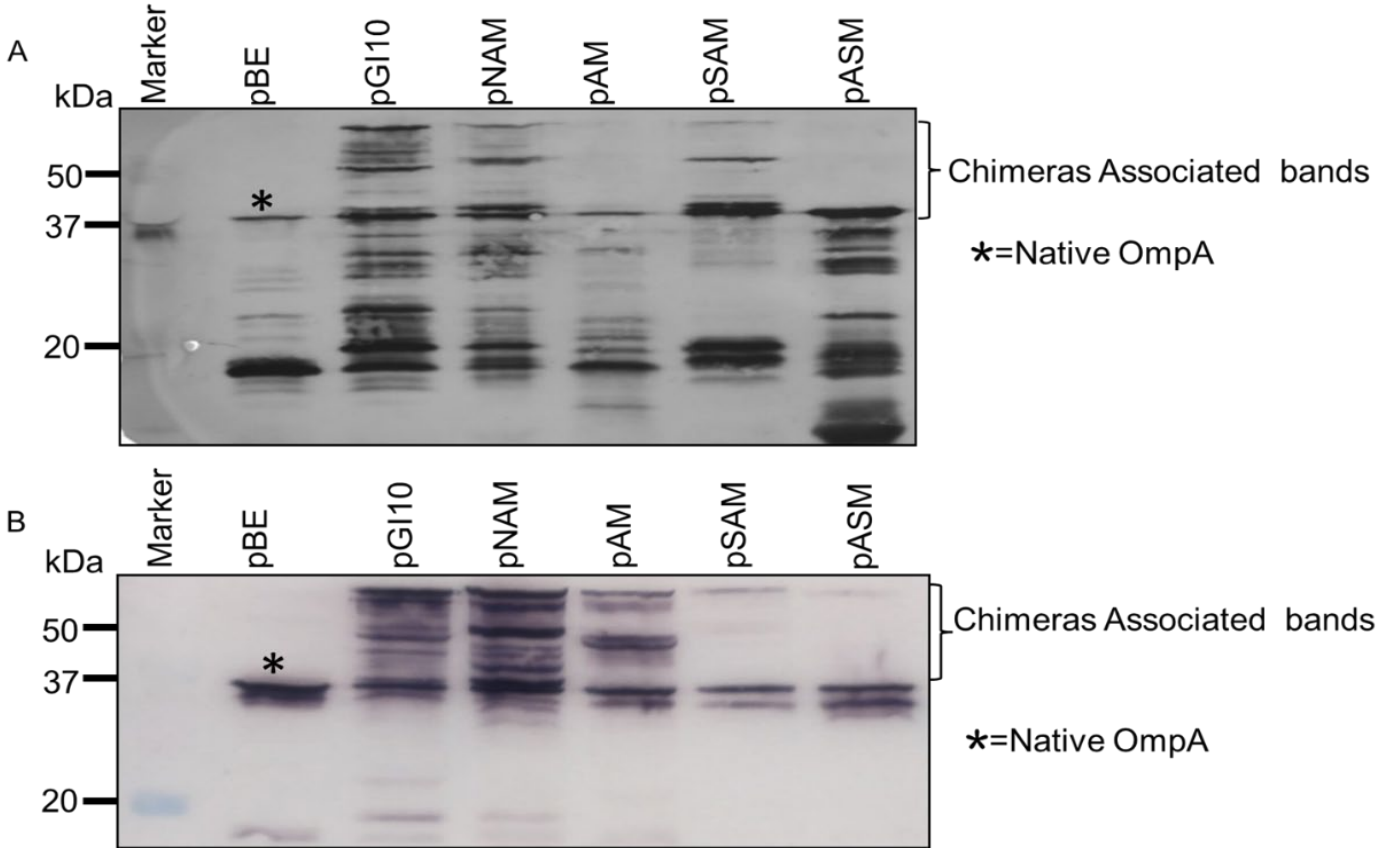

Figure 4.8: Western blot analyses of whole cell and Outer Membrane (OM) fractions.

Escherichia coli BL21 cells were transformed separately using the new OmpA-mCherry chimeras (pNAM, pAM, pSAM, pASM), pGI10 as a positive control (Verhoeven *et al.*, 2013), and pBAD empty vector as a negative control. (A) Western blot of the whole bacterial cell with the expression of the new OmpA-mCherry chimeras using the anti-OmpA antibody. (B) Western blot of the OM fractions. Rabbit polyclonal OmpA and the goat anti-rabbit alkaline phosphatase conjugate antibody were used as the primary and secondary antibodies, respectively, presented in A and B. * denotes the native OmpA.

4.2.5 Analysis of protein fluorescence

Each culture transformed with a OmpA fusion protein producing plasmid previously described in section 4.2.3, was screened using a plate reader to quantify the level of fluorescence as a measure of protein expression. All transformed cell cultures from the plasmids were induced with various concentrations of arabinose (0, 0.05, and 0.1% (w/v)). Plasmid pGI10 was induced with 1 mM isopropyl-β-d-thiogalactopyranoside (IPTG) as a positive control. 200 μl of each culture was then incubated at 37°C for 12 hours in a 96-well plate with the addition of 100 μg/ml ampicillin to pGI10 and 20 μg/ml chloramphenicol to the pBAD plasmids. Fluorescence was measured using a plate reader at OD_{600} at 584 nm as a measure of growth. Data was recorded every 10 minutes, up to 720 minutes and then plotted (**Figures 4.10 and 4.11)**. In **Figure 4.10,** all cell cultures, regardless of induction condition, had similar stationary phases. Growth curves followed the traditional exponential growth curve regardless of induction condition, however, induction of the OM proteins enhanced cell growth, ensuring faster growth than the pBAD empty vector (pBE). The cultures exhibited increases in fluorescence over time that were similar to the increases of OD_{600} (**Figure 4.11**), Overall, the OD_{600} and fluorescence intensity remained stable until the end of the 12-hour experiment. pGI10 containing the full length OmpA-mCherry had the highest fluorescence intensity regardless of induction. Plasmid persistence and strong signal intensity of pGI10 due to the leaky expression, is likely to be the primary reason for a strong fluorescent signal at 0% induction. This can explain why the colour of the pellets following centrifugation were red (**Figure 4.9**). We observed a lower level of fluorescence in the new chimeras when compared to the positive control, pGI10. Thus, none of the modifications were able to improve upon pGI10, suggesting all samples were similarly susceptible to proteolytic breakdown despite their varied structures. Amongst all the chimeras, pAM had the highest fluorescence intensity, which is perhaps because it also includes the full length OmpA along with mCherry.

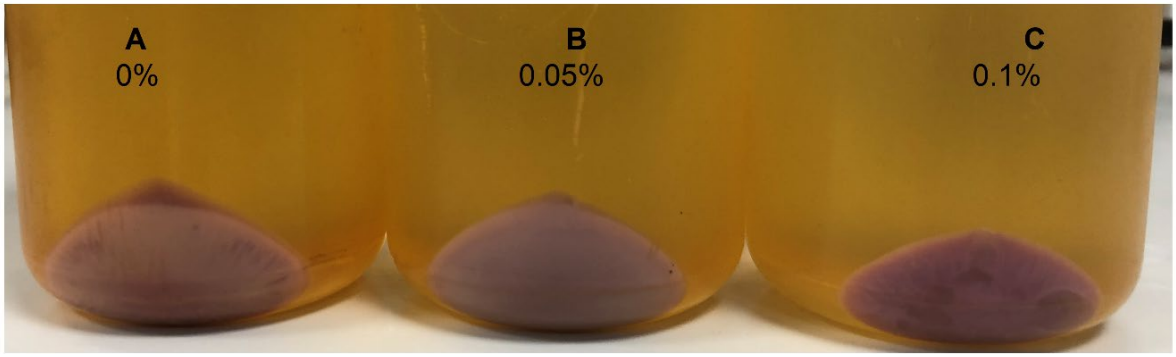

Figure 4.9: pGI10 pellets following centrifugation.

Escherichia coli transformed with pGI10. Cell cultures were grown for 8 hours in 500 ml Luria-Bertani (LB) with the appropriate antibiotic (100 µg/ml ampicillin). Cell pellets were generated using centrifugation at 10,000 rpm for 40 minutes. All pellets were red in colour.

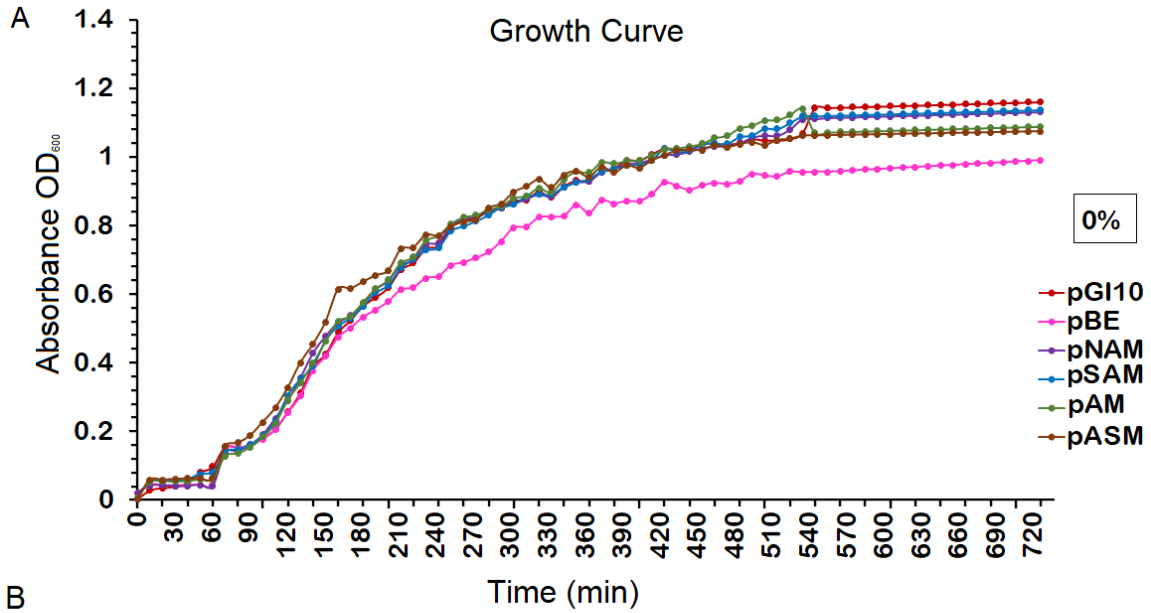
A
Growth Curve
Absorbance OD600
Time (min)
0%
pGI10
pBE
pNAM
pSAM
pAM
pASM

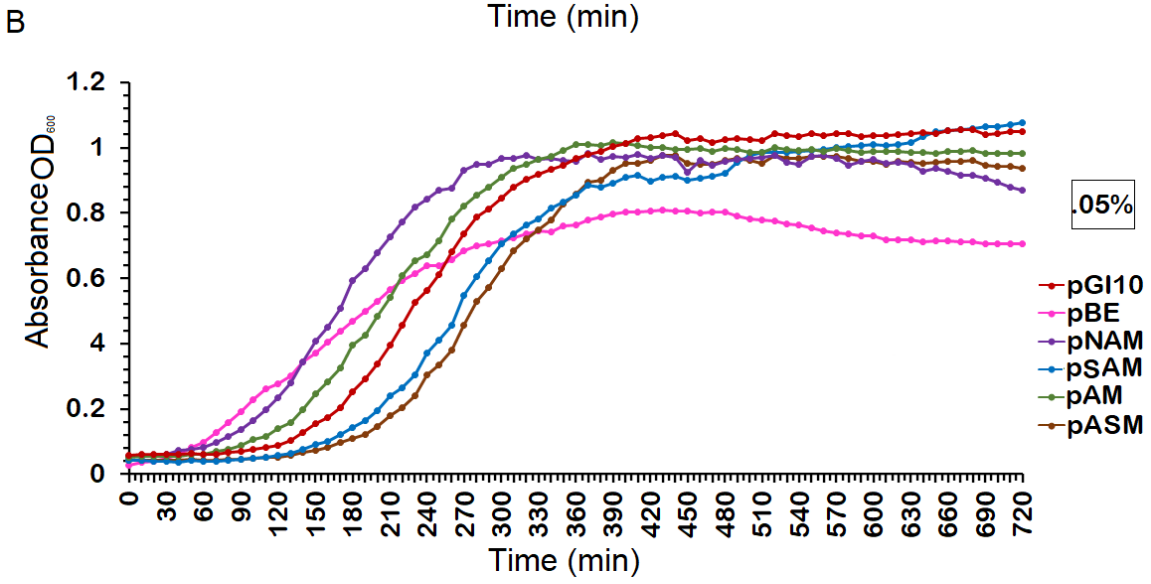
B
Absorbance OD600
Time (min)
.05%
pGI10
pBE
pNAM
pSAM
pAM
pASM

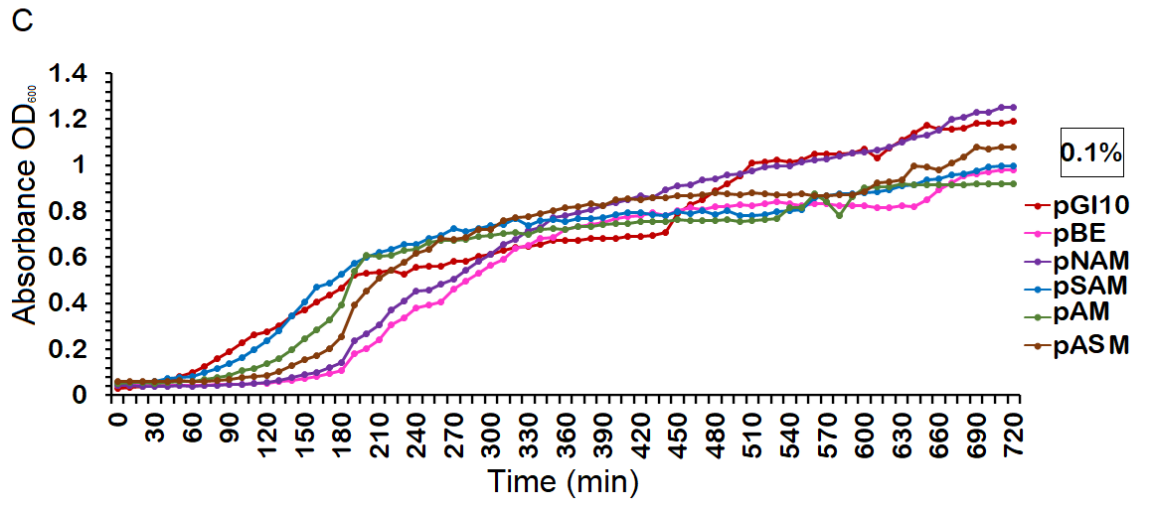
C
Absorbance OD600
Time (min)
0.1%
pGI10
pBE
pNAM
pSAM
pAM
pASM

Figure 4.10: Cell growth measured by OD_{600}.

Escherichia coli was transformed separately with six plasmids (pGI10, pBE, pNAM, pSAM, pAM, and pASM) with the appropriate antibiotics (100 µg/ml ampicillin for pGI10 and 20 µg/ml chloramphenicol for the pBAD plasmids). Cell cultures were incubated at 37°C. Upon reaching OD_{600}, 0.6 approximately after 120 minutes, all cultures were induced either with arabinose or with IPTG for pGI10. Readings of OD_{600} for all plasmids were recorded every 10 minutes using a plate reader at 595 nm. A) OD_{600} readings for all plasmids without induction (0% w/v arabinose). B) and C) OD_{600} readings for all plasmids with induction (0.05 and 0.1% w/v arabinose, respectively). pGI10 was induced with 1 mM IPTG.

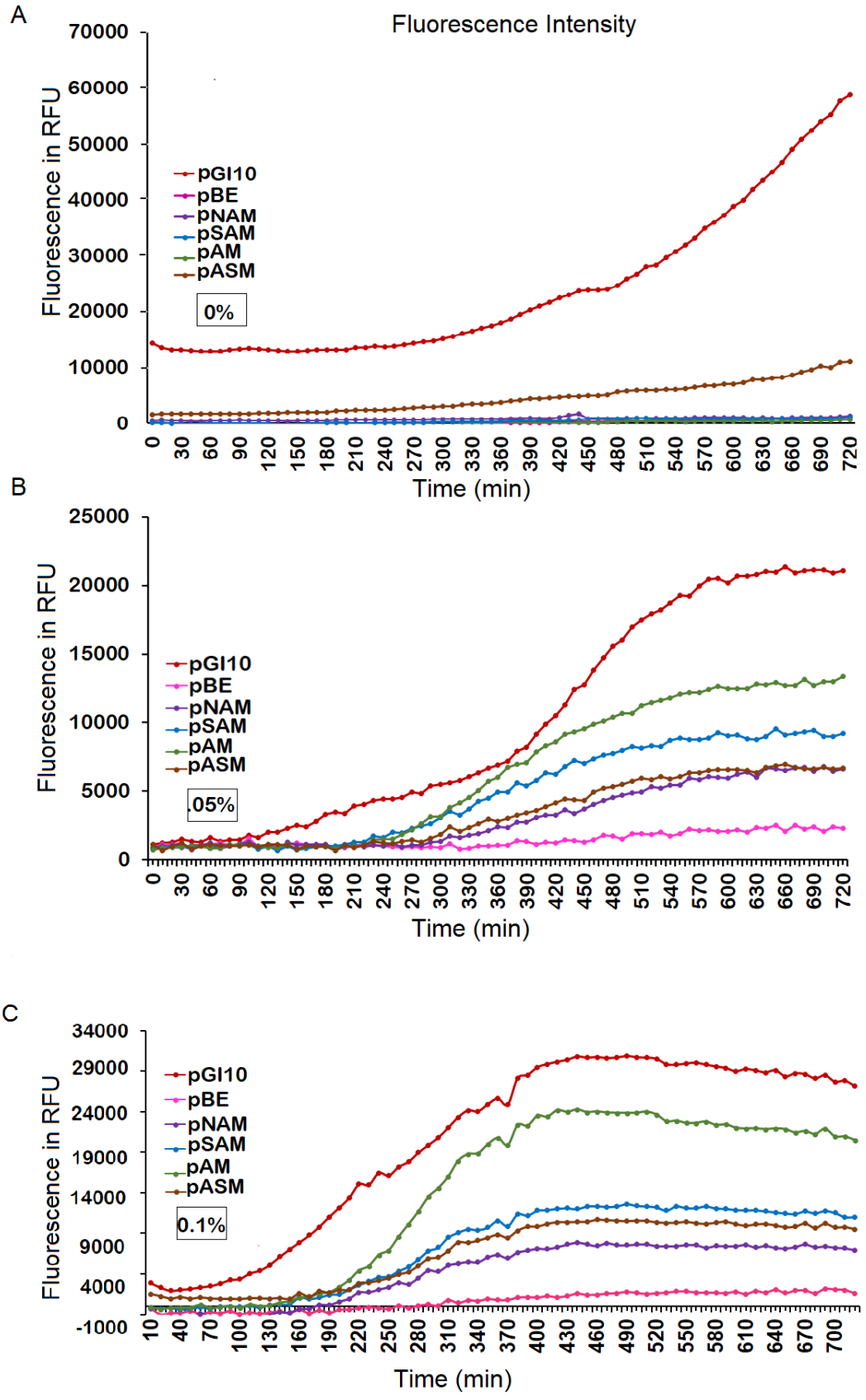
A
Fluorescence Intensity
Fluorescence in RFU
70000
60000
50000
40000
30000
20000
10000
0
pGI10
pBE
pNAM
pSAM
pAM
pASM
0%
0 30 60 90 120 150 180 210 240 270 300 330 360 390 420 450 480 510 540 570 600 630 660 690 720
Time (min)
B
Fluorescence in RFU
25000
20000
15000
10000
5000
0
pGI10
pBE
pNAM
pSAM
pAM
pASM
.05%
0 30 60 90 120 150 180 210 240 270 300 330 360 390 420 450 480 510 540 570 600 630 660 690 720
Time (min)
C
Fluorescence in RFU
34000
29000
24000
19000
14000
9000
4000
-1000
pGI10
pBE
pNAM
pSAM
pAM
pASM
0.1%
10 40 70 100 130 160 190 220 250 280 310 340 370 400 430 460 490 520 550 580 610 640 670 700
Time (min)

Figure 4.11: Analysis of fluorescence intensity.

Escherichia coli was transformed separately with six plasmids (pGI10, pBE, pNAM, pSAM, pAM, and pASM) with the appropriate antibiotics (100 µg/ml ampicillin for pGI10 and 20 µg/ml chloramphenicol for pBAD plasmids). Cell cultures were incubated at 37°C. Upon reaching OD_{600}, approximately 0.6 after 120 minutes, all cultures were induced with arabinose and IPTG for pGI10. Fluorescence intensity was measured in all plasmids every 10 minutes using fluorescence (n=9) excitation at 587 nm and read at 610 nm. Induction was initiated at 120 minutes. A) OD_{600} readings for all plasmids without induction (0% w/v arabinose), B) and C) OD_{600} readings for all plasmids with induction (0.05 and 0.1%, w/v arabinose respectively). All measurements were carried out in 96-well plate using FLUOstar Omega plate reader. pGI10 was induced with 1 mM IPTG.

4.2.6 Production of OmpA-Cys motif proteins without mCherry

Of the new OmpA-mCherry chimeras, pSAM and pASM possess the tetra-cysteine motif (TCM) (Cys-Cys-Pro-Gly-Cys-Cys). In pSAM the motif is in an extracellular loop (V-107 and Y-110), ensuring the exogenous dye is able to easily bind to the motif, which is in contrast to pASM, where the motif is located within the periplasm. The 4,5-bis (1,3,2-dithiarsolan-2-yl) fluorescein (FlAsH-EDT$_2$) Invitrogen Detection Technologies reagents (**Figure 4.12**). The green-emitting fluorophore FlAsH-EDT$_2$ dye has a molecular mass of 664.5 g/mol, and a small membrane-permeant fluorogenic biarsenical dye (Griffin *et al.*, 1998) which exhibits considerable affinity and specificity of binding towards a specific peptide sequence, such as the tetra-Cysteine motif (TCM) (Adams *et al.*, 2002; Griffin *et al.*, 1998). These compounds have been shown to bind covalently to the TCM almost immediately following addition to a target protein (Hoffmann *et al.*, 2010).

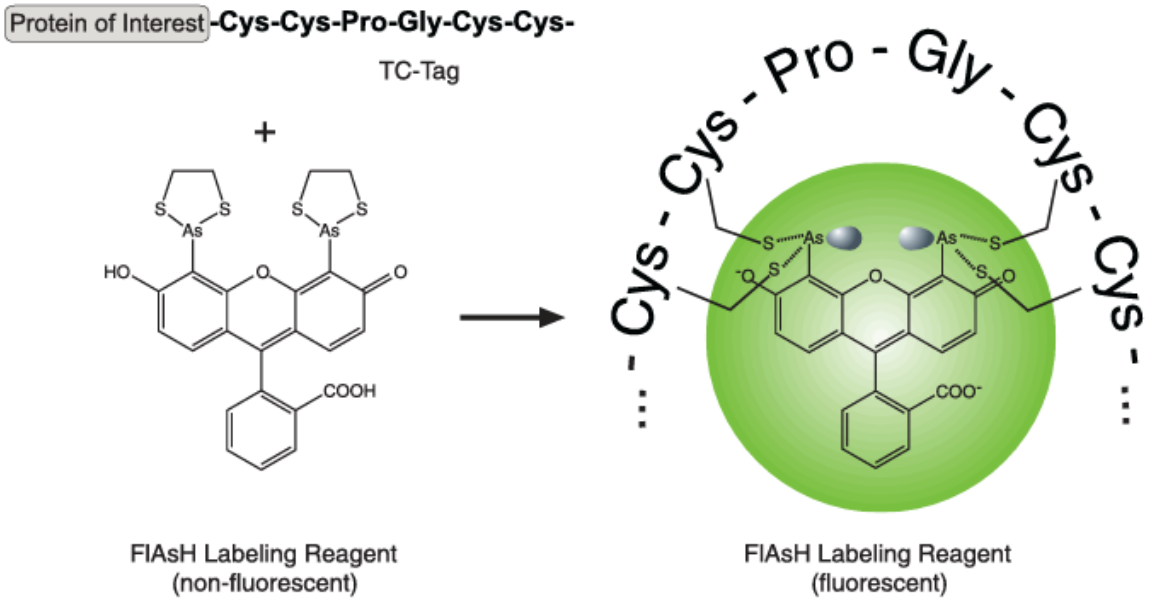

Figure 4.12: FlAsH-EDT2 Labelling Reagent

Diagram showing the non-fluorescent FlAsH-EDT$_2$ labelling reagent bound with the tetra-Cysteine motif (TC-Tag). FlAsH-EDT$_2$ labelling reagent generates a strong fluorescent signal upon binding with the TC-Tag. Adapted from Thermo Fisher manuals (Invitrogen, 2011).

The new constructs pSA and pAS involved the deletion of mCherry from the two constructs (pSAM) and (pASM) respectively utilising the Infusion HD cloning kit (**Figure 4.13 A and B, Table 4.4**).

Table 4.4: Oligonucleotide primers for the deletion of mCherry.

Primer	Nucleotide sequence (5' to 3')
∆mCherry-Forward	ACTCAGCCGCAGGCTTGATAA TCTAGAGTCGACCTGCAGGC ATGCAAG
∆mCherry-Reverse	AGCCTGCGGCTGAGTTACAA CGTCTTTGATACCTTTAACTTC GAT

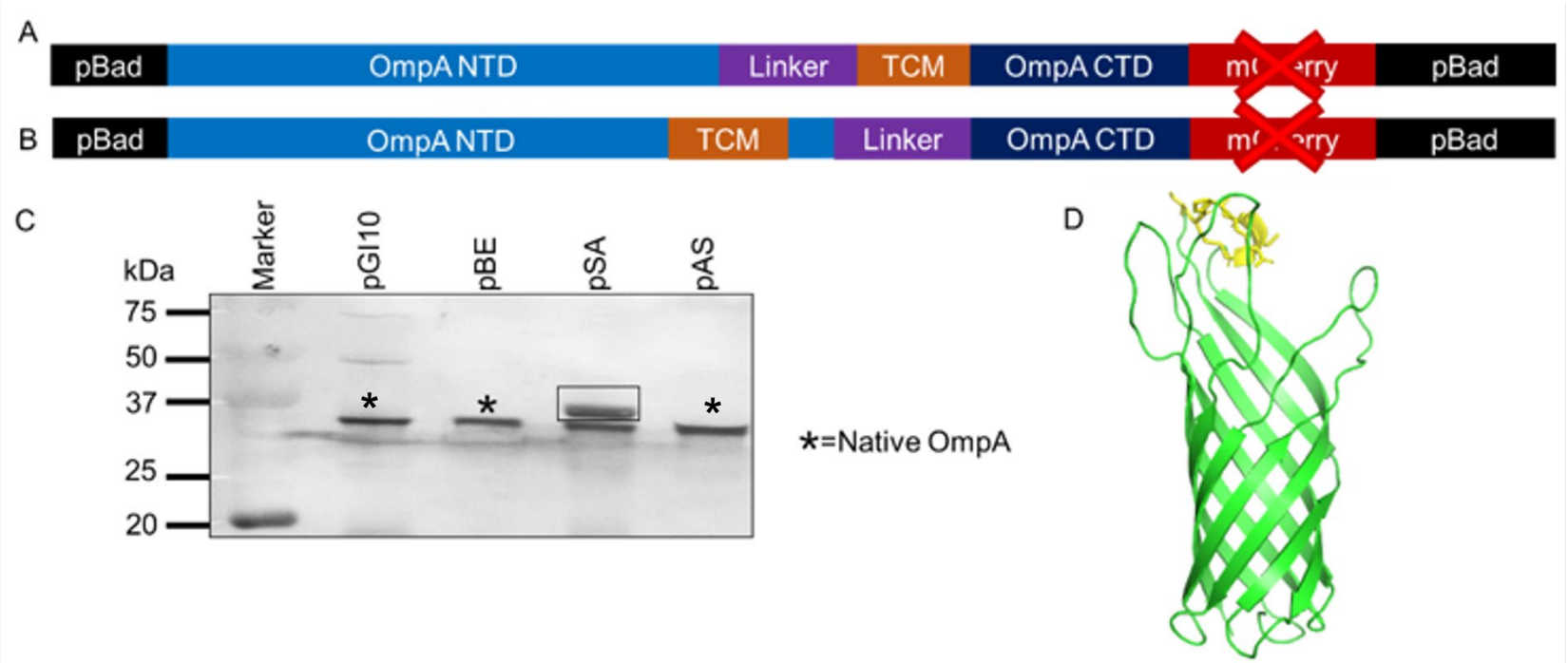

Figure 4.13: Design and western blot of the OmpA-Cys motif protein pSA, pAS.

A) and B) proposed constructs of pAS and pSA, respectively. pAS has the tetra cysteine motif (TCM) inserted immediately after the OmpA natural linker, whereas in pSA the TCM is inserted between V-107 and Y-110. C) western blot analysis confirming protein expression with a band at 39 kDa (above natural OmpA) for pSA construct only. *Escherichia coli* BL21 (DE3) cells were transformed separately with four plasmids (pGI10, pBE, pSA, and pAS). Samples were prepared using the outer membrane fractionation method. Samples were transferred from Sodium dodecyl-sulfate polyacrylamide gel electrophoresis (SDS-PAGE) onto a nitrocellulose membrane. Rabbit polyclonal OmpA and goat anti-rabbit alkaline phosphatase conjugate were used as the primary and secondary antibodies, respectively. (*) donates the native OmpA band. D) Swiss model for the insertion of the TCM into the outer loop of OmpA. PDB file:1BXW (Pautsch *et al.*, 1998).

The labelling with FlAsH-EDT_2 was performed in accordance with the TC-FlAsH™ TC-ReAsH™ II In-Cell Tetracysteine Tag Detection protocol (www.thermofisher.com). Tris (2-carboxyethyl) phosphine (TCEP)-Melford Laboratories LTD) was also used as a reducing agent to ensure the cysteine remained in a reduced form and was therefore likely to react with FlAsH-EDT_2. Samples of the OM fractions were diluted 1:10 with a final volume of 400 µl for each sample. All samples were then incubated in the dark with 1.25 µM FlAsH for 90 and 180 minutes. We added the reducing agent TCEP in order to demonstrate that TCEP enhanced labelling. We observed very low level of labelling when FlAsH alone was incubated with pSA for 90 and 180 minutes. In contrast, when incubating samples with the reducing agent TCEP at 1 mM and 0.5 mM, we observed significantly increased labelling **Figure 4.14**. This data was obtained with the protein pSA, whereas pAS samples showed no enhancement (**Figure 4.14**) which is in agreement with the absence of a pAS band on SDS-PAGE (**Figure 4.13**). The FlAsH labelling reagent has been shown to bind specifically to the tetra cysteine motif inserted into proteins (CCPGCC) (Granier *et al.*, 2007), and their data is similar to that presented here where FlAsH binds with the protein (pSA). Importantly, this demonstrates that we are able to specifically detect the presence of OmpA and potentially quantify OmpA in the OM fraction. This is suggesting a novel approach to measuring OMVs. Further work is required to validate these findings and perform confirmatory studies that this novel method can be used to quantify OMVs.

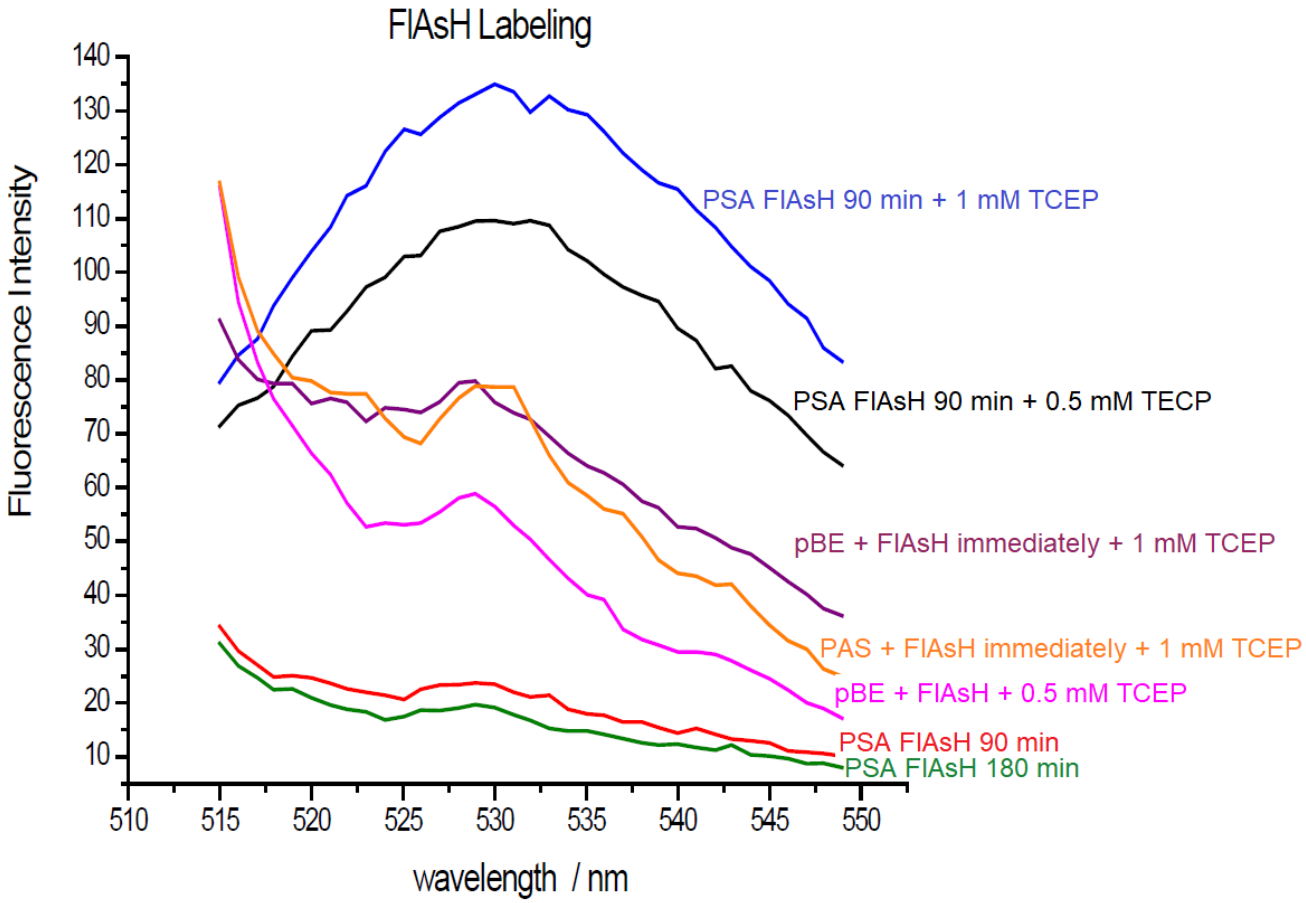

Figure 4.14: FlAsH fluorescence spectra of the outer membrane (OM) samples.

OM preparations were incubated with 1.25 µM FlAsH for 90 minutes, unless stated. Tris (2-carboxyethyl) phosphine hydrochloric acid (TCEP) was added where indicated. Samples were placed in 5 mm pathlength Hellma 101.016-40 Quartzglass cuvette at room temperature. Spectra were collected using a Cary Eclipse fluorimeter with an excitation wavelength of 505 nm. Both excitation and emission band widths were set to 20 nm. Blue; pSA+FlAsH from 90 minutes+ 1.0 mM TCEP, black; pSA+FlAsH from 90 minutes+ 0.5 mM TCEP, purple; pBE+FLASH 1 mM TCEP measured immediately, pink; pBE+FlAsH+0.5 mM TCEP, orange; pAS+FlAsH immediately+1.0 mM TCEP, red; pSA+FlAsH from 90 minutes, green; pSA+FlAsH from 180 minutes. pSA is the insertion of tetracysteine motif in an extra cellular loop of OmpA between V-107 and Y-110. pBE is pBAD empty vector which does not produce recombinant OmpA protein.

4.2.7 Detection of Outer Membrane Vesicles (OMVs) using fluorescent OmpA.

To detect the presence of the OMVs, pAM was co-expressed separately with pCaf1ΔA, pCaf1ΔR, and pGEMT. pGI10 was also co-expressed with pCaf1ΔA, pCaf1ΔR, and pGEMT whilst pSAM was co-expressed separately with pCaf1ΔA. To induce Caf1 expression, cells were grown for 7 h at 35 ˚C. OMVs were prepared as described in Chapter **II** Section **2.** OMV samples from each culture were then prepared as previously described (Section **3.2.6,** Chapter **III**). We used the three following approaches to analyse the OMV samples; 1) OMV fluorescence was measured using a plate reader (**Figure 4.15**); 2) quantification of OmpF present in the OMV by using western blot (**Figure 4.16**) and 3) images of the OMVs were examined using total internal reflection fluorescence (TIRF) microscopy (**Figures 4.17, 4.18 and 4.19**).

The plate reader experiment (**Figure 4.15**) showed a significant increase in the fluorescence in pCaf1ΔR and pCaf1ΔA compared to pGEMT. Thus, the expected increase in OMV levels in pCaf1ΔA are reflected in this simple assay.

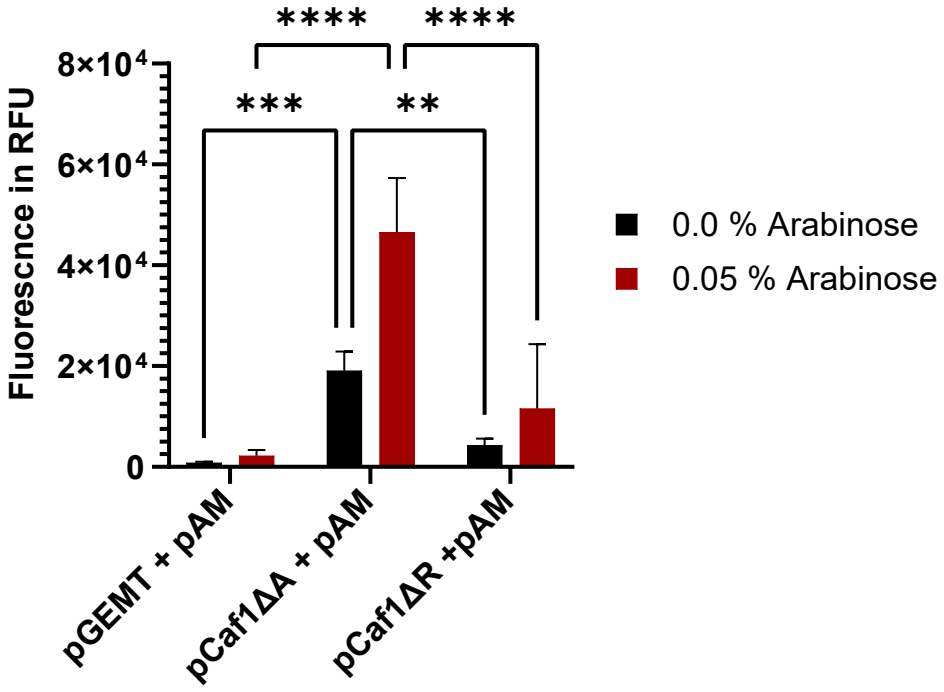

Figure 4.15: Relative amount of fluorescence in outer membrane vesicle (OMV) samples.

Relative fluorescence immediately following OMV preparation. 200 µl of each sample was transferred into a 96-well plate and fluorescence was measured immediately at 610 nm. Error bars represent standard error of the mean. Asterisks represent significant differences between groups (**** p<0.0001, *** p < 0.001, ** p<0.01) determined by One-Way ANOVA. Biological replicates = 2.

Using the same cultures described previously in this section (**4.2.7**) , we aimed to confirm the production and fluorescence of the OMVs using western blots with a rabbit anti-OmpF and a goat anti-rabbit alkaline phosphatase conjugate as the primary and secondary antibodies, respectively. **Figure 4.16B**, depicts an increase in OmpF in the pCaf1ΔA sample, supported by the largest fluorescence data of all constructs, suggesting that pCaf1ΔA cultures are rich with OMVs, supporting our previous data presented in Chapter **III**.

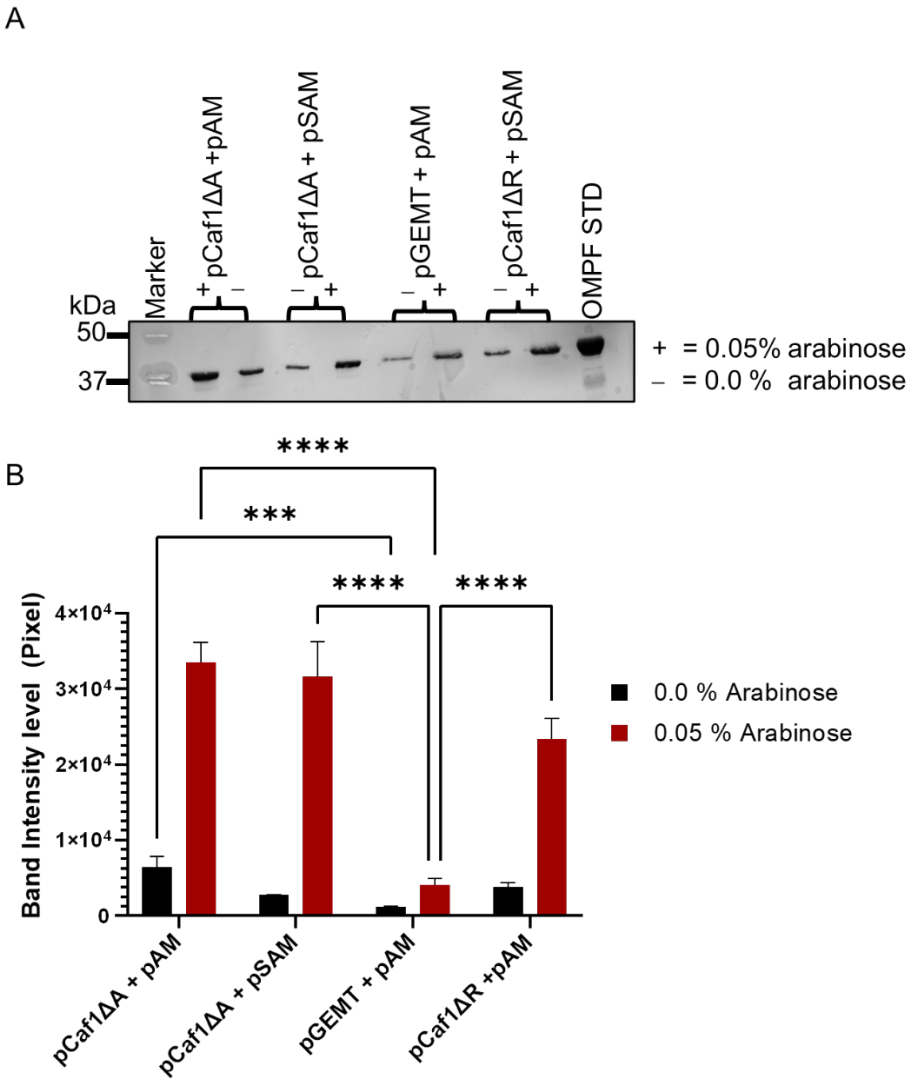

Figure 4.16: Relative amount of OmpF in Outer Membrane Vesicle (OMV) samples.

A) OmpF level detection in OMV samples prepared by transferring OMV samples from SDS-PAGE onto a nitrocellulose membrane. Samples were analysed using a rabbit anti-OmpF and goat anti-rabbit alkaline phosphatase conjugate as the primary and secondary antibodies, respectively. B) Densitometric quantification of OmpF bands using Image J. Biological replicates (n=2), technical replicates (n=6). Error bars represent the standard error of the mean. One way ANOVA test was used to determine the statistical significance of the differences among the samples. Significant differences between groups are indicated by asterisks, (****p< 0.0001, **(p< 0.001). pAM = OmpA + mCherry ; pSAM = OmpA +TCM; TCM = Tetra cysteine motive; OmpF STD = Loading control.

For TIRF wavelengths of 488 and 561, relating to blue and green lights, respectively, were used to excite the membrane with Mitotracker green membrane dye and to stimulate the mCherry, respectively. The Mitotracker green membrane dye and the mCherry were used to track the OMVs. The plasmid pAM was selected as it has previously been shown to have the largest fluorescent from our new chimeras, whilst containing the full length OmpA and mCherry. We selected the pGI10 plasmid as a positive control, as this contained the full length OmpA and mCherry. Images from the TIRF microscope analysis of pAM and pCaf1∆A cultures are displayed in Figure 4.17. We observed bright particles in which the membrane dye and OMP signal colocalise. The increase in such objects is clear in the comparison of the empty pGEMT and pAM-pCaf1∆R construct (Figure 4.18) which confirms the effect of Caf1 expression on OMV production. The positive control using the published pGI10 plasmid with pCaf1∆A also shows co localisation of the Mitotracker and OMP fluorescence expected of OMV, These observations suggest an increased presence of OMV due to Caf1 expression , confirmed by an increase in fluorescence pGEMT < pCaf1∆R < pCaf1∆A in (**Figure 4.15**). These data suggest that a fluorescent OMP is an efficient probe for the quantification of OMVs.

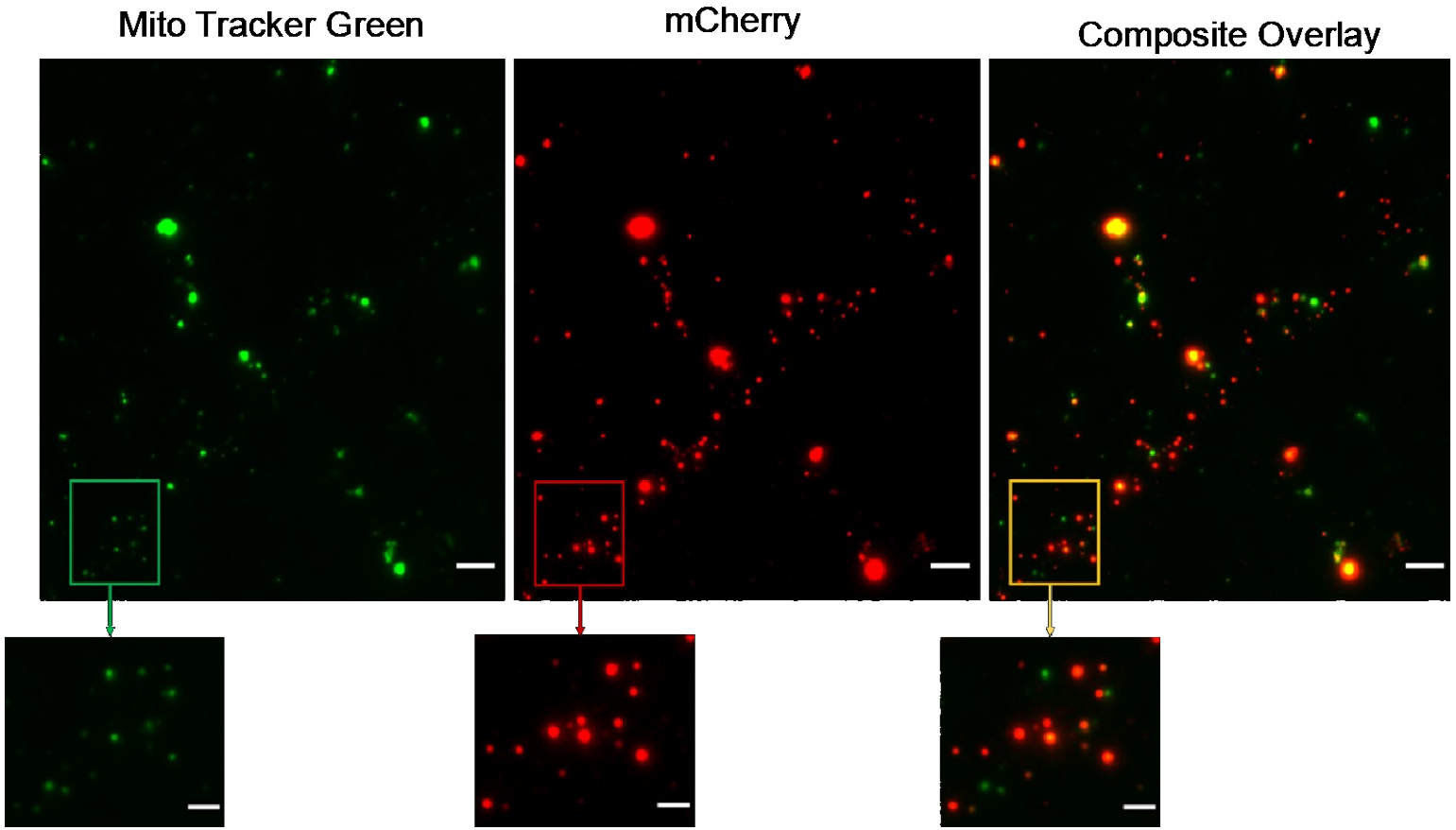

Figure 4.17: Total internal reflection fluorescence (TIRF) of OMV from pAM and pCaf1ΔA cultures.

All samples were diluted in phosphatase-buffered saline (PBS) buffer at a ratio of 1:100 before being stained with 100 nm MitoTracker green (MTG) membrane dye for 10 minutes at room temperature before being immobilised on a 1.2 % agarose slides and photographed at 488 and 561 nm. Scale bar = 3 µm. *Escherichia coli* BL21 cells were co-transformed with pAM and pCaf1ΔA. All the outer membrane vesicle samples were prepared as previously described in Chapter III, section 3.2.6. All microscopy analyses were performed using the Nikon Eclipse Ti2 equipped with Photometric Kinetix sCMOS camera Nikon CFI SR HP Apo TIRF 100XAC Oil.

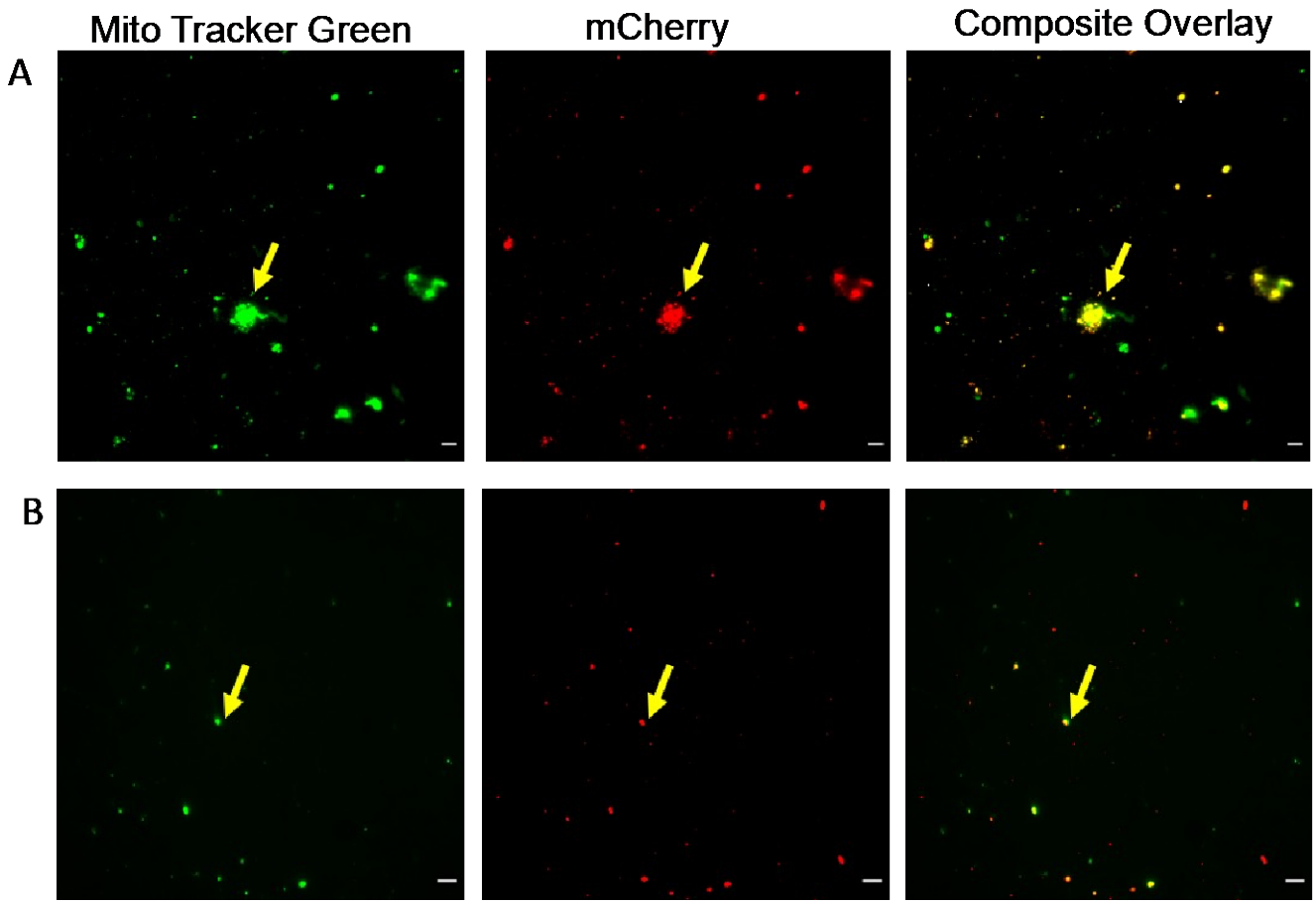

Figure 4.18: TIRF of outer membrane vesicles (OMVs).

(A) *Escherichia coli* BL21 cells were co-transformed using pAM and pCaf1ΔR. Large clumps and scatters of OMVs are depicted here. B) *E. coli* BL21 cells was transformed using pAM and pGEMT. OMVs appear as dots ≥250 nm). Scale bar = 2 µm. All OMV samples were prepared as previously described in Chapter III, section 3.2.6. All microscopy analyses were performed using the Nikon Eclipse Ti2 equipped with Photometric Kinetix sCMOS camera Nikon CFI SR HP Apo TIRF 100XAC Oil. pAM = OmpA + mCherry ; pGEMT = Empty vector.

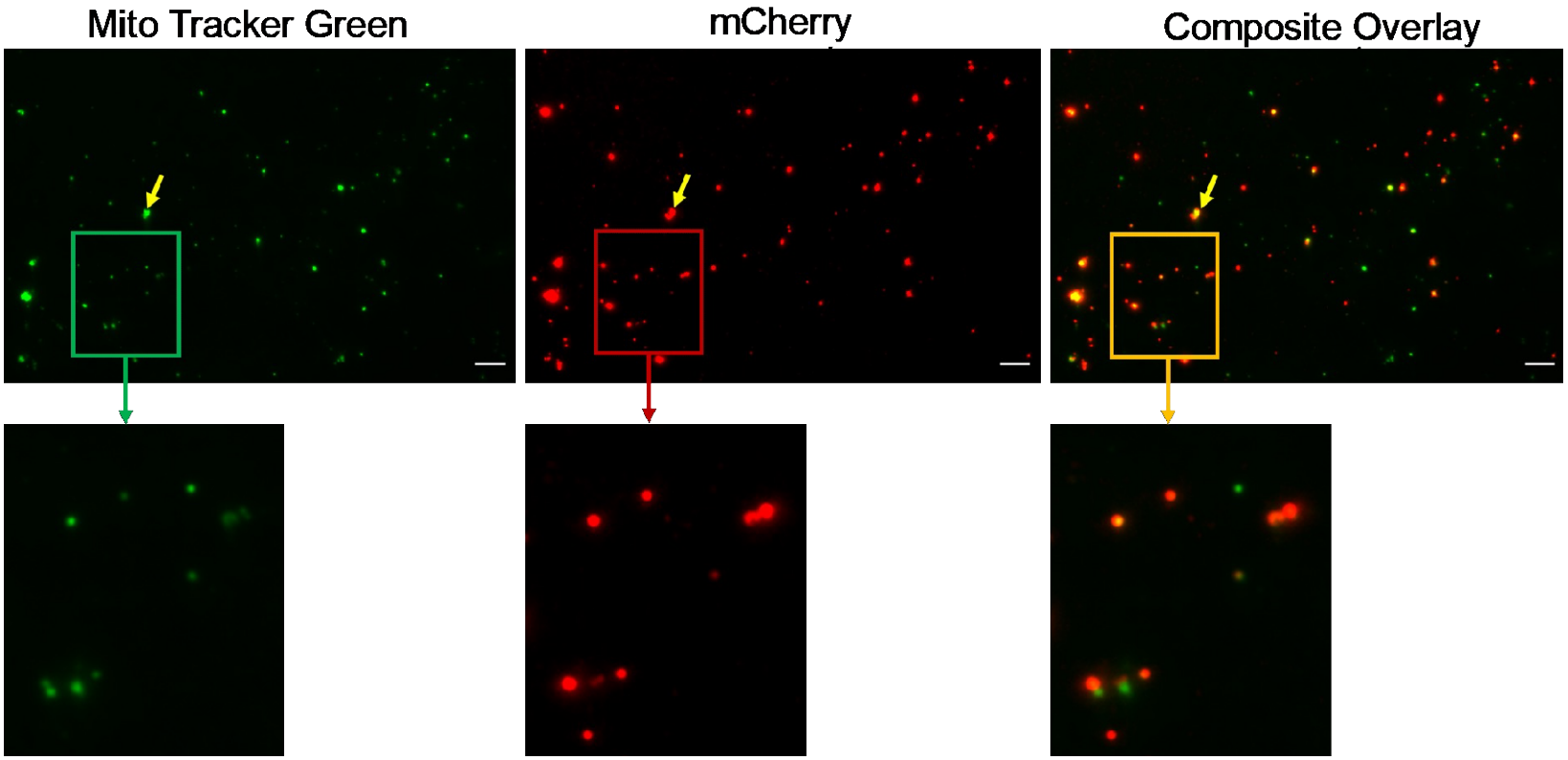

Figure 4.19: TIRF of OMV from pGI10 and pCaf1ΔA cultures.

Escherichia coli BL21(DE3) cells were co-transformed using pGI10 and pCaf1ΔA. OMVs appear clearer with scatterings. All OMV samples were prepared as previously described in Chapter III, section 3.2.6. All microscopy analyses were performed using the Nikon Eclipse Ti2 equipped with Photometric Kinetix sCMOS camera Nikon CFI SR HP Apo TIRF 100XAC Oil. pGI10 = OmpA + mCherry (Verhoeven *et al.*, 2013).

4.3 Discussion

OMVs have been identified as prospective candidates for the creation of OMV-based vaccines against infectious diseases (Bartolini *et al.*, 2013; Kulkarni *et al.*, 2014). One biotechnological design of OMV-based applications involves endogenous loading of surface-exposed antigens based on the expression of proteins which insert into the OM (Furuyama *et al.*, 2021). OmpA is a monomeric protein that functions as a primary surface antigen of Gram-negative bacteria and has been shown to be abundant on the surface of bacterial cells and their derived OMVs. It has been found that mutants lacking OmpA in *Salmonella* significantly increase their OMV formation (Deatherage *et al.*, 2009). Because of its monomeric nature and small size, OmpA has served as an ideal model for studying the biophysical principles and mechanisms by which membrane proteins insert and fold into the OM (Pautsch *et al.*, 1998; Kleinschmidt, 2003).

The subject of surface-exposed antigens, including OmpA, being produced in OMV has previously been investigated extensively. Kesty *et al.* (2004) found that expressed heterologous OMPs and periplasmic proteins, such as Ail and GFP, can be used to alter the characteristics of OMVs and deliver them to host cells (Kesty *et al.*, 2004). In a recent study into the use of OMVs as a potential vaccine, Weyant and colleagues have demonstrated that a biotinylated target protein antigen, such as GFP, can bind to artificial antigen receptors containing avidin on the exterior of genetically engineered OMVs (Weyant *et al.*, 2023). Genetic engineering of OMVs is utilised to improve and expand their potential to trigger humoral immune responses in the host and are based on pathogen-associated molecular patterns (PAMPs), triggering cell-mediated immunity (Kashyap *et al.*, 2022). In the present study, we investigated if fluorescently tagged OmpA could be utilised as a probe to measure Caf1 induced OMV formation and production. To achieve this, we employed different variants of fluorescent OmpA in *E. coli*, including co-transformation with pCaf1ΔA. This approach also allowed us to validate the results presented in Chapter III where we reported an increase in OMV production when cells produced Caf1 in the absence of the Caf1A usher protein.

We initially constructed the OmpA-sfGFP plasmid, expressing OmpA-sfGFP, to serve as a fluorescent marker for the quantification of OMVs. In our OmpA-sfGFP

construct the natural C-terminal domain of OmpA was replaced by sfGFP, including the natural linker joining the N and C terminal domains, notable due to its proline rich sequence that is capable of forming helical spacers between domains (Maiti *et al.*, 2011). However, through the use of microscopic analysis following separation of the IM and OM using the osmotic shock method, we observed that the OmpA-sfGFP fusion protein was trapped in the IM rather than in the OM. Generally, OMPs are translocated from the cytoplasm into the periplasm across the IM with the mediation of the Sec translocon in the general secretion pathway (Dalbey *et al.*, 2012; Rigel *et al.*, 2012; Tsukazaki *et al.*, 2008; Fairman *et al.*, 2011). Once across the IM, the OMPs are able to interact with periplasmic chaperones, such as SurA and Skp, that can then deliver the OMPs to the β-barrel assembly machine (BAM) complex for insertion into the OM (Sklar *et al.*, 2007; Hagan *et al.*, 2011; Kleinschmidt, 2015; Wang *et al.*, 2021).

Previous research from Kim *et al.* (2008), whose study demonstrated that GFP fused directly to the C-terminus of the pore-forming cytolysin protein (ClyA) was efficiently translocated across the IM and co-localised in OMVs. De Boer and colleagues also showed that several components of the periplasmic Tol-Pal complex, consisting of several proteins connecting the IM with the OM in *E. coli*, could be successfully labelled with GFP (Gerding *et al.*, 2007). Finally, in a recent study by Hale and co-workers, they observed successful transportation of a series of periplasmic proteins fused with GFP were able to cross the IM (Hale *et al.*, 2022). The data presented here contradicts these studies, where trapping of the OmpA-sfGFP fusion protein in the IM, suggests that the first step in this process, secretion into the periplasm, was prevented. Although there is clear evidence supporting the successful export of GFP fusion proteins into the periplasm, this study demonstrated that replacing the OmpA C-terminal domain with sfGFP prevented secretion across the IM. Clearly unsuccessful fusions of this type are rarely published, and this problem may be more common than appears. To further our understanding on the exact mechanisms of why the OmpA-sfGFP fusion protein was unable to pass across the IM requires more research.

The successful fusion of mCherry to both truncated and full length OmpA has been widely employed as an efficient fluorescent reporter for monitoring gene expression and protein localisation (Fages-Lartaud *et al.*, 2022).The work of Verhoeven *et al.* (2013) provided evidence that has facilitated the ability to explore the use of this fluorescent proteins for OMVs detection. We developed second-generation

experimental designs with a full length OmpA linked to the C-terminal mCherry to examine if we were able to improve the control of protein expression and stability by using arabinose inducible vectors with different fusion designs. We generated OmpA-mCherry chimeras that were subsequently inserted into pBAG following the deletion of the *sfGFP* gene. The data presented in this chapter demonstrates that the full length OmpA-mCherry fusion protein from pGI10 had the largest fluorescent intensities, both with and without induction of the IPTG when compared to our constructs which were induced with arabinose.

To assess the localisation of the new OmpA-mCherry chimeras in the OM, we used four different synthetic genes described in **Table 4.2,** two of which pSAM and pASM contain the TC motif. We extracted samples from the cell cultures of each of the four chimeras and examined them using a modified OM fractionation method (Wolf-Watz *et al.*, 1973), and subsequently analysed the data from these samples using an SDS-PAGE, western blot and microscopic analyses. The SDS-PAGE analysis detected the presence of a strong unanticipated band at approximately 14 kDa (**Figure 4.7**). We identified this band as the breakdown product of periplasmic glutamine-binding protein (glnH), confirmed using mass spectrometry. The glnH protein is an OMV-associated protein normally located in the periplasm and is essential for bacterial survival and pathogenicity (Bai *et al.*, 2014). Using western blot analysis and an anti-OmpA antibody, we also observed endogenous OmpA expression with a band at 35 kDa (**Figure 4.9)**.

The SDS-PAGE analysis revealed that all the OmpA-mCherry fusions exhibited similar susceptibility to proteolytic degradation to the published protein from pGI10, and therefore our alternative constructs did not noticeably improve fusion protein stability. However, our data did demonstrate that the full length OmpA can be used as a fluorescent marker suitable for quantifying the production of OMVs. Furthermore, our findings align with the work of Stephan and colleagues who analysed the ability of *Salmonella Typhimurium* OMVs to defend against bacteriophage P22 (Stephan *et al.*, 2020). The same research group also revealed that co-expression of an OmpA-mCherry construct as an OM marker protein revealed that it was localised in the OMV fraction. Interestingly, they also demonstrated that the OmpA-sfGFP localises in the IM but was also present in the OMV fraction (Stephan *et al.*, 2020).

In an attempt to identify an alternative approach using the full length OmpA as a fluorescent probe for detecting and measuring OMV production, we utilised two of the original OmpA-mCherry chimeras, pASM and pSAM. These also contained tetra cysteine (TC) motifs that bind the fluorescent probe FlAsH-EDT_2, which has gained traction in recent years due to its selectivity for the TC motif, and its capacity to be absorbed by cells (Piras *et al.*, 2017). This produced two new constructs pAS and pSA from each of which the mCherry was deleted A western blot analysis confirmed protein expression with a band at 39 kDa (above natural OmpA) for the mutant OmpA (pSA) construct only. The results in **Figure 4.15** showed that the fluorescence intensities of the OM fraction samples incubated with FlAsH increased as the reducing agent TCEP concentration increased (1 mM, 0.5 mM).

In summary, the data presented in this chapter demonstrate that OmpA based fluorescent proteins can be used when investigating OMV trafficking and formation. These findings are similar to the previously published work of Kesty *et al.* (2004) who indicated that in order to understand OMV production and OMV-mediated transport and trafficking inside the host cell, the OMV content needs to be engineered (Kesty *et al.*, 2004). Recent advances in OMV therapeutic applications pertaining to *meningitis* serogroup B (MenB) vaccine has provided proof that OMVs can be genetically manipulated to produce safe and effective OMV particle vaccine products (van der Pol *et al.*, 2015). The use of fluorescent OmpA derivatives can help in the quantification of OMV production and the visualisation of OMVs using microscopy. The detection and quantification of OMVs is essential for providing a platform for the development of non-infectious and nanoparticle vaccines against a host of pathogens (Bartolini *et al.*, 2013; Weyant *et al.*, 2021).

Chapter Five

Effect of overexpression of Caf1A usher on OMV and Caf1 polymer production

"Nothing can come of nothing"

William Shakespeare

5 Effect of the overexpression of the *caf1A* usher protein gene on OMV and Caf1 polymer production

5.1 Introduction

A diverse group of Gram-negative pathogenic bacteria utilise the chaperone–usher (CU) pathway to assemble non-flagellar, surface-located proteinaceous appendages, such as virulence factors pili, fimbriae ,and capsules (Hatkoff *et al.*, 2012; Dubnovitsky *et al.*, 2010). These virulence factors, which are filamentous extracellular organelles, are essential in the dissemination of cells, protection against the host immune system during infection and in the mediation of bacterial pathogen-host interactions (Dubnovitsky *et al.*, 2010; Remaut *et al.*, 2008). Based on their morphological properties and antigenic determinants, these virulence factors such as pili, fimbriae and capsules, are hair-like virulence-associated surface fibres that are commonly categorised into different classes. The most commonly used method for characterisation are the adhesive type I pili (mannose-sensitive hemagglutination represented by the Fim system), the pyelonephritis-associated pili (represented by the Pap system) and the F1 antigen of *Yersinia pestis* (Y. *pestis*) (represented by the Caf system) (Runco *et al.*, 2008; Proft *et al.*, 2009; Dalbey *et al.*, 2012; Werneburg *et al.*, 2017). The generic CU chromosomal genes are commonly clustered into operons. Each CU gene encodes at least one major structural subunit, a periplasmic chaperone, an outer membrane (OM) pore-forming usher, and/or regulatory proteins (Wurpel *et al.*, 2013; Sauer *et al.*, 2004; Nuccio *et al.*, 2007). Each subunit exhibits an incomplete immunoglobulin (Ig)-like structure lacking a seventh C-terminal β-strand (Geibel *et al.*, 2014).

The primary functions of the boomerang-shaped, 25 kDa periplasmic chaperone (PapD, FimC or Caf1M) involves facilitating the folding of structural subunits, preventing premature polymerisation and aggregation in the periplasm and allowing transportation of the folded subunits into the OM-spanning usher (PapC, FimD or Caf1A). The main function of the OM-spanning usher is to serve as an assembly platform for recruiting chaperone–subunit complexes from the periplasm, coordinating their assembly into a growing polymer and secreting this linear, unbranched fibre to the cell surface through its channel (Waksman *et al.*, 2009; Omattage *et al.*, 2018).

The pilus ushers have been shown to function autonomously and independently of a hydrolysable energy source or a proton motive force generated across the inner membrane (IM) (Jacob-Dubuisson *et al.*, 1994).

The assembly of the F1 antigen via the CU secretion system produces an amorphous anti-phagocytic capsule consisting of a polymerised capsular antigen fraction 1 (Caf1) polypeptide subunit (Zavialov *et al.*, 2003). The membrane-integral usher (Caf1A) is a 90.4 kDa porin-like outer membrane protein (OMP) that serves as a binding scaffold for organising the polymerisation of Caf1 into a capsule and promoting its anchorage into the OM (Zavialov *et al.*, 2001; Du *et al.*, 2002; Dubnovitsky *et al.*, 2010; Yu *et al.*, 2009). The initial step in the CU mechanism of the F1 antigen biogenesis involves synthesising each Caf1 subunit in the cytoplasm and then translocating it as an unfolded polypeptide across the IM via the Sec system to the periplasm. In the periplasm, Caf1M binds to the Caf1 subunit by the donor strand complementation (DSC) system, forming a soluble and stable Caf1M-Caf1 complex. The DSC system involves Caf1M donation of a ß-strand to complete the incomplete Ig-like fold of the subunit in a noncanonical manner. This binary complex is then transferred to the OM-localised Caf1A usher where Caf1M disassociates from Caf1, allowing for the Caf1-Caf1 interaction to ensue. Caf1A catalyses the replacement of the Caf1M-Caf1 complex with the Caf1-Caf1 interaction (Nuccio & Bäumler, 2007). It has previously been observed that Caf1A only binds to the chaperone-subunit complexes and differentiates between free Caf1M and Caf1M-Caf1 intermediates(Di Yu *et al.*, 2012).

Polymerised via the donor strand exchange (DSE) system, the Caf1 subunit then is incorporated into the growing fibre and eventually secreted to the surface of the bacterium (Soliakov *et al.*, 2010). The DSE system involves a strand invasion event in which the N-terminal extension of an incoming pilus subunit displaces the donated chaperone ß-strand in the preceding subunit, linking the two subunits together via formation of a canonical Ig fold. The resulting 15 kDa Caf1 provides producing cells with a shield to protect themselves from phagocytosis by minimising their interaction with the macrophage surface (cell adhesion) and by obscuring innate receptor-binding sites and mechanisms needed for ingestion (Werneburg *et al.*, 2017; Sauer *et al.*, 2004; Peters *et al.*, 2022).

The structure of OM ushers consists of a central transmembrane β-barrel domain (TM), an N-terminal periplasmic domain (NTD), a β-sandwich middle plug domain (PD), and two carboxy-terminal periplasmic domains (CTD1 and CTD2) (Phan *et al.*, 2011) (**Figure 5.1)**. The TM consists of a 24-stranded β-barrel and represents the secretion pore for the assembly of fibres and their export to the surface of the bacterium. The NTD is responsible for the initial binding site for the chaperone-subunit complexes with high affinity and recruitment of new subunits for the growing fibre. Located in the periplasm underneath the TD, the PD plays an essential role in the CU pathway since its deletion hinders the ability of the usher to assemble the fibre (Remaut *et al.*, 2008; Yu *et al.*, 2009; Phan *et al.*, 2011). CTD consists of a seven-stranded β-barrel whose presence is crucial for Caf1A to function (Dubnovitsky *et al.*, 2010).

Volkan *et al.* (2012) reported on the interactions between the NTD and PD, suggesting a biophysical basis for usher gating. The authors also demonstrated that the interaction between NTD and PD can bind chaperone-subunit complexes, indicating that the middle plug domain actively recruits chaperone–subunit complexes to the PapC usher and is the sole recruiter of the chaperone-terminator subunit (PapDH). Ford *et al.* (2010) demonstrated that the PapC CTD is indispensable for the pilus biogenesis and that there is a homology between the CTD of PapC and the PD of the same protein (Ford *et al.*, 2010). In a more recent study, Omattage *et al.* (2018) presented data from X-ray crystal structure analysis of the full length PapC usher from *Escherichia coli (E. coli)* in a PapC-PapDG ternary (usher-chaperone-adhesion) complex, elucidating the mechanism by which PapC is primed for activation and the process of its transition to a post-activation state (Omattage *et al.*, 2018). The findings from Omattage *et al.* (2018) showed that the NTD-CTD2 interaction is crucial for maintaining a stable association between PapDG and PapC, and translocation of subunits from the NTD to CTDs. Furthermore, their results suggest that CTD2 drives subunit transfer, perhaps by using the avidity of its interactions with both the NTD and PapD to competitively displace subunits from the NTD during pilus biogenesis.

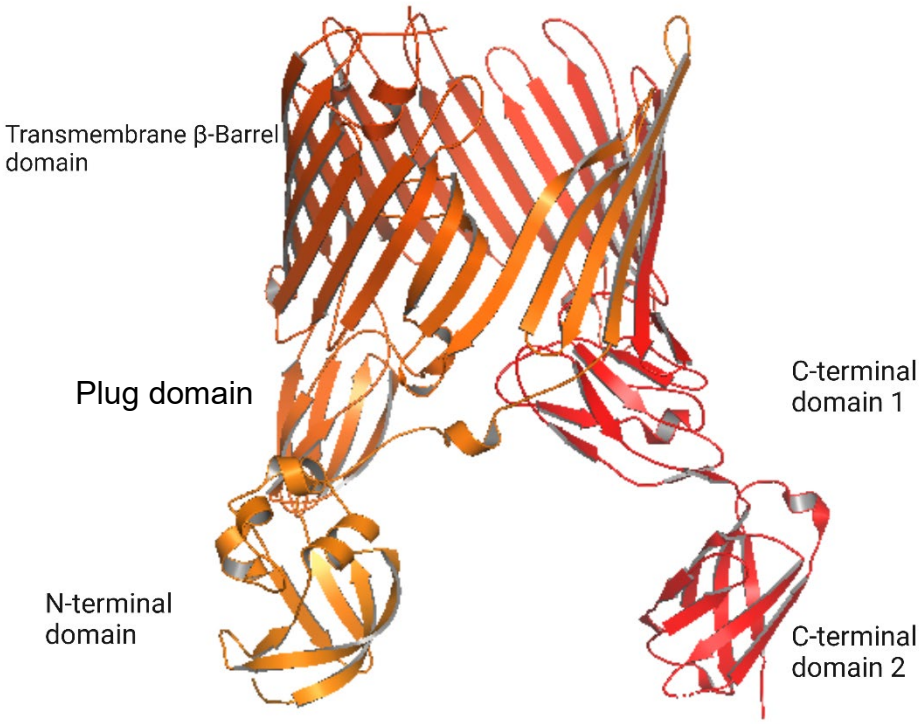

Figure 5.1: Caf1A usher structure

Caf1A usher structural model generated using PyMOL software and based on the crystal structure of FimD (PDB code: 3RFZ) (Phan *et al.*, 2011).

Departing from these findings, the recent work of Du *et al.* (2021) proposed a sequential model for P pilus biogenesis at PapC (Du *et al.*, 2021). The model proposed by Du et al. (2021) indicates that the activation of PapC results from the recruitment of the PapDF complex since PapC accommodates two-subunit domains below its channel entrance. These findings are in accordance with the earlier work of Remaut *et al.* (2008) who observed that FimD possess two periplasmic sites that are required for successive rounds of subunit binding and fibre assembly; one of which is formed by the NTD, and the second is formed by CTD1 and CTD2 (Remaut *et al.*, 2008). Furthermore, Du *et* al. (2021) reported that the usher CTD2 is able to adopt three different conformational states in the pilus assembly process. Conformer I involve the DSE, which is located between the adaptor PapF and PapG, which subsequently forms the first pilus link and releases CTD2. Conformer II binds to the vertex of the periplasmic chaperone PapD and shifts on PapD to generate an NTD-PapD-CTD interface. Conformer III destabilases the NTD binding to PapD (Du *et al.*, 2021).

The non-covalently assembled Caf1 polymer is a major constituent of Yersinia outer membrane vesicles (OMVs) (Eddy *et al.*, 2014). These nanostructures are believed to be utilised by pathogenic bacteria to regulate the activation or inhibition of the innate

immune system (Kaparakis-Liaskos *et al.*, 2015). Eddy *et al.* (2014) demonstrated that the abundance of Caf1 is responsible for causing other virulence determinants, such as proteases Pla and adhesion Ail, to disassociate from *Y. pestis* OMVs. In Chapter III, we presented results showing that OMVs are a major constituent of the flocculent layer, indicating Caf1 polymer production, and that the absence of this layer could be a determining factor of OMV release (**Figure 3.19**). Our results also demonstrated that Caf1A deletion prevents Caf1 polymer formation at the cell surface, causing aggregation of Caf1 in the periplasm, which may in turn exert stress on the OM to augment OMV production. Building on these results, the present study was designed to enhance our knowledge and understanding of the actions and dynamics of the Caf1A usher, whose expression is required for Caf1 formation. The primary aim of this chapter is to test the hypothesis that an increased expression of Caf1A will lead to an increase in Caf1 polymer production, with a subsequent reduction in OMV formation due to a reduction in the accumulation of Caf1 monomers in the periplasm. Moreover, we will also examine whether reducing stress stemming from the aggregation of Caf1 monomers in the periplasm will result in a decrease in the flocculent levels.

5.2 Results

5.2.1 Expression of caf1A

Here we aimed to test the hypothesis that an increased expression of Caf1A will lead to an increase in Caf1 polymer production, with a subsequent reduction in OMV formation due to a reduction in the accumulation of Caf1 monomers in the periplasm. Initially, we aimed to control Caf1A levels in the OM by inserting the *caf1A* gene into a plasmid with tightly regulated expression (pBAD). In the absence of a Caf1A specific antibody, and to ensure that we were able to detect and quantify Caf1A required the construction of the plasmid pBADCaf1AFLAG (pBA^{FLAG}) for subsequent experiments. To construct pBA^{FLAG}, an additional DNA sequence was added, using the In-Fusion HD cloning method, which coded for residues of the FLAG tag (DYKDDDDK) that were inserted into the middle extracellular loop of Caf1A (**Table 5.1**).

We used a previously identified site within Caf1 for the insertion of FLAG tags that had no impact upon the process of Caf1 polymer secretion (Al-jawdah, 2019). Using a model of Caf1A based on the crystal structure of the homologous FimD usher (PDB code: 3RFZ) (Phan *et al.*, 2011) allowed us to identify a suitable external loop and insert the FLAG sequence (**Table 5.1**) between proline 467 and asparagine 468 without affecting Caf1 production (**Figure 5.2**). Using AlphaFold (Jumper *et al.*, 2021; Mirdita *et al.*, 2022) we created another model of Caf1A to confirm the correct location for the FLAG tag insertion. The previous work from our group used $Caf1A^{FLAG}$ that was produced from a pCaf1 plasmid (Al-jawdah, 2019). Here, the purpose of this set of experiments was to increase Caf1A levels from a second inducible plasmid resulting in an increased expression of Caf1A, using a novel inducible expression vector containing Caf1AFLAG.

Table 5.1: Oligonucleotide primers for the insertion of the FLAG tag into the caf1A gene

Primer name	Nucleotide sequence (5' to 3')
Forward pBADCaf1A^{FLAG}	GATTATAAAGATGATGATGATAAAAATACCCGTAATGATTGCCGC
Reverse pBADCaf1A^{FLAG}	ATCATCTTTATAATCCGGTTTACAATAGGTATTCAGGG

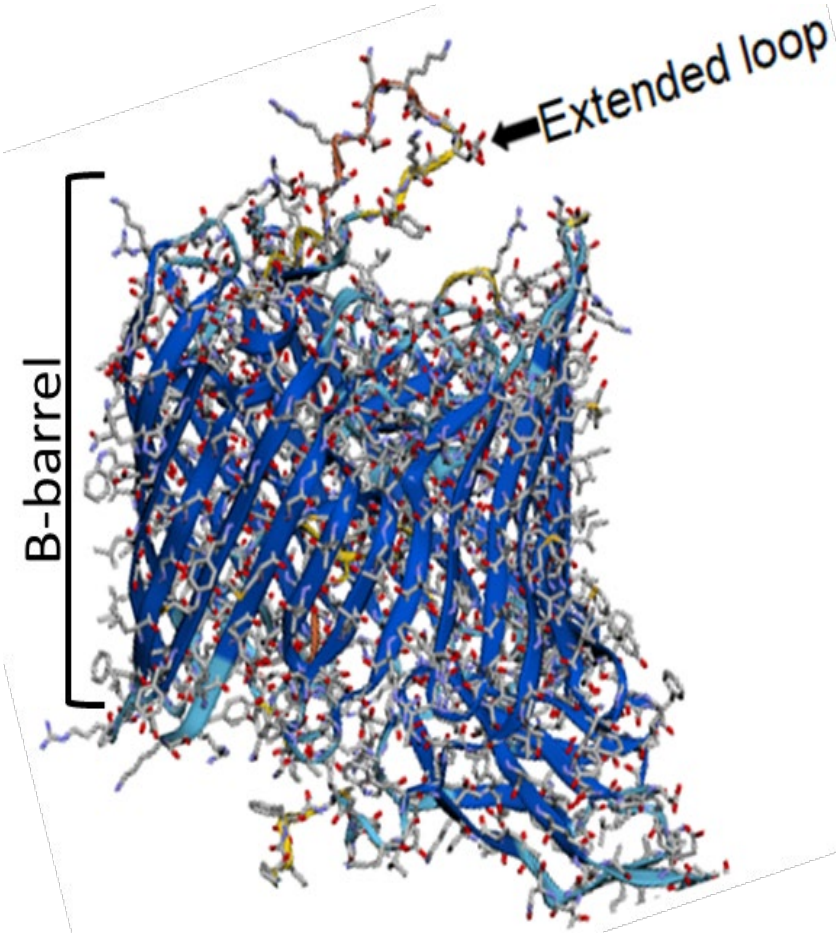

Figure 5.2: Caf1A usher outer membrane protein Alphafold model.

A β-barrel representation of the outer membrane (OM) Caf1A usher with the addition of the FLAG tag insertion within the central loop located between proline and asparagine (P-467 and N-468) facing the outer surface. PDB code: 3RFZ (Phan et al., 2011). The protein structure was created by AlphaFold.

The following experiment was conducted to test the expression of *caf1A*. *E. coli* BL21 (DE3) cells were transformed using pBA^{FLAG}. Cell cultures were grown for 7 and 22 h in TB media containing the appropriate antibiotic (20 µg/ml chloramphenicol) at 35°C with rotary agitation at 180 rpm. Induction with different L-arabinose concentrations (0, 0.05, 0.1 and 0.2% w/v) were started after the OD_{600} reached 0.6. Cells were then grown for 7 and 22 h and the subsequent collected cell pellets were centrifuged at 2367 x g for 20 minutes before being harvested. The supernatants were discarded. To ensure consistent loading volumes in each well across the gel, the cell pellets were diluted to the same OD with a lysis buffer. The samples were then resuspended in sample buffer before being heated at 100°C and then applied to SDS-PAGE. A western blot was used to identify the expression levels of Caf1A in the different concentrations of L-arabinose using an anti-FLAG antibody (**Figure 5.3**). We observed that Caf1A was expressed at all concentrations of the inducer L-arabinose. The expression of Caf1A was consistent at 7 h across different L-arabinose concentrations (0.05–0.2% w/v), indicating there was not a concentration dependent effect of the inducer L-arabinose. Similarly, the 22 h incubation time did not lead to higher levels of Caf1A in varying concentrations of L-arabinose. These findings demonstrate that we are able to express Caf1A using alternative vectors than pCaf1.

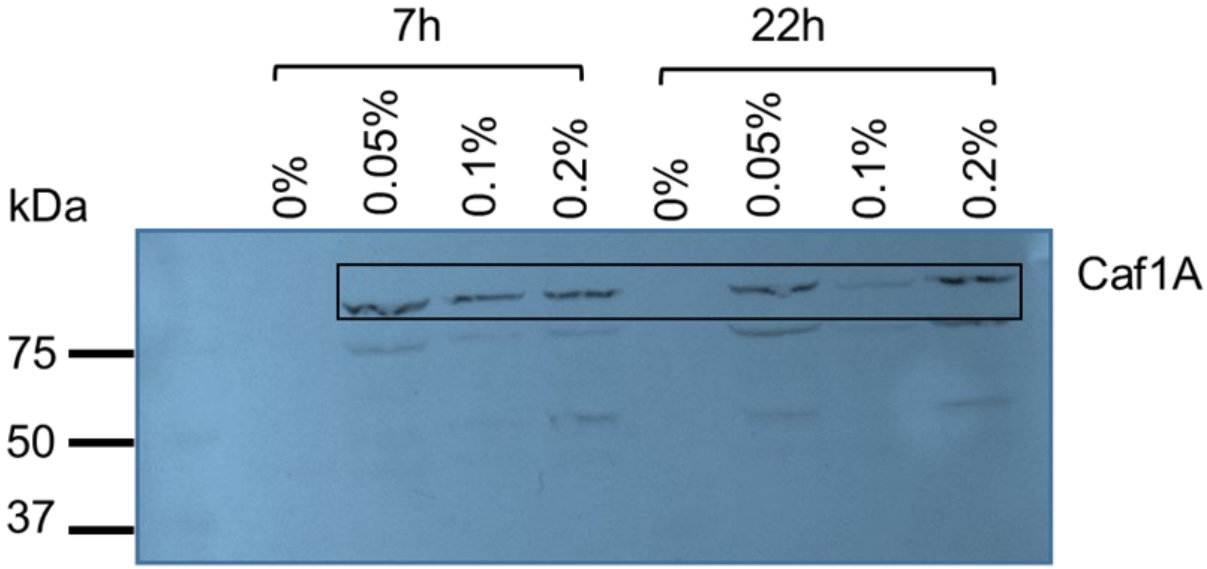

Figure 5.3: Caf1A expression.

A western blot analysis of the cultures of *Escherichia coli* BL21(DE3) cells transformed using the pBA^{FLAG}. The cultures used for expression were induced with different L-arabinose concentrations of 0, 0.05, 0.1, and 0.2% w/v, and then incubated for 7 and 22 hours at 35ºC whilst being shaken at 180 rpm. The cell pellets were harvested by centrifugation at 2367 x g for 20 minutes. All pellets were then diluted to the same OD with lysis buffer to ensure the same loading level in each well. Twenty µl samples of each cell pellet were then resuspended in sample buffer before being heated at 100°C and then loaded separately SDS PAGE. A western blot was used to identify the expression levels of Caf1A in different L-arabinose concentrations using rabbit polyclonal anti-FLAG and Goat anti-rabbit AP conjugate for the primary and secondary antibodies, respectively. Caf1A runs at ~90 kDa.

5.2.2 Effect of overexpression of caf1A on Caf1 production

We hypothesised that the presence of higher levels of the usher Caf1A would result in an increased production of the Caf1 polymer, with a subsequent reduction in OMV production because the periplasm is not under stress. The role of the usher is to act as an assembly platform for the periplasmic recruitment of chaperone-subunit complexes, coordinating their assembly into growing polymer and secreting this linear polymer to the surface through its channel. To test this hypothesis, we first investigated if we were able to increase the concentration of Caf1A. We utilised *E. coli* BL21 (DE3) cells that were co-transformed using the previously described pBA^{FLAG} and the following six different pGEMT based plasmids and the empty pGEMT vector:

1. pCaf1A^{FLAG} and an empty pBAD where the pGEMT based vector will be the sole source of Caf1A^{FLAG}

2. pCaf1ΔA + pBA^{FLAG} to identify levels of Caf1A^{FLAG} from pBA^{FLAG} in the absence of wild type (WT) Caf1A production

3. pCaf1A^{FLAG} + pBA^{FLAG} to observe the combined expression levels of both FLAG tagged constructs

4. pCaf1 + pBA^{FLAG} to observe the effect of WT Caf1 expression on Caf1A^{FLAG} levels

5. pCaf1ΔR + pBA^{FLAG} to observe effect of Caf1R *in trans,*

6. pGEMT + pBA^{FLAG}, to observe the effect of the empty vector

NB It is important to note here that, unless stated, these pCaf1 plasmids do not carry the caf1R deletion present in the pCaf1 plasmids used so far in this thesis.

Cultures were grown at 35ºC for 12 hours with continuous shaking 180 rpm, with 0.05% arabinose induction.

A western blot analysis revealed that the majority of Caf1A^{FLAG} was produced from the pCaf1 vector (**Figure 5.4A, lane 1**). Somewhat surprisingly, lanes 2 and 3 presented with low levels of Caf1A^{FLAG} when produced from the pBAD vector, or when both vectors were combined and then compared with the Caf1A^{FLAG} expression from pCaf1A^{FLAG} alone, respectively. In Lane 4 we utilised the complete *caf1* operon (*i.e.,* without FLAG) that was co-expressed with pBA^{FLAG}. We observed the lowest level of Caf1A^{FLAG} expression out of all the lanes, however, the levels of Caf1A^{FLAG} increased when *caf1R* was deleted, depicted in lane 4 (**Figure 5.4B**). These data suggest caf1R acting *in trans* has an inhibitory effect on the expression of Caf1A^{FLAG} obtained from

the pBAD vector. This is a novel finding in the thesis and demonstrates that Caf1R is regulating the production of Caf1A. These findings align with previous results that have revealed that in the presence of caf1R, Caf1 production from heterologous promoters is reduced, evidenced by an increase in Caf1 production following the deletion of caf1R (Karlyshev *et al.*, 1992a; Al-Jawdah *et al.*, 2019). The presence of caf1R shown here may in part contribute to explaining the difference between lanes 4 and 5 in (**Figure 5.4A**).These data clearly demonstrate that Caf1A is expressed in both lanes 5 and 6 from just the pBAD vector, where Caf1A produced in lane 5 from the pCaf1 is not FLAG-tagged, and Caf1A produced in lane 6 is only from the pBAD vector as the pGEMT vector has no production of Caf1A. Furthermore, we observed similar levels of FLAG-tagged Caf1A, regardless of whether it is produced from the pCaf1 or not.

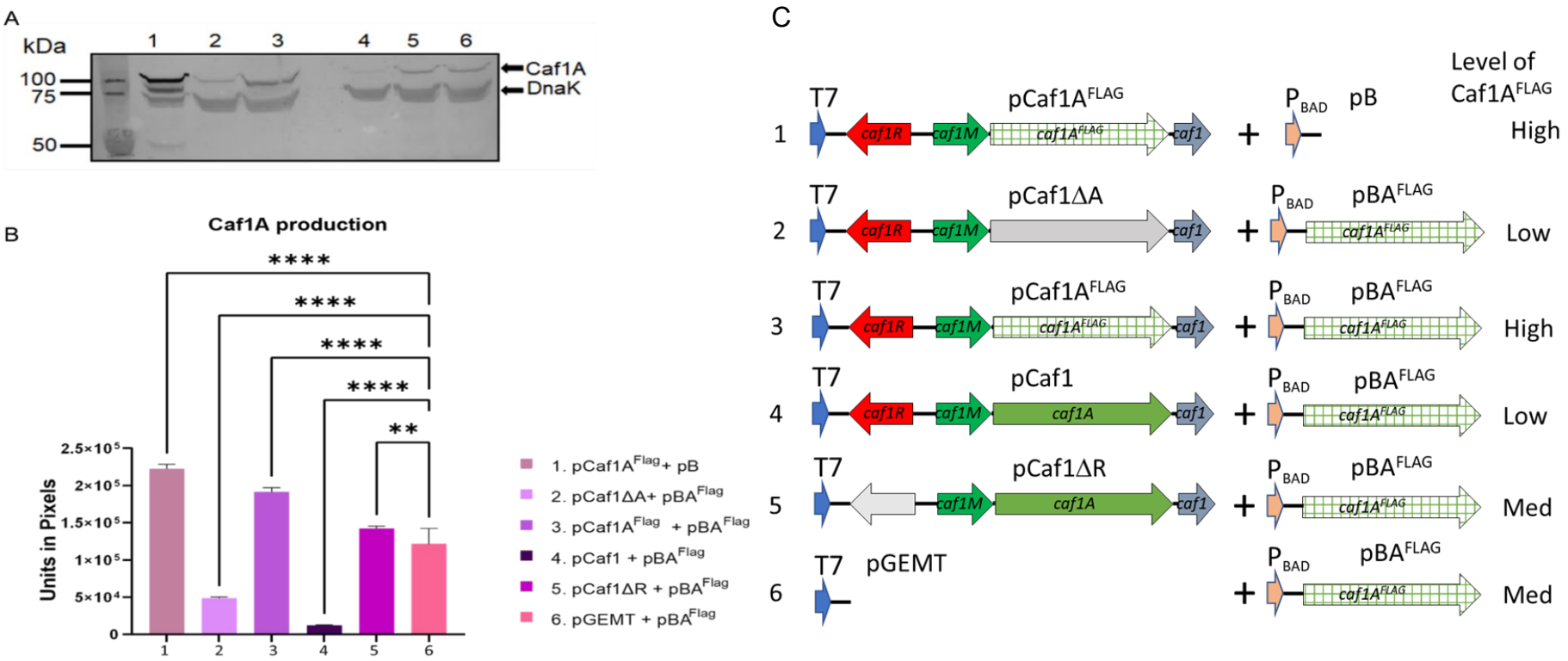

Figure 5.4: Caf1A Production

A) Western blot analysis of Caf1A production from six different plasmid combinations using an anti-FLAG- tag Rabbit polyclonal antibody and Goat anti-rabbit AP conjugate. Bands correspond to Caf1A production in pellets of different cultures. *Escherichia coli* BL21 cells were transformed with six different plasmid pairs (1-6). Cultures were grown at 35ºC for 12 hours. B) Bar chart depicting the standard error of the mean (+ S.E.M) densitometric quantification of Caf1A production. Biological replicates (n=2) and technical replicates (n=6). Between group differences were compared using a one-way ANOVA **** and ** denote significant differences at $p < 0.001$ and $p < 0.01$, respectively. The data from lanes 4&5 show that the low levels of Caf1AFLAG obtained from the pBAFLAG vector are due to the negative influence of caf1R acting in trans. C) Schematic representation of the plasmid combinations.

5.2.3 Comparison of flocculent layer production between Escherichia coli BL21(DE3) and BL21-AI cells

It is known that arabinose can inhibit lac promoters (Ammar *et al.*, 2018) and the data presented earlier in section **5.2.2** of this chapter indicate that using the pGEMT-based pCaf1 plasmids, which use leaky T7 expression alongside L-arabinose may not be suitable for expressing Caf1A. In **Figure 5.4,** lanes 2 and 4 demonstrate a potential inhibitory effect of L-arabinose on Caf1A production, when L-arabinose induced culture is used. Thus, in addition to Caf1R effects we needed to understand whether L-arabinose is repressing the leaky expression of T7 polymerase. We therefore performed the following comparisons without L-arabinose induction, by comparing the use of *E.coli* BL21 (DE3) and BL21-AI cells for flocculent layer production. Cell lines of *E.coli* BL21 (DE3) and BL21AI cells were co-transformed with both pCaf1ΔA and pBA^{FLAG}. In the pBAD vector only the *caf1A* gene was present to complement the *Δcaf1A* mutation. The two cell types were compared using the same methods of flocculent preparation previously described in Section **2.2.8** of Chapter **II**. The comparison of the flocculent layers generated between the BL21 (DE3), and BL21-AI cells is depicted in **Figure 5.5**. In Tube A, a clear flocculent layer was present when L-arabinose was not used to induce the BL21 (DE3) cells.

Previous research has suggested that Caf1 is produced from the leaky expression of the T7 promoter present in pGEMT (Roque, 2012; Roque *et al.*, 2014). To produce a flocculent layer in uninduced cells containing pCaf1ΔA, Caf1A must also be produced by the leaky expression of *caf1A* from pBAD, although the western blot in **Figure 5.3** indicates that it may not be sensitive enough to detect the low levels of Caf1A in uninduced cells. These data suggest that very low levels of Caf1A are sufficient for producing relatively normal flocculent layers. This may also provide insight into the data presented in **Figure 5.4A lane 1**, where Caf1A^{FLAG} may have been produced by the leaky expression of *caf1A* from pBAD. However, the results depicted in **Figure 5.5** indicate that the low levels of Caf1A present in BL21 (DE3) cells are sufficient to produce a flocculent layer (**Figure 5.5, Tube A**). Furthermore, we were unable to identify the presence of a flocculent layer in Tube B (**Figure 5.5**), where BL21 (DE3)

cells were induced with 0.05% w/v L-arabinose. These data are somewhat surprising given that we previously confirmed the presence of *caf1A* expression from the pBAD vector and the presence of a band for Caf1A^{FLAG} on the western blot (**Figure 5.3**). One potential explanation for these results is the possible inhibition of lac induced pCaf1 gene expression by L-arabinose.

Based on the results presented here, we made the decision to use BL21-AI cells for future experiments. The expression of T7 polymerase is tighter in the BL21-AI cells as it is controlled by the highly regulated arabinose-inducible pBAD promoter (Guzman *et al.*, 1995; Bhawsinghka *et al.*, 2020). This tight control should prevent leaky expression of *caf1* or flocculent layer. We would therefore expect there to be no leaky expression of caf1 and as a result no flocculent layer, depicted in Tube C (**Figure 5.5**). However, when the BL21-AI cells were induced with 0.05% w/v L-arabinose, Tube D (**Figure 5.5**), both pBADcaf1A and pCaf1 genes are expressed and as a result a clear flocculent layer was present. The presence of a similar flocculent layer in uninduced BL21 (DE3) cells and L-arabinose induced BL21-AI cells in tubes A and D, respectively, indicates that the leaky expression from pBADcaf1A is able to provide sufficient Caf1A activity to imitate that from the induced cells (**Table 5.2**). Taken together these data suggest that only a very low level of Caf1A is needed to produce a flocculent layer and that the level of Caf1A usher protein present in the OM may not be the limiting factor in polymer production.

Table 5.2: Flocculent layer production by induced and non-induced L-arabinose in *Escherichia coli* BL21 (DE3) and BL21-AI cells.

Cells	**Non-induced arabinose (-)**	**Induced arabinose (+)**
BL21(DE3)	Yes	No
BL21-AI	No	Yes

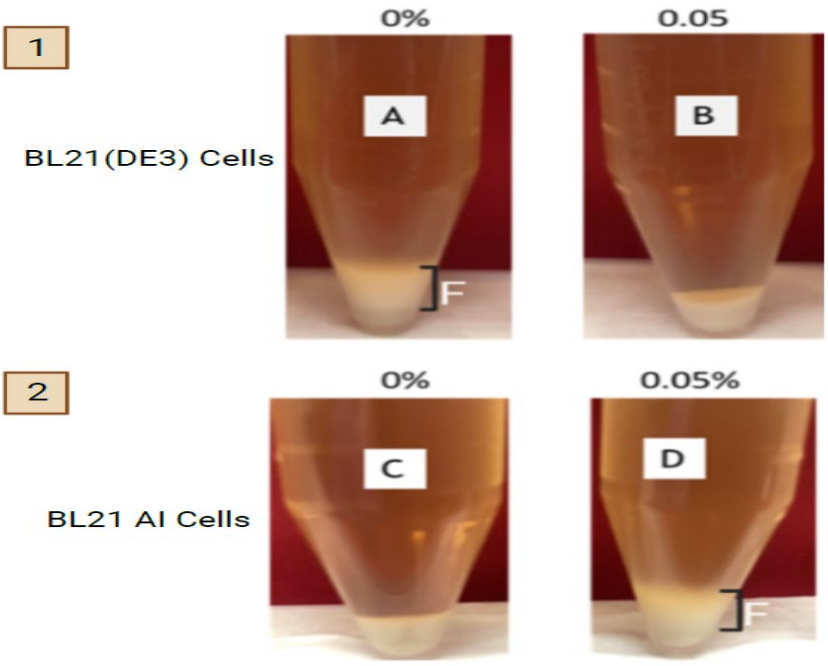

Figure 5.5: Flocculent layer production by *Escherichia coli* BL21 and BL21-AI cells.

1) *E.coli* BL21 (DE3) and 2) BL21-AI cells were transformed with pCaf1ΔA and pBA^{FLAG}. Cultures were then grown at 35°C for 12 hours before being centrifuged at 2367 x g for 20 minutes in 5 ml Eppendorf tubes. Following centrifugation any flocculent layer generated could be viewed. A flocculent layer is present in Tube A, which contained pCaf1 with the caf1A gene deleted, however, the flocculent layer is likely to be due to the Caf1A gene present on the pBAD, complementing the loss of Caf1A from the pCaf1. The flocculent layer is likely to be produced from a leaky expression of Caf1 and Caf1M from pCaf1 with very low leaky expression of Caf1A from the pBAD. Tube B, which did not have a flocculent layer is from BL21 (DE3) cells induced with 0.05% L-arabinose. The lack of flocculent layer is likely to be because the L-arabinose is able to modulate the pCaf1, thus inhibiting the lactose-induced expression and the leaky expression of the pGEMT. These mechanisms are also likely to be responsible for the lack of flocculent layer in Tube C, containing BL21-AI cells. The BL21-AI cells in Tube D were induced with 0.05% w/v L-arabinose, resulting in a large flocculent layer and Caf1 production. The pBAD is expressing Caf1A, and pCaf1 is also induced as a result a flocculent layer is observed.

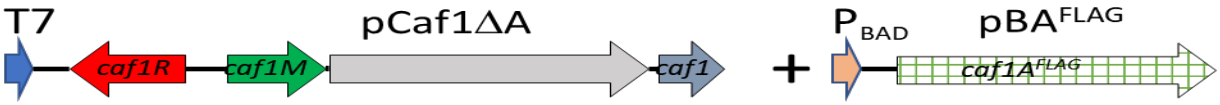

Figure 5.6: Schematic diagram of the pCaf1ΔA and pBADCaf1^{FLAG} plasmids.

The flocculent layer in *Escherichia coli* BL21 DE3 cells arises from leaky expression in both plasmids and the production of Caf1 is repressed by the addition of arabinose. In AI cells the Caf1 is repressed until arabinose is added (see Figure 5.5) and there is no repression of T7 in these cells because the L-arabinose inducible promoter of araB is missing in the BL21-AL cells.

5.2.3.1 Caf1A production in Escherichia coli BL21-AI cells

Following the expression of the flocculent layer in *E. coli* BL21-AI cells, we investigated if we were able to quantify the expression of Caf1A^{FLAG} in the BL21-AI cells. *E. coli* BL21-AI cells were transformed with pBA^{FLAG}. The expression cultures were then grown at 35°C with the appropriate antibiotic (chloramphenicol 20 µg/ml) whilst being continually shaken at 180 revolutions per minute (rpm) for 7 and 22 hours. Expression cultures were then induced after the value of OD_{600} had reached 0.6 by adding 20% w/v L-arabinose stock solution to produce concentrations including of 0, 0.05, 0.1 and 0.2% w/v. The samples were then collected and centrifuged at 2367 x g for 20 minutes in 5 ml Eppendorf tubes. Following centrifugation, the supernatants were discarded, and the cell pellets were diluted to an OD of 1.0 and resuspended in sample buffer and heated at 100°C for 10 minutes. The samples were then separated on SDS-PAGE prior to analysis using a western blot. Anti-FLAG antibodies were used in the western blot to reveal the expression levels of Caf1A^{FLAG} at the different L-arabinose concentrations. DnaK was employed as a loading control and probed with an anti-DnaK antibody. The data presented here demonstrates that the BL21-AI cells generated similar protein expression levels as the BL21 (DE3) cells (**Figure 5.7** and **Figure 5.3**, respectively). In a similar manner to the BL21 (DE3) cells, the highest concentrations of Caf1A^{FLAG} expression present in the BL21-AI cells was in those cells induced with the 0.05% (w/v) L-arabinose concentration (**Figure 5.7)**. Caf1AFLAG production identified using a western blot from *Escherichia coli* (*E.coli)* BL21-AI cells following induction with various concentrations of L-arabinose.

We thus observed no subsequent L-arabinose concentration dependent increases in Caf1A^{FLAG} or with an increased incubation period.

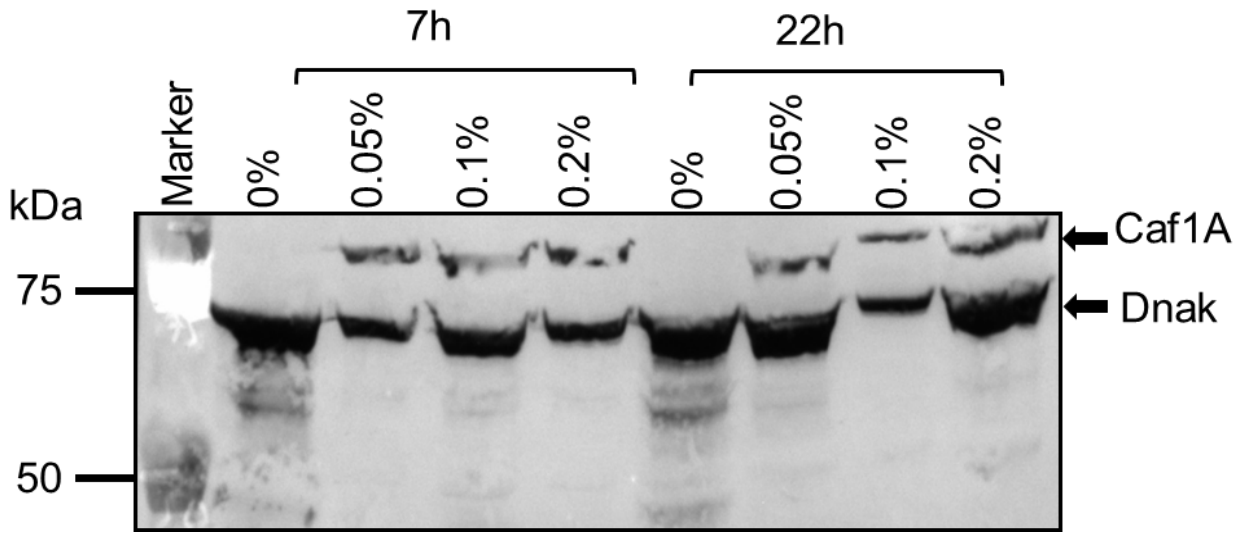

Figure 5.7: Caf1A^{FLAG} production identified using a western blot from *Escherichia coli* BL21-AI cells following induction with various concentrations of L- arabinose.

A western blot of Caf1A^{FLAG} from *E. coli* BL21-AI cells was transformed using pBA^{FLAG}. Expression of Caf1A^{FLAG} was detected using FLAG-tag Rabbit polyclonal antibody and a Goat anti-rabbit alkaline phosphatase conjugate were used as the primary and secondary antibodies, respectively. The western blot revealed that Caf1A^{FLAG} was expressed at all L-arabinose concentrations. A mouse monoclonal anti-DnaK antibody was used to probe DnaK, which was used as a loading control.

5.2.3.2 Overexpression of Caf1A in Escherichia coli BL21-AI cells

Here we aimed to identify if Caf1A^{FLAG} produced by *E. coli* BL21-AI cells was elevated in comparison with BL21 (DE3) cells. We transformed *E. coli* BL21-AI cells with the same six plasmids described in Section **5.2.2.** One additional sample with both control plasmids was added with the appropriate antibiotics (chloramphenicol and ampicillin at 20 and 100 µg /ml, respectively). The same conditions applied to the BL21 (DE3) cells, described in Section **5.2.2** were replicated in the BL21-AI cells. *E. coli* BL21-AI cells were co-transformed with the pBA^{FLAG} plasmid along with the following seven pGEMT plasmids:

1. pCaf1A^{FLAG}, Caf1A^{FLAG} from the pGEMT vector only

2. pCaf1∆A + pBA^{FLAG} to determine levels of Caf1A^{FLAG} from pBA^{FLAG} in the absence of WT Caf1A

3. pCaf1A^{FLAG} + pBA^{FLAG} to observe the combined expression levels of both vectors

4. pCaf1 + pBA^{FLAG} to examine the effect of WT Caf1 expression on Caf1A ^{FLAG}

5. pCaf1∆R + pBA^{FLAG} to observe levels of expression in the absence of the regulator Caf1R

6.pGEMT + pBA^{FLAG} to assess the level of Caf1A production from the pBAD vector

7. pGEMT + pB are empty vectors to serve as a control

Cell cultures were grown at 35°C for 12 hours and induced with an L-arabinose concentration at 0.05% w/v. The cell pellets were then analysed using a western blot (**Figure 5.8A**). In lane 1, Caf1A expression from pCaf1A^{FLAG} was lower than anticipated. This may be counterintuitive as the T7 promoter in pCaf1 is tightly regulated in the BL21-AI cells, however, the presence of 0.05% arabinose, as shown previously should have been sufficient to produce some protein, this may not be detectable using the western blot (**Figure 5.8A**). As the pCaf1 expressed protein is not visible in lane 1, the protein expressed in lanes 2 and 3 is presumably Caf1A expressed from the pBAD only. The band present in lane 4 is Caf1A expressed by pBAD but taking into account the lack of protein detected in lane 1, these results are likely to be from the WT Caf1A. However,

expression of WT Caf1A in lane 4 when compared to ΔCaf1A reduces the amount of Caf1A^{FLAG} produced by pBA^{FLAG}. Taken together these data demonstrate that BL21-AI cells containing pBA^{FLAG} produce more Caf1A than in the BL21 (DE3) cells (**Figure 5.4,lane 2**).

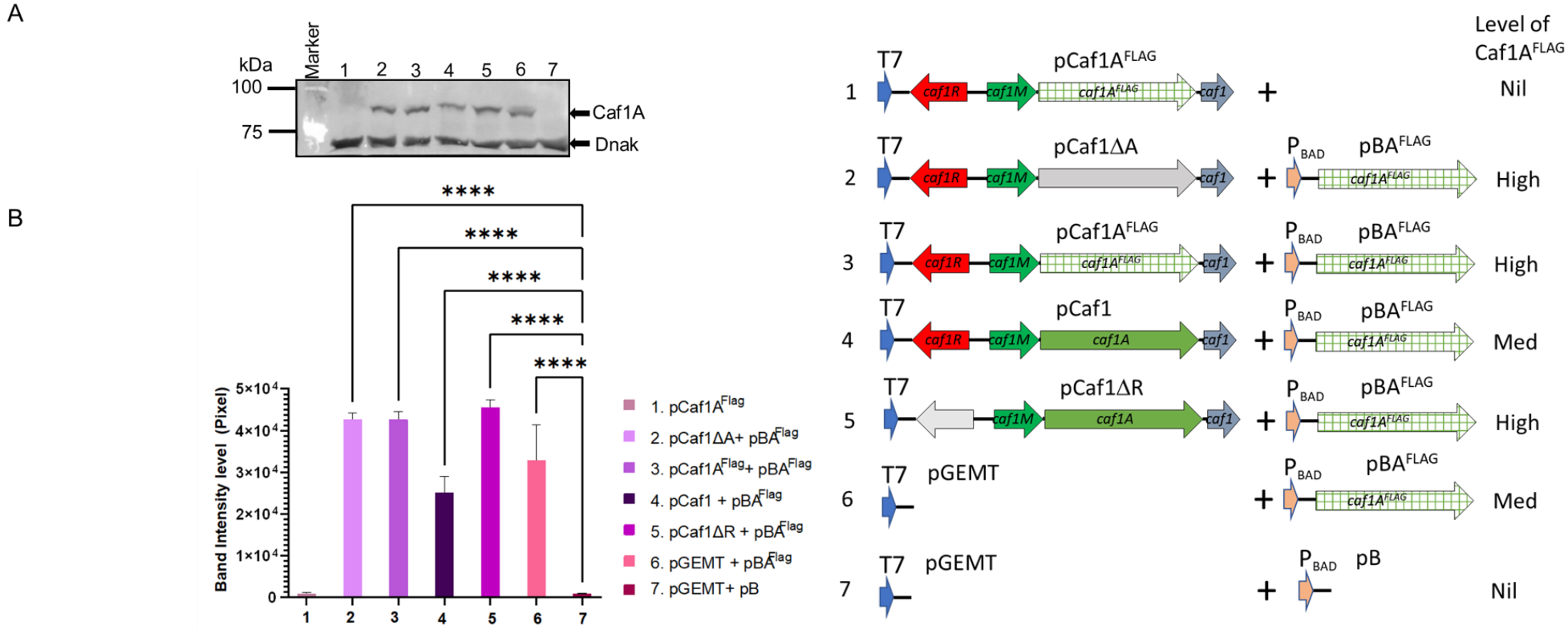

Figure 5.8: Caf1A production in the *Escherichia coli* BL21AI cells

A) Western blot analysis of cell pellets for cultures of *E. coli* BL21-AI cells that have been co-transformed with pBA^{FLAG} and seven different pGEMT plasmids. Cell pellets were collected from cell cultures grown for 12 hours at 35°C following induction with 0.05% w/v L-arabinose. All pellets were diluted to an OD_{600} of 1. Cell pellets were then mixed with sodium dodecyl-sulfate polyacrylamide gel electrophoresis (SDS-PAGE) sample buffer and heated at 100°C for 10 minutes. The pellets were then probed with anti-FLAG-tag rabbit polyclonal and goat anti-rabbit alkaline phosphatase conjugate as the primary and secondary antibodies, respectively. DnaK was applied as a loading control and probed with a mouse monoclonal anti-DnaK antibody. B) Bar graph of Caf1A production measured by densitometry from the western blots depicted in figure A. Data are presented as the mean and standard error of the mean (± S.E.M) presented as error bars. Between group differences were analysed using a one-way ANOVA. **** denotes a significant difference at p <0.0001. The result from lane 1 is unclear . The expression of WT Caf1 (4) when compared to ΔCaf1A (2) reduced the amount of Caf1 FLAG production by pBADCaf1A^{FLAG}. In addition, deleting Caf1R (5) was able to reverse the reduction in Caf1 FLAG expression. The result in lane 6 is unclear and may be due to large error bars. In BL21-AI cells, pBA^{FLAG} produces more Caf1 than in DE3 see lane 2 in **Figure 5.4.**

5.2.4 Effect of Caf1A expression on Caf1 production in Escherichia coli BL21 (DE3) cells

We previously hypothesised that an increase in the expression of Caf1A would lead to an increase in Caf1 polymer production. An increase in Caf1A expression may increase the amount of flocculent and/or decrease the stress placed on the Caf1 monomers in the periplasm and subsequently reduce OMV production. In contrast to our hypothesis, we have presented data here indicating that Caf1A is not the rate-limiting step in the Caf1 system. In previous research, Caf1 production was shown to be increased when using the pGEMT-Caf1ΔR mutation (Al-Jawdah *et al.*, 2019) or L-arabinose induction in BL21-AI cells (Unpublished data from our group done by Dr.Hellen Waller). The data depicted in **Figure 5.9** illustrates the effect of L-arabinose induction on the production of Caf1 from the pCaf1 plasmid in BL21 (DE3) cells. L-arabinose induction has previously been shown to inhibit the T7 promoter by reducing the lac-dependent T7 polymerase levels, therefore inhibiting the leaky expression of pGEMT (Ammar *et al.*, 2018), and is likely to be responsible for the lower levels of Caf1 production observed in the lanes where samples were induced with L-arabinose (Guzman *et al.*, 1995). These findings do not align with our hypothesis that pBAD-based expression of Caf1A would increase Caf1 production. This may in part be due to the effects of L-arabinose on Caf1 production, however when induction was not performed using L-arabinose and BL21-AI cells were used, the levels of Caf1A remained comparable with the WT levels. Moving forward, future experiments should therefore replicate the same experiments depicted in **Figure 5.9** , but instead use BL21-AI cells instead of BL21 (DE3) cells with a range of L-arabinose concentrations. Alternatively, we could investigate the use of other vectors co-transformed with the pCaf that are not dependent on L-arabinose. Finally, the higher levels of Caf1A produced from pCaf1 where the pBAD vector was missing and no L-arabinose induction used (**Figure 5.9 A lane 4**) could also be due to the lack of chloramphenicol in these samples.

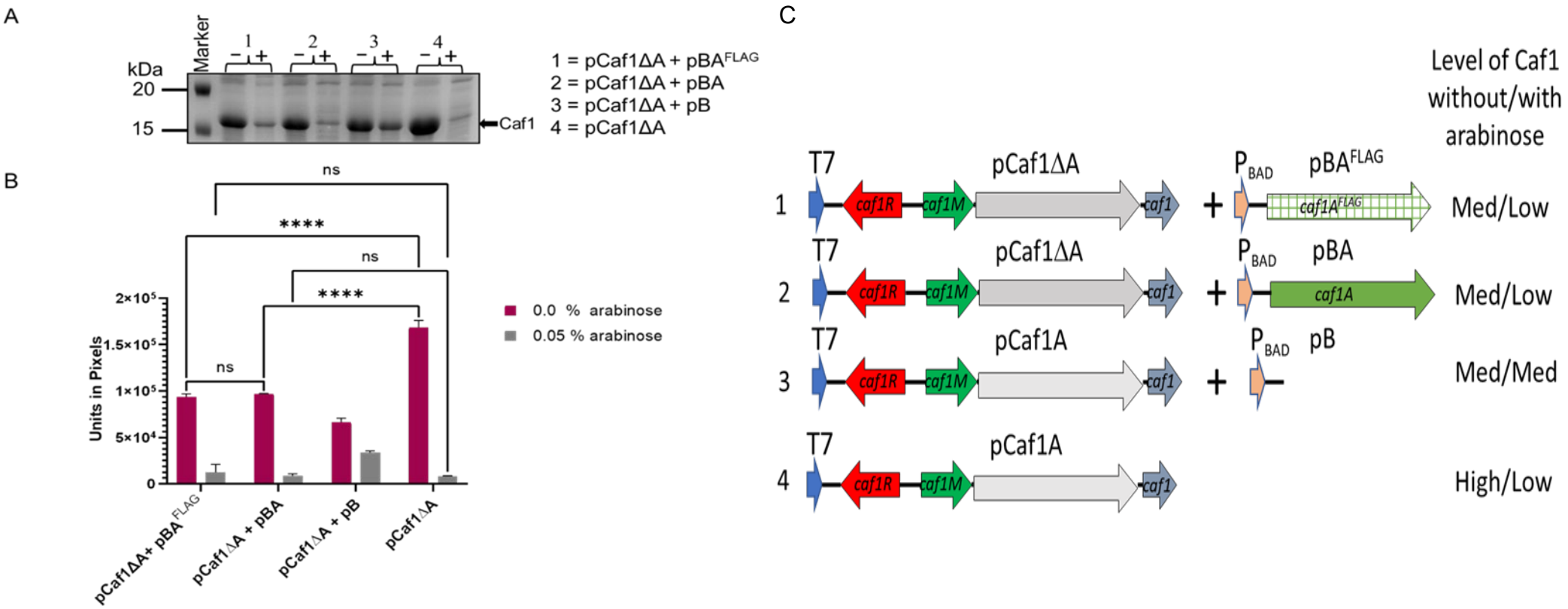

Figure 5.9: Caf1 production in cell pellets from *Escherichia coli* BL21(DE3) cells.

A) Sodium dodecyl sulfate polyacrylamide gel electrophoresis (SDS-PAGE) analysis of cell pellets samples from *E. coli* BL21 cells. *E. coli* BL21 cells co-transformed separately with 1: pCaf1ΔA+pBA^{FLAG}, 2: pCaf1ΔA+pBA, 3: pCaf1ΔA+pB, and 4: pCaf1ΔA). Cell cultures were grown for 12 hours at 35°C with 0.05% (w/v) L-arabinose. Samples were centrifuged at 2367 x g for 20 minutes in 5 ml Eppendorf tubes to isolate the cell pellets. Supernatants were discarded. Each pellet was resuspended and then diluted in lysis buffer to the same optical density (OD). The cell pellets were then mixed with SDS-PAGE sample buffer and heated for 10 minutes at 100°C. B) Mean and standard error of the mean (± S.E.M) presented as error bars. Data depicts Caf1 production from different plasmids. Two biological replicates (n=2) and 6 technical replicates (n=6). Between group differences were analysed using a one-way ANOVA. **** denotes a significant difference at $p<0.0001$. C) Inhibition of Caf1 production by arabinose and lastly a possible effect of the antibiotic chloramphenicol, which was not included in the last lane where Caf1 expression is very high.

5.3 Correlation between Caf1A expression and Outer Membrane Vesicle (OMV) production.

To conclude this chapter, we investigated if there was an association between the expression of Caf1A and OMV production. In this investigation, *E. coli* BL21 (DE3) cells were transformed separately with four plasmid combinations: pCaf1ΔR, pCaf1ΔA+pBA^{FLAG}, pCaf1ΔA, and pCaf1ΔRA^{FLAG}+pBA^{FLAG}. The cells were cultured for 7 hours at 35°C. OMV samples from each culture were prepared as previously described in Section **3.7** of Chapter **III**. Samples were heated 100°C or not heated, for 10 minutes before being analysed using a western blot. OmpF was detected using a rabbit anti-OmpF and goat anti-rabbit alkaline phosphatase conjugate as the primary and secondary antibodies, respectively. Caf1 was detected using an anti-Caf1 antibody. The data presented in **Figure 5.11 A**&**B** demonstrate OmpF levels in the OMV samples. We have previously identified that pCaf1ΔA generated the largest abundance of vesicle production, likely due to a stress response in the periplasm and the lack of a trapping polymer layer. We have previously observed that pCaf1ΔR released fewer OMVs than pCaf1ΔA (**Figure 3.9, Figure 3.10** in Section **3.2** of Chapter **III**). Although the data presented in this chapter indicates that L-arabinose may have an inhibitory effect on the pCaf plasmid, we still observed similar OMV production as previously presented in Section **3.2** of Chapter **III**, illustrated here in lanes 1 and 3 (**Figure 5.10A&B**). Caf1A produced from both plasmids may have overloaded the periplasm and/or in the OM, which could also cause an increase in the OMV level, but not to the same extent as pCaf1ΔA (**Figure 5.10A&B, lane 4**). However, in lane 2 (**Figure 5.10A&B**), Caf1A is only produced from the pBAD vector, which complements the lack of Caf1A in the pCaf1ΔA plasmid and produced fewer vesicles. Caf1 oligomers, which can form in the periplasm in the absence of Caf1A, are present in the non-heated lanes of **Figure 5.10C**. Taken together these findings demonstrate again that the expression of Caf1A does affect the production of OMVs.

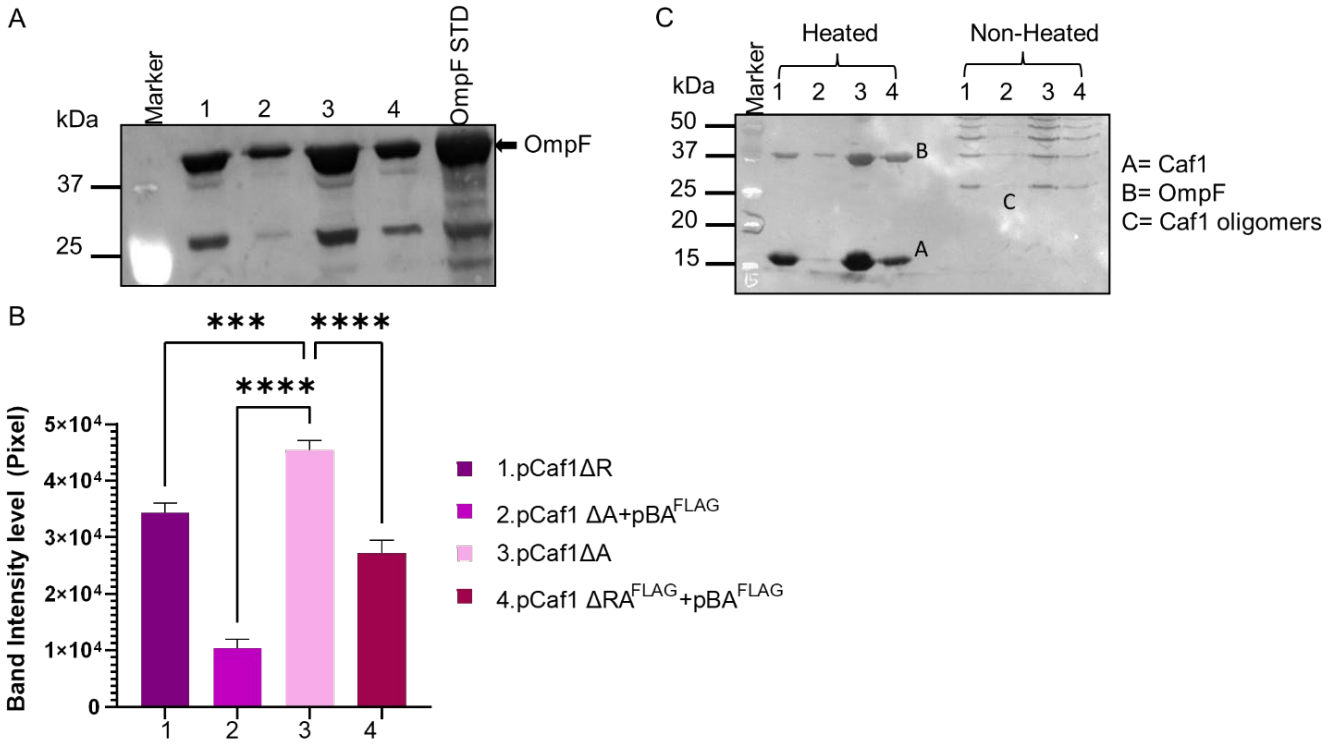

Figure 5.10: Relative amount of OmpF in Outer Membrane Vesicles (OMV) samples.

A) *E.coli* BL21(DE3) cells transformed separately with four plasmids. Samples from OMV preparation of the four different constructs were loaded onto the western blot. Detection was performed using a rabbit anti-OmpF and goat anti-rabbit alkaline phosphatase conjugate as the primary and secondary antibodies, respectively. B) OmpF levels in the OMV samples depicted as a bar graph presented as the mean and standard error of the mean (± S.E.M). Two biological replicates (n=2). C) Labelled A, this is a duplication of the western blot of Figure A. Samples were detected using two different antibodies. The primary antibody was to detect OmpF using a rabbit anti-OmpF antibody, and the secondary was a Goat anti-rabbit alkaline phosphatase (AP) conjugate antibody. The second antibody was to detect Caf1 protein by using an anti-Caf1 antibody as primary antibody and Goat anti-mouse AP conjugate as a secondary antibody. The samples were divided into those that were exposed to heat at 100°C for 10 minutes, and those that were not exposed to heat.

5.4 Discussion

Pilus biogenesis via the chaperone-usher mechanism requires an OM-localised usher to function as an assembly platform for receiving chaperone-subunit complexes. The next step is to incorporate the subunit complexes into a growing pilus (polymerisation), before finally transporting the polymerising pilus to the external face of the OM (secretion). Further emphasising of the importance of chaperone usher, it has been shown that FimD acts as a catalyst to enhance the polymerisation of type 1 pilus rod by a factor of over a thousand (Nishiyama *et al.*, 2008). In the absence of the molecular usher, typified by PapC, FimD or Caf1A, chaperone-subunit complexes aggregate in the periplasm, and are unable to move across the OM for assembly into fibres (pili, fimbriae, or capsules) on the bacterial surface (Thanassi *et al.*, 1998). The surface fibres of bacteria play an essential role in bacterial virulence by mediating adhesion to host cells and aiding bacteria in evading the host immune system (Yu *et al.*, 2009). We have previously demonstrated that Caf1A is the most abundant source of OMVs, and that deletion of Caf1A inhibits Caf1 polymer formation at the cell surface, leading to the accumulation of Caf1 in the periplasm and, ultimately, straining the OM to enhance OMV production. The primary aim of this chapter was to investigate if Caf1A expression is able to increase Caf1 polymer formation while decreasing OMV production through a reduction in Caf1 aggregation in the periplasm.

To increase the levels of Caf1A expression we inserted the *caf1A*^{FLAG} gene into the L-arabinose-regulated pBAD plasmid (Guzman *et al.*, 1995) (Schleif, 2000). Caf1A expression at different concentrations of L-arabinose as the inducible promoter was examined and analysed using a western blot (**Figure 5.3**). We concluded that Caf1A may be expressed in plasmids other than pGEMT and that the expression of Caf1A in pBAD can be initiated but is not regulated by the addition of L-arabinose, evident by all different L-arabinose concentrations generating similar levels of Caf1A^{FLAG} protein. We subsequently co-transformed *E. coli* BL21 (DE3) cells using six different pGEMT plasmids with pBA^{FLAG} to investigate the effect of Caf1A expression on Caf1 production. We observed a low level of Caf1A^{FLAG} from the pBAD vector, suggesting that the presence of pCaf1 may inhibit the production of Caf1A from pBAD. The inhibitory effect may be attributed to the presence of the *caf1R* gene that is regulating *caf1A in trans* between the two different genetic constructs. The earlier work of Al-Jawdah *et al.* (2019) observed that high levels of Caf1R, a highly basic protein belonging to the widely distributed AraC/XylS (A/X) family of positive

transcriptional regulators resulted in a decrease in Caf1 polymer production. Furthermore, this was confirmed by deleting Caf1R, resulting in a subsequent increase in Caf1 biogenesis (Gahlot *et al.*, 2021). Since Caf1R is a transcriptional regulator the data presented here suggests that the *caf1R* gene produces a protein that directly regulates the *caf1A* gene.

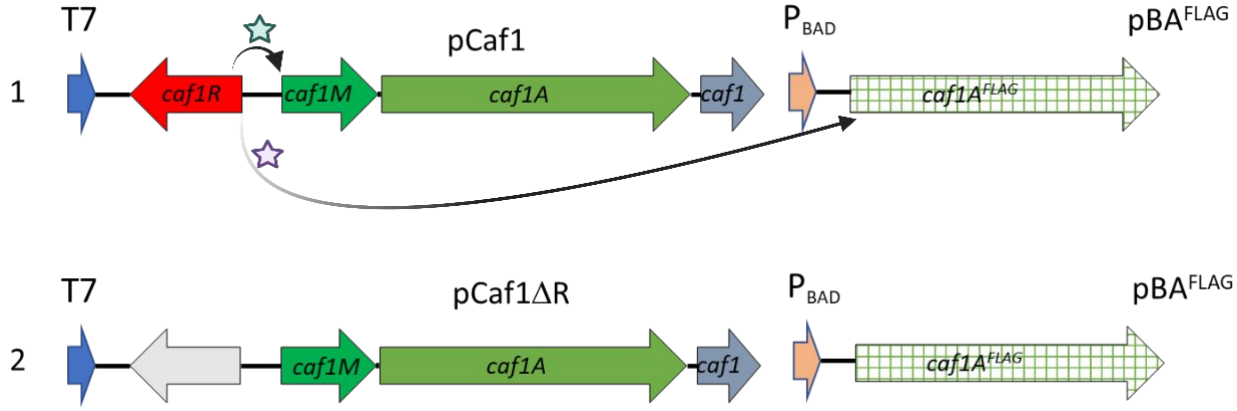

Figure 5.11: The effect of caf1R on the expression of caf1AFLAG on pBAD

1) In the absence of the T7 promoter, Caf1 operon expression is dependent upon the Caf1R protein which has been shown to bind upstream of *caf1MI* (Green star) (Gahlot *et al.*, 2021; Al-Jawdah *et al.*, 2019). 2) Removal of the *caf1R* increases T7 promoter dependent expression of the Caf operon, presumably since bound Caf1R blocks T7 RNA polymerase progression. The ability of caf1R to inhibit $caf1A^{FLAG}$ expression in trans (Figure 5.4, lane 4 and 5) suggests a previously unknown interaction of Caf1R with the *caf1A* gene (Purple Star) since the pBAD contains only the $caf1A^{FLAG}$ gene and no upstream components.

The possible effect of L-arabinose on the leaky expression of the pCaf1 operon was investigated by comparing *E. coli* BL21 (DE3) and BL21-AI cells, with both pCaf1 and pBAD vectors, with BL21-AI cells being induced. Using pCaf1ΔA and pBA^{FLAG} ensured that only when both vectors were induced would a flocculent layer appear. Comparisons of non-induced L-arabinose BL21 (DE3) and BL21-AI cells with cells induced with 0.05% w/v L-arabinose are summarised in **Table 5.3.** In cells not induced with L-arabinose, a flocculent layer was observed in the BL21 (DE3) cells, but the level of Caf1A was low in the western blot. This layer is likely to be produced from a leaky expression of Caf1 and from the pCaf1 with a low leaky expression of Caf1A from the pBAD. Nonetheless, a flocculent layer was not produced when the BL21 (DE3) cells were induced with 0.05% w/v L-arabinose. These findings are likely to be due to the inhibitory effect of L-arabinose on the T7 leaky expression of *caf1* on pCaf1, through modulation of the lac-dependent T7 polymerase levels and inhibition of the leaky expression of pGEMT (Guzman *et al.*, 1995). In a study by Ammar *et al.* (2018), the authors studied the effect of catabolite repression, postulating that *E. coli* is able to employ a myriad of mechanisms to facilitate the use of non-glucose sugars, such as lactose and L-arabinose. The authors reported that lactose represses the utilisation of L-arabinose, and that lactose-mediated repression of the L-arabinose genes is independent of L-arabinose metabolism (Ammar *et al.*, 2018). The same authors also demonstrated that repression is reciprocal in the sense that both lactose and L-arabinose repress each other's metabolism in rich media, although lactose is the preferred sugar in minimal medium. The authors further established that cyclic AMP receptor protein (cAMP) can regulate the selective utilisation of lactose and L-arabinose and that the addition of exogenous cAMP partially relieved lactose-mediated repression of L-arabinose gene expression (Ammar *et al.*, 2018).

Since L-arabinose will repress *lac* induction, Isopropyl β-D-1-thiogalactopyranoside (IPTG)-inducible T7 promoter can be induced at 0.05% w/v L-arabinose. L-arabinose repression of lactose needs Ara metabolism, including the promoter *ara*BAD (P_{BAD}). The L-arabinose-inducible promoter system of *araB* is missing in BL21-AI cells, meaning that L-arabinose will not be able to inhibit the BL21-AI cells. Previous research has demonstrated that L-arabinose inducibility is host-dependent and is less observable in strains with a mutation in the *ara* operon (Narayanan *et al.*, 2006). Furthermore, earlier work has been shown that P_{BAD} cloned

under the control of *araC*-P_{BAD} are efficiently repressed, allowing for high level and tightly regulated expression (Terpe, 2006). Mayer (1995) has also demonstrated that in bacterial strains with the deletion in the *ara* genes required 0.001% L-arabinose for full induction, however, a 1% concentration of L-arabinose is required in strains that are able to ferment.

Table 5.3: Flocculent layer production by induced and non-induced L-arabinose *E. coli* BL21(DE3) and BL21-AI cells

Cells	Non-induced arabinose (-)	Induced arabinose (+)
BL21(DE3)	Yes	No
BL21-AI	No	Yes

As an expression system, BL21 (DE3) have been shown to be less suitable for the induction of toxic proteins and was the driving force for the development of BL21-AI cells, in an attempt to alleviate the leaky nature of the BL21 (DE3) cells (Bhawsinghka *et al.*, 2020). In the present study, when BL21-AI cells were induced with 0.05% w/v L-arabinose, a clear flocculent layer was detected. The presence of a similar flocculent layer was present in the 0 and 0.05% w/v L-arabinose in *E. coli* BL21 (DE3) and BL21-AI cells, respectively. These data indicate that the leaky expression from T7 promoter can provide sufficient Caf1A activity, which is responsible for the flocculent layers observed here. Our data suggests that the level of Caf1A usher protein present in the OM may not be the limiting factor in polymer production and that only a very low level of Caf1A is needed to produce flocculent. These data do not support our original hypothesis, with no clear link between *caf1A* expression, Caf1A levels, or the production of OMV formation. There may be several reasons for these findings, but is likely to be due to a restriction in the amount of Caf1A that can be inserted into the OM.

In recent years, many membrane proteins (MPs) have been unable to effectively express *E. coli*, which has led to the development of an array of modifiable gene expression systems for expression of toxic proteins. In a recent study, Stargardt *et al.* (2021) constructed a new *E. coli* BL21-AI expression host, which they named BL21-AI<*gp2*>. The authors were motivated by their view that T7 expression system cannot be modified to modulate expression as it exerts an all-or-nothing induction

profile that fails to permit expression modulation. The authors also demonstrated the presence of an IPTG-inducible $P_{T7\text{-}lacO}$ promoter, inducible solely with L-arabinose in BL21-AI<*gp2*>, concluding that BL21-AI<*gp2*> was able to outperform the parental strain by improving the MP-GFP fusion proteins by 2.7-fold (Stargardt *et al.*, 2021). Future work should look to replicate the experiments described here using the novel BL21-AI<*gp2*> strain.

In conclusion, in this chapter, we demonstrated that the flocculent layer in BL21 (DE3) can be generated from a leaky expression in pCaf1ΔA and pBA^{FLAG}, and the tight regulation L-arabinose prevent leaky expression of *caf1*. We also observed that in BL21-AI cells, the *caf1* is repressed until the additon of L-arabinose, but there was no repression of the T7 expression system in these cells. Moving forward, further work is required to investigate more sensitive approaches that can detect lower levels of protein, such as enhanced chemiluminescence (ECL). One additional approach may be RT-PCR, which would allow for measurement of the relative expression of Caf1 genes (Al-jawdah, 2019). Finally, further experiments using different vectors that can produce Caf1A without the need for L-arabinose are required.

Chapter VI

Conclusions and Future Work

"Modest doubt is called the beacon of the wise"

William Shakespeare

6 Conclusions and future work

6.1 Conclusions

Preliminary unpublished data from our research group provided insight into potential associations between the Caf1 polymer and outer membrane vesicle (OMV) formation. This thesis focused on the association between Caf1 polymer production and OMV formation. The primary aim was to investigate if the production of OMV could be reduced, while maintaining high yields of Caf1. This could improve the bioprocess which produces Caf1 for biomaterial applications. The main conclusions of this study will be described in further detail as follows:

6.1.1 Effect of Caf1 protein expression on OMV production

Caf1 is expressed from the *caf* gene cluster and is assembled by the chaperone-usher secretion system. In this study we demonstrated the composition of a flocculent layer, which is often used as an indicator of Caf1 polymer production in bacterial cells. The flocculent layer contains OMVs that are confined in a polymeric network of Caf1. We demonstrated that deletion of the Caf1A usher prevented polymer and flocculent production and resulted in a significant increase in OMVs in the supernatant. Furthermore, we demonstrated that deletion of Caf1A resulted in a significant increase in lipopolysaccharide (LPS) levels in the supernatant which is another indicator of OMV release. This suggests that a Caf1-dependent flocculent layer is required to restrain OMVs. OMV production in the absence of Caf1A is not only caused by the presence of high levels of Caf1 in the periplasm but can also be induced by Caf1M chaperone expression in the absence of Caf1. However, we observed that cells with a deletion of Caf1M exhibited the largest increase of Caf1 in their OMVs. The accumulation of Caf1 or the chaperone-subunit Caf1M-Caf1 complexes in the periplasm due to the absence of Caf1A suggests a hypervesiculation cellular response. This indicates that OMV production is likely to be a stress response to an overloaded periplasm. Other studies show that the level of vesiculation can be modulated by a myriad of factors, including temperature, antibiotics, oxidation, and nutrient availability (Kashyap *et al.*, 2022; Jan, 2017; Fulsundar *et al.*, 2014).

6.1.2 Development of fluorescent OmpA to measure OMV production

Whilst we developed a method to analyse the production of OMVs using centrifugation steps followed by blots for OmpF and LPS we wished to more easily quantify the levels of OMVs in these samples. OMVs predominantly contain outer membranes (OM) and periplasmic materials and OmpA is an abundant monomeric protein located within the OM of Gram-negative bacterial cells. The primary objective of this experiment was to determine if a fluorescent OmpA could be used as a probe, enabling us to detect and quantify the formation of OMV. We therefore created several different versions of fluorescent OmpA constructs in *E.coli* and these were subsequently transformed into cells along with pCaf1ΔA as probes for OMV production. We observed that, contrary to expectations, the fluorescent marker OmpA-sfGFP fusion was located in the IM rather than the OM. As an alternative approach we used a second-generation experimental design employing a full length OmpA fused to the C-terminal mCherry. We were able to demonstrate that the full length OmpA-mCherry fusion protein generated from a positive control provided by another group had the largest fluorescence intensity either with or without the induction of the Isopropyl β-D-1-thiogalactopyranoside (IPTG) when compared to other chimeras induced by L-arabinose. We also demonstrated FlAsH-EDT_2specific fluorescence from OmpA as a result of the OmpA mutant containing the tetra cysteine motif (TCM). We observed that the full length OmpA-mCherry fusions were strongly expressed and present in the OM. These data support the use of the full length OmpA fused to the C-terminal mCherry as a suitable fluorescent marker of OMV levels.

6.1.3 Effect of overexpression of caf1A gene on OMV and Caf1 polymer production

The purpose of this chapter was to determine if the over expression of Caf1A led to an increase in Caf1 polymer formation and reductions in OMV production. The data presented in this chapter indicates that absolute Caf1A levels in the OM are able to influence Caf1 polymer production, however, there are likely to be several factors contributing to Caf1 polymer production. Furthermore, we demonstrated that only a very low level of Caf1A was required to produce a flocculent layer. We observed low levels of Caf1A produced from the pBAD vector in the presence of pCaf, suggesting that a product of this plasmid is inhibiting the production of Caf1A from pBAD. The inhibiting effect of Caf1 on Caf1A may be attributed to the presence of the *caf1R* gene, which directly regulates the *caf1A* gene. We observed that a comparable

flocculent layer in non-induced *E. coli* B21(DE3) and 0.05% w/v L-arabinose-induced *E. coli* B21-AI cells. These data demonstrate the presence of leaky expression from the T7 promoter that can provide adequate Caf1A activity. The *caf1A* overexpression had no affect on Caf1A levels, did not increase Caf1 polymer production, or decrease OMV formation by lowering Caf1 aggregation in the periplasm. These data may be due to a maximum quantity of Caf1A that can be inserted into the outer membrane.

6.2 Future work

Although we know that Caf1 polymer and OMV formation are inherently linked, the exact mechanisms are yet to be fully elucidated. In this thesis we have demonstrated some key novel findings, and future research should look to build on these findings and in doing so extend their biotechnological applicability. Previously published research has established evidence demonstrating a positive association between temperature and vesiculation in *E.coli*. Moreover, temperatures ranging between 26◦C and 35◦C have been identified as the ideal temperatures for the optimum production of Caf1. Thus, one possible suggestion for a future study is to examine the Caf1-OMV link at low temperatures. Preliminary data from this group has demonstrated that L-arabinose induction of a pBADCaf1M plasmid had no discernible impact on flocculent height, however, the production of Caf1 polymer was not examined (Al-Jawdah, 2019). These data provide the basis for future investigations into the effect of the Caf1M chaperone expression on the rate of monomer delivery to the Caf1A usher. A key finding presented in this thesis was the inhibitory effect of the *caf1R* gene on the *caf1A* gene. These findings require further research to understand its significance for Caf1 production. Future work is also required to determine if high concentrations of L-arabinose, which we have shown to inhibit Caf1 expression, elevate the gene expression levels of the T7 promoter from pCaf1. A further technique that may be useful in future research is the use of RT-PCR that will provide the ability to track the introduction and effects of desired genes. The use of other vectors that are able to produce Caf1A should also be considered to eliminate the need for L-arabinose. Finally, the development of an antibody for Caf1A would be a useful in future.

7 References

Abramov, V. M., Vasiliev, A. M., Khlebnikov, V. S., Vasilenko, R. N., Kulikova, N. L., Kosarev, I. V., Ishchenko, A. T., Gillespie, J. R., Millett, I. S., Fink, A. L. and Uversky, V. N. (2002) 'Structural and functional properties of Yersinia pestis Caf1 capsular antigen and their possible role in fulminant development of primary pneumonic plague', *Journal of Proteome Research,* 1(4), pp. 307-315.

Abramov, V. M., Vasiliev, A. M., Vasilenko, R. N., Kulikova, N. L., Kosarev, I. V., Khlebnikov, V. S., Ishchenko, A. T., MacIntyre, S., Gillespie, J. R., Khurana, R., Korpela, T., Fink, A. L. and Uversky, V. N. (2001) 'Structural and functional similarity between Yersinia pestis capsular protein Caf1 and human interleukin-1β', *Biochemistry,* 40(20), pp. 6076-6084.

Achouak, W., Heulin, T. and Pagès, J. M. (2001) 'Multiple facets of bacterial porins', *FEMS Microbiology Letters,* 199(1), pp. 1-7.

Adams, S. R., Campbell, R. E., Gross, L. A., Martin, B. R., Walkup, G. K., Yao, Y., Llopis, J. and Tsien, R. Y. (2002) 'New biarsenical ligands and tetracysteine motifs for protein labeling in vitro and in vivo: Synthesis and biological applications', *Journal of the American Chemical Society,* 124(21), pp. 6063-6076.

Al-Jawdah, A. D., Ivanova, I. G., Waller, H., Perkins, N. D., Lakey, J. H. and Peters, D. T. (2019) 'Induction of the immunoprotective coat of Yersinia pestis at body temperature is mediated by the Caf1R transcription factor', *BMC Microbiology,* 19(1), pp. 1-12.

Al-jawdah, A. D. M. (2019) *The thermo-responsive regulation of Yersinia pestis immune protective protein (F1) by the Caf1R transcription factor.* Unpublished PhD thesis, Newcastle University [Online] Available at: http://theses.ncl.ac.uk/jspui/handle/10443/4754 (Accessed: 13 February 2023).

Ammar, E. M., Wang, X. and Rao, C. V. (2018) 'Regulation of metabolism in Escherichia coli during growth on mixtures of the non-glucose sugars: Arabinose, lactose, and xylose', *Scientific Reports,* 8(1), pp. 1-11.

Anand, D. and Chaudhuri, A. (2016) 'Bacterial outer membrane vesicles: New insights and applications', *Molecular Membrane Biology,* 33(6-8), pp. 125-137.

Andrews, G. P., Heath, D. G., Anderson, G. W., Welkos, S. L. and Friedlander, A. M. (1996) 'Fraction 1 capsular antigen (F1) purification from Yersinia pestis CO92 and from an Escherichia coli recombinant strain and efficacy against lethal plague challenge', *Infection and Immunity,* 64(6), pp. 2180-2187.

Arora, A., Abildgaard, F., Bushweller, J. H. and Tamm, L. K. (2001) 'Structure of outer membrane protein A transmembrane domain by NMR spectroscopy', *Nature Structural Biology,* 8(4), pp. 334-338.

Arunmanee, W., Pathania, M., Solovyova, A. S., Le Brun, A. P., Ridley, H., Baslé, A., van den Berg, B. and Lakey, J. H. (2016) 'Gram-negative trimeric porins have specific LPS binding sites that are essential for porin biogenesis', *Proc Natl Acad Sci U S A,* 113(34), pp. E5034-43.

Auclair, S. M., Bhanu, M. K. and Kendall, D. A. (2012) 'Signal peptidase I: Cleaving the way to mature proteins', *Protein Science,* 21(1), pp. 13-25.

Avila-Calderón, E. D., Araiza-Villanueva, M. G., Cancino-Diaz, J. C., López-Villegas, E. O., Sriranganathan, N., Boyle, S. M. and Contreras-Rodríguez, A. (2014) 'Roles of bacterial membrane vesicles', *Archives of Microbiology,* 197(1), pp. 1-10.

Avila-Calderón, E. D., Ruiz-Palma, M. D. S., Aguilera-Arreola, M. G., Velázquez-Guadarrama, N., Ruiz, E. A., Gomez-Lunar, Z., Witonsky, S. and Contreras-Rodríguez, A. (2021) 'Outer Membrane Vesicles of Gram-Negative Bacteria: An Outlook on Biogenesis', *Front Microbiol,* 12, pp. 557902.

Bai, J., Kim, S. I., Ryu, S. and Yoon, H. (2014) 'Identification and characterization of outer membrane vesicle-associated proteins in Salmonella enterica serovar Typhimurium', *Infect Immun,* 82(10), pp. 4001-10.

Baker, E. E., Sommer, H., Foster, L. E., Meyer, E. and Meyer, K. F. (1952) 'Studies on immunization against plague. I. The isolation and characterization of the soluble antigen of Pasteurella pestis', *J Immunol,* 68(2), pp. 131-145.

Barnhart, M. M. and Chapman, M. R. (2006) 'Curli biogenesis and function', *Annual review of microbiology,* 60, pp. 131-147.

Bartolini, E., Ianni, E., Frigimelica, E., Petracca, R., Galli, G., Berlanda Scorza, F., Norais, N., Laera, D., Giusti, F., Pierleoni, A., Donati, M., Cevenini, R., Finco, O., Grandi, G. and Grifantini, R. (2013) 'Recombinant outer membrane vesicles carrying Chlamydia muridarum HtrA induce antibodies that neutralize chlamydial infection in vitro', *J Extracell Vesicles,* 2.

Baslé, A., Rummel, G., Storici, P., Rosenbusch, J. P. and Schirmer, T. (2006) 'Crystal structure of osmoporin OmpC from E. coli at 2.0 A', *J Mol Biol,* 362(5), pp. 933-42.

Bennion, D., Charlson, E. S., Coon, E. and Misra, R. (2010) 'Dissection of β-barrel outer membrane protein assembly pathways through characterizing BamA POTRA 1 mutants of Escherichia coli', *Molecular Microbiology,* 77(5), pp. 1153-1171.

Beveridge, T. J. and Kadurugamuwa, J. L. (1995) 'Virulence factors are released from Pseudomonas aeruginosa in association with membrane vesicles during normal growth and exposure to gentamicin : a novel mechanism of enzyme secretion . Virulence Factors Are Released from Pseudomonas aeruginosa in Associ', *Journal of bacteriology,* 177(14), pp. 3998-4008.

Bhawsinghka, N., Glenn, K. F. and Schaaper, R. M. (2020) 'Complete Genome Sequence of Escherichia coli BL21-AI', *Microbiol Resour Announc,* 9(10).

Bogdanov, A. M., Mishin, A. S., Yampolsky, I. V., Belousov, V. V., Chudakov, D. M., Subach, F. V., Verkhusha, V. V., Lukyanov, S. and Lukyanov, K. A. (2010) 'Green fluorescent proteins are light-induced electron donors Alexey', *Nat Chem Biol,* 5(7), pp. 459-461.

Bojkovic, J., Richie, D. L., Six, D. A., Rath, C. M., Sawyer, W. S., Hu, Q. and Dean, C. R. (2015) 'Characterization of an Acinetobacter baumannii lptD Deletion Strain: Permeability Defects and Response to Inhibition of Lipopolysaccharide and Fatty Acid Biosynthesis', *J Bacteriol,* 198(4), pp. 731-41.

Bonnington, K. E. and Kuehn, M. J. (2014) 'Protein selection and export via outer membrane vesicles', *Biochimica et Biophysica Acta - Molecular Cell Research,* 1843(8), pp. 1612-1619.

Bos, M. P., Robert, V. and Tommassen, J. (2007) 'Biogenesis of the Gram-Negative Bacterial Outer Membrane', *Annual Review of Microbiology,* 61(1), pp. 191-214.

Bouhss, A., Trunkfield, A. E., Bugg, T. D. H. and Mengin-Lecreulx, D. (2008) 'The biosynthesis of peptidoglycan lipid-linked intermediates', *FEMS Microbiology Reviews,* 32(2), pp. 208-233.

Braun, V. and Rehn, K. (1969) 'Chemical characterization, spatial distribution and function of a lipoprotein (murein-lipoprotein) of the E. coli cell wall. The specific effect of trypsin on the membrane structure', *Eur J Biochem,* 10(3), pp. 426-38.

Brown, L., Wolf, J. M., Prados-Rosales, R. and Casadevall, A. (2015) 'Through the wall: Extracellular vesicles in Gram-positive bacteria, mycobacteria and fungi', *Nature Reviews Microbiology,* 13(10), pp. 620-630.

Brubaker, R. R. (2003) 'Interleukin-10 and inhibition of innate immunity to Yersiniae: Roles of Yops and LcrV (V antigen)', *Infection and Immunity,* 71(7), pp. 3673-3681.

Bruneteau, M. and Minka, S. (2003) 'Lipopolysaccharides of bacterial pathogens from the genus Yersinia: a mini-review', *Biochimie,* 85(1-2), pp. 145-52.

Bulieris, P. V., Behrens, S., Holst, O. and Kleinschmidt, J. H. (2003) 'Folding and insertion of the outer membrane protein OmpA is assisted by the chaperone Skp and by lipopolysaccharide', *J Biol Chem,* 278(11), pp. 9092-9.

Busch, A. and Waksman, G. (2012) 'Chaperone-usher pathways: Diversity and pilus assembly mechanism', *Philosophical Transactions of the Royal Society B: Biological Sciences,* 367(1592), pp. 1112-1122.

Butler, T. (2014) 'Plague history: Yersin's discovery of the causative bacterium in 1894 enabled, in the subsequent century, scientific progress in understanding the disease and the development of treatments and vaccines', *Clinical Microbiology and Infection,* 20(3), pp. 202-209.

Campbell, R. E., Tour, O., Palmer, A. E., Steinbach, P. A., Baird, G. S., Zacharias, D. A. and Tsien, R. Y. (2002) 'A monomeric red fluorescent protein', *Proc Natl Acad Sci U S A,* 99(12), pp. 7877-82.

Caroff, M. and Karibian, D. (2003) 'Structure of bacterial lipopolysaccharides', *Carbohydr Res,* 338(23), pp. 2431-47.

Cepas, V. and Soto, S. M. (2020) 'Relationship between virulence and resistance among gram-negative bacteria', *Antibiotics,* 9(10), pp. 1-11.

Chai, T. J. and Foulds, J. (1977) 'Purification of protein A, an outer membrane component missing in Escherichia coli K-12 ompA mutants', *Biochim Biophys Acta,* 493(1), pp. 210-5.

Chalfie, M. and Ma, J. (1995) 'Green fluorescent protein', *Photochemistry and Photobiology,* 62(4), pp. 651-656.

Chalfie, M., Tu, Y., Euskirchen, G., Ward, W. W. and Prasher, D. C. (1994) 'Green fluorescent protein as a marker for gene expression', *Science,* 263(5148), pp. 802-5.

Chapman, D. A. G., Zavialov, A. V., Tatiana, V., Karlyshev, A. V., Zav, G. A., Vasiliev, A. M., Dudich, I. V., Vyacheslav, M., Zav, V. P., Macintyre, S. and Chernovskaya, T. V. (1999) 'Structural and Functional Significance of the FGL Sequence of the Periplasmic Chaperone Caf1M of Yersinia pestis Structural and Functional Significance of the FGL Sequence of the Periplasmic Chaperone Caf1M of Yersinia pestis', 181(8), pp. 2422-2429.

Chatterjee, S. N. and Chaudhuri, K. (2012) *Outer Membrane Vesicles of Bacteria.* Berlin, Heidelberg: Springer

Chen, T. H. and Elberg, S. S. (1977) 'Scanning electron microscopic study of virulent Yersinia pestis and Yersinia pseudotuberculosis type I', *Infection and Immunity,* 15(3), pp. 972-977.

Choi, U. and Lee, C. R. (2019a) 'Antimicrobial Agents That Inhibit the Outer Membrane Assembly Machines of Gram-Negative Bacteria', *J Microbiol Biotechnol,* 29(1), pp. 1-10.

Choi, U. and Lee, C. R. (2019b) 'Distinct Roles of Outer Membrane Porins in Antibiotic Resistance and Membrane Integrity in Escherichia coli', *Frontiers in Microbiology,* 10(APR), pp. 1-9.

Choudhury, D., Thompson, A., Stojanoff, V., Langermann, S., Pinkner, J., Hultgren, S. J. and Knight, S. D. (1999) 'X-ray Structure of the FimC-FimH Chaperone-Adhesin Complex from Uropathogenic Escherichia coli', 285(August), pp. 1061-1067.

Cinelli, R. A., Ferrari, A., Pellegrini, V., Tyagi, M., Giacca, M. and Beltram, F. (2000) 'The enhanced green fluorescent protein as a tool for the analysis of protein dynamics and localization: local fluorescence study at the single-molecule level', *Photochem Photobiol,* 71(6), pp. 771-6.

Clifton, L. A., Skoda, M. W. A., Le Brun, A. P., Ciesielski, F., Kuzmenko, I., Holt, S. A. and Lakey, J. H. (2015) 'Effect of Divalent Cation Removal on the Structure of Gram-Negative Bacterial Outer Membrane Models', *Langmuir,* 31(1), pp. 404-412.

Cowan, S. W., Garavito, R. M., Jansonius, J. N., Jenkins, J. A., Karlsson, R., König, N., Pai, E. F., Pauptit, R. A., Rizkallah, P. J., Rosenbusch, J. P., Rummel, G. and Schirmer, T. (1995) 'The structure of OmpF porin in a tetragonal crystal form', *Structure,* 3(10), pp. 1041-50.

Cowan, S. W., Schirmer, T., Rummel, G., Steiert, M., Ghosh, R., Pauptit, R. A., Jansonius, J. N. and Rosenbusch, J. P. (1992) 'Crystal structures explain functional properties of two E. coli porins', *Nature,* 358(6389), pp. 727-733.

Dalbey, R. E. and Kuhn, A. (2012) 'Protein Traffic in Gram-negative bacteria - how exported and secreted proteins find their way', *FEMS Microbiology Reviews,* 36(6), pp. 1023-1045.

Dammeyer, T. and Tinnefeld, P. (2012) 'Engineered fluorescent proteins illuminate the bacterial periplasm', *Computational and Structural Biotechnology Journal,* 3(4), pp. e201210013-e201210013.

Davidson, M. W. and Campbell, R. E. (2009) 'Engineered fluorescent proteins: innovations and applications', *Nat Methods,* 6(10), pp. 713-17.

Deatherage, B. L., Lara, J. C., Bergsbaken, T., Barrett, S. L. R., Lara, S. and Cookson, B. T. (2009) 'Biogenesis of bacterial membrane vesicles', *Molecular Microbiology,* 72(6), pp. 1395-1407.

Di Yu, X., Dubnovitsky, A., Pudney, A. F., MacIntyre, S., Knight, S. D. and Zavialov, A. V. (2012) 'Allosteric mechanism controls traffic in the chaperone/usher pathway', *Structure,* 20(11), pp. 1861-1871.

Diane Williamson, E., Eley, S. M., Griffin, K. F., Green, M., Russell, P., Leary, S. E. C., Oyston, P. C. F., Easterbrook, T., Reddin, K. M., Robinson, A. and Titball, R. W. (1995) 'A new improved sub-unit vaccine for plague: the basis of protection', *FEMS Immunology and Medical Microbiology,* 12(3-4), pp. 223-230.

Dinh, T. and Bernhardt, T. G. (2011) 'Using superfolder green fluorescent protein for periplasmic protein localization studies', *J Bacteriol,* 193(18), pp. 4984-7.

Drew, D., Newstead, S., Sonoda, Y., Kim, H. and Heijne, G. V. (2009) 'Drew, D., Newstead, S., Sonoda, Y., Kim, H., von Heijne, G., and Iwata, S. (2008) GFP-based optimization scheme for the overexpression and pu- rification of eukaryotic membrane proteins in Saccharomyces cerevisiae', 3(5), pp. 784-798.

Drew, D. E., Heijne, G. V. and Gier, J.-w. L. D. (2001) 'Green Fluorescent protein as an indicator to monitor membrane protein.pdf', *FEBS Letters,* 507, pp. 220-224.

Drummen, G. P. (2012) 'Fluorescent probes and fluorescence (microscopy) techniques--illuminating biological and biomedical research', *Molecules,* 17(12), pp. 14067-90.

Du , D. J. F., Nouwen, N. and Driessen, A. J. M. (2011) 'The Sec translocase', *Biochimica et Biophysica Acta - Biomembranes,* 1808(3), pp. 851-865.

Du, M., Yuan, Z., Werneburg, G. T., Henderson, N. S., Chauhan, H., Kovach, A., Zhao, G., Johl, J., Li, H. and Thanassi, D. G. (2021) 'Processive dynamics of the usher assembly platform during uropathogenic Escherichia coli P pilus biogenesis', *Nature Communications,* 12(1), pp. 1-9.

Du, Y., Rosqvist, R. and Forsberg, A. (2002) 'Role of fraction 1 antigen of Yersinia pestis in inhibition of phagocytosis', *Infect Immun,* 70(3), pp. 1453-60.

Dubnovitsky, A. P., Duck, Z., Kersley, J. E., Härd, T., MacIntyre, S. and Knight, S. D. (2010) 'Conserved Hydrophobic Clusters on the Surface of the Caf1A Usher C-Terminal Domain Are Important for F1 Antigen Assembly', *Journal of Molecular Biology,* 403(2), pp. 243-259.

Dura, G., Peters, D. T., Waller, H., Yemm, A. I., Perkins, N. D., Ferreira, A. M., Crespo-Cuadrado, M., Lakey, J. H. and Fulton, D. A. (2020) 'A Thermally Reformable Protein Polymer', *Chem,* 6(11), pp. 3132-3151.

Dura, G., Waller, H., Gentile, P., Lakey, J. H. and Fulton, D. A. (2018) 'Tuneable hydrogels of Caf1 protein fibers', *Materials Science and Engineering C,* 93(July), pp. 88-95.

Dutzler, R., Rummel, G., Albertí, S., Hernández-Allés, S., Phale, P., Rosenbusch, J., Benedí, V. and Schirmer, T. (1999) 'Crystal structure and functional characterization of OmpK36, the osmoporin of Klebsiella pneumoniae', *Structure,* 7(4), pp. 425-34.

Eddy, J. L., Gielda, L. M., Caulfield, A. J., Rangel, S. M. and Lathem, W. W. (2014) 'Production of outer membrane vesicles by the plague pathogen Yersinia pestis', *PLoS ONE,* 9(9), pp. 1-11.

Elhenawy, W., Bording-Jorgensen, M., Valguarnera, E., Haurat, M. F., Wine, E. and Feldman, M. F. (2016) 'LPS remodeling triggers formation of outer membrane vesicles in salmonella', *mBio,* 7(4), pp. 1-12.

Ellis, T. N. and Kuehn, M. J. (2010) 'Virulence and immunomodulatory roles of bacterial outer membrane vesicles', *Microbiol Mol Biol Rev,* 74(1), pp. 81-94.

Evans, M. L. and Chapman, M. R. (2014) 'Curli biogenesis: Order out of disorder', *Biochimica et Biophysica Acta - Molecular Cell Research,* 1843(8), pp. 1551-1558.

Fages-Lartaud, M., Tietze, L., Elie, F., Lale, R. and Hohmann-Marriott, M. F. (2022) 'mCherry contains a fluorescent protein isoform that interferes with its reporter function', *Front Bioeng Biotechnol,* 10, pp. 892138.

Fairman, J. W., Noinaj, N. and Buchanan, S. K. (2011) 'The structural biology of β-barrel membrane proteins: a summary of recent reports', *Current opinion in structural biology,* 21(4), pp. 523-531.

Fernández, L. A. and Berenguer, J. (2000) 'Secretion and assembly of regular surface structures in Gram-negative bacteria', *FEMS Microbiology Reviews,* 24(1), pp. 21-44.

Florez, C., Raab, J. E., Cooke, A. C. and Schertzer, J. W. (2017) 'Pseudomona quinolone signal modulates outer membrane vesicle production on Pseudomona aeruginosa', *mBio,* 8(4), pp. 1-13.

Ford, B., Rêgo, A. T., Ragan, T. J., Pinkner, J., Dodson, K., Driscoll, P. C., Hultgren, S. and Waksman, G. (2010) 'Structural homology between the C-terminal domain of the PapC usher and its plug', *Journal of Bacteriology,* 192(7), pp. 1824-1831.

Froning, M., Helmer, P. O. and Hayen, H. (2020) 'Identification and structural characterization of lipid A from Escherichia coli, Pseudomonas putida and Pseudomonas taiwanensis using liquid chromatography coupled to high-resolution tandem mass spectrometry', *Rapid Communications in Mass Spectrometry,* 34(21), pp. 1-9.

Fronzes, R., Remaut, H. and Waksman, G. (2008) 'Architectures and biogenesis of non-flagellar protein appendages in Gram-negative bacteria', *EMBO Journal,* 27(17), pp. 2271-2280.

Fulsundar, S., Harms, K., Flaten, G. E., Johnsen, P. J., Chopade, B. A. and Nielsen, K. M. (2014) 'Gene transfer potential of outer membrane vesicles of Acinetobacter baylyi and effects of stress on vesiculation', *Appl Environ Microbiol,* 80(11), pp. 3469-83.

Furuyama, N. and Sircili, M. P. (2021) 'Outer membrane vesicles (OMVs) produced by gram-negative bacteria: Structure, functions, biogenesis, and vaccine application', *BioMed Research International,* 2021, pp. 15-17.

Gahlot, D. K., Ifill, G. and Macintyre, S. (2021) 'Optimised Heterologous Expression and Functional Analysis of the Yersinia pestis F1-Capsular Antigen Regulator Caf1R', pp. 1-21.

Galdiero, S., Falanga, A., Cantisani, M., Tarallo, R., Elena Della Pepa, M., D'Oriano, V. and Galdiero, M. (2012) 'Microbe-Host Interactions: Structure and Role of Gram-Negative Bacterial Porins', *Current Protein and Peptide Science,* 13(8), pp. 843-854.

Galyov, E. E., Smirnov, O. Y., Karlishev, A. V., Volkovoy, K. I., Denesyuk, A. I., Nazimov, I. V., Rubtsov, K. S., Abramov, V. M., Dalvadyanz, S. M. and Zav'yalov, V. P. (1990) 'Nucleotide sequence of the Yersinia pestis gene encoding F1 antigen and the primary structure of the protein. Putative T and B cell epitopes', *FEBS Letters,* 277(1-2), pp. 230-232.

Galyovl, E. E., Chernovskayal, T. V., Dolgikhr, D. A., Volkovoyz, K. I. and Abramovl, V. M. (1991) 'Expression of the envelop antigen F1 of Yersinia pestis is mediaated by the product of caf1M gene having homology with the chaperone protein PapD of Escherichia coli', 286(1), pp. 79-82.

García-Weber, D. and Arrieumerlou, C. (2021) 'ADP-heptose: a bacterial PAMP detected by the host sensor ALPK1', *Cell Mol Life Sci,* 78(1), pp. 17-29.

Garde, S., Chodisetti, P. K. and Reddy, M. (2021) 'Peptidoglycan: Structure, Synthesis, and Regulation', *EcoSal Plus,* 9(2).

Geibel, S. and Waksman, G. (2014) 'The molecular dissection of the chaperone-usher pathway', *Biochimica et Biophysica Acta - Molecular Cell Research,* 1843(8), pp. 1559-1567.

Gerding, M. A., Ogata, Y., Pecora, N. D., Niki, H. and De Boer, P. A. J. (2007) 'The trans-envelope Tol-Pal complex is part of the cell division machinery and required for proper outer-membrane invagination during cell constriction in E. coli', *Molecular Microbiology,* 63(4), pp. 1008-1025.

Gohrbandt, M., Lipski, A., Baig, Z., Walter, S., Kurre, R., Strahl, H. and Deckers-Hebestreit, G. (2019) 'Low membrane fluidity triggers lipid phase separation and protein segregation in vivo', *bioRxiv*, pp. 852160-852160.

Gohrbandt, M., Lipski, A., Grimshaw, J. W., Buttress, J. A., Baig, Z., Herkenhoff, B., Walter, S., Kurre, R., Deckers-Hebestreit, G. and Strahl, H. (2022) 'Low membrane fluidity triggers lipid phase separation and protein segregation in living bacteria', *The EMBO Journal,* 41(5), pp. 1-21.

Gorman, A. and Golovanov, A. P. (2022) 'Lipopolysaccharide Structure and the Phenomenon of Low Endotoxin Recovery', *Eur J Pharm Biopharm,* 180, pp. 289-307.

Granier, S., Kim, S., Shafer, A. M., Ratnala, V. R. P., Fung, J. J., Zare, R. N. and Kobilka, B. 2007. Structure and conformational changes in the C-terminal domain of the β2-adrenoceptor: Insights from fluorescence resonance energy transfer studies.

Griffin, B. A., Adams, S. R. and Tsien, R. Y. (1998) 'Specific covalent labeling of recombinant protein molecules inside live cells', *Science,* 281(5374), pp. 269-272.

Gunasinghe, S. D., Webb, C. T., Elgass, K. D., Hay, I. D. and Lithgow, T. (2017) 'Super-Resolution Imaging of Protein Secretion Systems and the Cell Surface of Gram-Negative Bacteria', *Front Cell Infect Microbiol,* 7, pp. 220.

Guzev, K. V., Isaeva, M. P., Novikova, O. D., Solov'Eva, T. F. and Rasskazov, V. A. (2005) 'Molecular characteristics of OmpF-like porins from pathogenic yersinia', *Biochemistry (Moscow),* 70(10), pp. 1104-1110.

Guzman, L. M., Belin, D., Carson, M. J., Beckwith, J., Guzman, L.-m., Belin, D. and Carson, M. J. (1995) 'Tight regulation , modulation , and high-level expression by vectors containing the arabinose PBAD promoter . These include : Tight Regulation , Modulation , and High-Level Expression by Vectors Containing the Arabinose P BAD Promoter', *Journal of bacteriology,* 177(14), pp. 4121-4130.

Hagan, C. L., Silhavy, T. J. and Kahne, D. (2011) 'B-Barrel Membrane Protein Assembly By the Bam Complex', *Annual Review of Biochemistry,* 80, pp. 189-210.

Hale, C. A., Persons, L. and de Boer, P. A. J. (2022) 'Recruitment of the TolA Protein to Cell Constriction Sites in Escherichia coli via Three Separate Mechanisms, and a Critical Role for FtsWI Activity in Recruitment of both TolA and TolQ', *Journal of Bacteriology,* 204(1).

Harris, J. R. (2007) 'Negative staining of thinly spread biological samples', *Methods in Molecular Biology,* 369(1), pp. 107-142.

Harris, J. R. and Carlo, S. D. (2014) *Chapter 11. Negative Staining and Cryo-negative Staining: Applications in Biology and Medicine.* (42 vols). Oxford, england: *Micron*.

Hatkoff, M., Runco, L. M., Pujol, C., Jayatilaka, I., Furie, M. B., Bliska, J. B. and Thanassi, D. G. (2012) 'Roles of chaperone/usher pathways of Yersinia pestis in a murine model of plague and adhesion to host cells', *Infection and Immunity,* 80(10), pp. 3490-3500.

Hejair, H. M. A., Zhu, Y., Ma, J., Zhang, Y., Pan, Z., Zhang, W. and Yao, H. (2017) 'Functional role of ompF and ompC porins in pathogenesis of avian pathogenic Escherichia coli', *Microbial Pathogenesis,* 107(December 2019), pp. 29-37.

Hinnebusch, B. J., Rudolph, A. E., Cherepanov, P., Dixon, J. E., Schwan, T. G. and Forsberg, A. (2002) 'Role of Yersinia murine toxin in survival of Yersinia pestis in the midgut of the flea vector', *Science,* 296(5568), pp. 733-5.

Hoffmann, C., Gaietta, G., Zürn, A., Adams, S. R., Terrillon, S., Ellisman, M. H., Tsien, R. Y. and Lohse, M. J. (2010) 'Fluorescent labeling of tetracysteine-tagged proteins in intact cells', *Nature Protocols,* 5(10), pp. 1666-1677.

Högbom, M. and Ihalin, R. (2017) 'Functional and structural characteristics of bacterial proteins that bind host cytokines', *Virulence,* 8(8), pp. 1592-1601.

Holtzman, T., Levy, Y., Marcus, D., Flashner, Y., Mamroud, E., Cohen, S. and Fass, R. (2006) 'Production and purification of high molecular weight oligomers of Yersinia pestis F1 capsular antigen released by high cell density culture of recombinant Escherichia coli cells carrying the caf1 operon', The 4th Re, pp. 4-7.

Horne, J. E., Brockwell, D. J. and Radford, S. E. (2020) 'Role of the lipid bilayer in outer membrane protein folding in Gram-negative bacteria', *J Biol Chem,* 295(30), pp. 10340-10367.

Hsia, C. Y., Chen, L., Singh, R. R., DeLisa, M. P. and Daniel, S. (2016) 'A Molecularly Complete Planar Bacterial Outer Membrane Platform', *Scientific Reports,* 6(August), pp. 1-14.

Hsiao, C. D., Sun, Y. J., Rose, J. and Wang, B. C. (1996) 'The crystal structure of glutamine-binding protein from Escherichia coli', *J Mol Biol,* 262(2), pp. 225-42.

Hu, P., Elliott, J., McCready, P., Skowronski, E., Garnes, J., Kobayashi, A., Brubaker, R. R. and Garcia, E. (1998) 'Structural organization of virulence-associated plasmids of Yersinia pestis', *Journal of Bacteriology,* 180(19), pp. 5192-5202.

Huang, Z., Li, G., Zhang, C. and Xing, X. H. (2016) 'A study on the effects of linker flexibility on acid phosphatase PhoC-GFP fusion protein using a novel linker library', *Enzyme Microb Technol,* 83, pp. 1-6.

Huszczynski, S. M., Lam, J. S. and Khursigara, C. M. (2020) 'The role of Pseudomonas aeruginosa lipopolysaccharide in bacterial pathogenesis and physiology', *Pathogens,* 9(1), pp. 1-22.

Inouye, S. and Tsuji, F. I. (1994) 'Aequorea green fluorescent protein. Expression of the gene and fluorescence characteristics of the recombinant protein', *FEBS Lett,* 341(2-3), pp. 277-80.

Ishida, H., Garcia-Herrero, A. and Vogel, H. J. (2014) 'The periplasmic domain of Escherichia coli outer membrane protein A can undergo a localized temperature dependent structural transition', *Biochimica et Biophysica Acta - Biomembranes,* 1838(12), pp. 3014-3024.

Jacob-Dubuisson, F., Striker, R. and Hultgren, S. J. (1994) 'Chaperone-assisted self-assembly of pili independent of cellular energy', *Journal of Biological Chemistry,* 269(17), pp. 12447-12455.

Jan, A. T. (2017) 'Outer Membrane Vesicles (OMVs) of gram-negative bacteria: A perspective update', *Frontiers in Microbiology,* 8(JUN), pp. 1-11.

Jeanteur, D., Lakey, J. H. and Pattus, F. (1991) 'The bacterial porin superfamily: sequence alignment and structure prediction', *Molecular Microbiology,* 5(9), pp. 2153-2164.

Jumper, J., Evans, R., Pritzel, A., Green, T., Figurnov, M., Ronneberger, O., Tunyasuvunakool, K., Bates, R., Žídek, A. and Potapenko, A. (2021) 'Highly accurate protein structure prediction with AlphaFold', *Nature,* 596(7873), pp. 583-589.

Kaparakis-Liaskos, M. and Ferrero, R. L. (2015) 'Immune modulation by bacterial outer membrane vesicles', *Nature Reviews Immunology,* 15(6), pp. 375-387.

Karlyshev, A. V., Galyov, E. E., Abramov, V. M. and Zav'yalov, V. P. (1992a) 'Caf1R gene and its role in the regulation of capsule formation of Y. pestis', *FEBS Letters,* 305(1), pp. 37-40.

Karlyshev, A. V., Galyov, E. E., Smirnov, O. Y., Guzayev, A. P., Abramov, V. M. and Zavyalov, V. P. (1992b) 'A new gene of the f1 operon of Yersinia pestis involved in the capsule biogenesis', *FEBS Lett.,* 297(1,2), pp. 77-80.

Kashyap, D., Panda, M., Baral, B., Varshney, N., R, S., Bhandari, V., Parmar, H. S., Prasad, A. and Jha, H. C. (2022) 'Outer Membrane Vesicles: An Emerging Vaccine Platform', *Vaccines (Basel),* 10(10).

Kesty, N. C. and Kuehn, M. J. (2004) 'Incorporation of heterologous outer membrane and periplasmic proteins into Escherichia coli outer membrane vesicles', *J Biol Chem,* 279(3), pp. 2069-76.

Khalid, S., Bond, P. J., Carpenter, T. and Sansom, M. S. P. (2008) 'OmpA: Gating and dynamics via molecular dynamics simulations', *Biochimica et Biophysica Acta - Biomembranes,* 1778(9), pp. 1871-1880.

Kim, J. Y., Doody, A. M., Chen, D. J., Cremona, G. H., Shuler, M. L., Putnam, D. and DeLisa, M. P. (2008) 'Engineered Bacterial Outer Membrane Vesicles with Enhanced Functionality', *Journal of Molecular Biology,* 380(1), pp. 51-66.

Kim, Y. S., Choi, E. J., Lee, W. H., Choi, S. J., Roh, T. Y., Park, J., Jee, Y. K., Zhu, Z., Koh, Y. Y., Gho, Y. S. and Kim, Y. K. (2013) 'Extracellular vesicles, especially derived from Gram-negative bacteria, in indoor dust induce neutrophilic pulmonary inflammation associated with both Th1 and Th17 cell responses', *Clinical and Experimental Allergy,* 43(4), pp. 443-454.

Kleinschmidt, J. H. (2003) 'Membrane protein folding on the example of outer membrane protein A of Escherichia coli', *Cellular and Molecular Life Sciences,* 60(8), pp. 1547-1558.

Kleinschmidt, J. H. (2015) 'Folding of β-barrel membrane proteins in lipid bilayers - Unassisted and assisted folding and insertion', *Biochimica et Biophysica Acta - Biomembranes,* 1848(9), pp. 1927-1943.

Kleinschmidt, J. H., Den Blaauwen, T., Driessen, A. J. M. and Tamm, L. K. (1999) 'Outer membrane protein A of Escherichia coli inserts and folds into lipid bilayers by a concerted mechanism', *Biochemistry,* 38(16), pp. 5006-5016.

Klimentová, J. and Stulík, J. (2015) 'Methods of isolation and purification of outer membrane vesicles from gram-negative bacteria', *Microbiological Research,* 170, pp. 1-9.

Knight, S., Rao, V. B., Black, L. W. and Knight, S. (2007) 'Structure and assembly of bacteriophage', *Virology Journal,* 7(1), pp. 356-356.

Knight, S. D., Berglund, J. and Choudhury, D. 2000. Bacterial adhesins: Structural studies reveal chaperone function and pilus biogenesis. Elsevier Current Trends.

Koebnik, R. (1999) 'Structural and functional roles of the surface-exposed loops of the beta-barrel membrane protein OmpA from Escherichia coli', *J Bacteriol,* 181(12), pp. 3688-94.

Koebnik, R., Locher, K. P. and Van Gelder, P. (2000) 'Structure and function of bacterial outer membrane proteins: Barrels in a nutshell', *Molecular Microbiology,* 37(2), pp. 239-253.

Kubas, M., Zabad, A., Alqadhi, D. and Al-Azab, M. (2018) 'Antibiotic Resistance Trends of Gram-negative Bacteria Most Frequently Isolated from Inpatients in a Tertiary Care Hospital in Sana'a, Yemen', *Yemeni Journal for Medical Sciences,* 12(1), pp. 22-30.

Kudryakova, I. V., Shishkova, N. A. and Vasilyeva, N. V. (2016) 'Outer membrane vesicles of Lysobacter sp. XL1: biogenesis, functions, and applied prospects', *Applied Microbiology and Biotechnology,* 100(11), pp. 4791-4801.

Kuehn, M. J. and Kesty, N. C. (2005) 'Bacterial outer membrane vesicles and the host-pathogen interaction', *Genes and Development,* 19(22), pp. 2645-2655.

Kulkarni, H. M. and Jagannadham, M. V. (2014) 'Biogenesis and multifaceted roles of outer membrane vesicles from Gram-negative bacteria', *Microbiology (United Kingdom),* 160(2014), pp. 2109-2121.

Kulp, A. and Kuehn, M. J. (2010) 'Biological Functions and Biogenesis of Secreted Bacterial Outer Membrane Vesicles', *Annual Review of Microbiology,* 64(1), pp. 163-184.

Kulp, A. J., Sun, B., Ai, T., Manning, A. J., Orench-Rivera, N., Schmid, A. K. and Kuehn, M. J. (2015) 'Genome-wide assessment of outer membrane vesicle production in Escherichia coli', *PLoS ONE,* 10(9), pp. 1-16.

Kumamoto, C. and Nagata, Y. (1994) 'NOTES Localization of', 176(22), pp. 7074-7078.

Kunsmann, L., Rüter, C., Bauwens, A., Greune, L., Glüder, M., Kemper, B., Fruth, A., Wai, S. N., He, X., Lloubes, R., Schmidt, M. A., Dobrindt, U., Mellmann, A., Karch, H. and Bielaszewska, M. (2015) 'Virulence from vesicles: Novel mechanisms of host cell injury by Escherichia coli O104:H4 outbreak strain', *Scientific Reports,* 5(1), pp. 13252-13252.

Laemmli, U. K. (1970) 'Cleavage of structural proteins during the assembly of the head of bacteriophage T4', *Nature,* 227(5259), pp. 680-5.

Lee, D. H., Kim, S. H., Kang, W., Choi, Y. S., Lee, S. H., Lee, S. R., You, S., Lee, H. K., Chang, K. T. and Shin, E. C. (2011) 'Adjuvant effect of bacterial outer membrane vesicles with penta-acylated lipopolysaccharide on antigen-specific T cell priming', *Vaccine,* 29(46), pp. 8293-8301.

Levy, Y., Vagima, Y., Tidhar, A., Aftalion, M., Gur, D., Nili, U., Chitlaru, T., Zauberman, A. and Mamroud, E. (2018) 'Targeting of the Yersinia pestis F1 capsular antigen by innate-like B1b cells mediates a rapid protective response against bubonic plague', *npj Vaccines,* 3(1), pp. 2-9.

Lewenza, S., Mhlanga, M. M. and Pugsley, A. P. (2008) 'Novel inner membrane retention signals in Pseudomonas aeruginosa lipoproteins', *J Bacteriol,* 190(18), pp. 6119-25.

Li, B. and Yang, R. (2008) 'Interaction between Yersinia pestis and the host immune system', *Infection and Immunity,* 76(5), pp. 1804-1811.

Lima, S., Guo, M. S., Chaba, R., Gross, C. A. and Sauer, R. T. (2013) 'Dual molecular signals mediate the bacterial response to outer-membrane stress', *Science,* 340(6134), pp. 837-841.

Liu, C., Chen, Z., Tan, C., Liu, W., Xu, Z., Zhou, R. and Chen, H. (2012) 'Immunogenic characterization of outer membrane porins OmpC and OmpF of porcine extraintestinal pathogenic Escherichia coli', *FEMS Microbiology Letters,* 337(2), pp. 104-111.

Luirink, J., Yu, Z., Wagner, S. and De Gier, J. W. (2012) 'Biogenesis of inner membrane proteins in Escherichia coli', *Biochimica et Biophysica Acta - Bioenergetics,* 1817(6), pp. 965-976.

MacIntyre, S., Zyrianova, I. M., Chernovskaya, T. V., Leonard, M., Rudenko, E. G., Zav'Yalov, V. P. and Chapman, D. A. G. (2001) 'An extended hydrophobic interactive surface of Yersinia pestis Caf1M chaperone is essential for subunit binding and F1 capsule assembly', *Molecular Microbiology,* 39(1), pp. 12-25.

Macnab, R. M. (2003) 'How Bacteria Assemble Flagella', *Annual Review of Microbiology,* 57, pp. 77-100.

Maiti, B., Shetty, M., Shekar, M., Karunasagar, I. and Karunasagar, I. (2011) 'Recombinant outer membrane protein A (OmpA) of Edwardsiella tarda, a potential vaccine candidate for fish, common carp', *Microbiol Res,* 167(1), pp. 1-7.

Maldonado, R. F., Sá-Correia, I. and Valvano, M. A. (2016) 'Lipopolysaccharide modification in gram-negative bacteria during chronic infection', *FEMS Microbiology Reviews,* 40(4), pp. 480-493.

Mapingire, O. S., Henderson, N. S., Duret, G., Thanassi, D. G. and Delcour, A. H. (2009) 'Modulating effects of the plug, helix, and N- and C-terminal domains on channel properties of the PapC usher', *Journal of Biological Chemistry,* 284(52), pp. 36324-36333.

Mashburn-Warren, L. M. and Whiteley, M. (2006a) 'Special delivery: vesicle trafficking in prokaryotes', *Mol Microbiol,* 61(4), pp. 839-46.

Mashburn-Warren, L. M. and Whiteley, M. (2006b) 'Special delivery: Vesicle trafficking in prokaryotes', *Molecular Microbiology,* 61(4), pp. 839-846.

Mathelié-Guinlet, M., Asmar, A. T., Collet, J. F. and Dufrêne, Y. F. (2020) 'Lipoprotein Lpp regulates the mechanical properties of the E. coli cell envelope', *Nat Commun,* 11(1), pp. 1789.

Mayer, M. P. (1995) 'A new set of useful cloning and expression vectors derived from pBlueScript', *Gene,* 163(1), pp. 41-46.

McBroom, A. J., Johnson, A. P., Vemulapalli, S. and Kuehn, M. J. (2006) 'Outer membrane vesicle production by Escherichia coli is independent of membrane instability', *Journal of Bacteriology,* 188(15), pp. 5385-5392.

McBroom, A. J. and Kuehn, M. J. (2007) 'Release of outer membrane vesicles by Gram-negative bacteria is a novel envelope stress response', *Molecular Microbiology,* 63(2), pp. 545-558.

McMahon, K. J., Castelli, M. E., Vescovi, E. G. and Feldman, M. F. (2012) 'Biogenesis of outer membrane vesicles in Serratia marcescens is thermoregulated

and can be induced by activation of the Rcs phosphorelay system', *Journal of Bacteriology,* 194(12), pp. 3241-3249.

Meyers, A., Furtmann, C., Gesing, K., Tozakidis, I. E. P. and Jose, J. (2019) 'Cell density-dependent auto-inducible promoters for expression of recombinant proteins in Pseudomonas putida', *Microb Biotechnol,* 12(5), pp. 1003-1013.

Micciulla, S., Gerelli, Y. and Schneck, E. (2019) 'Structure and Conformation of Wild-Type Bacterial Lipopolysaccharide Layers at Air-Water Interfaces', *Biophysical Journal,* 116(7), pp. 1259-1269.

Miller, J., Williamson, E. D., Lakey, J. H., Pearce, M. J., Jones, S. M., Titball, R. W., Julie, M., E. Diane, W., Jeremy H, L., Martin J, P., Steven, J. M., Titball, R. W., Miller, J., Williamson, E. D., Lakey, J. H., Pearce, M. J., Jones, S. M. and Titball, R. W. (1998) 'Macromolecular organisation of recombinant Yersinia pestis F1 antigen and the effect of structure on immunogenicity', *FEMS Immunology and Medical Microbiology,* 21(3), pp. 213-221.

Miller, S. I. (2016) 'Antibiotic resistance and regulation of the Gram-negative bacterial outer membrane barrier by host innate immune molecules', *mBio,* 7(5), pp. 1-3.

Mirdita, M., Schütze, K., Moriwaki, Y., Heo, L., Ovchinnikov, S. and Steinegger, M. (2022) 'ColabFold: making protein folding accessible to all', *Nature methods,* 19(6), pp. 679-682.

Miyawaki, A., Shcherbakova, D. M. and Verkhusha, V. V. (2012) 'Red fluorescent proteins: chromophore formation and cellular applications', *Curr Opin Struct Biol,* 22(5), pp. 679-88.

Mozaheb, N. and Mingeot-Leclercq, M. P. (2020) 'Membrane Vesicle Production as a Bacterial Defense Against Stress', *Frontiers in Microbiology,* 11(December).

Nagakubo, T., Nomura, N. and Toyofuku, M. (2020) 'Cracking Open Bacterial Membrane Vesicles', *Frontiers in Microbiology,* 10(January).

Nakae, T. (1976) 'Outer membrane of Salmonella. Isolation of protein complex that produces transmembrane channels', *J Biol Chem,* 251(7), pp. 2176-8.

Nakamura, S. and Minamino, T. (2019) 'Flagella-driven motility of bacteria', *Biomolecules,* 9(7).

Narayanan, N., Hsieh, M. Y., Xu, Y. and Chou, C. P. (2006) 'Arabinose-induction of lac-derived promoter systems for penicillin acylase production in Escherichia coli', *Biotechnology progress,* 22(3), pp. 617-625.

Nevermann, J., Silva, A., Otero, C., Oyarzún, D. P., Barrera, B., Gil, F., Calderón, I. L. and Fuentes, J. A. (2019) 'Identification of Genes Involved in Biogenesis of Outer Membrane Vesicles (OMVs) in Salmonella enterica Serovar Typhi', *Front Microbiol,* 10, pp. 104.

Nie, D., Hu, Y., Chen, Z., Li, M., Hou, Z., Luo, X., Mao, X. and Xue, X. (2020) 'Outer membrane protein A (OmpA) as a potential therapeutic target for Acinetobacter baumannii infection', *Journal of Biomedical Science,* 27(1), pp. 1-8.

Nikaido, H. (2003) 'Molecular basis of bacterial outer membrane permeability revisited', *Microbiological Reviews,* 49(1), pp. 1-32.

Nikaido, H., Rosenberg, E. Y. and Foulds, J. (1983) 'Porin channels in Escherichia coli: studies with beta-lactams in intact cells', *J Bacteriol,* 153(1), pp. 232-40.

Nishiyama, M., Ishikawa, T., Rechsteiner, H. and Glockshuber, R. (2008) 'Reconstitution of pilus assembly reveals a bacterial outer membrane catalyst', *Science,* 320(5874), pp. 376-9.

Noinaj, N., Rollauer, S. E. and Buchanan, S. K. (2015) 'The β-barrel membrane protein insertase machinery from Gram-negative bacteria', *Curr Opin Struct Biol,* 31, pp. 35-42.

Nuccio, S.-P. and Bäumler, A. J. (2007) 'Evolution of the Chaperone/Usher Assembly Pathway: Fimbrial Classification Goes Greek', *Microbiology and Molecular Biology Reviews,* 71(4), pp. 551-575.

Obeng, E. M., Dullah, E. C., Razak, N. S. A., Danquah, M. K., Budiman, C. and Ongkudon, C. M. (2017) 'Elucidating endotoxin-biomolecule interactions with FRET: extending the frontiers of their supramolecular complexation', *J Biol Methods,* 4(2), pp. e71.

Ojima, Y., Nguyen, M. H., Yajima, R. and Taya, M. (2015) 'Flocculation of Escherichia coli cells in association with enhanced production of outer membrane vesicles', *Applied and Environmental Microbiology,* 81(17), pp. 5900-5906.

Omattage, N. S., Deng, Z., Pinkner, J. S., Dodson, K. W., Almqvist, F., Yuan, P. and Hultgren, S. J. (2018) 'Structural basis for usher activation and intramolecular subunit transfer in P pilus biogenesis in Escherichia coli', *Nat Microbiol,* 3(12), pp. 1362-1368.

Oparka, K. J. (1994) 'Plasmolysis: new insights into an old process', *New Phytologist,* 126(4), pp. 571-591.

Ormo, M., Cubitt, A., Kallio, K., Gross, L., Tsien, R. and Remington, J. 1996. Crystal structure of the Aequorea victoria green fluorescent protein.

Pagès, J. M., James, C. E. and Winterhalter, M. (2008) 'The porin and the permeating antibiotic: A selective diffusion barrier in Gram-negative bacteria', *Nature Reviews Microbiology,* 6(12), pp. 893-903.

Pajerski, W., Ochonska, D., Brzychczy-Wloch, M., Indyka, P., Jarosz, M., Golda-Cepa, M., Sojka, Z. and Kotarba, A. (2019) 'Attachment efficiency of gold nanoparticles by Gram-positive and Gram-negative bacterial strains governed by surface charges', *Journal of Nanoparticle Research,* 21(8).

Park, E. and Rapoport, T. A. (2012) 'Bacterial protein translocation requires only one copy of the SecY complex in vivo', *Journal of Cell Biology,* 198(5), pp. 881-893.

Parkhill, J., Wren, B. W., Thomson, N. R., Titball, R. W., Holden, M. T., Prentice, M. B., Sebaihia, M., James, K. D., Churcher, C., Mungall, K. L., Baker, S., Basham, D., Bentley, S. D., Brooks, K., Cerdeño-Tárraga, A. M., Chillingworth, T., Cronin, A., Davies, R. M., Davis, P., Dougan, G., Feltwell, T., Hamlin, N., Holroyd, S., Jagels, K., Karlyshev, A. V., Leather, S., Moule, S., Oyston, P. C., Quail, M., Rutherford, K., Simmonds, M., Skelton, J., Stevens, K., Whitehead, S. and Barrell, B. G. (2001) 'Genome sequence of Yersinia pestis, the causative agent of plague', *Nature,* 413(6855), pp. 523-7.

Parthasarathy, A., Cross, P. J., Dobson, R. C. J., Adams, L. E., Savka, M. A. and Hudson, A. O. (2018) 'A Three-Ring Circus: Metabolism of the Three Proteogenic Aromatic Amino Acids and Their Role in the Health of Plants and Animals', *Front Mol Biosci,* 5, pp. 29.

Paul, C. and Rosenbusch, J. P. (1985) 'Folding patterns of porin and bacteriorhodopsin', *Embo j,* 4(6), pp. 1593-7.

Pautsch, A. and Schulz, G. E. (1998) 'Nsb1198_1013', 5(11), pp. 1013-1017.

Pautsch, A. and Schulz, G. E. (2000) 'High-resolution structure of the OmpA membrane domain', *J Mol Biol,* 298(2), pp. 273-82.

Pédelacq, J. D., Cabantous, S., Tran, T., Terwilliger, T. C. and Waldo, G. S. (2006) 'Engineering and characterization of a superfolder green fluorescent protein', *Nat Biotechnol,* 24(1), pp. 79-88.

Perry, R. D. and Fetherston, J. D. (1997) 'Yersinia perstis - Etiologic agent of plague', *Clinical Microbiology Reviews,* 10(1), pp. 35-66.

Peters, D. T., Reifs, A., Alonso-Caballero, A., Madkour, A., Waller, H., Kenny, B., Perez-Jimenez, R. and Lakey, J. H. (2022) 'Unraveling the molecular determinants of the anti-phagocytic protein cloak of plague bacteria', *PLoS Pathog,* 18(3), pp. e1010447.

Phan, G., Remaut, H., Wang, T., Allen, W. J., Pirker, K. F., Lebedev, A., Henderson, N. S., Geibel, S., Volkan, E., Yan, J., Kunze, M. B. A., Pinkner, J. S., Ford, B., Kay, C. W. M., Li, H., Hultgren, S. J., Thanassi, D. G. and Waksman, G. (2011) 'Crystal structure of the FimD usher bound to its cognate FimC-FimH substrate', *Nature,* 474(7349), pp. 49-53.

Pilizota, T. and Shaevitz, J. W. (2013) 'Plasmolysis and cell shape depend on solute outer-membrane permeability during hyperosmotic shock in E. coli', *Biophys J,* 104(12), pp. 2733-42.

Piras, L., Avitabile, C., D'Andrea, L. D., Saviano, M. and Romanelli, A. (2017) 'Detection of oligonucleotides by PNA-peptide conjugates recognizing the biarsenical fluorescein complex FlAsH-EDT(2)', *Biochem Biophys Res Commun,* 493(1), pp. 126-131.

Power, M. L., Ferrari, B. C., Littlefield-Wyer, J., Gordon, D. M., Slade, M. B. and Veal, D. A. (2006) 'A naturally occurring novel allele of Escherichia coli outer membrane protein A reduces sensitivity to bacteriophage', *Appl Environ Microbiol,* 72(12), pp. 7930-2.

Prasher, D. C., Eckenrode, V. K., Ward, W. W., Prendergast, F. G. and Cormier, M. J. (1992) 'Primary structure of the Aequorea victoria green-fluorescent protein', *Gene,* 111(2), pp. 229-33.

Proft, T. and Baker, E. N. (2009) 'Pili in Gram-negative and Gram-positive bacteria - Structure, assembly and their role in disease', *Cellular and Molecular Life Sciences,* 66(4), pp. 613-635.

Psonis, J. and Thanassi, D. (2019) 'Therapeutic approaches targeting the assembly and function of chaperone-usher pili', *EcoSal Plus.,* 8(2), pp. 1-16.

Qing, G., Gong, N., Chen, X., Chen, J., Zhang, H., Wang, Y., Wang, R., Zhang, S., Zhang, Z., Zhao, X., Luo, Y. and Liang, X.-J. (2019) 'Natural and engineered bacterial outer membrane vesicles', *Biophysics Reports,* 5(4), pp. 184-198.

Raetz, C. R. and Whitfield, C. (2002) 'Lipopolysaccharide endotoxins', *Annu Rev Biochem,* 71, pp. 635-700.

Ransom, E. M., Ellermeier, C. D. and Weiss, D. S. (2015) 'Use of mCherry red fluorescent protein for studies of protein localization and gene expression in Clostridium difficile', *Applied and Environmental Microbiology,* 81(5), pp. 1652-1660.

Rao, S., Bates, G. T., Matthews, C. R., Newport, T. D., Vickery, O. N. and Stansfeld, P. J. (2020) 'Characterizing Membrane Association and Periplasmic Transfer of

Bacterial Lipoproteins through Molecular Dynamics Simulations', *Structure,* 28(4), pp. 475-487.e3.

Remaut, H., Tang, C., Henderson, N. S., Pinkner, J. S., Wang, T., Hultgren, S. J., Thanassi, D. G., Waksman, G. and Li, H. (2008) 'Fiber formation across the bacterial outer emmbrane by the chaperone/usher pathway', *Cell,* 133(4), pp. 640-652.

Remington, S. J. (2011) 'Green fluorescent protein: a perspective', *Protein Sci,* 20(9), pp. 1509-19.

Rigel, N. W. and Silhavy, T. J. (2012) 'Making a beta-barrel: assembly of outer membrane proteins in Gram-negative bacteria', *Curr Opin Microbiol,* 15(2), pp. 189-93.

Roier, S., Zingl, F. G., Cakar, F., Durakovic, S., Kohl, P., Eichmann, T. O., Klug, L., Gadermaier, B., Weinzerl, K., Prassl, R., Lass, A., Daum, G., Reidl, J., Feldman, M. F. and Schild, S. (2016) 'A novel mechanism for the biogenesis of outer membrane vesicles in Gram-negative bacteria', *Nature Communications,* 7(6), pp. 257-259.

Rollauer, S. E., Sooreshjani, M. A., Noinaj, N. and Buchanan, S. K. (2015) 'Outer membrane protein biogenesis in Gram-negative bacteria', *Philosophical Transactions of the Royal Society B: Biological Sciences,* 370(1679).

Römling, U., Bian, Z., Hammar, M., Sierralta, W. D. and Normark, S. (1998) 'Curli fibers are highly conserved between Salmonella typhimurium and Escherichia coli with respect to operon structure and regulation', *Journal of Bacteriology,* 180(3), pp. 722-731.

Roque, A. I. (2012) *Protein Scaffolds for Cell Culture.* PhD thesis, Newcastle Unversity

Roque, A. I., Soliakov, A., Birch, M. A., Philips, S. R., Shah, D. S. H. H. and Lakey, J. H. (2014) 'Reversible non-stick behaviour of a bacterial protein polymer provides a tuneable molecular mimic for cell and tissue engineering', *Advanced Materials,* 26(17), pp. 2704-2709.

Rosenbusch, J. P. (1974) 'Characterization of the major envelope protein from Escherichia coli. Regular arrangement on the peptidoglycan and unusual dodecyl sulfate binding', *J Biol Chem,* 249(24), pp. 8019-29.

Ruiz, N., Gronenber, L. S., Kahne, D. and Silhavy, T. J. (2008) 'Identification of two inner-membrane proteins required for transport of lipopolysaccharide to the outer membrane of Escherichia coli', *Journal of Bacteriology,* 190(13), pp. 4460-4469.

Ruiz, N., Kahne, D. and Silhavy, T. J. (2006) 'Advances in understanding bacterial outer-membrane biogenesis', *Nature Reviews Microbiology,* 4(1), pp. 57-66.

Runco, L. M., Myrczek, S., Bliska, J. B. and Thanassi, D. G. (2008) 'Biogenesis of the fraction 1 capsule and analysis of the ultrastructure of Yersinia pestis', *Journal of Bacteriology,* 190(9), pp. 3381-3385.

Sahoo, H. (2012) 'Fluorescent labeling techniques in biomolecules: a flashback', *RSC advances,* 2(18), pp. 7017-7029.

Salih, O., Remaut, H., Waksman, G. and Orlova, E. V. (2008) 'Structural Analysis of the Saf Pilus by Electron Microscopy and Image Processing', *Journal of Molecular Biology,* 379(1), pp. 174-187.

Samsudin, F., Boags, A., Piggot, T. J. and Khalid, S. (2017) 'Braun's Lipoprotein Facilitates OmpA Interaction with the Escherichia coli Cell Wall', *Biophys J,* 113(7), pp. 1496-1504.

Sauer, F. G., Fu, K., Pinkner, J. S., Dodson, K. W., Hultgren, S. J. and Waksman, G. (1999) 'Structural Basis of Chaperone Function and Pilus Biogenesis', 285(August), pp. 1058-1062.

Sauer, F. G., Knight, S. D., Waksman and, G. J. and Hultgren, S. J. (2000) 'PapD-like chaperones and pilus biogenesis', *Seminars in Cell and Developmental Biology,* 11(1), pp. 27-34.

Sauer, F. G., Remaut, H., Hultgren, S. J. and Waksman, G. (2004) 'Fiber assembly by the chaperone-usher pathway', *Biochimica et Biophysica Acta - Molecular Cell Research,* 1694(1-3 SPEC.ISS.), pp. 259-267.

Schertzer, J. W. and Whiteley, M. (2012) 'A bilayer-couple model of bacterial outer membrane vesicle biogenesis', *mBio,* 3(2).

Schindler, M. and Rosenbusch, J. P. (1984) 'Structural transitions of porin, a transmembrane protein', *FEBS Lett,* 173(1), pp. 85-9.

Schleif, R. (2000) 'Regulation of the L-arabinose operon of Escherichia coli', *Trends Genet,* 16(12), pp. 559-65.

Schubert, S., Rakin, A. and Heesemann, J. (2004) 'The Yersinia high-pathogenicity island (HPI): Evolutionary and functional aspects', *International Journal of Medical Microbiology,* 294(2-3), pp. 83-94.

Schwechheimer, C. and Kuehn, M. J. (2015) 'Outer-membrane vesicles from Gram-negative bacteria: biogenesis and functions', *Nat Rev Microbiol,* 13(10), pp. 605-19.

Schwechheimer, C., Kulp, A. and Kuehn, M. J. (2014) 'Modulation of bacterial outer membrane vesicle production by envelope structure and content', *BMC Microbiology,* 14(1).

Selkrig, J., Leyton, D. L., Webb, C. T. and Lithgow, T. (2014) 'Assembly of β-barrel proteins into bacterial outer membranes', *Biochimica et Biophysica Acta - Molecular Cell Research,* 1843(8), pp. 1542-1550.

Shaner, N. C., Campbell, R. E., Steinbach, P. A., Giepmans, B. N., Palmer, A. E. and Tsien, R. Y. (2004) 'Improved monomeric red, orange and yellow fluorescent proteins derived from Discosoma sp. red fluorescent protein', *Nat Biotechnol,* 22(12), pp. 1567-72.

Sherman, D. J., Xie, R., Taylor, R. J., George, A. H., Okuda, S., Foster, P. J., Needleman, D. J. and Kahne, D. (2018) 'Lipopolysaccharide is transported to the cell surface by a membrane-to-membrane protein bridge', *Science,* 359(6377), pp. 798-801.

Silhavy, T. J., Kahne, D. and Walker, S. (2010) 'The bacterial cell envelope', *Cold Spring Harb Perspect Biol,* 2(5), pp. a000414.

Singh, R., Kumar, M., Mittal, A. and Mehta, P. K. (2017) 'Microbial metabolites in nutrition, healthcare and agriculture', *3 Biotech,* 7(1), pp. 15.

Sklar, J. G., Wu, T., Kahne, D. and Silhavy, T. J. (2007) 'Defining the roles of the periplasmic chaperones SurA, Skp, and DegP in Escherichia coli', *Genes and Development,* 21(19), pp. 2473-2484.

Smith, S. G., Mahon, V., Lambert, M. A. and Fagan, R. P. (2007) 'A molecular Swiss army knife: OmpA structure, function and expression', *FEMS Microbiol Lett,* 273(1), pp. 1-11.

Soliakov, A., Harris, J. R., Watkinson, A. and Lakey, J. H. (2010) 'The structure of Yersinia pestis Caf1 polymer in free and adjuvant bound states', *Vaccine,* 28(35), pp. 5746-5754.

Sperandeo, P., Lau, F. K., Carpentieri, A., De Castro, C., Molinaro, A., Dehò, G., Silhavy, T. J. and Polissi, A. (2008) 'Functional analysis of the protein machinery required for transport of lipopolysaccharide to the outer membrane of Escherichia coli', *Journal of Bacteriology,* 190(13), pp. 4460-4469.

Sperandeo, P., Martorana, A. M. and Polissi, A. (2017) 'The lipopolysaccharide transport (Lpt) machinery: A nonconventional transporter for lipopolysaccharide assembly at the outer membrane of Gram-negative bacteria', *Journal of Biological Chemistry,* 292(44), pp. 17981-17990.

Stargardt, P., Striedner, G. and Mairhofer, J. (2021) 'Tunable expression rate control of a growth-decoupled T7 expression system by L-arabinose only', *Microb Cell Fact,* 20(1), pp. 27.

Stepanenko, O. V., Stepanenko, O. V., Kuznetsova, I. M., Verkhusha, V. V. and Turoverov, K. K. (2013) 'Beta-barrel scaffold of fluorescent proteins: folding, stability and role in chromophore formation', *Int Rev Cell Mol Biol,* 302, pp. 221-78.

Stephan, M. S., Broeker, N. K., Saragliadis, A., Roos, N., Linke, D. and Barbirz, S. (2020) 'In vitro Analysis of O-Antigen-Specific Bacteriophage P22 Inactivation by Salmonella Outer Membrane Vesicles', *Front Microbiol,* 11, pp. 510638.

Storek, K. M., Chan, J., Vij, R., Chiang, N., Lin, Z., Bevers, J., 3rd, Koth, C. M., Vernes, J. M., Meng, Y. G., Yin, J., Wallweber, H., Dalmas, O., Shriver, S., Tam, C., Schneider, K., Seshasayee, D., Nakamura, G., Smith, P. A., Payandeh, J., Koerber, J. T., Comps-Agrar, L. and Rutherford, S. T. (2019) 'Massive antibody discovery used to probe structure-function relationships of the essential outer membrane protein LptD', *Elife,* 8.

Strahl, H. and Hamoen, L. W. (2010) 'Membrane potential is important for bacterial cell division', *Proc Natl Acad Sci U S A,* 107(27), pp. 12281-6.

Sugawara, E., Steiert, M., Rouhani, S. and Nikaido, H. (1996) 'Secondary structure of the outer membrane proteins OmpA of Escherichia coli and OprF of Pseudomonas aeruginosa', *J Bacteriol,* 178(20), pp. 6067-9.

Sun, W. and Singh, A. K. (2019) 'Plague vaccine: recent progress and prospects', *npj Vaccines,* 4(1), pp. 11-11.

Tamber, S. and Hancock, R. E. W. (2003) 'On the mechanism of solute uptake in Pseudomonas', *Frontiers in Bioscience,* 8, pp. 472-483.

Tamm, L. K., Arora, A. and Kleinschmidt, J. H. (2001) 'Structure and Assembly of β-Barrel Membrane Proteins', *Journal of Biological Chemistry,* 276(35), pp. 32399-32402.

te Winkel, J. D., Gray, D. A., Seistrup, K. H., Hamoen, L. W. and Strahl, H. (2016) 'Analysis of antimicrobial-triggered membrane depolarization using voltage sensitive dyes', *Frontiers in Cell and Developmental Biology,* 4(APR), pp. 1-10.

Terpe, K. (2006) 'Overview of bacterial expression systems for heterologous protein production: from molecular and biochemical fundamentals to commercial systems', *Appl Microbiol Biotechnol,* 72(2), pp. 211-22.

Thanassi, D. G., Saulino, E. T., Lombardo, M. J., Roth, R., Heuser, J. and Hultgren, S. J. (1998) 'The PapC usher forms an oligomeric channel: implications for pilus

biogenesis across the outer membrane', *Proc Natl Acad Sci U S A,* 95(6), pp. 3146-51.

Titball, R. W., Howells, A. M., Oyston, P. C. F. and Williamson, E. D. (1997) 'Expression of the Yersinia pestis capsular antigen (F1 antigen) on the surface of an aroA mutant of Salmonella typhimurium induces high levels of protection against plague', *Infection and Immunity,* 65(5), pp. 1926-1930.

Titball, R. W. and Williamson, E. D. (2001) 'Vaccination against bubonic and pneumonic plague', *Vaccine,* 19(30), pp. 4175-4184.

Tokuda, H. (2009) 'Biogenesis of outer membrenes in gram-negative bacteria', *Bioscience, Biotechnology and Biochemistry,* 73(3), pp. 465-473.

Toyofuku, M., Nomura, N. and Eberl, L. (2018) 'Types and origins of bacterial membrane vesicles', *Nature Reviews Microbiology*.

Tseng, T. T., Tyler, B. M. and Setubal, J. C. (2009) 'Protein secretion systems in bacterial-host associations, and their description in the Gene Ontology', *BMC Microbiology,* 9(SUPPL. 1), pp. 1-9.

Tsukazaki, T., Mori, H., Fukai, S., Ishitani, R., Mori, T., Dohmae, N., Perederina, A., Sugita, Y., Vassylyev, D. G., Ito, K. and Nureki, O. (2008) 'Conformational transition of Sec machinery inferred from bacterial SecYE structures', *Nature,* 455(7215), pp. 988-991.

Ulusu, Y., Dura, G., Waller, H., Benning, M. J., Fulton, D. A., Lakey, J. H. and Peters, D. T. (2017) 'Thermal stability and rheological properties of the 'non-stick' Caf1 biomaterial', *Biomedical Materials (Bristol),* 12(5).

Valbuena, F. M., Fitzgerald, I., Strack, R. L., Andruska, N., Smith, L. and Glick, B. S. (2020) 'A photostable monomeric superfolder green fluorescent protein', *Traffic,* 21(8), pp. 534-544.

Valeru, S. P., Shanan, S., Alossimi, H., Saeed, A., Sandström, G. and Abd, H. (2014) 'Lack of Outer Membrane Protein A Enhances the Release of Outer Membrane Vesicles and Survival of Vibrio cholerae and Suppresses Viability of Acanthamoeba castellanii', *Int J Microbiol,* 2014, pp. 610190.

van der Pol, L., Stork, M. and van der Ley, P. (2015) 'Outer membrane vesicles as platform vaccine technology', *Biotechnology Journal,* 10(11), pp. 1689-1706.

Vanaja, S. K., Russo, A. J., Behl, B., Banerjee, I., Yankova, M., Deshmukh, S. D. and Rathinam, V. A. K. (2016) 'Bacterial Outer Membrane Vesicles Mediate Cytosolic Localization of LPS and Caspase-11 Activation', *Cell,* 165(5), pp. 1106-1119.

Verhoeven, G. S., Dogterom, M. and Den Blaauwen, T. (2013) 'Absence of long-range diffusion of OmpA in E. coli is not caused by its peptidoglycan binding domain', *BMC Microbiology,* 13(1), pp. 1-9.

Volgers, C., Savelkoul, P. H. M. and Stassen, F. R. M. (2018) 'Gram-negative bacterial membrane vesicle release in response to the host-environment: different threats, same trick?', *Critical Reviews in Microbiology,* 44(3), pp. 258-273.

Volkan, E., Ford, B. A., Pinkner, J. S., Dodson, K. W., Henderson, N. S., Thanassi, D. G., Waksman, G. and Hultgren, S. J. (2012) 'Domain activities of PapC usher reveal the mechanism of action of an Escherichia coli molecular machine', *Proceedings of the National Academy of Sciences of the United States of America,* 109(24), pp. 9563-9568.

Vollmer, W., Blanot, D. and de Pedro, M. A. (2008) 'Peptidoglycan structure and architecture', *FEMS Microbiol Rev,* 32(2), pp. 149-67.

Volokhina, E. B., Grijpstra, J., Stork, M., Schilders, I., Tommassen, J. and Bos, M. P. (2011) 'Role of the periplasmic chaperones Skp, SurA, and DegQ in outer membrane protein biogenesis in Neisseria meningitidis', *Journal of Bacteriology,* 193(7), pp. 1612-1621.

Waksman, G. (2017) 'Structural and Molecular Biology of a Protein-Polymerizing Nanomachine for Pilus Biogenesis', *Journal of Molecular Biology,* 429(17), pp. 2654-2666.

Waksman, G. and Hultgren, S. J. (2009) 'Structural biology of the chaperone-usher pathway of pilus biogenesis', *Nature Reviews Microbiology,* 7(11), pp. 765-774.

Waldo, G. S., Standish, B. M., Berendzen, J. and Terwilliger, T. C. (1999) 'Rapid protein-folding assay using green fluorescent protein', *Nat Biotechnol,* 17(7), pp. 691-5.

Walton, T. A., Sandoval, C. M., Fowler, C. A., Pardi, A. and Sousa, M. C. (2009) 'The cavity-chaperone Skp protects its substrate from aggregation but allows independent folding of substrate domains', *Proceedings of the National Academy of Sciences of the United States of America,* 106(6), pp. 1772-1777.

Wang, L., Qu, W. and Reeves, P. R. (2001) 'Sequence analysis of four Shigella boydii O-antigen loci: implication for Escherichia coli and Shigella relationships', *Infect Immun,* 69(11), pp. 6923-30.

Wang, X., Peterson, J. H. and Bernstein, H. D. (2021) 'Bacterial Outer Membrane Proteins Are Targeted to the Bam Complex by Two Parallel Mechanisms', *mBio,* 12(3).

Wang, X., Teng, D., Guan, Q., Mao, R., Hao, Y., Wang, X., Yao, J. and Wang, J. (2017) 'Escherichia coli outer membrane protein F (OmpF): an immunogenic protein induces cross-reactive antibodies against Escherichia coli and Shigella', *AMB Express,* 7(1), pp. 155.

Wang, Y. (2002) 'The function of OmpA in Escherichia coli', *Biochemical and Biophysical Research Communications,* 292(2), pp. 396-401.

Weiss, M. S., Wacker, T., Weckesser, J., Welte, W. and Schulz, G. E. (1990) 'The three-dimensional structure of porin from Rhodobacter capsulatus at 3 A resolution', *FEBS Lett,* 267(2), pp. 268-72.

Welte, W., Nestel, U., Wacker, T. and Diederichs, K. (1995) 'Structure and function of the porin channel', *Kidney International,* 48(4), pp. 930-940.

Wendel, S., Fischer, E. C., Martínez, V., Seppälä, S. and Nørholm, M. H. H. (2016) 'A nanobody: GFP bacterial platform that enables functional enzyme display and easy quantification of display capacity', *Microbial Cell Factories,* 15(1), pp. 1-13.

Werneburg, G. and Thanassi, D. (2017) *Pili assembled by the chaperone/usher pathway in Escherichia coli and Salmonella.*

Weyant, K. B., Liao, J., Jesus, M. R.-D., Jaroentomeechai, T., Moeller, T. D., Hoang-Phou, S., Pal, S., Gilmore, S. F., Singh, R. and Putnam, D. (2021) 'A modular platform for on-demand vaccine self-assembly enabled by decoration of bacterial outer membrane vesicles with biotinylated antigens', *bioRxiv*, pp. 2021.08.24.457488.

Weyant, K. B., Oloyede, A., Pal, S., Liao, J., Jesus, M. R., Jaroentomeechai, T., Moeller, T. D., Hoang-Phou, S., Gilmore, S. F., Singh, R., Pan, D. C., Putnam, D., Locher, C., de la Maza, L. M., Coleman, M. A. and DeLisa, M. P. (2023) 'A modular vaccine platform enabled by decoration of bacterial outer membrane vesicles with biotinylated antigens', *Nat Commun,* 14(1), pp. 464.

Williamson, E. D., Packer, P. J., Waters, E. L., Simpson, A. J., Dyer, D., Hartings, J., Twenhafel, N. and Pitt, M. L. M. (2011) 'Recombinant (F1 + V) vaccine protects cynomolgus macaques against pneumonic plague', *Vaccine,* 29(29-30), pp. 4771-4777.

Wimley, W. C. (2003) 'The versatile beta-barrel membrane protein', *Curr Opin Struct Biol,* 13(4), pp. 404-11.

Wolf-Watz, H., Normark, S. and Bloom, G. D. (1973) 'Rapid method for isolation of large quantities of outer membrane from Escherichia coli K-12 and its application to the study of envelope mutants', *J Bacteriol,* 115(3), pp. 1191-7.

Wu, K. Y. and Yang, T. X. (2020) 'A Novel Improved Gram Staining Method Based on the Capillary Tube', *Polish Journal of Microbiology,* 69(4), pp. 503-508.

Wurpel, D. J., Beatson, S. A., Totsika, M., Petty, N. K. and Schembri, M. A. (2013) 'Chaperone-usher fimbriae of Escherichia coli', *PLoS ONE,* 8(1), pp. 1-11.

Yan, Z., Yin, M., Chen, J. and Li, X. (2020) 'Assembly and substrate recognition of curli biogenesis system', *Nature Communications,* 11(1), pp. 1-10.

Yoshida, T., Qin, L., Egger, L. A. and Inouye, M. (2006) 'Transcription regulation of ompF and ompC by a single transcription factor, OmpR', *Journal of Biological Chemistry,* 281(25), pp. 17114-17123.

Yu, X., Visweswaran, G. R., Duck, Z., Marupakula, S., MacIntyre, S., Knight, S. D. and Zavialov, A. V. (2009) 'Caf1A usher possesses a Caf1 subunit-like domain that is crucial for Caf1 fibre secretion', *Biochemical Journal,* 418(3), pp. 541-551.

Yu, X. D., Fooks, L. J., Moslehi-Mohebi, E., Tischenko, V. M., Askarieh, G., Knight, S. D., MacIntyre, S. and Zavialov, A. V. (2012) 'Large is fast, small is tight: Determinants of speed and affinity in subunit capture by a periplasmic chaperone', *Journal of Molecular Biology,* 417(4), pp. 294-308.

Zavialov, A., Zav'yalova, G., Korpela, T. and Zav'yalov, V. (2007a) 'FGL chaperone-assembled fimbrial polyadhesins: Anti-immune armament of Gram-negative bacterial pathogens', *FEMS Microbiology Reviews,* 31(4), pp. 478-514.

Zavialov, A. V. (2005) 'Resolving the energy paradox of chaperone/usher-mediated assembly', *Biochemical Society,* 389(2), pp. 685-694.

Zavialov, A. V., Batchikova, N. V., Korpela, T., Petrovskaya, L. E., Korobko, V. G., Kersley, J., MacIntyre, S. and Zav`yalov, V. (2001) 'Secretion of Recombinant Proteins via the Chaperone / Usher Pathway in Escherichia coli', *Applied and environmental microbiology,* 67(4), pp. 1805-1814.

Zavialov, A. V., Berglund, J., Pudney, A. F., Fooks, L. J., Ibrahim, T. M., MacIntyre, S. and Knight, S. D. (2003) 'Structure and biogenesis of the capsular F1 antigen from Yersinia pestis: Preserved folding energy drives fiber formation', *Cell,* 113(5), pp. 587-596.

Zavialov, A. V., Kersley, J., Korpela, T., Zav'yalov, V. P., MacIntyre, S. and Knight, S. D. (2002) 'Donor strand complementation mechanism in the biogenesis of non-pilus systems', *Molecular Microbiology,* 45(4), pp. 983-995.

Zavialov, A. V. and Knight, S. D. (2007b) 'A novel self-capping mechanism controls aggregation of periplasmic chaperone Caf1M', *Mol Microbiol,* 64(1), pp. 153-64.

Zhou, D., Han, Y. and Yang, R. (2006) 'Molecular and physiological insights into plague transmission, virulence and etiology', *Microbes and Infection,* 8(1), pp. 273-284.

Zhu, H., Rollier, C. S. and Pollard, A. J. (2021) 'Recent advances in lipopolysaccharide-based glycoconjugate vaccines', *Expert Review of Vaccines,* 20(12), pp. 1515-1538.